Development and characterisation of anti-MCAM chimeric antigen receptor T cells

A thesis submitted to the University of Manchester for the degree of Doctor of Philosophy in the Faculty of Biology, Medicine and Health

2023

Holly J Mole

School of Medical Sciences, Division of Cancer Sciences

Table of Contents

Final word count: 56542

List of tables

List of figures

List of abbreviations

ACT	Adoptive cellular therapies
AICD	Activation induced cell death
Akt	Protein kinase B
ALL	Acute lymphoblastic leukaemia
APC	Antigen presenting cell
BCR	B cell receptor
BSA	Bovine serum albumin
CAIX	Carbonic anhydrase IX
CAR	Chimeric antigen receptor
CCR	Chimeric costimulatory receptor
CDR	Complementarity determining region
CEA	Carcinoembryonic antigen
CEACAM	Carcinoembryonic antigen-related cell adhesion molecule
CFSE	Carboxyfluorescein succinimidyl ester
CLL	Chronic lymphocytic leukaemia
CREB	cAMP response element binding protein
CREB	cAMP response element-binding protein
CRES	CAR related encephalopathy syndrome
CRS	Cytokine release syndrome
Csk	C-terminal Src kinase
DMEM	Dulbecco's Modified Eagles Medium
ECM	Extracellular matrix
EMT	Epithelial-mesenchymal transition
EMT	Epithelial–mesenchymal transition
HUVEC	Human umbilical vein endothelial cell
FAK	Focal adhesion kinase
FBS	Fetal bovine serum
Fc	Immunoglobulin fragment crystallisable region
FDA	Food and Drug Administration
GFP	Green fluorescent protein
HCC	Hepatocellular carcinoma
HER2	Receptor tyrosine-protein kinase erbB-2
HMW-MAA	High molecular weight melanoma-associated antigen
IFN-γ	Interferon gamma
Ig	Immunoglobulin
IL	Interleukin
ITAM	Immunoreceptor tyrosine-based activation motif
IV	Intravenous
JNK	c-Jun N-terminal kinase
LAT	Linker for activation of T cells
Lck	Lymphocyte-specific protein tyrosine kinase

LDL	Low density lipoprotein
LTR	Long terminal repeat
MAGE	Melanoma antigen gene
MAPK	mitogen-activated protein kinase
MCAM	Melanoma cell adhesion molecule (also referred to as MUC18, CD146 and MelCAM)
MHC	Major histocompatibility complex
MMP	Matrix metalloproteinase
MoMLV	Moloney murine leukaemia virus
NFAT	Nuclear factor of activated T cells
NF-κB	Nuclear factor kappa-light-chain-enhancer of activated B cells
NICE	National Institute for Heath and Care Excellence
NIK	NF-κB inducing kinase
NRAS	Neuroblastoma RAS viral oncogene homolog
PBMC	Peripheral blood mononuclear cells
PBS	Phosphate buffered saline
PHA	Phytohemagglutinin
PI3K	Phosphatidylinositol 3-kinase
PKC	Protein kinase C
PLC	Phospholipase C
PMA	Phorbol 12-myristate 13-acetate
PSMA	Prostate-specific membrane antigen
RPMI	Roswell Mark Memorial Institute -1640
scFv	Single chain variable fragment
SH2	Src homology 2
SHP-1	Src homology 2 domain-containing protein tyrosine phosphatase 1
TAA	Tumour-associated antigen
TBS	Tris-buffered saline
TCR	T cell receptor
TIL	Tumour infiltrating lymphocyte
TM	Transmembrane
TMB	Tetramethylbenzidine
TNFR	Tumour necrosis factor receptor
TNFα	Tumour necrosis factor alpha
TRAF	TNFR associated factor
UTR	Untranslated region
VEGF	Vascular endothelial growth factor
V_H	Immunoglobulin variable light domain
V_L	Immunoglobulin variable heavy domain
VSVG	Vesicular stomatitis virus G

Abstract

OBJECTIVES

One in two patients with stage 4 melanoma will not survive their first year after diagnosis. Although recent treatment advances have improved survival, there is an unmet need for alternative therapeutics. Chimeric antigen receptor (CAR) T cell therapy involves re-directing autologous T lymphocytes against tumour-associated antigens via a receptor which couples an antigen-binding domain to CD3ζ and costimulatory signalling domains. Melanoma cell adhesion molecule (MCAM) is upregulated in melanoma, promotes invasive cell behaviour and angiogenesis, and predicts poor survival. CAR T cells redirected against this tumour-associated antigen could represent a novel treatment option in late-stage melanoma.

METHODS

5 single chain variable fragments (scFvs), derived from MCAM-specific antibody sequences, were cloned into a retroviral second-generation, 4-1BB costimulated CAR construct with CD8 hinge and transmembrane regions. CARs were screened for their ability to activate the JRT3-T3.5 cell line in response to MCAM-expressing cells. Selected CAR constructs were then expressed in primary T cells, and T cell effector functions were assessed in response to target cells. CAR T cells were also cocultured with HUVEC cells in monolayers and networks.

RESULTS

M1.BBz and M40.BBz CARs drove modest activation of the JRT3-T3.5 cell line in response to target cells expressing the MCAM ectodomain. These CARs redirected primary T cells effector functions, causing MCAM-dependent pro-inflammatory cytokine release, upregulation of cell surface activation markers and tumour cell lysis. However, the CAR T cells also targeted HUVEC cells, causing significant destruction of capillary-like networks.

CONCLUSIONS

Whilst this study demonstrates the feasibility of generating MCAM-specific CAR T cells, further work is needed to confirm their anti-tumour efficacy *in vivo*. Ultimately, the potential for on-target/off-tumour toxicity, particularly towards the vasculature, must be considered. Further engineering has the potential to increase their safety and specificity, but the risk of toxicities may ultimately preclude the safe targeting of MCAM in this context.

Declaration

I hereby declare that no portion of the work referred to in the thesis has been submitted in support of an application for another degree or qualification of this or any other university or other institute of learning.

Copyright statement

i. The author of this thesis (including any appendices and/or schedules to this thesis) owns certain copyright or related rights in it (the "Copyright") and s/he has given The University of Manchester certain rights to use such Copyright, including for administrative purposes.

ii. Copies of this thesis, either in full or in extracts and whether in hard or electronic copy, may be made only in accordance with the Copyright, Designs and Patents Act 1988 (as amended) and regulations issued under it or, where appropriate, in accordance with licensing agreements which the University has from time to time. This page must form part of any such copies made.

iii. The ownership of certain Copyright, patents, designs, trademarks and other intellectual property (the "Intellectual Property") and any reproductions of copyright works in the thesis, for example graphs and tables ("Reproductions"), which may be described in this thesis, may not be owned by the author and may be owned by third parties. Such Intellectual Property and Reproductions cannot and must not be made available for use without the prior written permission of the owner(s) of the relevant Intellectual Property and/or Reproductions.

iv. Further information on the conditions under which disclosure, publication and commercialisation of this thesis, the Copyright and any Intellectual Property University IP Policy (see http://documents.manchester.ac.uk/display.aspx?DocID=24420, in any relevant Thesis restriction declarations deposited in the University Library, The University Library's regulations (see http://www.library.manchester.ac.uk/about/regulations/) and in The University's policy on Presentation of Theses.

Funding

This PhD was funded by the Medical Research Council as a doctoral training partnership (MRC-DTP). Additional funding for extensions to mitigate the impact of COVID-19 was provided by UKRI and the charity Melanoma UK.

Acknowledgements

First and foremost, I would like to thank my supervisors, Adam Hurlstone and Paul Lorigan. Adam, thank you for giving me the opportunity to work in your lab. Your patience, help and guidance has been invaluable. I would like to thank Paul for all his clinical insight and encouragement over the last 4 years.

A big thank you goes to all the members of the Hurlstone lab, past and present. Thank you for sharing your knowledge and for making the lab a great place to work, these 4 years would not have been the same without you. A special thank you must go to Gemma Johnson for her wisdom in all things scientific, and for being a source of friendship and encouragement throughout my PhD. To the current members of the Hurlstone lab, Alex Wong, Maca Fernandez Carro, Erez Uzuner, Rotem Salmi-Leshem and Kieran Sefton: thank you for the support and the laughs, it has been great working with you all!

My grateful thanks also goes to all the staff of the University of Manchester core facilities, including the BSF technical staff, the bioimaging team, and Gareth Howell and David Chapman of the flow cytometry facility. Their expertise and help was invaluable.

I would like to thank my wonderful family: without the support of my mum, dad and brother this would not have been possible. Thank you so much for all your love and encouragement over the years.

Finally, the biggest thank you of all goes to my fiancé, Sam. Words can't quite capture how grateful I am for all that you are and all that you do. Coming home to you, Edie, Nora and Morris is the highlight of every day and has kept me grounded over the last 4 years. I simply could not have done this PhD without the love and support you have shown me every step of the way.

Chapter 1. Introduction

1.1. Adoptive immunotherapy for cancer

Cancer immunotherapy is a diverse and growing field, encompassing various strategies in which components of the immune system are utilised to mediate anti-cancer effects. Significant success has been achieved in certain malignancies, leading to its introduction as standard therapy in some contexts [1, 2].

The innate and adaptive arms of the human immune system perform various functions, including protection from infection, cancer immunosurveillance and the prevention of autoimmunity. The adaptive immune system is formed of antigen-specific B and T lymphocytes and has been utilised in many immunotherapies to date [1, 3]. Lymphocytes are characterised by the expression of unique antigen receptors known as the B cell receptor (BCR)/surface immunoglobulin (Ig) and the T cell receptor (TCR), respectively. Despite sharing similar structural organisation, Ig and the TCR differ in respect to the types of antigens they can recognise. Ig can bind to native protein, lipid and carbohydrate antigens expressed on the cell surface, with the typical TCR only binding processed peptides presented by the major histocompatibility complex (MHC) I and II [4]. The αβ TCR is a heterodimer of 2 chains, each of which has a membrane-proximal constant region and an N-terminal unique variable domain through which they bind antigen [5, 6].

Whilst binding of the TCR to its cognate peptide: MHC complex is an essential step for T cell activation and effector function, activation of naïve T cells also requires the presence of various co-receptors, accessory proteins, and costimulatory receptors. The CD4 and CD8 coreceptors are expressed on T cells, and bind to distinct sites on MHCII and MHCI, respectively, increasing the stability of the interaction between the TCR and antigen presenting cell [4]. The tyrosine kinase Lck is found constitutively associated with the cytoplasmic tail of CD4/8 [7], and binding to a peptide: MHC complex localises it to the membrane where it can phosphorylate signalling proteins such as those in the TCR-associated CD3 complex [8]. The CD3 signalling complex comprises ε, γ and δ chains and a CD3ζ homodimer, all of which contain immunoreceptor tyrosine-based

activation motifs (ITAMs). Each ITAM has a canonical sequence of YXXL/I X_{6-12} YXXL/I, and phosphorylation of the two tyrosine residues by Lck creates binding sites for SH2 domain-containing proteins, such as ZAP70. Membrane-localised ZAP70 is phosphorylated by Lck, activating downstream signalling pathways [9]. Ultimately, this results in upregulation of the transcription factors nuclear factor of activated T cells (NFAT), AP1 and NF-κB, promoting interleukin-2 (IL-2) production, survival, proliferation, and differentiation into effector clones. Signalling through the CD28 costimulatory receptor, which binds CD80 and CD86 on antigen presenting cells, serves to amplify the signal through the TCR/CD3 complex, and is necessary for activation of naïve T cells [5, 10].

Naïve T cells differentiate into different effector subsets depending on their expression of CD4/CD8 and the presence of cytokines in the microenvironment during the early phases of antigen encounter and activation (Figure 1.1). 5 canonical subsets of T helper cells exist, which have lineage specific transcription factors and inducer and effector cytokines [11, 12]. Th1-polarisation occurs in response to interferon gamma (IFN-γ) from activated dendritic cells, with the resulting T-bet-expressing Th1 cells playing a role in host immunity against intracellular pathogens through their expression of IFN-γ and TNF-alpha (TNF-α). GATA-3-expressing Th2 cells protect against helminth infection by producing various cytokines including IL-4, IL-5 and IL-13, which serve to activate and recruit macrophages, eosinophils and basophils. Meanwhile Th17 cells, characterised by their expression of RORγt, IL-17, IL-21 and IL-22 play a role in controlling extracellular bacterial infections. In contrast, regulatory T cells (Treg) are defined by their expression of Foxp3, CD25 and IL-10, and dampen down immune responses to prevent autoimmunity. Lastly, T follicular helper (Tfh) cells promote humoral immunity by B cells. Although direct cytotoxicity was originally considered a canonical CD8+ T cell effector function, cytotoxic CD4+ T cells which produce granzyme B and perforin have also been described [13–16].

Several subsets of cytotoxic CD8+ T cells have also been reported: Tc1 cells are typical cytotoxic T cells, lysing target cells through the release of granzyme B and perforin; Tc2 cells are similarly cytotoxic, but differ in that they express IL4, IL-5 and IL-13 instead of IFNγ and TNFα; Tc9 and Tc17 cells are poorly cytotoxic due to their limited production

of granzyme B, instead producing IL-9 and IL-17, respectively; whilst Tc22 cells, defined by their production IL-22, are also cytotoxic [17].

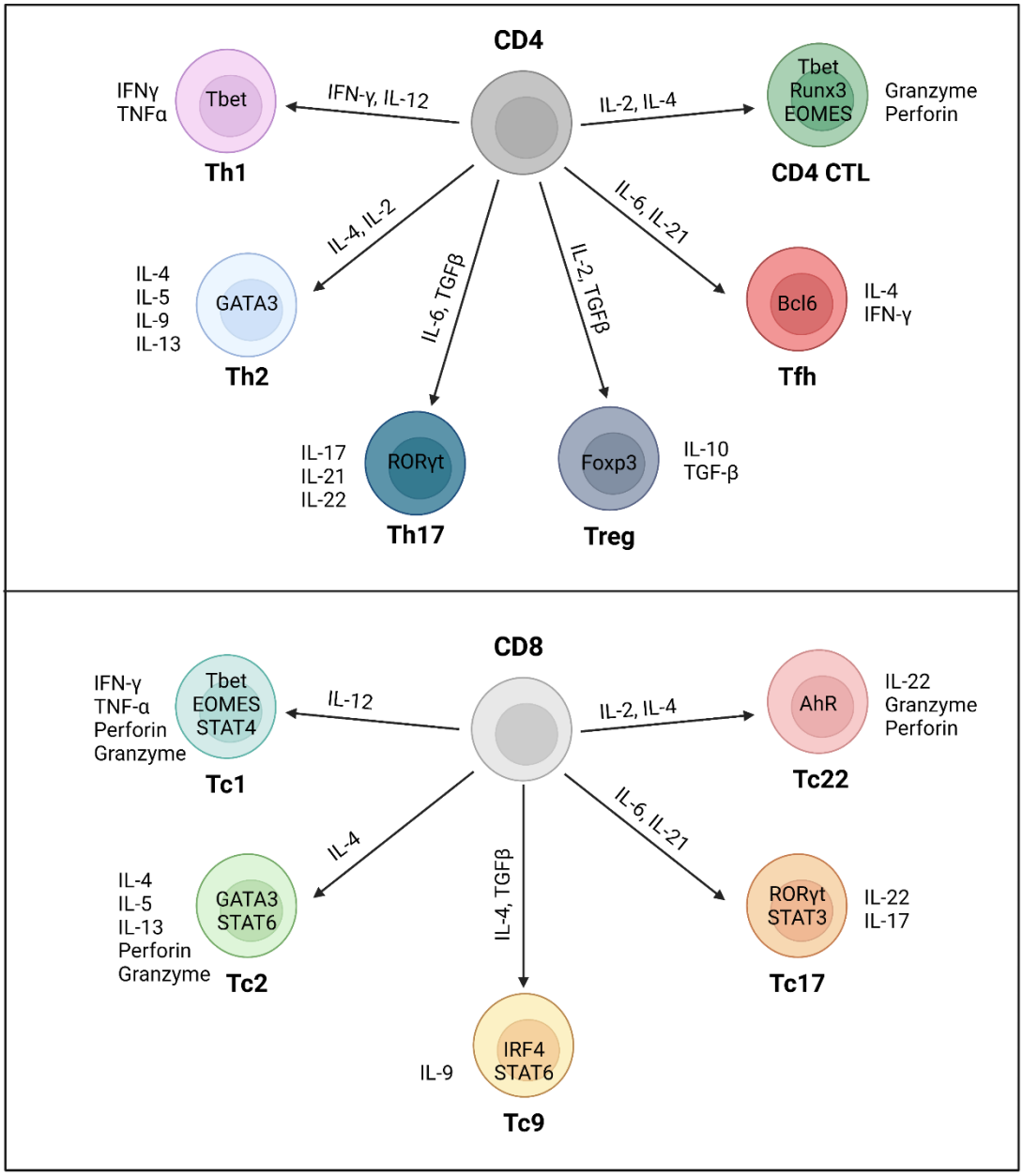

Figure 1.1 CD4+ and CD8+ T cell effector subsets.
Upon TCR engagement, CD4+ and CD8+ T cells differentiate into different subsets with unique effector functions and cytokine profiles. This process is determined by the presence of polarising cytokines and is controlled by the lineage specific transcription factors. Th, T helper; CTL, cytotoxic T lymphocyte; Tfh, T follicular helper; Treg, regulatory T cell; IL, interleukin; IFN, interferon; TNF, tumour necrosis factor. Adapted from Zhu et al, 2020 [12] and Paul et al, 2020 [17]. Figure created with Biorender.com.

Given their diverse effector functions, the potential use of T cells as immunotherapies has received significant interest. T cells receive inhibitory signals through the receptors CTLA-4 and PD-1, and blocking antibodies targeted to these have proven effective, particularly in metastatic melanoma [18–20]. A recent meta-analysis found that their use significantly improved progression free survival in this context compared to the standard regimen of chemotherapy [21]. However, survival rate for advanced cancers such as metastatic melanoma is still poor, and responses to checkpoint blockers are not observed in all patients [18–20].

Adoptive cell transfer (ACT) based therapies involve the infusion of tumour reactive T cells into patients to drive anti-cancer responses. One of the first examples of this was the pioneering use of tumour infiltrating lymphocytes (TILs) for the treatment of metastatic melanoma by Rosenberg et al [22]. In this therapy, tumour tissue is surgically removed, and fragments are cultured with IL-2 to drive the preferential expansion of T cells within the tumour. Following this initial outgrowth, a rapid expansion protocol is initiated which involves culturing TILs with anti-CD3 antibodies, irradiated feeder cells and IL-2 to achieve the high cell numbers required for transfer. Patients are pre-treated with either non-myeloablative chemotherapy or total body irradiation in order to deplete endogenous lymphocytes prior to infusion of the prepared TILs. IL-2 is often also administered to support TIL survival [23].

A 2019 meta-analysis by Dafni et al of 13 trials covering 410 patients with cutaneous melanoma estimated the overall response rate to be 41% and the complete response rate to be 12% [24]. Encouraging results have also been reported in the context of cervical cancer [25], colorectal cancer [26], cholangiocarcinoma [27], breast cancer [28] and non-small cell lung cancer [29]. However, toxicities are common, often relating to the administration of IL-2 or to preconditioning lymphodepletion: febrile neutropenia was the most frequently identified toxicity in the above meta-analysis, occurring in around a third of patients. Autoimmune toxicities linked to the TILs themselves have also been reported in the context of melanoma (Yeh et al., 2009).

TIL therapies require an immune response to have already been mounted against the tumour, which does not always occur on account of the rarity of naturally occurring tumour reactive T cells. This is in part due to the lack of neoantigens expressed on

cancer cells and the deletion of self-reactive T cells by central tolerance processes during development in the thymus. To overcome this barrier, transgenic TCR T cells were developed which are genetically engineered to express a pre-defined TCR construct. A significant benefit of this method over TIL-based therapies is that such T cells can be specifically re-directed against antigens which they otherwise would be tolerant towards, such as tumour associated antigens (TAAs) or lineage specific antigens. Tumour associated antigens are expressed on normal tissues at low levels but become significantly upregulated on cancerous cells, whilst lineage specific antigens are only expressed on cells of one developmental lineage.

This approach allows an expanded population of T cells specific to a known antigen to be infused into patients, typically combined with preconditioning lymphodepletion and systemic IL-2 infusions. This is an active area of research with over one hundred clinical trials registered to date in various malignancies [31]. The cancer germline antigen, NY-ESO-1, has received particular attention as a potential target for such therapies: phase I clinical trials of NY-ESO-1 TCR engineered T cells, typically recruiting patients with melanoma or synovial sarcoma, have achieved promising albeit variable ORRs of 20% to 58% [32–37]. Other commonly targeted antigens include MART-1, MAGE A1/A3/A4, gp100 and viral antigens from the human papilloma (HPV), Epstein-Barr (EBV) and Hepatitis B (HBV) viruses [31]. As with TIL therapies, toxicities often relate to the preconditioning lymphodepletion and systemic IL-2 administration. Toxicities relating to recognition of the target antigen on normal tissues have also been reported [38–40], as have incidences of fatal cross-reactivity against other target peptides [41, 42].

The potential repertoire of TCRs is large as they can recognise both intracellular and extracellular antigens with high sensitivity compared to other types of genetically engineered T cells [43, 44]. However, binding is limited to peptide antigens expressed on a particular MHC molecule. Often tumour cells down-regulate MHC expression and antigen presentation [45], and the utility of such therapies is restricted as they can only be offered to individuals with the required MHC haplotype. There is also a theoretical risk of mispairing between the endogenous and engineered TCRs, although several strategies have been developed to mitigate this risk [46].

Chimeric antigen receptor (CAR) T cells are single chain receptors with an antibody derived antigen-recognition domain termed a single chain variable fragment (scFv). When antibody variable heavy and variable light domains are arranged in tandem in an scFv they retain their antibody specificity [47], allowing CAR T cells to be generated against a wide range of potential protein, lipid, and carbohydrate antigens in a non-MHC restricted manner. The prototypical CAR contains either one or two costimulatory domains and the CD3ζ activation domain downstream of the scFv, so on antigen engagement through the CAR the normal TCR signalling pathways are induced [3, 48, 49]. This results in cytokine production and the lysis of target cells through perforin/granzyme and Fas pathways [50].

1.1.1. Development of CAR T cells

The advent of chimeric T cell receptors began in 1987, with the development of a receptor construct which comprised the V regions of immunoglobulin light and heavy chains fused to the constant region of the TCR α and β chains [51]. On expression in T cells, the α and β chains dimerised, allowing the adjoining variable regions to assume the form of the antigen binding domain from the original anti-phosphorylcholine antibody. T cells bearing these receptors were able to specifically respond to phosphorylcholine-expressing bacterial strains, evidenced by elevations in intracellular calcium [51].

It was first demonstrated that single chain constructs could be used to activate T cells in 1991 with the development of a chimera incorporating the CD8 ectodomain in tandem with the intracellular domain from CD3ζ [52]. Inclusion of this ITAM-containing activation domain recapitulated the normal T cell signalling events [52], and similar receptor constructs were able to mediate target cell lysis and cytokine expression [53, 54].

The first use of an antibody-derived single chain variable fragment (scFv) as the extracellular domain of a chimeric T cell receptor was described in 1993 by Eshhar et al [55]. In this design, the first of its kind to resemble what is now conventionally

understood as a CAR, antibody-derived variable heavy and variable light domains were arranged in tandem and fused to the intracellular CD3 zeta signalling domain (Figure 1.2). Activation of the receptor by antigen expressing cells or immobilised antigen induced IL-2 production and lysis of target cells in a dose-dependent manner [55].

Whilst this scFv-CD3ζ chimera was to become the basis of the prototypical CAR, such so-called first-generation CARs had significant functional limitations. Their signalling was unable to prime resting T lymphocytes [56], with stimulated first-generation CAR T cells displaying only minimal cytokine production [56, 57], limited proliferation [58], poor cytolytic activity [56] and a susceptibility to anergy and cell death [59].

During a normal immune response, T cells receive both activating and costimulatory signals, whereas cross-linking of first-generation CARs can only mediate the former. Exposure of first-generation CAR T cells to target-expressing cells transduced with CD80/CD86 costimulatory molecules could rescue priming [56, 60], protect from anergy [59, 60], and increase the production of IL-2 [57], IFNγ and TNFα [60], demonstrating the importance of costimulation for a full and sustained T cell response.

Therefore, second-generation CARs were developed, characterised by the addition of costimulatory domains in the cytoplasmic region of the receptor (Figure 1.2). Given its important role in physiological responses, CD28 was the first domain to be included in the receptor construct [59]. This resulted in an increase in target-induced T cell proliferation [58, 59, 61, 62], protection from anergy [59] and increased levels of Bcl-2 [58]. Such receptors were able to mediate increased production of IL-2 [59, 62], TNFα and IFNγ [58], activation of phosphoinositide 3-kinase (PI3K) [58], and modest increases in target cell-lysis [58]. Correspondingly, the use of second-generation CAR T cells in *in vivo* tumour models was able to inhibit tumour growth [62, 63]. Importantly, these effects appear only to be mediated when the CD28 costimulatory domain is located 5’ of the CD3ζ domain [59]. Various other costimulatory regions have been incorporated instead of CD28, most notably 4-1BB (CD137).

The hypothesis that different costimulatory domains may have additive effects on CAR T cell survival and effector functions led to the development of third-generation CAR T cells which have 2 costimulatory domains followed by a C-terminal CD3ζ region (Figure

1.2) [64]. The prototypical third-generation CAR combines CD28 and 4-1BB signalling domains, can increase expression of anti-apoptotic markers, and can significantly improve *in vivo* engraftment, persistence, and tumour control [62]. Several third generation CAR T cells have been tested clinically with some success [65–67], although whether they perform better than their second-generation counterparts is currently unclear due to a lack of head-to-head comparisons.

In physiological conditions, T cells receive cytokine signals alongside TCR engagement and costimulation. As CARs only include costimulatory and CD3ζ domains, their signalling does not fully replicate this. Furthermore, CAR T cells are required to function in an immunosuppressive tumour microenvironment with low levels of cytokines required for T cell survival and activity [68]. Fourth-generation CAR constructs, also termed 'TRUCKs' ('T cells redirected for universal cell killing') circumvent this through the constitutive or inducible expression of cytokines and chemokines, including IL-7 [69–72], IL-15 [73], IL-12 [74–76], IL-18 [77], CCL21 [71] and CCL19 [69, 70, 72], and have been shown to mediate promising responses in pre-clinical studies. Meanwhile, fifth generation CAR T cells incorporate elements of cytokine receptor signalling domains into the CAR itself, triggering the respective signalling pathways on CAR engagement and leading to augmented *in vivo* tumour control [78]. To date, few fourth and fifth generation CAR T cells have been tested clinically, but several trials are underway in this area [79].

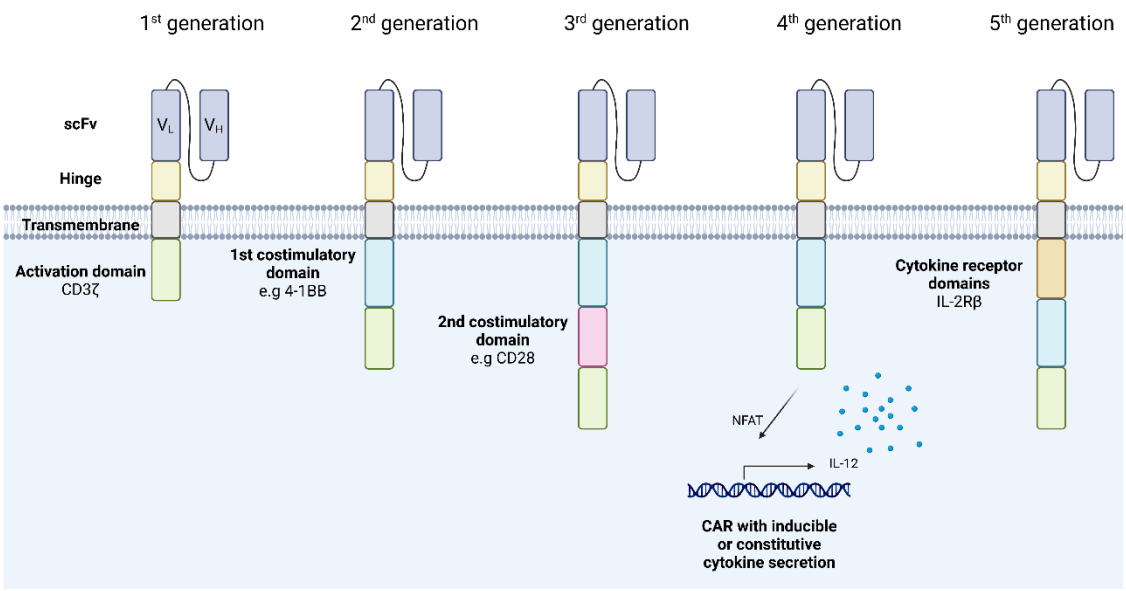

Figure 1.2 Generations of chimeric antigen receptors.
First-generation CAR constructs comprised an antibody derived scFv with/without a hinge domain, coupled to the CD3ζ intracellular domain via a transmembrane region. Second- and third-generation constructs incorporated additional costimulatory domains, typically derived from 4-1BB and CD28. 4th generation CARs, also termed T cells redirected for universal cell killing, are further engineered with genes to drive constitutive or inducible cytokine production, whilst 5th generation CARs incorporate cytokine receptor signalling domains into the CAR intracellular domain. scFv, single chain variable fragment; V_L, variable light domain; V_H, variable heavy domain; IL-12, interleukin 12; NFAT, nuclear factor of activated T cells.
Figure created with Biorender.com.

1.1.2. CAR T cell design considerations

The extent of CAR T cell activity against a given target depends on several factors: the design of the CAR construct, the starting material for CAR generation, and the generation and expansion protocol. CAR intrinsic factors include the choice of scFv, the presence and design of a hinge domain and the number and type of costimulatory domains.

1.1.2.1. Antigen targeting domain

As described above, the prototypical antigen binding domain comprises an antibody-derived scFv. By incorporating scFv domains with different affinities for the target, it is possible to modulate the antigen density required for T cell activation [80]. Whilst high affinity scFv domains confer on T cells the ability to respond to tumours with low

antigen expression, lower affinity scFvs may be more appropriate where there are concerns about on-target/off tumour toxicities due to low level antigen expression on normal tissues.

Work by Long et al [81] demonstrated that the framework regions of the variable heavy and variable light domains in a range of scFvs triggered antigen independent CAR clustering. This led to tonic signalling, with phosphorylation of the CAR-CD3ζ domain in the absence of target. Such cells showed increased expression of exhaustion markers, poor effector functions, and limited persistence *in vivo*. This was not observed for identical CAR T cells with the FMC63 anti-CD19 scFv, suggesting that the clinical success of anti-CD19 CAR T cells may be in part due to unique properties of the scFv. Notably, the 3 main CAR T cell therapies recommended by the National Institute for Health and Care Excellence (NICE) all utilise FMC63 (Axicabtagene ciloleucel, tisagenlecleucel and brexucabtagene autoleucel).

Consideration must also be given to the immunogenicity of any given scFv. Many scFvs are of mouse origin and are therefore targets of human anti-mouse antibodies (HAMA), which have the potential to abrogate T cell activity by impairing scFv binding or causing T cell apoptosis [82]. Pre-existing anti-CAR antibodies against the mouse FMC63 scFv have been reported in several trials, but do not appear to be correlated with clinical outcomes [82]. However, in trials of CAR T cells directed against the folate receptor (FR) and carbonic anhydrase IX (CAIX) poor CAR T cell persistence and functionality was partly attributed to an anti-CAR humoral response [83, 84]. In addition, one patient treated with a mesothelin specific CAR rapidly developed severe anaphylaxis following infusion [85]. Anti-CAR cellular immune responses have also been documented and are associated with poor persistence and treatment failure [82, 84, 86, 87], but may be prevented to some extent by preconditioning chemotherapy [87, 88].

Work is ongoing to develop CARs using human or humanised scFvs which are predicted to be less immunogenic [89, 90]. However, but the risk is not entirely resolved: the junctions created by the tandem arrangement of variable heavy and light domains would not normally be encountered by the immune system, and the gene

recombination and somatic hypermutation required to produce antibodies may also give rise to non-self-antigens [82].

Attention must also be paid to the flexible linker between the variable domains, which generally consists of a repeated glycine-serine motif. Singh et al [91] demonstrated that the length of the linker has a significant impact on CAR functioning. Specifically, shortening the linker length of a CD22 specific CAR from 20 to 5 amino acids led to clustering at the cell surface, which was associated with stronger signalling following antigenic stimulation. Such cells displayed improved effector functions *in vitro* and mediated stronger anti-tumour responses in mouse models. This correlated with known clinical experience, where the complete response rate was elevated in trials using the 5-amino acid linker containing CAR [92, 93] versus patients treated with CARs utilising the longer linker [91].

Bispecific or tandem CARs contain 2 linked scFv domains so can bind to two separate antigens through the same receptor [94–97]. This aims to prevent the outgrowth of antigen negative tumour cells which is a common mechanism of acquired resistance to anti-CD19 CAR T cells [98] but could increase the potential impact of the scFv on CAR functionality.

1.1.2.2. Hinge and transmembrane domain

The ability of the CAR to contact its cognate epitope has been shown to be affected by both the hinge/spacer region between the scFv and transmembrane domain and the proximity of the epitope to the target cell membrane [99]. Various hinge regions have been used, including CD8 [60–63], CD29 [60] and the CH2-CH3 region of IgG1 [58, 64]. The inclusion of a spacer region improves cell lysis and cytokine production by CAR T cells targeted against epitopes close to the target cell membrane [99, 100] or those requiring greater receptor flexibility [101], whilst it can impair the activity of CAR T cells against membrane-distal epitopes [99]. Thus, whilst a spacer region may be necessary to facilitate contact between the scFv and certain epitopes, their use is not a universal requirement.

The use of IgG derived spacer regions may also result in off-target effects due to interactions with host Fc receptors (FcR). Interactions between FcRs and the IgG1 CH2-CH3 CAR spacer domain leads to reciprocal activation of innate immune cells and CAR T cells. This resulted in the production of pro-inflammatory cytokines from activated monocytes and NK cells, which are themselves simultaneously targeted by cytolytic CAR T cells [102]. *In vivo*, such CAR T cells are sequestered in the lungs and take longer to distribute throughout the body due to interactions with lung resident, FcR-expressing innate immune cells [103, 104]. Mutating the residues in the CH2-CH3 domain responsible for this interaction can rescue CAR T cell trafficking [104, 105].

Numerous transmembrane domains have also been utilised, including CD8 [60], CD28 [63, 64], DAP10 [62], 4-1BB [62], CD29 [60], OX40 and CD3ζ [64]. Of the 3 anti-CD19 CAR T cells in clinical use, Axicabtagene ciloleucel and brexucabtagene autoleucel utilise hinge and transmembrane domains derived from CD28, whilst the corresponding domains in tisagenlecleucel are taken from CD8α. It has been reported that inclusion of the CD28 transmembrane region instead of CD8α leads to more efficient recruitment of ZAP70 and greater phosphorylation of CAR-CD3ζ on antigen encounter, leading to augmented anti-tumour responses in *in vitro* and *in vivo* assays [106]. However, the increased sensitivity might also confer an increased tendency to undergo activation induced cell death (AICD), with increased expression of exhaustion markers such as PD-1 and LAG3 [107]. Some reports also suggest that CAR expression and stability is increased by the CD28 transmembrane domain compared to alternative domains (30).

1.1.2.3. Costimulatory domain

All CARs which have been approved by NICE and the FDA have to date included either CD28 or 4-1BB costimulatory domains. Recent work has highlighted the differential effects of such domains, allowing a more rational approach to CAR design [108].

CD28, which is expressed constitutively by naïve and activated T cells, becomes cross-linked on binding to B7-family ligands on activated antigen presenting cells (APCs). This

results in the phosphorylation of certain residues in the CD28 cytoplasmic tail by the Src kinases Lck and Fyn, creating binding sites for Src-homology-2 (SH2) and -3 (SH3) domain-containing proteins [109]. This colocalises important signal transduction proteins such as Lck, Grb2 and PI3K, amplifying TCR signalling and ultimately increasing the activity of important transcription factors including NF-κB, NFAT and AP-1 [108, 110].

By contrast, 4-1BB is a member of the tumour necrosis factor receptor (TNFR) superfamily which is upregulated following T cell stimulation [111]. On binding to its APC-expressed ligand (4-1BBL), a signalling cascade is initiated following the association of TNFR-associated factors (TRAFs) to its intracellular tail. The resulting ubiquitination of TRAF proteins creates binding sites for other signalling complexes to form, which predominantly serves to promote NF-κB signalling and improve T cell survival through expression of anti-apoptotic proteins [108, 111].

It has been reported that stimulation of CD28-containing CAR T cells activates the endogenous 4-1BB signalling pathway, whilst phosphorylation of endogenous CD28 is detected following stimulation through 4-1BB CAR constructs, suggesting that these common pathways are activated irrespective of the CAR design [112]. Studies have also demonstrated that rapid calcium influx and phosphorylation of the CAR-CD3ζ ITAMs occurs on antigen stimulation, independent of the costimulatory domain [106, 112, 113]. However, the inclusion of CD28 appears to increase the magnitude of this effect, with more intense phosphorylation of CAR-CD3ζ, ZAP70 and LAT [106, 112–114].

The increased signalling activity of CD28-containing CAR constructs reportedly correlates with augmented *in vitro* functionality, including increased cytokine production [112, 113, 115, 116], proliferation [112] and target cell lysis [115]. *In vivo*, this reduces the antigen density requirements for CAR activity, allowing them to control tumours expressing lower levels of the target antigen [80, 106].

However, research in this field in ongoing, with several groups reporting contradictory findings in which 4-1BB containing constructs achieved optimal cytokine production and target cell lysis [81], even in response to repeated antigenic stimulation [117]. In

addition, *in vivo* the inclusion of a 4-1BB domain has been linked to augmented CAR T cell expansion [114] and persistence [81, 118], with greater generation of memory cells [80, 119], and improved tumour control [81, 112]. By contrast CD28-CAR T cells reportedly acquire an exhausted phenotype *in vivo*, ultimately predisposing mice to relapse [112, 117].

CD28-containing CARs are reportedly more prone to tonic signalling in the absence of antigen, leading to increased detection of apoptosis markers, inhibitory receptors and transcription factors associated with exhaustion [81, 113]. In accordance with this, Salter et al confirmed the basal phosphorylation of ZAP70 and CAR-CD3ζ in CD28-CAR constructs using liquid chromatography mass spectrometry and suggested that this was linked to increased association of Lck with such constructs [112, 113]. By contrast, 4-1BB-CARs associate with the protein THEMIS, which in turn binds to the phosphatase SHP-1, localising it to the CAR intracellular domain. SHP-1 antagonises the activity of Lck, which may account for the reduced tonic signalling observed with 4-1BB-containing CARs [113].

The differences between 4-1BB and CD28-CARs extend further than just their propensity for tonic signalling. 4-1BB containing CAR T cells consistently show enrichment of genes involved in memory [81, 115, 120], in addition to those involved in Th1 polarisation [120], NF-κB signalling [115, 120] and the hypoxia response [81]. By contrast, CD28-CARs are enriched for Th2 polarising genes [120], with higher expression of exhaustion markers [81, 115] and inhibitory receptors [81], a phenotype which has been associated with poor treatment responses in clinical trials [121, 122]. 4-1BB-CAR T cells are enriched for genes involved in fatty acid oxidation [119, 120], and have corresponding increases in basal oxygen consumption, fatty acid uptake and mitochondrial mass [119]. This preferential use of fatty acid oxidation is redolent of memory cells, and contrasts with the metabolic switch to glycolysis observed in CD28-CAR T cells [119].

Whilst a lack of direct head-to-head comparisons is lacking, clinical evidence suggests that 4-1BB costimulation may be preferential. Anti-CD19 CAR T cells with 4-1BB domains persisted for significantly longer and maintained B cell aplasia for a greater duration compared to patients receiving with CD28-costimulated CAR T cells [123–

126]. Meta-analyses of CAR T cells in the treatment of B-cell acute lymphoblastic leukaemia (B-ALL) and gastrointestinal cancers have also suggested that better treatment outcomes correlate with 4-1BB costimulation [127, 128]. However, differences in trial protocols, CAR construct design and T cell generation confound these direct comparisons and further research is needed.

1.1.2.4. CD3ζ activation domain

The inclusion of the intracellular, ITAM containing CD3ζ domain is a constant factor for nearly all published CARs, regardless of generation. However, research on this domain is contradictory. In one study, the inclusion of an additional CD3ζ domain conferred upon second generation CAR T cells the ability to kill target cells at low antigen densities. Conversely, reducing the number of ITAMs reduced CAR activity *in vivo* [106]. Optimal activity has been shown to depend upon the ability of the CAR to both homodimerise and to interact with other endogenous CD3 subunits, increasing the number of available ITAMS for downstream signalling [129].

However, Feucht et al [130] demonstrated that inactivating point mutations in the second and third CD3ζ ITAMs of a CD19.28ζ CAR improved *in vivo* tumour control and CAR T cell persistence. Such cells displayed reduced expression of exhaustion markers and were enriched for genes involved in memory responses. It is possible therefore that the optimal CD3ζ domain depends on the antigen density on the tumour cells and the other CAR design elements such as the transmembrane and costimulatory domain used.

Furthermore, inclusion of the CD3ε intracellular domain into the CAR design has been reported to augment CAR T cell activity *in vitro* and *in vivo* [131, 132]. The p85 subunit of PI3K is known to bind to CD3ε, localising it to the membrane and leading to increased downstream AKT activity [131]. Additionally, CD3ε recruits Csk, a kinase which phosphorylates CAR-associated Lck at Y505, inhibiting its activity and preventing tonic CAR-CD3ζ phosphorylation. This in turn appears to have a protective effect against exhaustion [131, 132].

1.1.2.5. Method of engineering

Similarly, there is significant variation in the literature in terms of the strategy used to engineer T cells to express the CAR. Viral systems are by far the most widely used, and can be sub-categorised according to their use of γ-retroviral or lentiviral vectors. For efficient γ-retroviral transduction, cells must be actively dividing, which is generally achieved through culture with IL-2 and anti-CD3 and -CD28 antibodies [133]. This is known to drive T cells down a route of terminal differentiation, which may impede their ability to proliferate and persist *in vivo*. Lentiviral based protocols have been favoured by some groups as these theoretically allow the transduction of non-dividing cells. Circosta et al demonstrated that unstimulated, lentivirally transduced T cells maintained a naïve phenotype, and correspondingly displayed superior expansion on antigen exposure when compared to CD3 pre-stimulated cells [134]. However, it has subsequently been demonstrated that the low-density lipoprotein (LDL) entry receptor for vesicular stomatitis virus glycoprotein (VSVG) pseudotyped virus is only expressed at appreciable levels on T lymphocytes following stimulation, and therefore lentiviral protocols typically require an activation step for optimal transduction [135].

Viral-based systems are limited in the size of the genetic payload they can deliver and are therefore potentially unsuitable for more complicated CAR cassettes [136]. There are also safety considerations relevant to the use of viral vectors, in particular the risks of replication competent virus and insertional mutagenesis. The integration of transgenes into the genome by viral vectors risks driving dysregulated expression of oncogenes and tumour suppressor genes. This was first reported in a trial of patients receiving gene therapy to treat X-linked severe combined immunodeficiency (SCID-X1) [137, 138], but to date no cases of therapy-linked leukemogenesis have been reported in the context of CAR T cell trials. The risk is generally considered to be higher with γ-retroviruses due to their propensity to integrate at regions involved in gene regulation [139–141], although clonal expansion linked to transgene insertion has also been observed with a lentiviral vector [142].

Current retroviral and lentiviral systems typically split the various viral genes between separate plasmids, requiring multiple recombination events to occur simultaneously

for replication competent virus to be produced [143]. Screening by several groups has found no evidence of replication competent virus in clinical CAR T cell products suggesting that the risk of occurrence is relatively low, however the requirement for extensive biosafety testing adds to the high cost of these therapies [144–147].

Other engineering systems harness transposase enzymes which catalyse the insertion of mobile genetic elements, known as transposons, into the genome [148]. The transgene of interest and the transposase enzyme can be introduced into T cells by electroporation, streamlining the manufacturing process, reducing production costs, and simplifying the biosafety testing requirements [149]. The utility of non-viral piggyBAC and Sleeping Beauty transposon systems has been demonstrated in the field of CAR T cell research [150–154], and is becoming more frequently used in clinical trials [154–156].

Transposon-based systems still pose a theoretical risk of insertional mutagenesis as they integrate into the genome, so the electroporation of non-integrating plasmids and mRNA may have safety benefits. Although efficient gene transfer can be achieved with this method, transgene expression is only transient [157–159]. Whilst this theoretically limits the duration of any toxicities, it is at the expense of the formation of a long-lasting memory response and may necessitate multiple CAR T cell infusions per patient. Non-integrating lentiviral vectors can also achieve short term gene expression, which can be extended by tethering the transgene-encoding episomes to the host chromosomes via scaffold/matrix attachment region (S/MAR) elements [160]. Lastly, the use of CRISPR-Cas9 or TALEN technology is gaining popularity as a means of targeting transgene insertion to defined loci, reducing the risk of insertional mutagenesis [161–163].

In vitro and *in vivo* efficacy of CAR T cells is not just determined by the receptor design but is also affected by the T cell population used. In a physiological immune response, activated naïve T cells proliferate, giving rise to progressively differentiated cell subsets: central memory T cells (T_{CM}), effector memory T cells (T_{EM}) and effector T cells (T_{EFF}) [164].

Clinical trials of TILs in metastatic melanoma have demonstrated a correlation between an extended telomere length in the infused cells and improved treatment responses [165, 166]. Differentiation from $T_N > T_{CM} > T_{EM} > T_{EFF}$ is associated with a progressive shortening of telomeres [164], potentially favouring the use of T_N and T_{CM} cells for adoptive cell therapies. Transgenic TCR engineered T cells derived from T_N and T_{CM} cells were significantly better at mediating anti-tumour responses in mice when compared to T_{EM} [167, 168], supporting this hypothesis.

The use of EBV-specific T cells may also improve responses by increasing CAR T cell persistence *in vivo*, via endogenous TCR stimulation and signalling. Whilst this is only feasible in previously infected individuals, it has been shown to increase CAR T cell persistence in clinical trials in the context of neuroblastoma [169].

The subtype of T cell used is likely therefore to have an impact on the clinical effectiveness of CAR T cells. However, currently a direct comparison between T cell subtypes in this context is lacking, with most clinical trials to date simply using peripheral blood T cells expanded *in vitro* to achieve sufficient cell numbers for infusion. Despite the lack of consensus on the optimal CAR design and T cell subtype, clinical trials in certain malignancies have had significant success.

1.1.3. CAR T cells in the clinic

1.1.3.1. CAR T cell clinical trials

The first reported use of CAR T cells in the clinic was in 2006, with the use of a first-generation anti-folate receptor (FR) CAR to treat ovarian cancer [170]. These T cells were unable to mediate any anti-cancer effects, and similarly disappointing results were obtained in other early clinical trials of first-generation CAR T cells in the context of solid tumours [169, 171, 172]. Promising results with CAR T cells were first achieved in a phase 1 clinical trial of second generation, anti-CD19 CAR T cells in 3 patients with chronic lymphocytic leukaemia (CLL) [173]. Infused cells proliferated and mediated complete responses in 2 out of 3 patients, which have been subsequently maintained

for 10 years [174]. More robust evidence of CAR T cell efficacy in this context was provided in 2014 by Maude et al [175]. Of 30 patients with relapsed/refractory leukaemia/lymphoma treated with CD19-CARs, 27 had achieved complete responses by one-month post-treatment, and 19 patients had sustained remissions at the end of follow up.

Numerous other studies followed, firmly establishing this as an active area of research: a recent review identified 878 ongoing clinical trials of CAR T cells worldwide [79]. The majority of CAR constructs which have been tested in the clinic are second generation CARs [79, 128], with a relatively even balance between those using 4-1BB or CD28 costimulatory domains [79, 128, 176]. Third and fourth generation CAR constructs have also been used but are yet to demonstrate significantly superior activity in this context [128].

Many of the trials conducted to date have been of CD19-specific second-generation CAR T cells and focused on the treatment of B cell malignancies, including acute and chronic leukaemia, Non-Hodgkin's lymphoma and follicular lymphoma [176–178]. CAR T cells have proved to be a promising treatment strategy for such conditions, with meta-analyses estimating the complete response rate in haematological malignancies to be between 54.4 % [178] and 60.0 % [176]. Treating B-cell acute lymphoblastic leukaemia (B-ALL) patients who achieve remission with anti-CD19 therapy with a subsequent allogenic haematopoietic stem cell transplant may further consolidate responses, increasing leukaemia free survival [179]. CAR T cells might also be leveraged in T cell haematological malignancies: recently a paediatric patient with T-cell acute lymphoblastic leukaemia (T-ALL) achieved remission after treatment with anti-CD7 CAR T cells which had been further engineered to inhibit expression of CD7, the TCR, and CD52 [180].

Based on these encouraging results in B cell leukaemia and lymphoma, tisagenlecleucel (Kymriah, Novartis) was licensed in United States in August 2017 for the treatment of acute lymphoblastic leukaemia in paediatric patients [181], with NICE approval following in November 2018 [182]. A similar second-generation CAR, axicabtagene ciloleucel (Yescata, Kite Pharmaceuticals), also received FDA approval in 2017 [183]. Subsequently, a further 4 CAR products have been approved: brexucabtagene

autoleucel [184] , Kite Pharmaceuticals; lisocabtagene maraleucel [185] and idecabtagene vicleucel [186], Bristol Myers Squibb; and ciltacabtagene autoleucel [187], Janssen. These CARs are all second-generation CARs, with 4-1BB or CD28 costimulatory domains, and use retroviral or lentiviral transduction systems. Except for idecabtagene vicleucel and ciltacabtagene autoleucel, which target B cell maturation antigen in multiple myeloma, the above CAR constructs all use the same FMC63 scFv to target CD19.

CAR T cells have also been trialled for solid tumours, including cancers of the nervous, hepatobiliary, and gastrointestinal systems, as well as melanoma, sarcoma, and breast, prostate and non-small cell lung cancer [177, 188]. CARs in such trials were directed against a multitude of targets, including GD-2, carcinoembryonic antigen (CEA), epidermal growth factor receptor (EGFR), HER2, prostate specific membrane antigen (PSMA), claudins 6 and 18.2, and tumour associated glycoprotein-72 (TAG72) [176, 177].

Historically, the clinical success of CAR T cells has been predominantly limited to the treatment of blood cancers. Complete response rates in solid tumours are estimated to be between 2.3 % [188] and 11.0 % [176], and such patients are approximately 4 to 8 times less likely than those with haematological malignancies to achieve an objective response to treatment [128, 176, 188]. The potential reasons for the poor efficacy of CAR T cells in solid tumours are numerous, with the difficulty in identifying appropriate antigens and the need for T cells to traffic to the tumour site and survive in the immunosuppressive tumour microenvironment likely having a significant impact [189].

Despite this, some encouraging albeit rare complete responses have been reported, including 3 patients with neuroblastoma treated with an anti-GD2 first generation CAR [190, 191], and one patient with rhabdomyosarcoma bone metastases treated with a second generation anti-HER2 CAR [192].

Several promising CAR T cell products are in development for the treatment of gastrointestinal cancers. Proteins such as claudin 18.2 (CLDN18.2) and guanylyl cyclase C (GUCY2C) are widely expressed in the normal gastrointestinal mucosa, however their sequestration at the apical and lateral surfaces of the epithelium means that they are

not easily accessible to circulating T cells [193]. Their expression is maintained during malignant progression, where the loss of normal tissue architecture leads to antigen exposure and therefore facilitates potential targeting by CAR T cells [194, 195].

CLDN18.2 is a transmembrane protein expressed selectively in the gastric mucosa, where it contributes to tight junction formation [193]. Following promising *in vivo* mouse data which demonstrated that second-generation CLDN18.2-specific CAR T cells could effectively target tumours in the absence of gastric toxicity, CARsgen's CT041 CAR entered clinical trials in 2019. The largest study to report to date was an investigator-initiated study (NCT03874897) including 37 patients with advanced digestive system cancers who received preconditioning chemotherapy followed by CT041 infusion [196]. The overall response rate was 48.6%, with 83.3% of lesions showing evidence of measurable regression following treatment. Although CRS and toxicities relating to the preconditioning chemotherapy regimen were common, the therapy had an acceptable safety profile with no dose-limiting toxicities. These results are broadly comparable with encouraging initial reports from ongoing studies of CT041 in patients with gastric cancer or pancreatic adenocarcinoma (NCT04404595) [197], or gastric and gastroesophageal junction adenocarcinoma (NCT04581473) [198].

GUCY2C is a transmembrane receptor expressed on the apical surface of intestinal epithelia. Proof of principle for GUCY2C-targeting CARs was demonstrated by Magee et al [199], who developed a second generation, mouse GUCY2C-specific CAR construct. Immunocompetent mice injected intravenously with GUCY2C-expressing CT26 cells were subsequently treated with non-myeloablative radiotherapy and syngeneic CAR T cells. GUCY2C-CAR T cell treatment significantly improved survival and reduced the number of lung metastases compared to recipients of control T cells, in the absence of any histopathological evidence of autoimmunity. Later work validated a similar human-GUCY2C-specific CAR construct, confirming its anti-tumour efficacy in a syngeneic immunocompetent mouse model of metastatic colon carcinoma [200]. A phase I clinical trial of GUCY2C CAR T cells for patients with advanced gastrointestinal neoplasms sponsored by Innovative Cellular Therapeutics is currently recruiting (NCT04652219). Pfizer is also targeting GUCY2C with its bispecific reagent PF-07062119, a diabody which binds to both CD3ε and GUCY2C to indirectly drive T cell

infiltration into the tumour. Based on encouraging efficacy data from syngeneic immunocompetent mouse models and toxicology studies in cynomolgus monkeys which demonstrated a manageable safety profile [195, 201], PF-07062119 has entered clinical trials.

Another member of the claudin family, claudin 6 (CLDN6), has also received attention as a CAR T cell target. CLDN6 is like CLDN18.2 in that it is a membrane protein involved in the tight junction, however it in differs in that it is a oncofoetal antigen with limited reported expression in healthy adult tissues. It is upregulated in various malignancies including male and female reproductive tract cancers, lung cancer and gastric cancer [202]. BioNTech have developed a 4-1BB-costimulated anti-CLDN6 CAR with a corresponding antigen-encoding RNA vaccine (termed CARVac), designed to promote in vivo CAR T cell expansion by driving CLDN6 expression by antigen presenting cells in the spleen and lymph nodes [202]. Promising results from *in vivo* mouse models led to the initiation of a phase I trial (NCT04503278) in 2020. Initial reports on the first 22 patients receiving CLDN6 CAR T cells (with or without CARVac) described a manageable safety profile with a 33% overall response rate [203].

Solid tumours clearly pose more of a challenge for CAR T cell therapeutics, which has typically meant that clinical success has been limited to the context of haematological malignancies. However, the identification of promising targets such as CLDN18.2 and CLDN6, alongside the development of novel engineering strategies, may represent a step towards effective CAR T cell therapies for patients with solid tumours, who represent the bulk of new cancer cases [147].

1.1.3.2. Clinical Manufacturing of CAR T cell products

Given their personalised nature and the requirements for GMP-compliance, manufacturing CAR T cell products for clinical applications is expensive. Typically, clinical trials harvest autologous PBMCs via leukapheresis using specialised equipment [204]. T cells may then be isolated with immunomagnetic beads, followed by activation with anti-CD3 antibody, either in its soluble form or presented on immunomagnetic beads or nanobeads. In most clinical trials, the CAR transgene is introduced by

lentiviral or retroviral transduction: whilst lentivirus is more frequently used in clinical trials reported to date [176, 178, 188], the lack of stable packaging lines does introduce potential lot-to-lot variability [204]. Gene transfer by mRNA electroporation [205] or transposon/transposase systems [149–151, 206] has also been reported but is yet to be fully adopted. CAR-T cells then undergo a period of expansion until the required numbers are generated, before being cryopreserved until treatment initiation [204]. To standardise the process and meet stringent GMP sterility requirements, several commercial devices have been developed such as the CliniMACS Prodigy, WAVE Bioreactor or G-Rex Platform, which are either fully- or semi-automated closed systems [204].

The turnaround time for CAR T cell therapeutics for clinical use is typically less than 20 days from the point of apheresis to infusion, according to a 2018 analysis by Vormittag et al [207]. Shortening production time benefits patients, who typically have advanced disease and risk rapid progression. Moreover, it was demonstrated by Ghassemi et al that CD19-specific CAR T cells progressively differentiate during the ex vivo culture period [208]. Various studies in adoptive cell therapy have suggested that optimal responses are mediated by less differentiated cells, including those in naïve and central memory subsets [167, 168]. As expected, Ghassemi et al observed CAR T cells engrafted 3 or 5 days after culture initiation showed improved tumour control and stronger expansion and persistence in *in vivo* xenograft models compared to cells harvested after the standard 9-day culture period. Subsequent work by the group demonstrated that it is possible to further reduce this culture period down to just 24 hours whilst retaining strong anti-leukaemic activity and persistence *in vivo* [209].

Pre-infusion lymphodepleting chemotherapy, which typically consists of cyclophosphamide (Cy) and fludarabine (Flu), has been demonstrated to improve clinical responses [178]. These regimens are incorporated into most trials for haematological malignancies [178], but are only used in around half of trials for solid tumours [188]. Combination treatment with Cy/Flu increases the persistence and expansion of adoptively transferred cells [88, 210], which has been attributed to the increased availability of IL-15 and IL-7 following the depletion of endogenous NK, B and T cells [88, 211, 212]. Lymphodepletion may also increase the activity of host dendritic

cells, enhancing their uptake and display of antigens and production of IL-12 [213, 214].

At the point of infusion, cryopreserved CAR T cell products are thawed and administered to patients intravenously. Reported target doses vary considerably between trials, but patients treated with the 6 FDA-approved CAR T cells receive between 0.5 and 5 x 10^6 cells/kg body weight [181, 183–187]. A meta-analysis of published trials for all cancers found that total doses <10^8 were associated with improved overall response rates [176], suggesting that quality rather than absolute quantity of cells is important.

1.1.3.3. Safety concerns

Whilst an effective therapy in B cell malignancies, the use of CAR T cells is associated with several significant risks, including potentially fatal toxicities [125, 210, 215]. One of the most common toxicities is cytokine release syndrome (CRS), which is characterised by elevations in IFNγ, IL-6, IL-1 and IL-10 [216–218]. It occurs because of massive cytokine release by both infused T cells and endogenous myeloid cells, following widespread cytotoxic T cell activity [216]. The systemic inflammatory response that is triggered causes varied symptoms, ranging from minor fever to severe hypotension, circulatory shock, and multiple organ failure. CRS is frequently reported in anti-CD19 clinical trials [177], resulting in several fatalities [125, 210]. The condition can be managed clinically using supportive measures, the IL-6R blocking antibody tocilizumab, and corticosteroids [219].

Associated adverse events include immune effector cell-associated neurotoxicity syndrome (ICANS; also known as CAR related encephalopathy syndrome (CRES)) and tumour lysis syndrome [218, 220]. ICANS is characterised by neurological disturbances following CAR T cell infusion, and it is thought to be linked to CRS-induced disruption of the blood brain barrier [216]. It is frequently reported [126, 177, 220–222], and can be fatal [210, 215]. Treatment in severe cases often consists of corticosteroids [223]. By contrast, tumour lysis syndrome occurs due to the release of substances from large

numbers of lysed tumour cells, causing electrolyte disturbances with similar symptoms to CRS [216].

As their aetiology is linked to CAR cell activation and activity, CRS, ICANS and tumour lysis syndrome are rarely reported in clinical trials in solid tumours [178]. However, this does not mean that the use of CAR T cells in such trials can be considered safe. With any CAR T cell design, especially those targeting tumour associated antigens, there is an inherent risk that they will react against the target antigen expressed on healthy tissues, causing on-target/off-tumour toxicities. This was first observed with first-generation CAR T cells against carbonic anhydrase IX (CAIX) [172], which induced liver toxicities in all patients treated due to recognition of the protein on hepatocytes. The severity of such on-target/off-tumour effects largely depends on the cell type recognised. Anti-CD19 CAR T cells can target healthy CD19+ B cells, however the resulting B cell aplasia can be managed with intravenous immunoglobulin infusions [220, 224, 225]. By contrast, the off-tumour recognition of HER2 on the lungs of a patient treated with a high dose of anti-HER2 CAR T cells designed to target her metastatic colon cancer proved fatal [226]. The development of acute respiratory toxicities in a trial of anti-CEACAM5 CAR T cells was also attributed to the potential on-target/off-tumour recognition of CEACAM5 on the lung epithelium [177].

Another potential risk of CAR T cells is the potential for cross-reactivity with other structurally related antigens, leading to off-target effects. Such toxicities have not yet been reported in the context of CAR T cells, which is likely in part due to the adoption of protein microarray technology for extensive cross-reactivity screening [227–230], but they have occurred in trials of TCR-engineered T cells.

2 patients who received autologous T cells bearing an HLA-A*01-restricted, affinity enhanced TCR specific to a peptide in MAGE-A3 (EVDPIGHLY) developed cardiac toxicities several days after T cell infusion [231]. One patient succumbed to a myocardial infarction, whilst the other developed a pericardial effusion which ultimately led to fatal cardiogenic shock. Autopsy findings revealed an inflammatory infiltrate consisting of engineered CD3+ cells in the myocardium. Subsequent analysis demonstrated that this was caused by cross-recognition of a titin-derived peptide in the heart muscle, and highlighted the difficulties in predicting off-target toxicities:

reactivity was only observed against a beating cardiomyocyte culture, but not against broad panel of primary cardiac cells in standard culture conditions [42].

Morgan et al also tested an HLA-A*0201-restricted MAGE-A3 TCR which recognised an alternative peptide (KVAELVHFL) [41]. 4 out of 9 patients treated with autologous T cells bearing this receptor developed neurological disturbances, which proved fatal in 2 cases. Necrosis and a T cell infiltrate were detected in the brain on autopsy. This was initially attributed to the cross-recognition of a MAGE-A12 peptide (KMAELVHFL) expressed at low levels in the brain, although subsequently it has also been suggested that it was instead due to reactivity against the protein EPS8L2 [232]. By contrast, in a later trial by Lu et al [233] 9 patients received autologous T cells bearing an alternative MAGE-A3 TCR which recognised the peptide QHFVQENYLEY, without developing cardiac or neurological toxicities.

Potential safety risks are also posed by the method of gene transfer used in CAR clinical trials. Retroviral and lentiviral based methods are frequently used, but risk the generation of replication competent virus or insertional mutagenesis. The likelihood of replication competent retrovirus/lentivirus production is minimised by segregating *gag, pol* and *env* genes onto different plasmids, thereby requiring multiple recombination events to occur [234, 235]. Self-inactivating lentiviral vectors are characterised by deletion of regions in the 3' UTR, further reducing the risk [236]. Although toxicities driven by replication competent retrovirus were detected in an early study in non-human primates by Donohue et al [237], several subsequent large-scale analyses of transduced cell products from clinical trials have found no evidence of replication competent retrovirus [146, 147] or lentivirus [144, 145], suggesting that the risk is relatively low.

Viral integration into the host genome also risks disrupting normal gene expression, thereby potentially leading to malignant transformation. The potential for insertional mutagenesis was first highlighted in clinical trials in which patients with X-linked severe combined immunodeficiency (SCID-X1) received autologous haematopoietic stem cells retrovirally transduced with the gamma cytokine receptor chain gene [238]. Although effective in correcting the immunodeficiency, several subjects subsequently developed T cell leukaemia caused by the clonal proliferation of transduced cells due to viral

integration events causing dysregulated expression of the *LMO2* proto-oncogene [137, 138].

Given their propensity to integrate at transcription start sites and enhancer regions [139–141, 239], retroviruses may in theory pose an increased risk of gene dysregulation compared to lentiviruses, which favour integration within actively transcribed genes [240]. However, there have been case reports of the clonal expansion of lentivirally transduced CAR T cells [142, 241], including a case in which insertion of the lentiviral vector caused disruption of the *TET2* gene, which combined with an existing mutation in the patient's second *TET2* allele led to T cell proliferation [142].

CAR T cell therapies are therefore not without risk, and these need to be balanced against the potential benefits for individual patients. However, the encouraging responses they have mediated in certain malignancies justify the continued interest in the development of such therapies.

1.1.4. CAR T cells for melanoma

Melanoma is the 5th most common cancer in the UK, accounting for 4 % of total cancer cases in the UK. Age standardised incidence rates are increasing, rising by 30 % in the last decade. 87 % of melanoma cases are attributable to exposure to preventable risk factors [242], the most significant of which is UV exposure, particularly through sunbed use [243, 244]. Common genetic driver mutations result in aberrant activation of the MAPK pathway [245], with mutations in BRAF, NRAS and NIK frequently reported [246–248]. Melanoma progresses through distinct histological phases: benign proliferation of melanocytes, forming a melanocytic nevus; development of a dysplastic nevus, characterised by atypical melanocyte appearance; radial growth phase melanoma, with transformed cells mainly limited to the epidermis; invasion into the dermis, classified as vertical growth phase melanoma; and metastatic melanoma with spread to distal sites [249, 250].

With appropriate diagnosis and treatment, the 5-year survival rate for patients diagnosed with early-stage melanoma approaches 100 %; however only 53 % of patients with stage 4 metastatic disease survive to 1 year post-diagnosis [251, 252]. Various immunotherapies have been used in such patients, including IL-2, interferon, immune checkpoint blockade and tumour infiltrating lymphocytes [253].

Melanoma-targeted CAR T cells against targets such as DNAM-1 [254], gp100/HLA-A2 [255] and HMW-MAA (high molecular weight melanoma associated antigen) [256] have shown promise in the lab. Several clinical trials in this area are currently registered (Table 1); however, they typically recruit patients with a variety of cancers and are mostly yet to report results.

Development of CAR T cells is restricted by a lack of suitable antigens, however one antigen which may hold promise as a potential target for melanoma immunotherapy is CD146, commonly known as melanoma cell adhesion molecule (MCAM).

Table 1: CAR T cell trials for melanoma registered on ClinicalTrials.Gov as of January 2023.

Trial ID	Target	Phase	Conditions	Intervention	Status
NCT02107963	GD2	Phase I	Sarcoma, osteosarcoma, neuroblastoma, melanoma	Cyclophosphamide, GD-2 specific, CD28 and OX40 stimulated autologous 3rd generation CAR T cells.	Completed. No results posted.
NCT03060356	cMET	Phase I	Breast cancer, melanoma	RNA-electroporated cMET-specific, autologous, 4-1BB costimulated CAR T cells.	Terminated (halt in funding)
NCT01218867	VEGFR2	Phase I/II	Metastatic melanoma, renal cancer.	Cyclophosphamide, fludarabine, VEGFR2-specific autologous CD8+ CAR T cells, recombinant IL-2.	Terminated (no objective responses)
NCT04119024	IL-13-Rα2	Phase I	Metastatic melanoma, stage III/IV cutaneous melanoma	Cyclophosphamide, fludarabine, IL-13Rα2-specific autologous, 4-1BB costimulated CAR T cells, recombinant IL-2.	Recruiting
NCT02830724	CD70	Phase I/II	Pancreatic, renal, breast and ovarian cancer, melanoma	Cyclophosphamide, fludarabine, CD70-specific autologous CAR T cells, recombinant IL-2.	Recruiting
NCT03893019	CD20	Phase I	Unresectable metastatic melanoma	CD20-specific, autologous CAR T cells enriched for CD4/8.	Recruiting
NCT04897321	B7-H3	Phase I	Multiple solid tumours with B7-H3 expression	Cyclophosphamide, fludarabine, B7-H3-specific autologous CAR T cells.	Recruiting
NCT03635632	GD2	Phase I	Neuroblastoma, osteosarcoma, Ewing Sarcoma, Rhabdomyosarcoma, uveal melanoma	Autologous CAR T cells co-engineered with a GD-2 specific CAR and a constitutively active IL-7 receptor.	Recruiting
NCT04483778	B7-H3	Phase I	Multiple solid tumours with B7-H3 expression	2nd generation 4-1BB costimulated B7-H3-specific autologous CAR T cells, with/without co-expression of a 2nd generation, 4-1BB costimulated CD19 CAR.	Recruiting
NCT05117138	AMT-253	Phase I/II	Melanoma, non-small cell lung cancer, head and neck squamous cell carcinoma	AMT-253, autologous, CAR T cells.	Not yet recruiting

1.2. Melanoma cell adhesion molecule

Melanoma cell adhesion molecule (MCAM) was first identified in 1987 [257], and has since acquired several names: CD146, MUC18, S-Endo1, A32 antigen and Mel-CAM. It is a single pass transmembrane protein of the Ig superfamily, with a predicted molecular weight of 113kDa [258]. The 646 amino acid protein is encoded by a 14 Kb gene on chromosome 11, q23.3 [259], and is comprised of 16 exons [260]. The full-length mRNA for MCAM is 3.3 kb in length and encodes the open reading frame flanked by a short 5' untranslated region (UTR) and large 3' UTR [260]. 2 different isoforms of MCAM exist (short and long), which are generated by alternative splicing at exon 15; they share the same extracellular and transmembrane domains, but differ in their cytoplasmic domains, which are 21 and 43 amino acids long, respectively [261].

The MCAM ectodomain is characterised by the presence of 5 immunoglobulin domains, which are each approximately 100 bp in length and contain prototypical cysteine residues (Figure 1.3) [262]. Domains 1 and 2 are V class, whilst domains 3 to 5 are C2 class Ig domains [260, 262]. Mature MCAM is highly glycosylated with a preponderance of sialic acids, alongside D-mannose and galactose [263], and 8 putative sites for asparagine-linked glycosylation have been identified [262]. The proteins can exist as monomeric or dimeric forms: dimers are stabilised by a disulphide bond between cysteine residues at positions 452 and 499 within the 5th Ig domain [264].

A 24 amino acid single pass transmembrane region separates the ectodomain from the short intracellular domain [265]. Both short and long MCAM isoforms contain a recognition site for protein kinase C (PKC) and a juxta-membrane KKGK motif, which is reported to interact with several proteins involved in signalling cascades and cytoskeletal arrangement [266–268]. The long form contains a second PKC-binding site, a cAMP dependent protein kinase domain [260] and a dileucine motif thought to play a role in controlling cellular localisation, whilst a PZD-binding domain is only found in the short form [260, 269].

MCAM also exists as a soluble form (sMCAM) which is generated by matrix metalloproteinase (MMP) mediated ectodomain shedding of the membrane anchored

form, from endothelial and cancerous cells (including melanoma) [270–272]. Although detectable in the blood of healthy individuals, sMCAM is elevated in patients with cancer and other in disease states [273–275]. It is biologically active, driving increased tumour growth and metastasis when administered in *in vivo* tumour implantation models [272, 276].

The murine form of MCAM has 75 % amino acid sequence similarity with its human ortholog and retains many of the same features including the 5 Ig domains and 6 of the 8 glycosylation motifs in the ectodomain [277, 278]. The intracellular region contains conserved PKC and casein kinase II domains but lacks the cAMP-dependent protein kinase domain [277]. The zebrafish ortholog of MCAM is significantly different at the amino acid level, with only approximately 30 % sequence similarity to human and mouse forms [279]. The 617 amino acid protein is characterised by a 5 Ig domain extracellular region and short cytoplasmic domain. As in the mouse form, the PKC site in the tail is conserved [279].

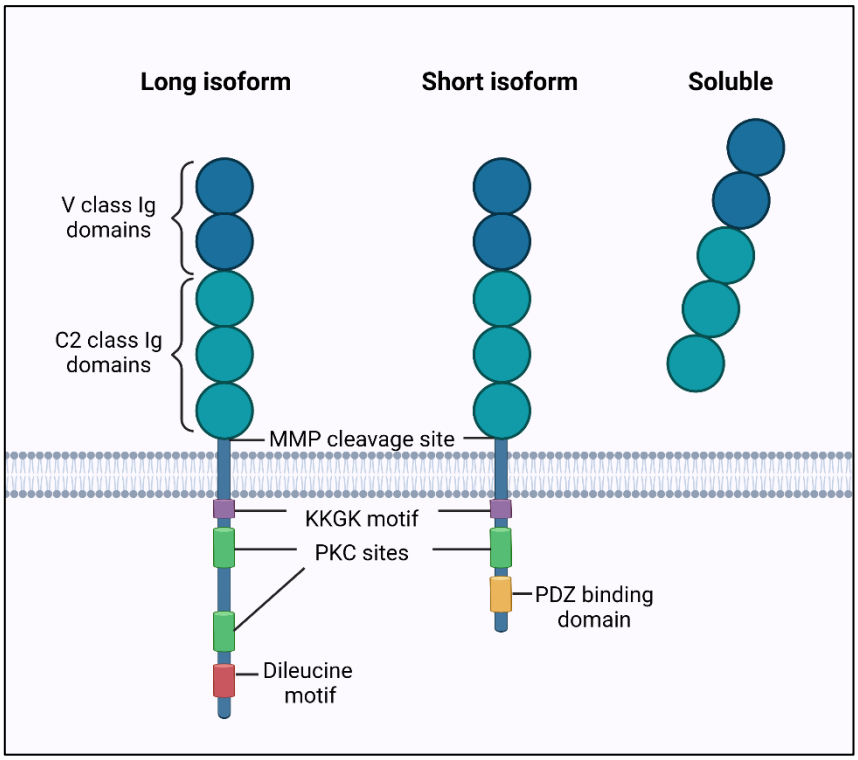

Figure 1.3 Three distinct forms of the MCAM protein.
Membrane bound MCAM exists as two distinct isoforms which share the same ectodomain but differ in their intracellular regions. Soluble MCAM is generated by MMP-mediated ectodomain shedding. Ig, immunoglobulin; MMP, matrix metalloproteinase; PKC, protein kinase C. Figure created using Biorender.com. Adapted from Leroyer et al, 2019 [280].

1.2.1. Regulation of expression

Numerous factors involved in the regulation of MCAM expression have been identified, suggesting that a complex interplay between inducing and suppressive factors ultimately determines its levels.

Regulation of MCAM-expression on melanocytes and melanoma cells was first attributed to cell-cell contact inhibition with keratinocytes [281]. Direct coculture with keratinocytes reduced the expression of MCAM on such cells, however advanced primary and metastatic melanoma cells were resistant to keratinocyte-mediated MCAM downregulation *in vitro*, suggesting that other mechanisms come into play which may allow this keratinocyte-mediated suppression to be bypassed [281].

Analysis of the MCAM promoter has identified several factors which may control its expression: aberrant promoter methylation has been implicated in MCAM

overexpression [282, 283], whilst binding sites have been identified for several transcription factors with known oncogenic activity. 2 motifs have been identified for cAMP response element binding protein (CREB) [284], a transcription factor which is upregulated in numerous cancers and is reported to promote tumour growth and metastasis [285]. Mutation of the CREB sites in the MCAM promoter can reduce expression by 70 % [284]. CREB induces target gene expression in response to various stimuli, including intracellular cAMP increases [286]; increasing intracellular cAMP levels in MCAM expressing cells by treating cells with an activator of adenylyl cyclase, a stable cAMP analogue or an inhibitor of cAMP breakdown upregulated MCAM mRNA and cell surface protein levels [287].

SP1 is a proto-oncogene which has been implicated in tumorigenesis and supports the proliferation and metastasis of cancer cells [288]. Mutation of the SP1 recognition motif significantly reduces MCAM promoter activity [284]. Similarly, SOX18, a transcription factor elevated in gastric cancer, has been shown to drive MCAM expression; expression of both markers is a negative prognostic factor in patients [289].

Contrastingly, deletion of the AP2 motif increased MCAM expression by up to 5-fold in melanoma cell lines [284]. The presence of AP2 bound to the MCAM promoter differentiates MCAM negative from positive cells, and its forced overexpression in $MCAM^{high}$ cells can significantly suppress expression [290]. AP2 has tumour suppressor activity in a number of tumours including melanoma [291, 292], an effect thought to be mediated in part by its direct interaction with p53 to increase the transcription of p53-regulated genes [293]. The transcription factor ZBTB7A [294], and the micro-RNA, miR329 [295] also inhibit MCAM expression. Loss of ZBTB7A frequently occurs in progressive melanoma, is associated with poor survival, and correlates with MCAM overexpression in clinical samples [294]. miR329 is a microRNA which is a post-transcriptional repressor of several genes, and acts as a tumour suppressor. Its overexpression can significantly reduce MCAM levels, alongside genes including VEGF and MMP9 [295].

Clearly therefore, the pathways controlling MCAM transcription and translation are complex and likely depend on the balance between stimulatory and inhibitory factors.

The involvement of several oncogenes in promoting its transcription fits with its known expression profile, with elevated levels widely reported in numerous malignancies.

1.2.2. Expression profile

MCAM was first identified in 1987 by Lehmann et al as a potential marker of melanoma [257]. What was then referred to as the MUC18 antigen was identified by its reactivity with a murine antibody raised against human metastatic melanoma tissue. Reactivity of the antibody was recorded against only 2 % of clinical samples of benign nevi, but this increased to 47 % in the context of primary melanoma and 69 % in metastatic melanoma.

Analyses of both protein and mRNA levels have confirmed the absent or low-level expression of MCAM on melanocytes and normal epidermal tissue [263, 281]. Contrastingly, MCAM shows a pattern of stepwise upregulation during the malignant progression from dysplastic nevus through to primary and metastatic melanoma [296]. Expression is also correlated with the vertical depth of melanoma lesions, suggesting a possible causal role of MCAM in the acquisition of an invasive phenotype by melanoma cells [296].

MCAM upregulation has also been reported in all 3 types of solid tumours: carcinomas of the stomach [297], breast [298–300], ovary [301], liver [302], prostate [277, 303] and kidney [304]; sarcomas including leiomyosarcoma, Kaposi's sarcoma, osteosarcoma and angiosarcoma [305–307]; and nervous system tumours such as schwannomas and neurofibromas [306].

In the context of melanoma, the presence of MCAM on clinical specimens correlates with the clinical staging descriptors Clark's level and Breslow thickness [308], and with disease burden in metastatic melanoma [309]. MCAM positivity is also predictive of poor outcome after non-surgical treatment [309], and of reduced 5-year survival [308]. Interestingly, the predictive value of MCAM has also been demonstrated in the context of circulating tumour cells, with its expression associated with advanced disease stage

and increased recurrence risk, as well as poor outcome following non-surgical treatment [309, 310].

The association between poor prognosis and MCAM in melanoma is also observed in other malignancies. 41 % of gastric tumours express MCAM, which is predictive of poor survival and increased risk of lymph node metastases [297]. Similarly, MCAM is expressed on approximately 7 % of breast cancers, where it is associated with high grade, basal triple negative cancers [298] and acts as a negative prognostic marker [298, 311]. Similar associations with poor survival have also been reported in ovarian cancer [312], clear cell renal cell carcinoma [313], osteosarcoma [307, 314, 315], and glioblastoma [316]. A 2017 meta-analysis which included the results of 12 studies covering 2600 patients found that MCAM overexpression was associated with poor overall survival and reduced time to progression [317]

Soluble MCAM also has value as a biomarker in non-cancer disease states, with elevated plasma levels detected in patients with heart failure [274], miscarriage [318], age-related macular degeneration [319] and systemic sclerosis [320].

Based on its widely reported overexpression on malignancies, MCAM has been characterised as a tumour-associated antigen. However, this categorisation is complicated by its expression on healthy cells. It has been frequently detected on vascular endothelial cells throughout the body, including in the lymph nodes, spleen, lung, tonsils, and placenta [265], to the extent that it can be used as a marker of circulating endothelial cells [321]. MCAM is predominantly limited to capillaries, and is generally low or undetectable on larger calibre vessels [265].

The location of MCAM on endothelial cells has mainly been investigated using human umbilical vein endothelial cells (HUVEC) cultured *in vitro* in monolayers or networks on Matrigel; notably, expression of the protein on HUVECs increases on *ex vivo* culture [265] which may be more representative of angiogenic vasculature rather than quiescent endothelium. Expressed at low levels in subconfluent cultures, the protein is upregulated on confluent HUVECs [322], where it is primarily localised to sites of cell-cell contact [323–325]. It does not appear to directly form part of adherens junctions or focal adhesions however [269, 326]. The short and long isoforms display different

subcellular localisation and are involved in different processes. The long isoform, which is found intracellularly in subconfluent cells [322], is directed to the basal membrane and cell-cell junctions in confluent cultures [269, 322]; it plays a role in the formation and stabilisation of HUVEC networks [322]. At confluency, the short isoform is relocated from the nucleus to the apical surface and the migrating edge of the cell where it promotes HUVEC proliferation and migration [322], potentially via its association with VEGFR1/R2 [272].

MCAM expression has also been reported on the smooth muscle of the tunica media [262, 263, 265, 305, 327] and non-vascular smooth muscle of the colon and stomach [265], with some reports suggesting it is also found on skeletal muscle [305]. In the nervous system it has been detected on the cerebellar cortex and on Schwann cells [305, 327], whilst elsewhere in the body it has been identified on tissues as varied as adipose tissue, the kidney, hair follicles [257, 263], parathyroid glands [305], and the epithelia of the lens, thymus, breast, and bronchi [305].

Furthermore, MCAM has been reported on a minority of cells of the haematopoietic lineage: MCAM expression in healthy participants is detected on approximately 3 % of peripheral CD3+ T cells [328–330], 1 % of B cells and 0.1 % of NK cells [329]. MCAM+ T cells are polyclonal, with conventional αβ TCRs [329, 330] and more commonly co-express CD4 over CD8 [328, 331, 332]. This population is reported to have a CD45RA-CD45RO+ CCR7- memory phenotype [329, 333–337], and its enrichment for genes including CCR6, IL-17, IL-22, IL-23R, IL-26, ROR and CD161 [331, 333, 338] has led several groups to conclude that MCAM demarks a CD4+ Th17 subset [333, 338]. It doesn't appear to be an exclusive marker for this group however, as MCAM+ CD8+ T cells have also been detected.

The expression of MCAM on immature thymocytes and the thymic epithelium [305, 339] suggested a potential role for MCAM in T cell development. Recently this was confirmed by Duan et al [340], who demonstrated that conditional knockout of MCAM in Lck-expressing cells interfered with the β-chain selection and positive selective steps of T cell development, reducing the total number of mature T cells in the periphery. Several groups have demonstrated that MCAM expressed in this context functions as an adhesion receptor, allowing T cells to bind to the endothelium and facilitating their

extravasation [331, 341]. Duan et al [340] also demonstrated that MCAM binds to Lck via its KKGK motif, driving Lck activation and augmented T cell signalling.

Although rare in healthy participants, MCAM-expressing T cells are elevated in the blood and affected tissues in several autoimmune and inflammatory conditions, including arthritis [336–338, 342, 343], contact dermatitis [342], multiple sclerosis [331], psoriasis [343] and Crohn's disease [333].

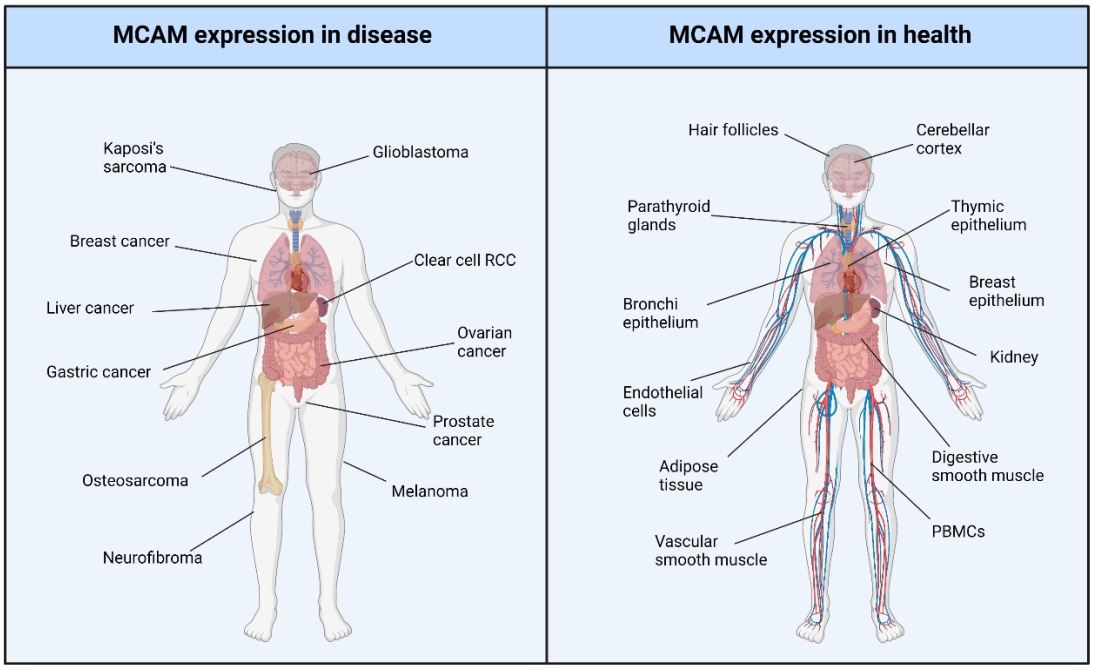

Figure 1.4 MCAM expression in health and disease.
MCAM is upregulated in a variety of malignant conditions, where it is associated with a poor prognosis. However, it is also expressed on healthy tissues throughout the body. Figure created with Biorender.com.

1.2.3. Function of MCAM

1.2.3.1. Membrane bound MCAM

Several studies have demonstrated a correlation between the expression of MCAM and the invasion and motility of various cell lines *in vitro* [277, 301, 344–348]. Acquisition of this invasive, migratory phenotype correlates with the increased expression of markers of the epithelial-mesenchymal transition (EMT) in MCAM-

expressing cells, including N-cadherin, vimentin, slug, and the matrix metalloproteinases MMP2 and MMP9, alongside downregulation of E-cadherin [297, 298, 344, 346]. The downregulation of E-cadherin and upregulation of N-cadherin and vimentin are considered to be essential for cellular migration and invasion, and favour cancer metastasis [349]. In an *in vitro* 3D skin model, MCAM-expressing melanoma cells implanted amongst keratinocytes were able to rapidly invade into the dermis, replicating the vertical growth phase of melanoma. This invasion through the basement membrane, a key step in cancer spread, was significantly impaired by MCAM knockdown [350].

Intravenous injection of MCAM-transfected cell lines and neo-transfected controls into immunocompromised or syngeneic mice confirmed a correlation between the expression of MCAM and metastatic ability [344, 351]. The magnitude of the effect differs between different models, and it is lost when tumour cells are implanted subcutaneously [344, 347], suggesting that MCAM may act to facilitate extravasation to a greater degree than intravasation.

Whilst there is consensus that MCAM favours the development of a migratory, invasive and metastatic phenotype, its role in cellular growth and tumorigenicity is less clear. The upregulation of MCAM has no demonstrable effect on cell proliferation *in vitro* [281, 344, 347], however siRNA knockdown has been linked with decreased cell proliferation [301, 348, 352]. Similar contradictory results have been obtained *in vivo*, with several studies finding a correlation between MCAM and tumour growth rate in mice [290, 344], with others finding that tumorigenicity was unaffected [347, 351] or in some cases reduced [345, 353].

Given its widespread expression on endothelial cells, several studies have investigated the role of MCAM in the context of angiogenesis. The expression of MCAM by HUVECs and endothelial cell lines promotes the VEGF-induced formation of capillary-like tubular structures on Matrigel [266], in a manner which can be inhibited by MCAM siRNA [264]. In a Matrigel plug model in which VEGF-containing Matrigel was implanted into wild type (WT) and $MCAM^{-/-}$ mice, the absence of MCAM significantly reduced endothelial invasion into the plug and the number of large diameter vessels [266]. Similar results were obtained in a model in which HUVEC cells were treated with

a MCAM-targeting micro-RNA, miR329 [295], which could also significantly reduce neovascularisation in a murine model of oxygen induced retinopathy [295].

Neovascularisation was also reduced in a zebrafish model in which human HCC, human gastric cancer and mouse melanoma cell lines were injected into the yolks of wild-type and MCAM-morpholino-oligonucleotide knock down embryos. Sprouting of vessels from the sub-intestinal vein into tumours was significantly impaired in the MCAM-knockdown animals [354]. Finally, further evidence for the importance of MCAM in angiogenesis was provided by a chick chorioallantoic membrane assay, in which a filter disk saturated with anti-MCAM antibody was directly placed on the membrane of fertilised eggs. Blood vessel formation after 24h exposure to anti-MCAM decreased in a dose dependent manner, resulting in avascular regions adjacent to the filter paper [355].

To summarise, MCAM-expression on tumour cells correlates with upregulation of markers of the EMT, the acquisition of an invasive motile phenotype, and increased metastatic ability *in vivo*. Its role in promoting cell growth and tumorigenicity by tumour cells is less clear, however expression on HUVECs promotes angiogenesis in response to pro-angiogenic factors *in vitro* and *in vivo*.

1.2.3.2. Soluble MCAM

The pro-tumour effects of MCAM are not just limited to the membrane bound isoforms. Soluble MCAM is generated by a calcium-dependent process which ultimately results in ectodomain shedding [271]. Originally MMP1 and MMP3 were identified as the mediators of this [271], with more recent work identifying TACE and ADAM10 as responsible for cleaving the short and long isoforms, respectively [320].

Soluble MCAM is secreted by numerous cancer cell lines as well as HUVECs and human microvascular endothelial cells [272]. sMCAM treatment drives the proliferation of UACC-1273, C8161 and PANC-1 cells, and increases the expression of proteins known to promote angiogenesis and invasion, including MMP-9, Ang2, c-Myc and Max [272],

along with markers of the EMT [276]. Accordingly, the motility and formation of capillary-like structures by an ovarian cancer cell line (HEY) was also increased in the presence of sMCAM [276]. Through the induction of the anti-apoptotic factor Bcl-X_L, sMCAM also protects cancer cells from free radical induced apoptosis [272]. *In vivo*, sMCAM treatment promoted the growth of ovarian and melanoma xenografts and increased the frequency and size of metastases [276].

1.2.4. MCAM as a receptor

Although the location and effects of MCAM expression have been well characterised, the exact signalling mechanisms by which it acts are still somewhat unclear. Numerous ligands have been identified; they can broadly be categorised as components of the extracellular matrix (ECM) involved in modulating cell adhesion and cytoskeletal rearrangements or signalling molecules which promote cell growth and angiogenesis [356].

It was first suggested that MCAM may be a cell adhesion molecule after cDNA analysis identified high sequence similarity with the adhesion molecules N-CAM, CEA, L1, fascilin II, and contactin [262]. Additionally, its expression at the cell surface is localised to sites of cell-cell contact [281, 323, 324], and is associated with the formation of spheroids *in vitro* [344, 351, 357]. Whilst it was initially thought to mediate cell adhesions through the formation of homodimers [263], evidence has since demonstrated that these MCAM-mediated adhesions are more likely to be the result of an interaction between MCAM and a heterophilic ligand [357]. Subsequently, it has been demonstrated that MCAM is the receptor for laminins 411 and 421, galectins 1 and 3, and S100A8/A9.

Laminins form a key component of the basement membrane, playing important structural roles throughout the body and interacting with the overlying endothelial and epithelial cells through cell membrane receptors. They consist of α, β and γ chains, and 16 isoforms have been identified in mammals which have tissue and cell-specific expression patterns and functions [358]. Laminins 421 and 411 (α4β2γ1) are reported

to promote the motility of cancer cells *in vitro* [359, 360]. Binding of MCAM to laminin 421 and laminin 411 is mediated by an interaction with the globular domain of the α4 laminin chain [361]. Migration of MCAM-expressing melanoma cells on the immobilised proteins can be abrogated by MCAM-blocking antibodies [362]. Studies suggest that MCAM on melanoma cells binds more strongly to laminin 421 [362], whilst laminin 411 serves as a vascular ligand for Th17 cells [363]. The cause for this differential binding is unclear but could indicate the presence of different MCAM epitopes on different cell types.

Galectins are a family of 15 soluble carbohydrate binding proteins, of which galectins -1 and -3 are most well characterised [364]. Galectin-1 has been implicated in the progression of a range of cancers, including breast, prostate, cervical, lung and brain cancers, as well as melanoma. Its effects are mediated through a range of mechanisms which result in tumour growth, metastasis, angiogenesis, and resistance to chemo- and radiotherapy. Galectin-3 expression has similarly been shown to increase invasion and metastasis of pancreatic, colon and breast cancer cells, and promotes angiogenesis in melanoma by inducing NFAT1 activity [364]. Clinical studies have demonstrated the altered expression of galectin-1 and -3 in numerous malignancies, with galectin-1 overexpression in particular predicting poor prognosis [365].

Galectin-1 binds to N-glycans on MCAM expressed by cultured endothelial cells, protecting them from galectin-1-induced apoptosis [366]. Galectin-1-MCAM interactions are also reported on melanoma cells, where they promote cell migration [367]. Studies from the Yu research group have similarly identified MCAM as a major binding partner for galectin-3 on endothelial cells [368] and melanoma [369]. This induces MCAM dimerisation and downstream AKT signalling, resulting in production of metastasis-inducing cytokines from the endothelium and promoting melanoma invasion and motility.

S100 proteins are another family of soluble dimeric proteins found in the extracellular environment which have diverse roles including promoting tumorigenesis [370]. The heterodimer S100A8/A9 is a ligand for MCAM on malignant cells, resulting in the activation of NF-κB and MAPK signalling pathways [371, 372]. This has been shown to

facilitate local invasion through the induction of MMP25 [371], and to promote distant lung metastases in mouse models [372].

Alongside alterations in cell adhesion to other cells and ECM components, local invasion and metastasis requires cytoskeletal reorganisation, a process which is regulated by RHO GTPases [373, 374]. MCAM interacts with meosin, an ERM protein which couples the transmembrane MCAM protein with the actin cytoskeleton, an interaction which facilitates migration *in vitro* [267]. MCAM also indirectly interacts with the cytoskeleton via paxillin: it associates with the kinase p59 FYN, which becomes phosphorylated following MCAM cross-linking. Activated p59 FYN phosphorylates and activates p125 FAK (focal adhesion kinase), which in turn recruits and phosphorylates paxillin, an adaptor protein which is coupled to the cytoskeleton through other proteins such as vinculin [326, 375].

Furthermore, MCAM also transmits signals which drive cytoskeletal rearrangement through its role as a receptor in non-canonical Wnt signalling. Wnt5a increases the motility of cultured endothelial cells through an interaction with the third extracellular Ig domain of MCAM: MCAM associates intracellularly with the protein dishevelled (Dvl), which becomes phosphorylated. This drives cytoskeletal rearrangement through the activation of JNK [376].

MCAM is involved in diverse and numerous signalling pathways linked to cell motility, in accordance with its role as a driver of cell invasion and metastasis in cancer cells. It is also known to promote angiogenesis, which may be in part mediated by its role as a co-receptor for VEGF-A. On cultured endothelial cells MCAM is found directly associated with VEGFR-2, and this interaction is necessary for VEGF-induced VEGFR-2 phosphorylation and NF-κB/AKT signalling [266]. Moreover, CD146 is a receptor for VEGF-C, playing an important role in lymphangiogenesis by lymphatic endothelial cells [377].

Although originally considered as a homophilic receptor simply involved in cell-cell adhesion, MCAM is now known to act as a receptor and signal transducer in numerous pathways. The relative contributions of these different MCAM-ligand interactions, and how these different pathways may interact, requires further research. Likewise, the

mechanisms underpinning the activity of sMCAM remain to be fully elucidated. Currently the only binding partner to be identified is angiomotin, which is expressed on endothelial cells. sMCAM-angiomotin interactions on endothelial progenitor cells upregulates phosphorylated AKT, FAK and JNK and promotes the formation of capillary-like networks in *in vitro* assays [378].

1.2.5. MCAM immunotherapies

The characterisation of MCAM as a tumour associated antigen led several groups to investigate its potential as an immunotherapy target. To date, several therapeutic antibodies have been developed to this end [379], as has a vaccine targeting MCAM.

1.2.5.1. Therapeutic Monoclonal Antibodies

ABX-MA1

The first reported anti-MCAM antibody, ABX-MA1, was generated by immunising Abgenix's proprietary XenoMouse against the human melanoma cell line SK-MEL-28, giving rise to an affinity matured, fully human antibody [380]. *In vitro*, ABX-MA1 blocks the adhesion of MCAM-expressing cells to HUVECs, and significantly impairs the invasion and migration of human melanoma and osteosarcoma cell lines, partly by reducing MCAM-induced protease activity by MMP2 [380]. Accordingly, therapeutic ABX-MA1 treatment was able to inhibit the metastasis of melanoma and osteosarcoma cell lines in nude mice [380, 381]. Interestingly, although it was able to slow the growth of tumours in mice with subcutaneous melanoma xenografts, osteosarcoma tumours were resistant to its tumouristatic effects [380, 381].

ABX-MA1 also appears to inhibit angiogenesis: *in vitro* it disrupts the formation of capillary networks by HUVECs on Matrigel [380], and IHC analysis of tumour sections from mice demonstrated that ABX-MA1 treatment significantly reduced the tumour micro-vessel density and increased the number of apoptotic cells [380].

AA98

The MCAM-specific monoclonal antibody AA98 was raised in mice against HUVEC cells stimulated with conditioned media from tumour cells to isolate a monoclonal antibody which bound selectively to angiogenic vasculature [355]. It is reported to preferentially label tumour vasculature over that in healthy tissues, binding to an epitope at the junction between the 4^{th} and 5^{th} Ig domains of MCAM [382]. This is thought to stabilise the protein in its monomeric form [382], antagonising the effects of VEGF and blocking downstream NF-κB signalling [266, 304]. AA98 treatment was shown to selectively inhibit the proliferation of stimulated HUVEC cells, prevent their migration towards a VEGF stimulus, and impair blood vessel formation in a chick chorioallantoic membrane (CAM) angiogenesis assay [355].

In vivo, AA98 could reduce the growth of human leiomyosarcoma, pancreatic cancer, uveal melanoma, and hepatic cell carcinoma in nude mice, and prevented the formation of micro-metastases to the lungs and lymph nodes [266, 355]. Conjugating AA98 to ^{131}I enhanced its inhibition of tumour growth and reduced micro-vessel density by 70 % compared to IgG-treated controls; those vessels which were present were characterised by narrowed lumens and the presence of thrombi [355]. Angiogenesis and vascular mimicry in a uveal melanoma model were also reduced following AA98 treatment [383].

tsCD146

The potential for unintended effects caused by reactivity of existing MCAM antibodies against healthy vasculature led Nollet et al to develop a novel antibody with higher selectivity for tumour specific (ts) MCAM [384]. Termed tsCD146, this rat monoclonal antibody was able to discriminate between cell lines of cancerous and vascular origin, suggesting that tumour expressed MCAM may contain distinct epitopes. This antibody selectively labelled tumour cells but not endothelial cells in biopsies of melanoma, renal carcinoma, colon adenocarcinoma and verrucous skin carcinoma. tsCD146 could also detect melanoma cancer microparticles in the plasma of patients, whilst radiolabelled tsCD146 provided a means of detecting melanoma in a xenograft model via PET imaging.

In vitro, tsCD146 caused a moderate decrease in the proliferation of a panel of cancer cell lines, and significantly induced apoptosis. Growth of melanoma and pancreatic tumours in NOD/SCID xenograft experiments was reduced by 30-50 % [384].

PRX-003

PRX-003 is the only anti-MCAM therapeutic that has been utilised clinically to date. This anti-MCAM antibody developed by Prothena reduces tumour size and bone metastases in SCID male mice xenografted with prostate cancer cells [385]. It was tested in phase 1 clinical trials for the treatment of psoriasis. Whilst it was well tolerated it did not achieve any meaningful clinical responses and therefore has not been developed further [386, 387].

MJ2-1

Given its role in promoting tumour growth and metastasis, the soluble form of MCAM presents a unique target for monoclonal antibody therapy. M2J-1, a rat monoclonal antibody which selectively binds to sMCAM but not the membrane-bound isoforms, was developed by Stalin et al [272]. M2J-1 antagonised the effects of sMCAM on ovarian, melanoma and prostate cancer cell lines *in vitro*, reducing their proliferation and inducing apoptosis and senescence [272, 276]. In mouse xenograft models, MJ2-1 treatment reduced tumour growth and dissemination, with mice developing fewer and smaller metastases compared to control groups, likely due to a reduction in circulating micro-metastases [272, 276]. Intra-tumoural vascularisation was reduced, and the number of apoptotic tumour cells was increased [276].

Photoimmunotherapy with therapeutic antibodies

Photoimmunotherapy is a new treatment modality which utilises antibody-conjugates to deliver the hydrophilic dye IR700 to the membrane of cancer cells. Near infrared light is then used to excite the antibody-IR700 complexes, which causes the production of reactive oxygen species and membrane damage. This ultimately leads to cell death and the release of DAMPs, eliciting an immune response [388]. Wei et al leveraged this technology in 2019, conjugating IR700 to an alternative murine anti-MCAM antibody, YY146. In mouse experiments IR700-YY164 treatment could reduce the growth of melanoma xenografts and induce production of reactive oxygen species [389]. To date,

only the YY146 antibody has been tested in this context, but it could represent a promising research direction.

1.2.5.2. Vaccination

The encouraging results mediated by monoclonal antibodies led to the development of a DNA vaccine against murine MCAM [390], which was used to vaccinate immunocompetent C57/BL6 mice prior to challenge with subcutaneous MCAM-overexpressing mouse melanoma cells. Prophylactic vaccination reduced tumour incidence by 50 % compared to a β-galactosidase vaccine control ($p<0.001$) and could also reduce metastasis formation in mice challenged with IV melanoma cells. However, vaccination was unable to mediate any anti-tumour effects in mice bearing established tumours [390].

Vaccination was demonstrated to induce the formation of MCAM-specific IgG2a antibodies and cytotoxic T lymphocytes which could selectively mediate the lysis of MCAM+ cells. Treatment of mice with a CD8 eliminating agent could abrogate the anti-tumour effects of the vaccine, suggesting that CTLs may play a major role in the response observed. Given that MCAM is known to be expressed on the vascular smooth muscle [278] and endothelium [391], a risk of autoimmunity exists with this vaccination strategy. No signs of toxicity were observed, however, potentially suggesting that full immune responses only occur in response to the high MCAM levels on melanoma cells [390].

1.2.6. MCAM as a CAR T cell target

MCAM-specific CAR T cells could represent a novel immunotherapy for several reasons. Firstly, the characterisation of MCAM as a tumour associated antigen with high expression not only in melanoma but in a variety of tumours would increase their utility. Its expression also correlates with poor prognosis and advanced disease, and it

is involved in several important signalling cascades, suggesting that it may play a causal role in disease progression. Furthermore, it appears to have an active effect on cell behaviour, with MCAM^{high} cells acquiring a migratory, invasive phenotype and upregulating markers of the EMT. As would be expected, this correlates with an increased risk of metastasis in *in vivo* models.

Not only is its expression on tumour cells upregulated, MCAM also facilitates angiogenesis, an essential step for tumour growth and survival. Moreover, disrupting the angiogenic vasculature with CAR T cells could potentially mediate significant anti-tumour effects without the need for such cells to extravasate and survive in the immunosuppressive tumour microenvironment. Given its active roles in tumour cell behaviour and angiogenesis, selectively targeting MCAM^{high} cells could remove tumour cells with an aggressive phenotype and reduce the chance of antigen loss variants occurring, a common cause of relapse in CD19-CAR trials [98].

However, as with all tumour-associated antigens, the expression of MCAM on healthy tissues means that this strategy carries a risk of on-target/off-tumour toxicities. MCAM is expressed at low levels in a range of different tissues: whilst certain sites of expression such as the central nervous system (CNS) and the eye may be protected from CAR activity due to immune privilege, other sites would certainly be accessible. CAR T cells have been tested in the clinic against a range of tumour associated antigens with diverse expression on normal tissues, including those targeting VEGFR2 [392], mesothelin [205], and EGFR [393, 394]. To date these therapies have been broadly well tolerated with no evidence of major on-target/off-tumour toxicity, although their anti-tumour activity has also been limited.

The expression of MCAM on the vasculature is a major concern. Whilst it may be that antigen density on normal blood vessels is insufficient to activate CAR T cells, there is little research directly comparing expression levels on healthy vasculature and tumour tissues, so it is not possible to be confident of this. However, the absence of autoimmunity in mice vaccinated against MCAM does suggest that there may be a therapeutic window for targeting it [390]. Additionally, it appears to localise to endothelial cell junctions, making it potentially less readily accessible to circulating CAR T cells compared to antigens on the apical surface.

A further complicating factor is its reported expression on a population of T cells enriched for Th17 and memory markers. Typical T cell expansion protocols do not utilise Th17 polarising cytokines, so this is likely to represent a minority of cells in the final CAR T cell product, limiting the degree of potential trans-activation at this stage. However, if subsequent T cell activation leads to MCAM upregulation this percentage could increase, potentially leading to cell death or exhaustion. Additionally, CAR T cells administered clinically would be exposed to the patient's Th17 cell population, risking further on-target/off-tumour toxicity. This could serve to reduce the persistence of transferred cells, which may limit the extent of any toxicities, albeit at the expense of tumour control.

These complications would clearly need to be taken into account during the development of any MCAM-directed therapy. Whether there is a therapeutic window in which MCAM can safely be targeted with CAR T cells remains to be seen. However, given its expression profile and function in cancer, MCAM may prove to be a rational target for CAR T cell therapy, with the potential applications in several malignancies.

1.3. Project Aims and Hypothesis

We hypothesised that primary human T cells could be redirected against MCAM through the expression of second generation, 4-1BB costimulated chimeric antigen receptors, and that this could provide a rational means of targeting MCAM-overexpressing melanoma cells, as assessed in preclinical assays. We also hypothesised that there may be a therapeutic window for such a therapy if MCAM expressed on normal tissues proved inaccessible or sufficiently low level to result in off-tumour CAR T cell activity.

The detailed aims of this project are therefore as follows:

- To generate a panel of second-generation, 4-1BB costimulated CAR constructs with MCAM-specific scFv domains.
- To screen these domains in an immortalised T cell line (JRT3-T3.5) and identify those constructs with MCAM-specific activity.
- To generate CAR-expressing primary T cells and assess their effector functions in a range of *in vitro* assays.
- To investigate potential on-target/off-tumour reactivity of anti-MCAM CAR T cells through coculture with HUVEC cells.
- To generate a zebrafish-based *in vivo* model to challenge CAR T cells with a more complex microenvironment.

Chapter 2. Materials and Methods

2.1. Materials and suppliers

2.1.1. Buffers and solutions

Table 2: List of buffers and respective components

Buffer/solution	Application	Components
SDS Blue buffer (1X)	Cell lysis for western blotting	62.5 mM TRIS pH 6.8 with 2 % (w/v) SDS, 10 % (v/v) Glycerol, 0.01 % (w/v) bromophenol blue and 3 % (v/v) β-mercaptoethanol
Running buffer (1X)	Western blotting	25 mM tris, 192 mM glycine, 1 % (w/v) SDS
Transfer buffer (1X)	Western blotting	25 mM TRIS, 192 mM glycine, 1 % (w/v) SDS, 20 % (v/v) methanol
WB blocking buffer	Western blotting	3 % (w/v) BSA in PBST
Cell dissociation buffer	Cell culture/flow cytometry	PBS with 5 mM EDTA
Cell staining buffer	Flow cytometry	PBS with 10 % (v/v) FBS and 5 mM EDTA.
FACS buffer	Flow cytometry	PBS with 5 % (v/v) FBS with 5 mM EDTA (optional).
RetroNectin blocking buffer	Retroviral transductions	PBS with 2 % (w/v) BSA.
MACS buffer	Cell sorting	PBS with 2 mM EDTA and 0.5 % (v/v) FBS.
TAE buffer	Gel electrophoresis	dH_2O with 40 mM tris-acetate and 1 mM EDTA.
LB broth	Bacterial culture	dH_2O with 2 % (w/v) yeast extract, 1 % (w/v) NaCl and 1 % (w/v) tryptone
Chorion water	Raising zebrafish embryos	dH_2O with 60 mg/mL instant ocean salt and 0.0001 % (w/v) methylene blue (optional).
MS222 stock solution	Zebrafish anaesthesia/euthanasia	dH_2O 4 g/L MS222 (15.4 mM) and 20 mM Tris, pH 8.5

2.1.2. Primary and secondary antibodies

Table 3: Primary and secondary antibodies for western blotting

Antibody Target	Host species	Target species	Clone	CAT number	Supplier	Dilution
PRIMARY ANTIBODIES						
MCAM ectodomain	Rabbit	Human	EPR3207	ab134065	Abcam	1:1000
MCAM endodomain	Rabbit	Human	EPR3208	ab75769	Abcam	1:1000
CD19	Mouse	Human	1C10A1	66298-1-Ig	Proteintech	1:1000
CD3ζ	Mouse	Human	8D3	551033	BD Biosciences	1:1000
GAPDH	Mouse	Human	1E6D9	60004-1	Proteintech	1:5000
Vinculin	Mouse	Human	VIN54	Ab130007	Abcam	1:5000
β Tubulin	Rabbit	Human	1D4A4	66240-1	Proteintech	1:5000
SECONDARY ANTIBODIES						
Anti-rabbit-HRP	Goat	Rabbit	Polyclonal	7074	Cell Signalling	1:5000
Anti-mouse-HRP	Horse	Mouse	Polyclonal	7076	Cell Signalling	1:5000

Table 4: Antibodies for flow cytometry

Target	Conjugate	Host species	Target species	Clone	CAT number	Supplier	Dilution
CD34	APC	Mouse	Human	561	343608	BioLegend	1:100
CD69	PECy7	Mouse	Human	FN50	310912	BioLegend	1:100
CD62L	BV605	Mouse	Human	DREG-56	562719	BD Biosciences	1:100
CD3	APC	Mouse	Human	UCHT1	300411	BioLegend	1:50
CD4	BV510	Mouse	Human	OKT4	317443	BioLegend	1:50
CD8	APC/H7	Mouse	Human	SK1	560273	BD Biosciences	1:100
CD34	BV650	Mouse	Human	561	343623	BioLegend	1:50
CD69	BV421	Mouse	Human	FN50	310929	BioLegend	1:100
CD25	BV785	Mouse	Human	BC96	302637	BioLegend	1:100
CD137	PE-Dazzle	Mouse	Human	4B4-1	309825	BioLegend	1:100
PD-1	BV785	Mouse	Human	EH12.2H7	329929	BioLegend	1:100
TIM3	BV421	Mouse	Human	F38.2E2	345007	BioLegend	1:100
LAG3	PE-Dazzle	Mouse	Human	11C3C65	369331	BioLegend	1:100
MCAM	PE	Mouse	Human	361005	P1H12	BioLegend	1:100
MCAM	APC	Mouse	Human	361015	P1H12	BioLegend	1:100
IgG	PE	Goat	Human	Polyclonal	P9170	Sigma	1:100
CD107a	PE	Mouse	Human	H4A3	555801	BD Biosciences	1:100

2.1.3. Kits, enzymes, and other reagents

Table 5: List of enzymes and other reagents

Reagent	CAT number	Supplier
KITS		
Monarch PCR & DNA Clean-up Kit	T1030S	New England Biolabs
Monarch DNA Gel Extraction Kit	T1020S	New England Biolabs
Monarch Plasmid Miniprep Kit	T1010S	New England Biolabs
PureLink Fast Low-Endotoxin Midi Plasmid Purification Kit	A36227	Invitrogen
CD34 Microbead Kit, Human	130-046-702	Miltenyi Biotec
Human IFN-γ DuoSet ELISA kit	DY285B	R&D Systems
Human TNF-α DuoSet ELISA kit	DY210	R&D Systems
Human IL-2 DuoSet ELISA kit	DY202	R&D Systems
Steady Glo Luciferase Assay	E2510	Promega
CELL CULTURE REAGENTS		
PBS (without calcium and magnesium)	D8537-500ML	Sigma-Aldrich
DMEM	D5796-500ML	Sigma-Aldrich
RPMI	R8758-500ML	Sigma-Aldrich
FBS	10500064	Gibco
Glutamax	35050-038	Gibco
Opti-MEM	31985062	Gibco
Fugene	E2311	Promega
Polybrene	TR-1003-G	Sigma-Aldrich
RetroNectin	T100B	Takara
Trypan Blue	15250-061	Gibco
Trypsin-EDTA Solution	T3924-100ML	Sigma-Aldrich
0.5M EDTA	15575-038	Invitrogen
DMSO	D12345	Thermo Fisher
PMA	P1585-1MG	Sigma-Aldrich
Ionomycin	9995S	Cell Signalling Technology
IL-2 (Proleukin)	N/A	Clinigen
EGM-2 Endothelial Cell Growth Medium Bullet-Kit	CC-3162	Lonza
Accutase Cell Dissociation Reagent	A1110501	StemPro
Cultrex Basement Membrane Extract	3432-005-01	R&D Systems
Vybrant DiO Cell Labelling Solution	V22886	Invitrogen
Vybrant DiI Cell Labelling Solution	V22885	Invitrogen
ANTIBIOTICS		
Penicillin/Streptomycin	P0781-100ML	Sigma-Aldrich
Ampicillin	11593027	Gibco
Puromycin Dihydrochloride	A1113803	Thermo

ENZYMES AND REACTION BUFFERS		
NotI-HF	R3189S	New England Biolabs
ClaI	R6551	Promega
NheI-HF	R3131S	New England Biolabs
EcoRI-HF	R3101S	New England Biolabs
HindIII-HF	R3104S	New England Biolabs
NEBuilder HiFi DNA Assembly Master Mix	E2621S	New England Biolabs
Cutsmart Buffer	B7204S	New England Biolabs
Q5 High Fidelity 2x mastermix	M0494S	New England Biolabs
T4 DNA ligase and reaction buffer	M0202S	New England Biolabs
Instant Sticky End Ligase Mastermix	M0370S	New England Biolabs
Antarctic phosphatase	M0289S	New England Biolabs
Taq DNA Polymerase with Thermopol Buffer	M0267S	New England Biolabs
KLD reaction mix	M0554S	New England Biolabs
FLOW CYTOMETRY REAGENTS		
DAPI	564907	BD Pharmingen
Live/Dead Fixable Blue Stain	L23105	Invitrogen
FcR Blocking Reagent	130-059-901	Miltenyi Biotech
Ultra-Comp eBeads Plus Beads	01-3333-42	Thermo Fisher
MCAM-Fc chimera	9709-MA-050	R&D Systems
Monensin	00-0405-51	eBiosciences
FITC Annexin V Apoptosis kit with PI	640914	BioLegend
Cell Trace Violet	C34571	Thermo
MOLECULAR BIOLOGY REAGENTS		
10uM dNTPs	N0447S	New England Biolabs
Hyperladder 1kB	H1-618106A	Bioline
Hyperladder 100bp	H4-216109	Bioline
Gel Loading Dye, Blue (6x)	17-1329-01	New England Biolabs
Agarose	BIO-41025	Bioline
Ethidium bromide	E8751-5G	Sigma-Aldrich
LB powder	L3522-1kg	Sigma-Aldrich
Agar powder	M1002	Melford
SOC media	15544-035	Invitrogen

2.1.4. Oligonucleotides

Table 6: List of oligonucleotides with respective sequences

Target	5'-3' Sequence	Supplier
PRIMERS FOR MYCOPLASMA TESTING		
Myco forward	TGCACCATCTGTCACTCTGTTAACCTC	Thermo Fisher
Myco reverse	GGGAGCAAACAGGATTAGATACCCT	Thermo Fisher
PRIMERS FOR SEQUENCING PMP71.CD34.2A.CAR.CD8.4-1BB PLASMID		
Seq Primer 1	CTCGAGAGCTTTGGCGTAATCATGG	Thermo Fisher
Seq Primer 2	GCGCCTTATCCGGTAACTATCGTC	Thermo Fisher
Seq Primer 3	GGTCCTGCAACTTTATCCGCCTC	Thermo Fisher
Seq Primer 4	GGGAATAAGGGCGACACGGAAAT	Thermo Fisher
Seq Primer 6	GGACTTTTTGGAGCTCCGCCA	Thermo Fisher
Seq Primer 7	GAAGTCAAACTGACACAGGGCATCT	Thermo Fisher
Seq Primer 8	GAACTTTGATCTGCTGAAGCTGGCC	Thermo Fisher
Seq Primer 11	CAGCTGTAGATTCCCCGAGGAAGA	Thermo Fisher
Seq Primer 14	AGGCGATTAAGTTGGGTAACGCC	Thermo Fisher
Seq Primer 15	GAAAGACCCCACCTGTAGGTTTGG	Thermo Fisher
Seq Primer 20	TTATCCAGGCTCATGAAGCC	Thermo Fisher
Seq Primer 21	GCAGAGCATCGTAGGTAT	Thermo Fisher
Seq Primer 22	GTATTTCAGCCACTTCGTGC	Thermo Fisher
PRIMERS FOR AMPLIFYING SCFVS AND GENEBLOCKS		
M1	F – GATCATCGATACAGGTGCAGCTGG R – GATCGCGGCCGCTAGGAC	Thermo Fisher
M40	F – GATCATCGATACAGGTGCAGCTGTT R – GATCGCGGCCGCTAGGAC	Thermo Fisher
B6-11	F – GATCATCGATAATGGCCGAGGTGCAGC R – GATCGCGGCCGCCGCGCCTAGGACGGTCA	Thermo Fisher
ABX-MA1	F – GATCATCGATACAGGTGCAGC R – GATCGCGGCCGCCTTAATCTC	Thermo Fisher
tsCD146	F – GATCATCGATAGAGGAGC R – GATCGCGGCCGCTTTCAATT	Thermo Fisher
String 1	F – GATTCCCCGAGGAAGAGGAA R – TTCTATCTATGGCTCGTGTT	Thermo Fisher
String 2	F – CTCTCCAAGCTCACTTACAG R – TCACAGCCCCCTTCCTCTTC	Thermo Fisher

2.1.5. Cell lines

Table 7: List of cell lines

Cell line	Type	Species	Supplier
Phoenix GP (PhGP)	Human Embryonic kidney cells	Human	Provided by Dr A Gilmore
PG13	Mouse embryonic fibroblast line.	Human	Provided by Dr E Cheadle
Lenti-X 293T	Human Embryonic kidney cells	Human	Provided by Dr A Malliri
JRT3-T3.5 Jurkats	T cell leukaemia	Human	Provided by Dr J Bridgeman
888-Mel	Metastatic melanoma	Human	Provided by Dr C Wellbrock
501-Mel	Metastatic melanoma	Human	Provided by Dr C Wellbrock
WM2664	Metastatic melanoma	Human	Provided by Dr C Wellbrock
C8161	Melanoma	Human	Provided by Dr C Wellbrock
HUVEC	Human umbilical vein endothelial cells, from pooled donors	Human	Lonza
Yumm1.1	Melanoma cell line	Mouse	Provided by Dr R Marais
Yumm1.7	Melanoma cell line	Mouse	Provided by Dr R Marais
Yumm2.1	Melanoma cell line	Mouse	Provided by Dr R Marais

2.2. Methods

2.2.1. Molecular biology

2.2.1.1. Standard PCR

For routine applications requiring high fidelity DNA amplification, PCR was performed using Q5 DNA polymerase. Reactions were set up on ice (see Table 8), using appropriate forward and reverse primers, and then thermocycled (Alpha Cycler 4, PCR Max) according to the cycling parameters detailed in Table 8. Where required on account of the amplicon length and primer design, cycling conditions were optimised.

Table 8: Reaction mix and cycling conditions for standard PCR

REACTION MIX			
Reagent	Volume	Final Concentration	
Q5-High Fidelity 2x Master Mix	12.5 µL	1x	
10uM forward primer	1.25 µL	0.5 µM	
10uM reverse primer	1.25 µL	0.5 µM	
Template DNA	X µL	40 ng/µl	
Nuclease-free water	To 25 µL	-	
THERMOCYCLING CONDITIONS			
Step	Temperature (˚C)	Time	Cycles
Initial denaturation	98	2 minutes	1
Denaturation	98	25 seconds	35
Annealing	60	25 seconds	
Extension	72	30 seconds/kb	
Final extension	72	10 minutes	1
Final store	4	∞	1

2.2.1.2. DNA gel electrophoresis

1 % (w/v) agarose gels for DNA electrophoresis were prepared by dissolving agarose powder (Bioline) in TAE buffer (Table 2) and heating. Ethidium bromide was then added to a final concentration of 0.5 µg/mL prior to gel casting. An appropriate volume of 6x Blue Gel Loading Dye (New England Biolabs) was added to each sample, and 15 µL was loaded into individual wells. According to fragment size, either a 100 bp (Bioline, H4-216109) or 1 Kb (Bioline, H1-618106A) molecular weight marker was also

loaded. Gel electrophoresis was performed at 120V for 35 minutes using a consort E132 powerpack, following which the gel was transferred into a Uvitec Geldoc Gel Light Imaging System to allow visualisation of DNA bands under UV light. Where required, the gel was imaged with the Uvitec Geldoc Gel Light Imaging System, and relevant bands were excised with a sterile scalpel.

2.2.1.3. Bacterial transformation and plasmid preparation

10 µL aliquots of XL-1 competent cells (Agilent) were thawed on ice for each required transformation reaction. 3µl per ligation reaction or 0.5µl of previously prepped plasmid DNA was then added to each aliquot. The reactions were gently mixed by flicking the tubes prior to a 30-minute incubation on ice. Cells were heat shocked by heating to 42 ˚C for 42 seconds then placed on ice for a further 2 minutes. 350 µL stable outgrowth media (Invitrogen) was added to each aliquot, which were then shaken at 225 rpm and 37 ˚C in a shaking incubator for 1 hour. 75 µL of this culture was then spread on selective agar plates, with 1:4 and 1:10 dilutions also plated to ensure appropriate colony confluency. Plates were then incubated for 12-16 hours at 37 ˚C.

Miniprep cultures were generated by picking individual colonies and inoculating 3 mL LB broth containing the appropriate selection antibiotic. Cultures were incubated for 12-16 hours at 37 ˚C and 225 rpm prior to plasmid preparation using the Monarch® Plasmid Miniprep Kit (New England Biolabs), according to the manufacturer's instructions. To generate larger yields of plasmid DNA, 100 µL of miniprep culture was added to 150 mL LB broth with selection antibiotic and incubated as above. Plasmid DNA was then harvested using the PureLink™ Fast Low-Endotoxin Midi Plasmid Purification Kit (Invitrogen) as per the manufacturer's protocol.

2.2.1.4. Colony screening PCR

Colony screening PCRs were performed to minimise the number of miniprep cultures required when cloning new constructs. For each colony, a PCR reaction mix was set up (Table 9) and a sterile pipette tip was used to pick a colony and introduce it first to the PCR reaction, and then into a well of a 96 well plate containing 100 µL LB/well. PCR reactions were thermocycled using the PCR Max Alpha Cycler 4, according to the cycling conditions in Table 9. Reactions were then electrophoresed, and PCR products visualised as above. Where PCR products were of the expected length, the 100 µL culture from the corresponding colony was used to generate a miniprep culture as above.

Table 9: Reaction mix and cycling conditions for colony screening PCR

REACTION MIX			
Reagent	Volume	Final Concentration	
10x Taq ThermoPol buffer	2.5 µL	1x	
10mM dNTP mix	0.5 µL	200 µM	
10uM forward primer	0.5 µL	0.2 µM	
10uM reverse primer	0.5 µL	0.2 µM	
Template DNA	x µL	40 ng/µL	
Taq DNA polymerase	0.125 µL	0.625 units/25 µL PCR	
Nuclease-free water	To 25 µL	-	
THERMOCYCLING CONDITIONS			
Step	Temperature (˚C)	Time	Cycles
Initial denaturation	95	5 minutes	1
Denaturation	95	15 seconds	30
Annealing	55	25 seconds	
Extension	72	30 seconds/kb	
Final extension	72	5 minutes	1
Final store	4	∞	1

2.2.1.5. Assessment of DNA/RNA levels

Plasmid concentrations were calculated according to the absorbance of the sample at 260 nm measured using a Nanodrop 2000 (Thermo Scientific). When performing mini- and midi-preps, plasmid DNA was eluted into molecular biology grade water, which was also used as the blanking solution for spectrophotometric assessment of DNA concentration. The ratios of the absorbance at 260nm and 280nm, and of that 260nm

and 230nm were used to determine sample purity, with pure DNA indicated by values of 1.8 and 2.2, respectively.

2.2.1.6. Western blotting

To prepare whole cell lysates for immunoblotting, adherent cells were gently washed with PBS then lysed in SDS blue lysis buffer (see Table 2). Non-adherent cells (JRT3-T3.5 Jurkats and primary T cells) were harvested and centrifuged. Supernatant was discarded and the cell pellet was washed by resuspension in PBS. Cells were then pelleted by centrifugation and resuspended in SDS blue lysis buffer. Lysates were then sonicated at 4˚C for 20 seconds at an amplitude of 25 % using the VCX130 Vibracell Sonicator (Sonics & Materials), prior to denaturing at 95 ˚C for 5 minutes. The Mini-Protean Tetra Cell system was used to cast SDS-polyacrylamide gels consisting of an 8 % (w/v) TRIS-SDS acrylamide running gel with a 5 % (w/v) TRIS-SDS acrylamide stacker. Gels were placed in running buffer (Table 2) and 10 µL of each sample was loaded per well along with a pre-stained molecular weight marker (Sigma, SDS7B2), prior to electrophoresis for 70 minutes at 68 mA and 135 V. Gels were then transferred in transfer buffer (Table 2) onto activated Immobilon P PVDF membrane (Millipore) via application of a current of 340 mA and 100 V for 70 minutes. Membranes were then blocked at room temperature for 1 hour in PBS-T with either 3 % (w/v) BSA or 5 % (w/v) skim milk (when more stringent blocking was required). Primary antibodies were diluted 1:1000 in 3 % (w/v) BSA/PBS-T and then applied to the membrane, which was incubated overnight at 4 ˚C with gentle agitation. Membranes were then washed for 5 minutes in 10 mL PBS-T for a total of 3 times, prior to incubation for 1-hour at room temperature with a 1:5000 dilution of the secondary antibody in 3 % (w/v) BSA/PBS-T. Following three further 5-minute washes, 500 µL each of Clarity Western Peroxide Reagent and Clarity Western Luminol/Enhancer Reagent (Clarity™ Western ECL Substrate, BioRad) was applied to the membrane, which was developed and imaged using the Chemidoc XRS+ and Imagelab software (both Biorad).

2.2.2. Cell culture methods

2.2.2.1. Cell culture maintenance

All cell lines used in this project are listed in Table 7, along with their respective cell type, origin species and supplier. All cell culture work was carried out in accordance with risk management protocols and was performed in sterile conditions in a category 2 laminar flow hood.

All packaging cell lines (Phoenix GP, lenti-X and PG13) and human melanoma cell lines (888-Mel, 501-Mel, WM266-4, A375 and C8161) were maintained in Dulbecco's Modified Eagles Medium (Sigma Aldrich) supplemented with 10 % (v/v) heat inactivated FBS (Gibco), 50 IU/mL penicillin (Sigma Aldrich), 50 µg/mL streptomycin (Sigma Aldrich) and 10µl/mL Glutamax (Gibco). Roswell Park Memorial Institute (RPMI) 1640 medium (Sigma Aldrich) was supplemented as above for the culture of JRT3-T3.5 cell lines and mouse melanoma cell lines (Yumm 1.1, Yumm 1.7 and Yumm 2.1). HUVECs were maintained in HUVEC media, comprising EGM-2 Endothelial Cell Growth Media supplemented with the EGM-2 BulletKit (Lonza). Primary T cells were kept in T cell medium (TCM) composed of RPMI supplemented with 10 % (v/v) heat inactivated FBS, 100 IU/mL penicillin, 100 µg/mL streptomycin, 10 µl/mL Glutamax, 25 mM HEPES (Sigma) and 100-200 IU/mL IL-2 (Proleukin, Clinigen). All human and mouse cell lines were incubated at 37 ˚C, 5 % (v/v) CO_2 unless otherwise indicated.

2.2.2.2. Mycoplasma testing

Cell lines were screened for mycoplasma contamination prior to freezing and use in *in vitro* and *in vivo* assays, in addition to regular routine screening every month. To prevent false negative results due to antibiotic-mediated suppression of mycoplasma growth, cell lines were maintained for a minimum of 5 days in media free from penicillin and streptomycin before testing. Samples of media were centrifuged to remove cell debris and heated to 95 °C for 10 minutes, prior to use in a PCR-based

detection assay (see Table 6 for primer sequence and Table 10 for PCR reaction mix and thermocycling conditions). Positive and negative control samples were included with every assay. PCR reactions were then loaded onto a 1 % (w/v) agarose gel for DNA electrophoresis, and PCR products were visualised under UV light with a Uvitec Geldoc Gel Light Imaging System (see section 2.2.1.2). The presence of 200 bp PCR products was indicative of mycoplasma infection, and such cell lines were discarded to prevent cross-contamination.

Table 10: Reaction mix and cycling conditions for mycoplasma screening PCR

REACTION MIX			
Reagent	Volume	Final Concentration	
10x Taq ThermoPol buffer	2.5 µL	1x	
10mM dNTP mix	0.5 µL	200 µM	
10uM forward primer	0.5 µL	0.2 µM	
10uM reverse primer	0.5 µL	0.2 µM	
Template DNA	x µL	40 ng/µl	
Taq DNA polymerase	0.125 µL	0.625 units/25ul PCR	
Nuclease-free water	To 25 µL	-	
THERMOCYCLING CONDITIONS			
Step	Temperature (˚C)	Time	Cycles
Initial denaturation	95	5 minutes	1
Denaturation	95	15 seconds	30
Annealing	55	25 seconds	
Extension	72	30 seconds/kb	
Final extension	72	5 minutes	1
Final store	4	∞	1

2.2.2.3. Passaging cell cultures

Cell lines were subcultured every 2 to 5 days depending on cell growth rate and optimal cell confluency. Adherent cells were subcultured using trypsin-EDTA mediated cell dissociation. All reagents were warmed to 37 ˚C prior to use. Briefly, cells were washed gently with PBS without magnesium or calcium (Sigma Aldrich) and incubated at 37 ˚C for up to 5 minutes following the addition of trypsin-EDTA (Sigma-Aldrich). 10 mL complete culture media with FBS was then added to the culture vessel and dissociated cells were transferred to a sterile conical centrifuge tube which was centrifuged at 400 g for 5 minutes. The supernatant was then aspirated, and the cell pellet was resuspended in fresh culture media to give a homogenous cell suspension.

An appropriate volume of cell suspension to achieve the required split ratio was then transferred to a sterile cell culture vessel containing sufficient complete media.

To subculture suspension cells, media was removed by centrifugation and the pellet was gently resuspended, prior to transfer of an appropriate volume into fresh media.

2.2.2.4. Freezing and thawing cell lines

For optimal cell survival on thawing, cell lines were ideally cryopreserved when they reached 80 % confluency and had a viability of above 90 %. The mycoplasma status of all cell lines was also verified before freezing (see section 2.2.2.2). Briefly, 2X sterile freezing medium consisting of heat inactivated FBS (Sigma-Aldrich) with 20 % (v/v) DMSO (Thermo Fisher) was prepared and stored at 4 ˚C. Cells were dissociated as above (section 2.2.2.3) and centrifuged at 400 g for 4 minutes. Supernatant was aspirated and cells were resuspended in complete media at a concentration of approximately 2 x 10^6 cells/mL for adherent cells and 2 x 10^7 cells/mL for primary T cells. An equal volume of freezing media was then added in a dropwise manner, with regular mixing to produce a homogenous cell suspension with DMSO at a final concentration of 10 % (v/v). 1 mL aliquots were dispensed into sterile cryovials which were placed in Mr Frosty™ freezing containers (Thermo Fisher) in order to control the rate of cooling to a final temperature of -80 ˚C. After a minimum of 4 hours in the -80 ˚C freezer, cryovials were then transferred to liquid nitrogen for long term storage.

In order to culture frozen cells, cryovials were quickly thawed at 37 ˚C in a water bath. The cell suspension was then transferred to a sterile conical centrifuge tube and 10 mL pre-warmed complete culture media was added prior to centrifugation at 400 g for 5 minutes. Supernatant was aspirated to remove DMSO and the cell pellet was gently resuspended in fresh pre-warmed complete media and transferred to a sterile tissue culture flask.

To achieve optimal recovery of cryopreserved HUVEC cells, tissue culture plates were first coated with fibronectin (Sigma) at 5 µg/ml in PBS for 1 hour at 37°c, followed by a

single wash in PBS. HUVEC cells were quickly thawed at 37 ˚C in a water bath, transferred to the fibronectin coated flask and topped up with EGM-2 Endothelial Cell Growth Media supplemented with the EGM-2 BulletKit (Lonza). After 8 hours the media was carefully aspirated and replaced to remove residual DMSO.

2.2.2.5. Establishment of cell populations by lentiviral transduction

HIV-1 based lentivirus was generated using a second generation lentiviral production system utilising the lenti-X cell line, a derivative of the HEK 293T cell line acquired for the purposes of this project from Dr A Malliri (see Table 7, section 2.2.2.5). In this system, lenti-X cells were transfected with 3 plasmids. The psPAX2 envelope plasmid encodes the *gag, pol, tat* and *rev* genes, while the pMD2.G envelope plasmid allows generation of VSVG-pseudotyped lentivirus. A third transfer plasmid encodes the gene of interest flanked by LTRs and Ψ packaging sequences, which enable its incorporation into virions. Briefly, 1 x 10^7 lenti-X cells were plated and incubated overnight, prior to transfection with 12 µg psPAX2, 6 µg pMD2.G and 9 µg lentiviral transfer plasmid, with 100 µL Fugene HD transfection reagent (Promega) and 900 µL OptiMEM Reduced Serum Media (Gibco). Lentivirus-containing culture supernatant was harvested after 48-hours, centrifuged, filtered through a 0.45 µM cellulose acetate filter, and either frozen at -80 ˚C or used immediately to transduce adherent cell lines. For the purposes of transduction, 3 mL viral supernatant was combined with 7 mL fresh culture media and Polybrene Infection/Transfection reagent (Merck) to a final concentration of 8 µg/mL and overlaid onto 5 x 10^6 pre-plated adherent cells. After a 24-hour incubation at 37 ˚C, virus-containing media was aspirated and replaced with fresh culture media.

2.2.2.6. Establishment of stable PG13 retrovirus producer cell lines for CAR expression

To maximise transduction efficiencies for JRT3-T3.5 and primary T cells, stable CAR-retrovirus-producing cell lines were generated. In the first step of this 2-step process,

MoMULV-based retrovirus was produced by Phoenix GP (PhGP) helper cells, which stably express *gag* and *pol* genes. PhGP cells were plated at 1 x 10^7 per T175 flask the day prior to transfection with 6 µg pMG2.G envelope plasmid (containing VSVG protein) and 9 µg of transfer plasmid encoding the CAR construct and required LTR and Ψ packaging sequences, using 100 µL Fugene HD Transfection Reagent (Promega) and 900 µL Opti-MEM Reduced Serum Media (Gibco). After 48 hours, the supernatant was harvested, centrifuged, filtered through a 0.45 µM filter and used to transduce sparsely plated PG13 cells (see section 2.2.2.5 for details of transduction of adherent cells). This process was repeated 24 hours later to maximise the number of successfully transduced PG13 cells. The PG13 cell line is derived from NIH 3T3 TK- mouse fibroblasts, and stably expresses MoMULV *gag* and *pol* genes in addition to the *env* gene from Gibbon Ape Leukaemia Virus (GALV). When the CAR construct with associated packaging sequences is delivered via VSVG-pseudotyped retrovirus, such cells can stably produce retrovirus.

The CAR constructs used in this project featured a truncated (non-functional) CD34 marker protein, separated from the CAR via a self-cleaving 2A linker. Successfully transduced PG13 cells were isolated using the CD34-microbead Kit (Miltenyi) which allows positive selection of CD34 expressing cells with antibody-conjugated microbeads and column based magnetic sorting. Stocks of $CD34^+$ PG13 cells were then mycoplasma tested and frozen. Supernatant from confluent plates of sorted cells was harvested, centrifuged, and filtered as above and used to transduce JRT3-T3.5 cells or primary human T cells (sections 2.2.2.7 and 2.2.2.10).

2.2.2.7. Generation of CAR positive JRT3-T3.5 cells

A RetroNectin-based protocol was used for the transduction of the JRT3-T3.5 cell line with GALV-pseudotyped CAR-encoding retrovirus produced by PG13 cells (see above). Non-TC treated, 6-well plates were coated with RetroNectin (Takara Bio) at 30 µg/mL and incubated for 2 hours at room temperature, followed by a 30-minute block with 2 % (w/v) BSA/PBS. Plates were then washed twice with 4ml/well PBS, prior to the

addition of 2 mL/well, filtered viral supernatant from $CD34^+$ PG13 cells. Plates were centrifuged for 2 hours at 2000 g and 32 ˚C. Supernatant was then aspirated, and wells were washed twice with 4 mL PBS/well prior to the addition of 2 x 10^6 cells/well (JRT3-T3.5 or primary human T cells). Following a final 5-minute centrifugation step at 200 g, plates were incubated for 48-hours.

2.2.2.8. FACS sorting of transduced cells

Cells were trypsinised if required, then resuspended at 5 x 10^6 cells per 100 µL FACS buffer (Table 2). Where cells were sorted according to expression of a cell surface marker, fluorophore-conjugated antibodies were added at manufacturer recommended dilutions (Table 4) and cells were incubated on ice in the dark for 1 hour. CAR-transduced cells were stained with APC-anti-human CD34 (BioLegend) at a 1:20 dilution to allow the isolation of CD34-positive cells. Cells were then washed 2 times in an excess of ice-cold PBS, prior to being resuspended in flow buffer and analysed on the BD FACS Aria Fusion (BD Biosciences).

The flow cytometers and sorters used in this project were accessed via the Flow Cytometry Core Facility. Thanks to Gareth Howell, Mike Jackson and David Chapman for their help in planning flow cytometry experiments and performing all cell sorting work.

2.2.2.9. Isolating and expanding primary T cells from leukocyte reduction system (LRS) cones

LRS cones were obtained from NHS-BT under ethical approval from the University of Manchester Proportionate University Research Ethics Committee. The contents of the cone were harvested and diluted with room temperature PBS at a 1:8 ratio. 20 mL of diluted suspension was then gently overlaid on top of 15 mL Ficoll Paque Plus (Cytiva) in a 50 mL falcon tube, which was then centrifuged at 400 g for 40 minutes, with no brake applied. The uppermost layer of serum was removed and discarded, and the

PBMC-containing buffy coat layer was collected. The PBMCs were then resuspended in unsupplemented RPMI and centrifuged at 300 g for 10 minutes, and the resulting cell pellet was resuspended in unsupplemented RPMI prior to counting.

2.2.2.10. Transducing and expanding primary T cells

2 days prior to the planned transduction, PBMCs were isolated from LRS cones (see above) and cultured in TCM with 50 ng/mL ULTRA-LEAF anti-human CD3 (BioLegend) and 50ng/mL anti-human CD28 (R&D Systems) antibodies and 300 IU/mL IL-2 (Clinigen), to promote selective activation and expansion of T cells. On the same day, CAR retrovirus producing PG13s (section 2.2.2.6) which had been previously sorted for CD34 were plated in TCM such that they would achieve 80 % confluence by the day of the transduction (generally a density of 2 x 10^4 cells/cm^2).

The day before the transduction, RetroNectin (Takara Bio) was diluted in PBS to 20 µg /mL and 2 mL/well was used to coat sterile, non-TC coated 6-well plates (CytoOne, Starlab). Plates were wrapped in cling film and incubated overnight at 4 ˚C. On the day of the transduction, the RetroNectin solution was removed and reserved, and the wells were blocked with 4 mL/well TCM for 30 minutes at room temperature. The reserved RetroNectin solution was transferred to new 6-well plates, which were incubated at 4 ˚C overnight until required for the second transduction.

Virus-containing supernatant from PG13 cells was harvested, centrifuged at 400 g for 5 minutes, and then filtered through a 0.45 µm cellulose acetate syringe filter. The TCM block was then removed, and wells were washed once with 4 mL/well PBS prior to the addition of 3 mL/well viral supernatant. Plates were centrifuged in a pre-warmed centrifuge at 2000 g/32 ˚C. After 1 hour, the viral supernatant was exchanged for 3 mL/well fresh supernatant, and plates were centrifuged as above for a further hour. The viral supernatant was then aspirated, and wells were washed with 4 mL/well PBS prior to the addition of 2 mL/well T cell suspension (containing 2 x 10^6 cells in TCM supplemented with 200 IU/mL IL-2). Following a brief centrifugation step (5 minutes at 400 g) to deposit the T cells on the RetroNectin-virus layer, plates were incubated at 37

˚C and 5% (v/v) CO_2 overnight. The following day, the above process was repeated using the second set of RetroNectin coated plates, and fresh viral supernatant from the PG13 cells. T cells were harvested from the first set of plates, resuspended in 2 mL/well TCM with 200 IU/mL IL-2, and transferred to the newly virus-coated plates, prior to centrifugation and incubation as above.

24 hours after the final transduction, T cells were harvested and counted. To generate sufficient cells for subsequent assays, they were then expanded using G-Rex 6-well cell culture plates (Wilson Wolf). Transduced T cells were seeded at 2 x $10^6/cm^2$ in 40 mL/well TCM supplemented with 200 IU/mL IL-2. Every 2 days, a 75 % media change was performed (without disturbing the cell layer), with the addition of fresh IL-2 to a final concentration of 200 IU/mL. After 12 days, CAR T cells were harvested and counted prior to use in functional assays.

2.2.2.11. Pre-assay characterisation of primary CAR T cells

Viability dye and Fc-R blocking:

Prior to use in functional assays, primary CAR T cells were first characterised by flow cytometry to quantify transduction efficiency and the CD3/4/8 composition of the expanded population. Cells were counted and plated at 2 x 10^5 cells/well of a 96-well round bottomed plate, then washed by centrifugation at 400 g and 4 ˚C for 5 minutes followed by removal of the supernatant. This wash step was repeated once more, then the cell pellet was resuspended in 100 µl/well of Live/Dead Fixable Blue stain (Thermo Fisher) diluted 1:1000 in PBS and incubated for 30 minutes at room temperature. To quench staining, cells were washed once in 200 µl/well FACS buffer (5 % (v/v) FBS in PBS). To prevent non-specific binding, an Fc-receptor blocking step followed, using FcR Blocking Reagent (Miltenyi) at a 1:100 dilution in FACS buffer. After a 20-minute incubation at 4 ˚C, cells were washed once in FACS buffer.

scFv labelling:

A 2-step staining protocol was used to label the anti-MCAM scFv on the MCAM-specific CAR T cells. Briefly, cells were incubated for 30 minutes at 4 ˚C with 5 µg/mL

recombinant human MCAM-Fc (R&D Systems) in FACS buffer, then washed twice with 200 µL/well FACS buffer to remove unbound protein. Anti-IgG-PE (Sigma) diluted 1:100 in FACS buffer was then used to label the Fc-portion of the MCAM-Fc chimeric protein. Following a 30-minute incubation at 4 ˚C, 2 wash steps were performed (with 200 µl/well FACS buffer).

Labelling cell surface markers:

Cells were incubated with 100 µl/well FACS buffer containing the required antibody mix (see Table 11) at 4 ˚C for 30 minutes. Unbound antibody was removed by a further 2 wash steps in FACS buffer, then cells were incubated for 15 minutes at room temperature in 2 % (w/v) PFA in PBS to fix. A final 2 wash steps were performed, and cells were resuspended in 200 µl/well FACS buffer prior to analysis.

Analysis:

Samples were analysed on the BD Fortessa using BD FACSDiva software (both BD Biosciences). Subsequent analysis was performed using FlowJo™ Software (Beckton, Dickinson and Company). Compensation for CD3-, CD4-, CD8- and CD34-conjugated fluorophores was performed using UltraComp eBeads™ Plus Compensation Beads (Thermo) labelled as per the manufacturer's instructions, while single stained cell samples were used to compensate for the Live/Dead Fixable Blue and MCAM-Fc/anti-IgG PE fluorophores. Fluorescence minus one (FMO) samples were used to set gates.

Table 11: Viability dye and antibodies used for pre-assay CAR T cell characterisation.

Target	Clone	Dilution
Live/Dead Fixable Blue	N/A	1:1000
APC Anti-CD3	UCHT1	1:50
BV510 Anti-CD4	OKT4	1:50
APC/H7 Anti-CD8	SK1	1:100
BV650 Anti-CD34	561	1:50
PE Anti-IgG	Poly	1:100

2.2.3. *In vitro* assays of CAR function

2.2.3.1. Assessment of CAR activity in the JRT3-T3.5 cell line

CAR activity in the JRT3-T3.5 cell line was assessed via flow cytometric analysis of surface CD69 and CD62L expression following coculture with a range of target cells. Adherent target cells were dissociated from tissue culture vessels and counted and plated in triplicate at 1x 10^4 cells/well in round-bottom, TC-treated 96-well plates. CD34+ CAR JRT3-T3.5 cells were then added at a 10:1 effector: target ratio. Pooled CAR JRT3-T3.5 cells were stimulated with 50 ng/µL PMA (Sigma-Aldrich) and 500 ng/µL ionomycin (Cell Signalling Technology), as a positive control. Plates were then incubated for 16 hours at 37 ˚C.

Cells were suspended by pipetting and were transferred to a new 96-well round bottomed plate for staining. Cells were pelleted by centrifuging the plate at 500 g for 5 minutes. Media was aspirated, and the cells were thoroughly resuspended in 100 µL/well FACS buffer (Table 2) with CD69-PECy7, CD34-APC and CD62L-BV605 antibodies at 1:100 dilutions (Table 12). Fluorescence-minus-one (FMO) controls were included for each fluorophore. Cells were then stained in the dark on ice for 1 hour. Cells were then washed 2 times in 200 µL/well flow buffer, prior to a final resuspension in flow buffer with DAPI Cell Viability Stain (BD Biosciences) at a 1:5000 dilution. Data was acquired on the BD Fortessa X20 using BD FACSDiva software (both BD Biosciences), with manual compensation. Subsequent analysis was performed using FlowJo™ Software (Beckton, Dickinson and Company).

Table 12: Viability dye and antibodies used for JRT3-T3.5 activation assay.

Target	Clone	Dilution
DAPI	N/A	1:5000
APC Anti-CD34	561	1:100
PECy7 Anti-CD69	FN50	1:100
BV605 Anti-CD62L	DREG-56	1:100

2.2.3.2. IFN-γ, TNF-α and IL-2 ELISAs

To quantify cytokine production by primary CAR T cells, cocultures were established using either the 888-Mel target cell lines, a panel of melanoma cell lines, or HUVECs. Target cells were plated at 2 x 10^4/well in TCM in round bottomed TC-coated 96-well plates. CAR T cells were then counted and equalised for transduction efficiency via the addition of mock T cells. They were then added to the target cells at 1 x 10^5 cells/well in 100 µl TCM or plated in media alone as a negative control. All conditions were plated in triplicate. After a 24-hour incubation period at 37 ˚C, the plates were centrifuged for 5 minutes at 400 rpm to pellet all cells, and the supernatant was transferred to new 96-well round bottomed non-TC coated plates and stored at -80 ˚C. When required, the culture supernatant was thawed at room temperature and appropriate dilutions (1:4 for IFN-γ, 1:2 for TNF-α and IL-2) were made using TCM. IFN-γ, TNF-α and IL-2 in the supernatant were quantified by sandwich ELISA, using Nunc Maxisorp flat-bottomed 96 well ELISA plates (Thermo) and Human DuoSet kits (R&D Systems), according to the manufacturer's instructions. Absorbance at 450 nm and 540 nm wavelengths was determined using a BioTek Synergy Plate reader. To correct for optical imperfections in the plate, the 540nm values were first subtracted from the 450 nm readings. Average background absorbance was determined for TCM alone, and this value was subtracted from the absorbance values for the test samples and standards. GraphPad Prism was then used to generate a sigmoidal 4 parameter logistic curve (for which X is concentration), from which the cytokine concentrations could be interpolated.

2.2.3.3. Expression of activation and exhaustion markers

To determine the expression of activation and exhaustion markers on CAR T cells following exposure to antigen expressing target cells, cocultures were set up as above (section 2.2.3.2) and incubated for 24 hours. Non-adherent cells were resuspended via gentle pipetting, and then transferred to a 96-well round bottomed non-TC coated

plate for staining. Briefly, cells were washed and underwent staining with Live/Dead Fixable Blue stain (Thermo) and Fc-R blocking, as described in section 2.2.2.11.

Cells were then washed and resuspended in 100 µl/well antibody solution containing the relevant fluorophore conjugated antibodies in FACS buffer (see Table 13 and Table 14). Staining proceeded for 30 minutes at 4 ˚C, followed by 2 wash steps in FACS buffer to remove unbound antibody. Fixation was performed at room temperature for 15 minutes with 2 % (w/v) PFA/PBS, followed by a final 2 wash steps and resuspension in 200 µl/well FACS buffer. Data acquisition and compensation was performed using the Fortessa flow cytometer as described in section 2.2.2.11.

Table 13: Viability dye and fluorophore-conjugated antibodies used for the CAR T cell activation marker panel.

Target	Clone	Dilution
Live/Dead Fixable Blue	N/A	1:1000
APC Anti-CD3	UCHT1	1:50
BV510 Anti-CD4	OKT4	1:50
APC/H7 Anti-CD8	SK1	1:100
BV650 Anti-CD34	561	1:50
BV421 Anti-CD69	FN50	1:100
BV785 Anti-CD25	BC96	1:100
PE-Dazzle Anti-CD137	4B4-1	1:100

Table 14: Viability dye and fluorophore-conjugated antibodies used for the CAR T cell exhaustion marker panel.

Target	Clone	Dilution
Live/Dead Fixable Blue	N/A	1:1000
APC Anti-CD3	UCHT1	1:50
BV510 Anti-CD4	OKT4	1:50
APC/H7 Anti-CD8	SK1	1:100
BV650 Anti-CD34	561	1:50
BV785 Anti-PD-1	EH12.2H7	1:100
BV41 Anti-TIM3	F38.2E2	1:100
PE-Dazzle Anti-LAG3	11C3C65	1:100

2.2.3.4. Luciferase-based cytotoxicity assays

CAR T cell mediated cytotoxicity was determined using a luciferase-based assay, which necessitated the generation of luciferase-expressing target cell lines. Briefly, Lenti-X cells were transfected (section 2.2.2.5) with psPAX2 and pMD2.G packaging plasmids and the pLenti CMV Puro Luciferase construct (w168-1), a gift from Eric Campeau & Paul Kaufman (Addgene plasmid # 17477; http://n2t.net/addgene:17477 ; RRID:Addgene_17477). This construct contains firefly luciferase and the puromycin resistance gene, under the CMV and murine pGK promoters, respectively. After 48 hours, the lentiviral supernatant was harvested, centrifuged for 5 minutes at 400 g and filtered through a 0.45 µM cellulose acetate membrane. Media on pre-plated target cells was changed to a lentiviral transduction mix, containing 3 mL of filtered viral supernatant, 7 mL fresh culture media and Polybrene Infection/Transfection reagent (Merck) to a final concentration of 8 µg/mL. Cells were incubated for 2 days, at which point the media was removed and cells were split into new flasks. Non-transduced target cells were cultured with serial dilutions of puromycin (Thermo) in a kill curve to establish the optimal selection concentration for each cell line, determined as the dose which achieves 100 % cytotoxicity by 2-4 days. This concentration was then applied to the transduced cell lines for a period of 5 days to select for successfully transduced target cells, which were then used in cytotoxicity assays.

Target cells were plated at 1 x 10^4 cells/well in 50 µL TCM in white walled, clear-bottomed TC-treated 96 well plates (Thermo). CAR T cells were equalised for transduction efficiency as above and added in 50 µL TCM at varying effector: target ratios from 5:1 to 0.5:1. Media-only and target cell-only wells were plated as negative controls. Cocultures were then incubated for 24 hours. 1 hour prior to assay development, plates were removed from the incubator and allowed to equilibrate to room temperature. 75 µL/well room temperature Steady Glo Luciferase Reagent (Promega) was added, and plates were incubated on an orbital shaker with gentle agitation at room temperature for 20 minutes. Luminescence (RLU) measurements were taken with the Biotek Synergy Plate reader, with background luminescence (measured using media-only wells) subtracted from the test values. Percentage cell

survival relative to the corresponding mock coculture for the appropriate cell line and effector: target ratio was calculated as 100 x (CAR T cell coculture RLU/mock coculture RLU).

2.2.3.5. Degranulation assays

Degranulation of primary CAR T cells was determined by quantifying cell surface CD107a expression following coculture with MCAM-expressing target cell lines. Melanoma cell lines (888-Mel, 501-Mel, C8161 and WM2664) were plated in 96 well round-bottomed, TC-treated plates at 1 x 10^5 cells/well in 100 µL TCM. CAR T cells were equalised for transduction efficiency and added to the coculture wells at a 1:1 effector: target ratio in 100 µL TCM. T cells were also plated with media only, or with 50ng/mL PMA and 1 µg/mL ionomycin, as negative and positive controls respectively. To inhibit intracellular protein transport, monensin solution (eBioscience) was added to all wells for a final concentration of 2 µM (1:1000 dilution), along with 2 µL/well CD107a-PE. Cells were incubated for 4 hours at 37 ˚C, at which point cells were stained with Live/Dead Fixable Blue viability dye and fluorophore-conjugated antibodies (see Table 15) against cell surface markers, as previously described (section 2.2.2.11). Data was acquired on the Fortessa, with compensation and post-acquisition analysis performed as described in section 2.2.2.11.

Table 15: Viability dye and fluorophore-conjugated antibodies for quantification of CAR T cell degranulation

Target	Clone	Dilution
Live/Dead Fixable Blue	N/A	1:1000
APC Anti-CD3	UCHT1	1:50
BV510 Anti-CD4	OKT4	1:50
APC/H7 Anti-CD8	SK1	1:100
BV650 Anti-CD34	561	1:50
PE Anti-CD107a	H4A3	1:100

2.2.3.6. Annexin PI assays

To determine CAR T cell toxicity against HUVEC cells, HUVEC apoptosis and necrosis was quantified following a period of coculture, using the FITC Annexin V Apoptosis kit with PI (BioLegend). CAR T cells were first resuspended at 5 x 10^5 cells/mL in PBS and stained for 10 minutes at 37 ˚C with Cell Trace Violet (Thermo), diluted 1:1000. Cells were washed twice with TCM to quench staining and remove any unbound CTV. HUVECs and CTV-stained CAR T cells were then plated at a 4:1 effector: target ratio (5 x 10^4 HUVECs and 2 x 10^5 T cells) in 200 µL/well HUVEC media and incubated at 37 ˚C for 20 hours. HUVEC cells were plated in media alone as negative controls. To generate positive control cells and Annexin-FITC and PI single stained samples for compensation, HUVECs were plated in media alone, and DMSO was added 1 hour prior to the end of the coculture period, at a final concentration of 10 %.

At the end of the coculture period, the plates were centrifuged to pellet all cells, and the supernatant was aspirated and discarded. Residual culture media was removed by adding 100 µL/well PBS, which was then aspirated and transferred to a separate plate to retain any non-adherent cells. 30 µL/well Accutase Cell Dissociation Reagent (StemPro) was added, and cells were incubated at 37 ˚C for 2 minutes to generate a single cell suspension. Dissociation was stopped by the addition of 170 µL/well RPMI + 10 % (v/v) FBS, and the 200 µL suspension was combined with the 100 µL/well PBS wash. Cells were then centrifuged and washed twice in 200 µL FACS buffer, prior to staining with 50 µL/well Annexin-V binding buffer containing 2.5 µL/well Annexin-V-FITC and 5 µL/well PI. Staining was allowed to proceed for 15 minutes at room temperature in the dark, at which point cells were transferred to polypropylene FACS tubes containing 250 µL Annexin-V binding buffer and analysed immediately on the Fortessa using BD FACS Diva Software (BD Biosciences). Compensation was performed using a mix of stained and unstained T cells (for CTV compensation), and DMSO-treated HUVECs single stained with either Annexin-V or PI. FMO samples were generated for each fluorophore and used to facilitate the setting of gates.

2.2.3.7. MCAM expression on activated T cells

To determine if activated CAR T cells displayed any detectable MCAM expression, T cells were plated at 1 x 10^4 cells/well in round-bottomed 96-well plates. Cells were cultured for 48 hours in TCM + 200 µL IL-2. At the end of the culture period, cells were washed and stained with Live/Dead Fixable Blue and antibodies against cell surface markers (Table 16) (see section 2.2.2.11 for full staining protocol). Data acquisition and analysis was performed as previously described (section 2.2.2.11).

Table 16: Viability dye and fluorophore-conjugated antibodies used to quantify MCAM expression on CAR T cells.

Target	Clone	Dilution
Live/Dead Fixable Blue	N/A	1:1000
APC Anti-CD3	UCHT1	1:50
PE Anti-MCAM	361015	1:100

2.2.4. HUVEC network models

2.2.4.1. Basic HUVEC network model

To promote the development of network-like structures by HUVECs, µ-plate 96-well angiogenesis plates (Ibidi) were pre-cooled on ice and coated with 10 µL/well ice-cold Cultrex Basement Membrane Extract (BME, R&D Systems). To set the coating layer, plates were then incubated for 1-hour at 37 ˚C. 70 µL/well HUVEC media was overlaid on top of the coating, and plates were incubated for 24-48 hours at 37 ˚C, to ensure the gel coating was fully hydrated to reduce optical drift during time-lapse imaging. HUVECs were resuspended at 1 x 10^6 cells/mL in serum-free DMEM and stained for 20 minutes at 37 ˚C with 1:200 Vybrant DiI Cell Labelling Solution (Invitrogen). Staining was quenched by the addition of DMEM containing 10 % FBS, and cells were washed twice in 200 µL serum supplemented DMEM.

The pre-coated angiogenesis plates were then prepared for the addition of the HUVECs by careful aspiration of the 70 µL/well EGM-2 medium. 1 x 10^4 HUVECs were gently

deposited on top of the basement membrane layer, in 50 µL EGM-2 medium. Plates were immediately transferred to the environmental control chamber of a LiveCyte Quantitative Phase Imaging microscope (Phasefocus), at 5 % (v/v) CO_2 and 37 ˚C. Hourly images were acquired over the next 20 hours, using a 10x/ 0.25 Plan N objective, C-MOS 52U camera (Hamamatsu) and LiveCyte Acquire software (Phasefocus). QPI Images were calculated using a proprietary algorithm (Phasefocus) to analyse diffraction patterns generated by transmitted 650nm laser light. Fluorescence images were created using a pE-300 LED light source (CoolLED) and Texas Red (Vybrant DiI) filter cubes (Olympus).

2.2.4.2. HUVEC network model with melanoma cells

To incorporate melanoma cells into the basic HUVEC network model, HUVEC networks were established as described in section 2.2.4.1, and allowed to develop over a 6-hour incubation period. WM2664 melanoma cells were resuspended in serum-free DMEM and stained with Vybrant DiO or DiD (Invitrogen), diluted 1:200, for 20 minutes at 37 ˚C, followed by 2 washes in DMEM containing 10 % (v/v) FBS. 2.5 x 10^3 cells/well DiO-labelled WM2664 cells in EGM-2 medium were then added to the HUVEC networks. Plates were then imaged immediately as previously described, with additional fluorescence images taken using the FITC (Vybrant DiO) or Cy5 (Vybrant DiD) filter cubes.

To investigate the interaction of CAR T cells with the HUVEC-WM2664 cultures, plates were set up as described above and for 4 hours to allow the WM2664s to incorporate into the network. CAR T cells were labelled with Cell Trace Violet (see section 2.2.3.6 for staining details) then added at 1 x 10^4 cells/well. Plates were then imaged (section 2.2.4.1), with fluorescence images acquired using the Texas Red (Vybrant DiI), FITC (Vybrant DiO) and DAPI (CTV) filter cubes.

2.2.4.3. Image analysis

Timelapse images were exported from the LiveCyte Analyse software (Phasefocus) as Tiff stacks for further image analysis in Image J (Fiji) [395]. Briefly, Tiff stacks were

renamed and saved to separate folders according to the channel; CTV+ T cells were imaged in the blue channel, DiI+ HUVECs in the red channel and DiO+ WM2664 cells in the green channel. Basic image processing was performed in batch to optimise contrast, following which all images were converted 8-bit and automatically thresholded to create new binary stacks. The inbuilt Fiji measurement tools were used to measure the thresholded area (HUVECs and WM2664) or count thresholded particles (T cells) for each image within a stack. To quantify the co-localisation of T cells with adherent cells, the Fiji Image Calculator application was used to create overlay images which mapped the common thresholded pixels for matched T cell and HUVEC images. These areas of overlap, corresponding to T cells co-localised with HUVECs, were quantified using the measurement tools as described above. This process was repeated for the WM2664 images.

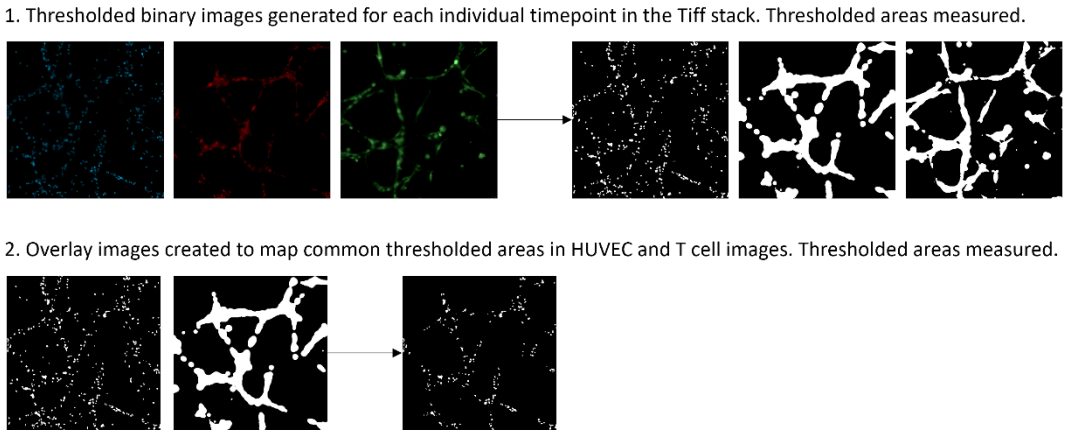

Figure 2.1 Image analysis protocol for HUVEC capillary-like network assay.

Separately, the Angiogenesis Analyzer tool by Gilles Carpentier [396] was run on the phase contrast images to estimate the total branching network length, with the following parameters: minimum object size, 25 pixels; minimum branch size, 50 pixels; artifactual loop size, 850 pixels; isolated element size threshold, 50 pixels; master segment size threshold, 30 pixels; 3 iterations.

2.2.5. Zebrafish husbandry and embryo xenograft assays

2.2.5.1. Licence details

All animal work was conducted under personal licence IFD3CD6DB, and project licence PF74F0848 (Dr Adam Hurlstone, '*Zebrafish models for investigating cancer formation and progression, immune responses and immunotherapy*'), according to National Home Office regulations under the Animals (Scientific Procedures) Act 1986.

2.2.5.2. General husbandry

Adult zebrafish were housed in the University of Manchester Biological Services Facility (BSF) where they were subject to a 14 h/10 h light/dark cycle and a set water temperature of 28.5 ˚C. Fish were fed twice-daily with an age-determined diet, comprising powdered food, brine shrimp and rotifers. For this study, all assays were carried out using *nacre* fish, which lack melanophores due to a nac^{W2} mutation [397].

2.2.5.3. Breeding

Zebrafish were bred either by marbling or by pairwise breeding in breeding boxes. For routine breeding purposes, a specialised crossing tank with mesh insert (Aquaneering) was half filled with marbles and placed in the main tank the evening before the planned mating. Breeding was initiated by the beginning the light cycle, and embryos were collected 1 hour later.

For zebrafish embryo assays requiring embryos of standardised age, pairwise mating was used to ensure synchronous fertilisation. Male and female zebrafish were placed in a crossing tank with mesh insert (Aquaneering) either side of a divider which spanned the width of the tank and left overnight. On initiation of the light cycle the next morning, the divider was removed, and breeding occurred, with fertilised eggs collected after 20 minutes.

Embryos were raised in petri-dishes (Greiner Bio-One) in chorion water (60 mg/L Instant Ocean Salts (Tropic Marin) with 0.0001 % (w/v) methylene blue in dH_20), at a maximum density of 50 animals per dish. Embryo water was exchanged daily, and screening was performed to remove any dead/abnormal animals. To raise new generations, fry were transferred to the BSF's nursery system at 5 days post fertilisation (dpf).

2.2.5.4. Zebrafish anaesthesia and euthanasia

MS222 (tricaine methanesulfonate, Sigma) was used for zebrafish embryo anaesthesia and euthanasia. A buffered stock solution of pH 8.5 containing 4 g/L MS222 (15.4 mM) and 20 mM Tris was diluted 1:25 for the purposes of anaesthetising embryos, and 1:10 for euthanasia. Adult zebrafish were euthanised using an overdose of anaesthetic (2000-2800 ppm Aqua-Sed) followed by rapid freezing.

2.2.5.5. Tumour and T cell xenotransplantation

Tumour and T cells were prepared for xenotransplantation as follows. 888-Mel MCAM GFP target cells were labelled with Vybrant DiI (Invitrogen), diluted 1:200 in serum-free DMEM for 20 minutes at 37 ˚C. T cells were labelled with Cell Trace Violet as previously described (2.2.3.6). Mixed suspensions were generated containing 1 x 10^7 cells/mL 888-Mel MCAM-GFP targets, with or without 5 x 10^5 cells/mL CAR T cells, in PBS with 1 % (v/v) polyvinylpyrrolidone solution (PVP, Sigma) to reduce clumping. Cell suspensions were kept on ice and xenotransplantation assays were performed immediately.

Needles for embryo injections were produced by pulling borosilicate glass capillaries (Harvard apparatus, GC100TF-10) in a Flaming/Brown micropipette puller (model P-97). 4 µL of cell suspension was back-loaded into the needle, which was mounted on a micro-manipulator attached to a PLI-90A Pico-Injector micro-injection station (Warner

instruments) with inverted microscope. The tip of the loaded needle was broken using forceps immediately prior to embryo injections.

Nacre embryos at 52 hpf were anaesthetised in MS222 (600 µM) in chorion water and placed on pre-made injection plates—9 mm petri-dishes (Greiner Bio-One) coated with 1.5 % (w/v) agarose (Bioline) in chorion water. The needle was advanced into the pericardial space (PCS) and approximately 1nL of cell suspension was injected.

Embryos were screened immediately using a microscope with UV source and fluorescent filter cubes, and successfully injected embryos were revived in fresh chorion water.

2.2.5.6. Imaging zebrafish embryos

For confocal imaging, xenografted embryos were embedded in 9mm petri-dishes in 1.5 % (w/v) low gelling temperature agarose (Sigma) in chorion water without methylene blue.

Images were acquired on a Leica SP8 Upright Confocal microscope, with 25x/0.95 NA water-immersion objective and the following confocal settings: format - 1024 x 1024, scan speed – 600Hz unidirectional, zoom factor - 1, pinhole – 1 airy unit. Images were acquired using hybrid detectors, with the below settings. Due to crosstalk, images using the blue diode and white light laser (WLL) were acquired sequentially. 3D optical stacks of the pericardiac space region were acquired using a z-step size of 1.4 µm.

Table 17: Laser and detector settings for the SP8 Upright Confocal Microscope.

Label	Laser line	Laser power	Hybrid detector setting
CTV	Blue Diode, 405 nm	20 %	408-463 nm
GFP	WLL, 488 nm	25 %	498-545 nm
DiI	WLL, 549 nm	20 %	559-726 nm

2.2.5.7. Image analysis

Z-stacks were exported from the Leica microscope as .lif files, for further processing in Image J (Fiji)[395]. The Fiji Bio-Formats tool was used to import each z-stack, splitting the images acquired on different channels. Basic image processing was performed on each z-stack to optimise contrast, following which maximum intensity projections were generated. These were converted into 8-bit thresholded binary images to facilitate measurement of the tumour and T cell area with the Fiji Analyse tool.

2.2.6. Statistical analysis

Figure generation and statistical analysis was performed in GraphPad Prism (Version 9.0, GraphPad Software Inc). Unless otherwise specified data are presented as mean ± standard deviation. Statistical analysis was by paired t-test, one-way or two-way ANOVA according to the assay design, followed by Tukey's multiple comparisons test where stated in figure legends. For the HUVEC network assays, best-fit curves were estimated using non-linear regression, and compared using the extra sum of squares F test. P values less than 0.05 were taken as significant.

Chapter 3. Initial assessment of CAR activity in the JRT3-T3.5 cell line.

3.1. Introduction

CAR specificity is determined by the binding properties of the incorporated scFv. To generate appropriate anti-MCAM CAR constructs for further study, a series of second generation 4-1BB-CD3ζ CARs with differing scFv regions were first screened for their ability to induce signalling in the JRT3-T3.5 cell line. JRT3-T3.5 is a CD3/TCR-deficient derivative of the E.6 (JM) Jurkat line, a T cell acute lymphoblastic leukaemia (T-ALL) line which was originally isolated from the peripheral blood of a 14-year-old male [398] Gamma-irradiated E.6 Jurkat cells were cultured in the presence of complement and antibody specific to the CD3ε chain (OKT3) in order to enrich for CD3- cells by negative selection [399]. Such cells were then isolated by FACS. Characterisation of the JRT3-T3.5 Jurkat line by flow cytometry confirmed that not only was cell surface CD3 lacking, but the TCR was also undetectable [399].

Subsequent Northern blot analysis for the TCRα and β chains revealed that JRT3-T3.5 cells express a truncated transcript of the β chain which lacks the variable and diversity gene segments [400]. Furthermore, transcription of the α chain is also significantly reduced. Transfection with TCRβ cDNA not only restored expression of the TCR (as determined by northern blot and flow cytometry) but also the cell surface CD3 complex, demonstrating a requirement for co-expression.

This feature makes the JRT3-T3.5 line an attractive model in which to screen CAR constructs, as it removes the potentially confounding effect of the endogenous TCR. JRT3-T.3 cells also have an oncogenic mutation in CDK6 [401], and non-functional tumour suppressor genes PTEN and SHIP (reported for the parental Jurkat line) [402–404], which likely contributes to their rapid and sustained proliferation. This has practical benefits in terms of cell culture, for example through facilitating the expansion of transduced cells following FACS. It also increases the cost-effectiveness of such a model when contrasted to sourcing primary T cells from multiple donors. The use of JRT3-T3.5 removes donor-to-donor variation observed with primary T cells,

allowing the differential activity of the CAR constructs to be more easily isolated. Lastly, as an established cell line, JRT3-T3.5 have fewer biosafety considerations than primary T cells.

Nevertheless, there are drawbacks to this system, principally that JRT3-T3.5 do not retain the full array of effector functions mediated by primary T cells. However, it is possible to determine whether CAR constructs can trigger activating signals when exposed to their cognate antigen, which is the first fundamental requirement of any new CAR. Expression of the early activation marker CD69 has successfully been used to detect the activation of CAR-expressing JRT3-T3.5 and predicts to an extent the degree of activation mediated by the same constructs in primary T cells [405, 406].

The production of CAR-expressing JRT3-T3.5 cells first requires an efficient transgene delivery system. Multiple gene transfer delivery methods exist, however most CARs tested to date have utilised retro- and lentiviral systems [407–414]. Retroviral systems generally require virus producer cell lines which stably express the viral *gag* and *pol* genes under the control of a strong promoter [415]. The third component of the viral genome, *env,* is either stably expressed or can be transiently introduced on a plasmid for customisable tropism. Typically, the producer cell lines are then transfected with a transfer plasmid which contains the transgene of interest flanked by 5´ and 3´ long terminal repeat (LTR) sequences and the ψ Psi packaging sequence [415].

Assembly of replication-incompetent retrovirus begins with the association between RNA dimers (in this case encoding the transfer cassette) and the Gag protein, contingent on the presence of the ψ sequence. These complexes assemble with Pol and are released from the cell, acquiring a lipid bilayer in the process on which the envelope proteins are expressed. Following release, the immature virions undergo a maturation process whereby Gag and Pol are cleaved, producing key structural (capsid, nucleocapsid and matrix) and functional (integrase and reverse transcriptase) proteins, respectively [416].

The mature virions infect target cells by a process triggered by binding of the envelope protein to its cellular target. This triggers the fusion of the viral envelope and the cell membrane, releasing the viral core. A cDNA copy of the RNA genome is generated by

reverse transcriptase and inserted into the host cell DNA by integrase, whereupon transgene expression is driven by promoters and enhancers contained within the LTR region [416].

Described herein is the initial work to express a panel of MCAM-specific second-generation CAR constructs in the JRT3-T3.5 cell line, and to quantify MCAM-dependent CAR activity. This necessitated cloning anti-MCAM scFvs into a retroviral CAR construct, optimising the protocols for Jurkat transduction and CAR-driven activation, and eventually selecting functional scFvs for further study.

3.2. Methods

3.2.1. Cloning CAR-encoding retroviral constructs

The pMP71.tCD34.2A.CD19.CD8.4-1BB.CD3ζ retroviral vector was kindly provided by Dr David Gilham [417]. An unmethylated preparation of the plasmid was purified from *dam*$^{-}$*/dcm*$^{-}$ competent *E.coli* (New England Biolabs), allowing a restriction enzyme digest to be performed with NotI-HF and ClaI (both New England Biolabs) which cleave the plasmid at sites immediately flanking the scFv. The reaction was treated with Antarctic Phosphatase and Antarctic Phosphatase Buffer (New England Biolabs) to prevent re-annealing, prior to gel purification of the 6.3kb backbone fragment using a 1 % agarose gel and Monarch DNA Gel Purification Kit (New England Biolabs; section 2.2.1.2).

Sequences for 3 MCAM-binding scFvs were kindly provided by Professor Bin Liu (M1 and M40 scFvs; University of California) and Dr Bridget Hantusch (B6-11 scFv; Medical University of Vienna). The sequence of the variable heavy and variable light domains from the MCAM-specific ABX-MA1 antibody was obtained from a lapsed antibody patent (US-7090844, Dr Bar-Eli et al 2006), whilst Dr Blot-Chabaud (Aix-Marseille University) kindly provided the corresponding sequences for the tsCD146 antibody. ABX-MA1 and tsCD146 derived scFvs were designed to match the M1, M40 and B6-11 scFvs, with 5' variable heavy domains and 3' variable light domains separated by a 15 amino acid (G4S)3 glycine-serine linker sequence.

Genestrings (Thermo Fisher) incorporating the various scFv sequences with flanking NotI and ClaI sites were designed and PCR amplified using Q5 Hot Start High Fidelity DNA polymerase (New England Biolabs) and complementary primers (see Table 6 for primer sequences and section 2.2.1.1 for PCR reaction mix and thermocycling conditions). PCR products were purified with Monarch DNA Clean-up Columns (New England Biolabs), digested with NotI-HF and ClaI to produce sticky ends compatible with the digested backbone, and gel purified as above. T4 DNA Ligase (New England Biolabs) was used to insert the scFv sequences into the vector backbone, using a 1:3 vector-to-insert molar ratio. Ligation reactions were incubated for 24 hours at room

temperature, prior to transformation into XL-1 competent cells (Agilent, section 2.2.1.3). Plasmid DNA was isolated with the Monarch DNA Plasmid Miniprep Kit (New England Biolabs; section 2.2.1.3), and bidirectional sequencing over the ligation sites (Eurofins Lightrun Services) was used to confirm successful cloning, prior to high quality plasmid preparation using the Purelink Fast Low Endotoxin Midi Plasmid Purification Kit (Invitrogen).

3.2.2. JRT3-T3.5 cell culture

The JRT3-T3.5 Jurkat cell line was maintained in RPMI-1640 medium supplemented with 10 % heat-inactivated FBS, 50 IU/ml penicillin, 50 µg/ml streptomycin and 10 ul/ml Glutamax. Cells were subcultured every 2-3 days to maintain a density of 1-2 x 10^6 cells/ml.

CAR-expressing Jurkat lines were generated by retroviral transduction. Briefly, PhGP retrovirus producer cells were transiently transfected with a plasmid bearing the VSVG envelope protein and the CAR encoding retroviral vectors (see section 2.2.2.6). Mock transfections lacking the pMP71 transfer plasmid were performed to generate mock retrovirus.

In early experiments the resulting retrovirus was used to directly transduce JRT3-T3.5 cells using a RetroNectin-based protocol (section 2.2.2.7). In later iterations of the protocol, stable retrovirus producer cell lines were generated by transducing the PG13 cell line with the PhGP retroviral supernatant. The resulting cell lines stably produced CAR-encoding, GaLV-pseudotyped retrovirus and were enriched for successfully transduced cells by magnetic sorting for CD34 (section 2.2.2.6). RetroNectin based Jurkat transductions then proceeded as described (section 2.2.2.7) using the PG13 retroviral supernatant. CAR^+ Jurkat were then isolated by flow cytometry, using CD34 expression as a proxy for CAR expression (section 2.2.2.8). CAR-Jurkat activation on coculture with target cell lines was quantified by assessing CD69 and CD62L expression by flow cytometry, as described in section 2.2.3.1.

3.2.3. Generating target cell lines

MCAM-expressing target cell lines were generated using the CSII_lenti_MCAM-GFP plasmid, which was kindly provided by Dr Natalie Ahn (University of Colorado). This third-generation lentiviral vector encodes full length human MCAM tagged with cytoplasmic GFP under the CMV promoter, with HIV-1-derived LTR and ψ packaging sequences. A truncated control construct lacking the 5 extracellular immunoglobulin domains (CSII_lenti_trunc.MCAM-GFP) was cloned as described below.

The sequence spanning the GFP tag, MCAM cytoplasmic and transmembrane domains and short (50 amino acid) extracellular stalk was PCR amplified using Q5 Hot Start High Fidelity DNA polymerase (See sections 2.1.4 and 2.2.1.1). Primers were designed to incorporate 5´ NheI and 3´ NotI restriction enzyme sites into the resulting PCR product, which was purified using Monarch DNA Clean-up Columns. Restriction enzyme digestion with NotI-HF and NheI (New England Biolabs) was performed to generate sticky ends, and the 1.2kb trunc.MCAM-GFP encoding PCR product was gel purified using a 1.5 % agarose gel and the Monarch DNA Gel Extraction kit.

Concurrently, the original CSII_lenti_MCAM-GFP vector underwent digestion with NotI-HF and NheI to cleave the plasmid at sites flanking the MCAM-GFP sequence. The 10kb vector backbone was gel purified as described above, and the trunc.MCAM-GFP encoding PCR product was ligated in at a 1:3 vector-to-insert ratio using Instant Sticky End Mastermix (New England Biolabs) as per manufacturer's recommendations. Ligation reactions were transformed into XL-1 competent cells with ampicillin selection. DNA isolation, sequencing and plasmid preparation were performed as described above.

VSVG-pseudotyped MCAM-GFP and trunc-MCAM-GFP encoding lentivirus was generated using the Lenti-X producer cells (as described in section 2.2.2.5) and used to transduce the 888-Mel cell line. Simultaneously, an 888-Mel line expressing human CD19 was generated for use as a target for the anti-CD19 positive control CAR. A Murine Moloney Leukaemia virus (MMLV) based retroviral vector encoding full length CD19 followed by an internal ribosome entry site and GFP sequence was kindly provided by Dr Eleanor Cheadle [418]. Retrovirus was produced by transient

transfection of PhGP cells with the vector and a VSVG-encoding plasmid, and 888-Mel cells were transduced as above. The resulting 888-Mel MCAM-GFP, 888-Mel trunc-MCAM-GFP and 888-Mel CD19-GFP cell lines were sorted for GFP expression by FACs (see section 2.2.2.8).

Protein expression was confirmed by western blot (section 2.2.1.6) and flow cytometry using the APC anti-MCAM antibody (BioLegend) and Live/Dead Fixable Blue Kit (Thermo).

3.2.4. Rearranging the pMP71 vector backbone

The pMP71.tCD34.2A.CD19.CD8.4-1BB.CD3ζ retroviral vector was rearranged to place the CAR in the 5´ position, separated by the 2A linker from the 3´ tCD34 marker gene. A HindIII/EcoRI restriction enzyme digest was performed to cleave the vector either side of the tCD34-2A-CAR transgene, and the remaining vector backbone was gel purified. The rearranged plasmid sequence was modelled in silico, allowing the design of 2 genestrings which spanned the scFv-CD8-4-1BB and CD3ζ-2A-TCD34 transgene sequences, respectively. Appropriate homology regions were added to the 5´ and 3´ ends of the Genestrings, which were PCR amplified and gel purified. Assembly of the DNA fragments into the cleaved vector backbone was performed using the NEBuilder HiFi DNA Assembly Master Mix (New England Biolabs) and a 1:2 vector-to-insert molar ratio. Bacterial transformation, DNA extraction, sequencing and plasmid preparation all proceeded according to standard protocols (see above). Once the correct sequence had been confirmed, the CD19 scFv was exchanged for the M1 and M40 scFvs via a NotI-HF and ClaI restriction enzyme digest, as described above. PG13 retrovirus producer cell lines were then generated and used to transduce Jurkat cells as previously described.

3.3. Results

3.3.1. Generation of MCAM-specific CAR-encoding vectors

To drive CAR expression on JRT3-T3.5 cells, we utilised a pMP71 retroviral vector kindly provided by Dr David Gilham (Figure 3.1a). In this plasmid, Murine Myeloproliferative Virus (MMPV) LTR regions surround the transgene cassette. pMP71 vectors are particularly efficient in primary human T cells and T cell lines when compared to earlier vectors containing LTRs derived from the Moloney Murine Sarcoma Virus (MMSV) [419]. The transgene cassette included: 1) a truncated form of human CD34, lacking the majority of its intracellular signalling domain but allowing cell surface labelling and sorting; 2) a self-cleaving 2A linker from the foot-and-mouth-disease virus [420, 421] to allow expression of two proteins from a single mRNA; and 3) the CAR itself downstream of an oncostatin M leader sequence for plasma membrane targeting) (Figure 3.1a and b). The CAR itself contained a scFv, comprising antibody V_H and V_L domains arranged in tandem with a flexible glycine-serine linker. The scFv is presented on a short extracellular stalk derived from human CD8α, which also contributes the CAR transmembrane domain. The intracellular portion of the receptor contains signalling domains derived from human 4-1BB and CD3ζ (inclusive of its 3 ITAMS) (figure 3.1b).

To redirect the above CAR construct against MCAM, the existing scFv was substituted for a panel of 5 different MCAM-specific scFvs. The M1 and M40 scFvs (sequences kindly provided by Professor Bin Liu, University of California, San Francisco) were originally characterised by a study aiming to identify internalising mesothelioma-specific scFvs, with a view to conjugating them to chemotherapeutic agents as a means of targeted drug delivery [422]. A phage display library of more than 500 million human scFv sequences underwent successive rounds of positive selection using mesothelioma cell lines. M1 and M40 were amongst the 21 candidate sequences which were selected for further study.

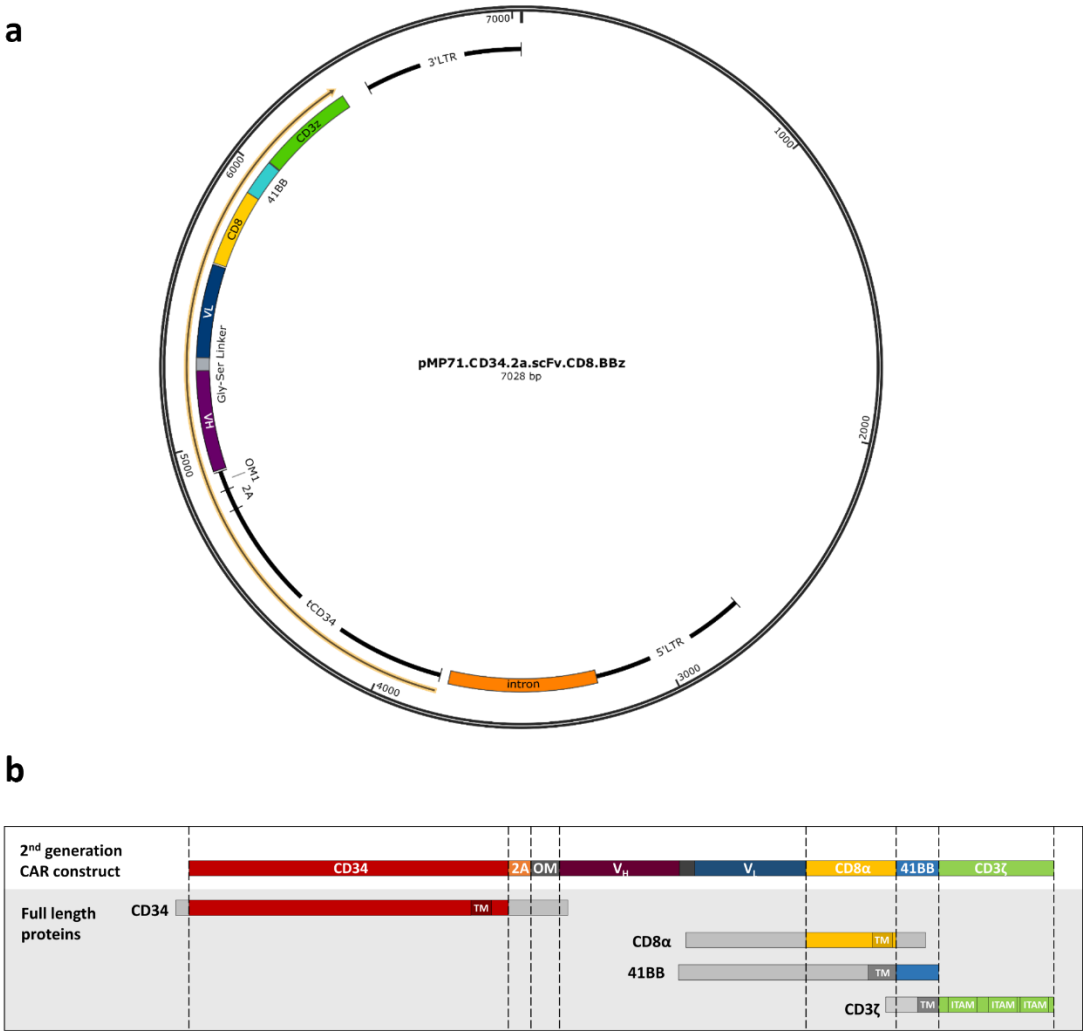

Figure 3.1 Schematic of the CAR construct.
(a) Plasmid map of the pMP71.tCD34.2A.CAR retroviral vector, inclusive of ampicillin resistance gene, truncated CD34, 2A linker sequence, oncostatin signal peptide and CAR construct. (b) Design of the construct, demonstrating relative contributions from CD34, CD8α, 4-1BB and CD3ζ. Top panel, schematic of the receptor; bottom panel, full length proteins. Coloured blocks represent protein domains included in the receptor, while grey regions are excluded. TM, transmembrane domain; ITAM, immunoreceptor tyrosine-based activation motif. Plasmid maps created on SnapGene.

Subsequent characterisation demonstrated the reactivity of the scFvs against epithelioid and sarcomatoid mesothelioma as well as cell lines derived from breast, ovarian and prostate cancer, with a lack of activity against the non-malignant cell lines tested. Competitive binding analysis using soluble and phage-displayed scFv confirmed that M1 and M40 bind to distinct epitopes. MCAM was subsequently identified as the target antigen by a screen performed using a yeast-displayed cDNA library of human cell surface proteins [423].

The B6-11 scFv (sequence kindly provided by Dr Bridget Hantusch, Clinical Institute of Pathology, Medical University of Vienna, Vienna, Austria) was similarly generated by phage display, with successive rounds of panning performed using blood endothelial cells [424]. MCAM was subsequently identified as its cognate antigen via liquid chromatography with tandem mass spectrometry and confirmed by co-labelling of B6-11 bound antigen with commercially available anti-MCAM antibodies. B6-11 also bound to melanoma cell lines and labelled the vasculature in human tissue sections in a comparable manner to known MCAM-specific antibodies.

For the purposes of this project, a fourth anti-MCAM scFv sequence was obtained from a lapsed antibody patent (antibody sequence C3.19.1 from patent US-7090844, published by Bar-Eli et al in 2006). ABX-MA1 is a fully human monoclonal antibody first described by Mills et al [425], which was raised against the SK-MEL-28 melanoma cell line in the XenoMouse line (Abgenix). These animals carry human heavy and light chain antibody genes in place of the murine counterparts, and therefore produce affinity matured human antibodies on immunisation [426].

The presence of ABX-MA1 in culture media has diverse cellular effects, including reduced proteolytic activity and corresponding reductions in invasiveness by melanoma cells, and impaired network formation by HUVECs. *In vivo*, ABX-MA1 treatment reduced the tumour burden in nude mice with subcutaneous A375SM or WM2664 tumours, and inhibited metastasis formation when tumours were inoculated intravenously. Ex vivo immunohistochemical analysis of the tumours revealed reduced tumour blood vessel formation and increased apoptosis, potentially accounting for the observed differences in tumour formation. Contrastingly, when this work was repeated with osteosarcoma cells no effect on tumour growth was observed, although the impact on metastasis and *in vitro* behaviour was conserved [427].

Sequence for the final anti-MCAM scFv was kindly provided by Dr Marcel Blot-Chabaud (Aix-Marseille University) [428]. tsCD146 was so named due to its apparent ability to discriminate between MCAM expressed on malignant cells (tumour-specific; ts) and the physiological form of the protein expressed on healthy tissues such as blood vessels. This rat monoclonal antibody displays reactivity against melanoma, pancreatic cancer and colon cancer cell lines, but differed from established MCAM-specific

antibodies in that it did not bind to HUVEC and HMEC-1. This selective binding was further demonstrated in immunofluorescence experiments using whole tissue sections, in which tsCD146 selectively labelled tumour cells and did not stain the vasculature. As with ABX-MA1, tsCD146 functionally impacted MCAM-expressing tumour cells, selectively reducing their proliferation and inducing apoptosis *in vitro,* and significantly reducing melanoma growth in NOD/SCID mice.

A positive control CAR was also generated using a validated anti-CD19 scFv (provided by Dr Eleanor Cheadle), originally derived from the HD37 hybridoma [429]. Expression of first-generation CARs bearing the CD19 scFv conferred on primary T cells the ability to recognise and kill $CD19^+$ target cells *in vitro,* as determined by cytokine production, degranulation, and target cell lysis [417, 418]. Such cells were also able to eradicate established B cell lymphoma in immunocompromised mouse models [417, 418].

3.3.2. Optimising the Jurkat transduction method

Initial attempts to express the CAR constructs in the JRT3-T3.5 Jurkat cell line utilised retrovirus generated by the Phoenix GP (PhGP) retroviral producer cell line [415]. PhGP cells are a 293T derivative which stably express *gag* and *pol* genes from the Moloney murine leukaemia virus (MoMLV) under the RSV promoter. As such, they are capable of short-term retrovirus production when provided *in trans* with an *env* gene and retroviral transfer plasmid containing LTR and ψ sequences.

The PhGP system was used to generate CAR-encoding retroviruses pseudotyped with the *env* gene from the vesicular stomatitis virus Indiana variant (VSVG), which confers greater stability and broad cellular tropism compared to earlier viruses bearing the MoMLV envelope protein [430]. VSVG-pseudotyped retrovirus and Jurkat cells can be colocalised on plates pre-coated with RetroNectin, a chimeric protein with C/CS-1 and heparin-binding domains which bind to cells and virions, respectively [431] (Figure 3.2, left panel). The VSVG transmembrane G-protein binds to the cell surface LDH receptor [432], triggering receptor-mediated endocytosis, and the viral core is released into the

cytoplasm by pH-dependent fusion of the viral envelope and endosomal membrane [433][434].

To test this protocol in the context of the Jurkat cell line, retrovirus was produced using the pMP71.tCD34.2A.M1.BBz construct. Mock retrovirus was generated by transfecting PhGP with the *env* plasmid alone. Jurkat transductions were performed (Figure 3.2a, left panel) and transduction efficiency was assessed 4 days later by flow cytometry. The tCD34 marker gene (a proxy measure for CAR expression) was detected on less than 30 % of Jurkat cells (Figure 3.2b), indicative of sub-optimal transduction.

The JRT3-T3.5 Jurkat line is highly proliferative and therefore could potentially be expanded from a low seeding density after sorting for successfully transduced cells. However, this model was to be used as an intermediary step prior to the use of primary T cells, which present additional challenges to successful transduction. In our hands, primary T cells proliferate at a much slower rate than Jurkats, so the actively dividing fraction which is amenable to transduction will represent a smaller proportion of the overall population. In addition, the LDH receptor to which VSVG binds is only upregulated on activated T cells [135]. Furthermore, primary T cells cannot be expanded ad infinitum, so sorting and expanding a small number successfully transduced cells would likely present difficulties.

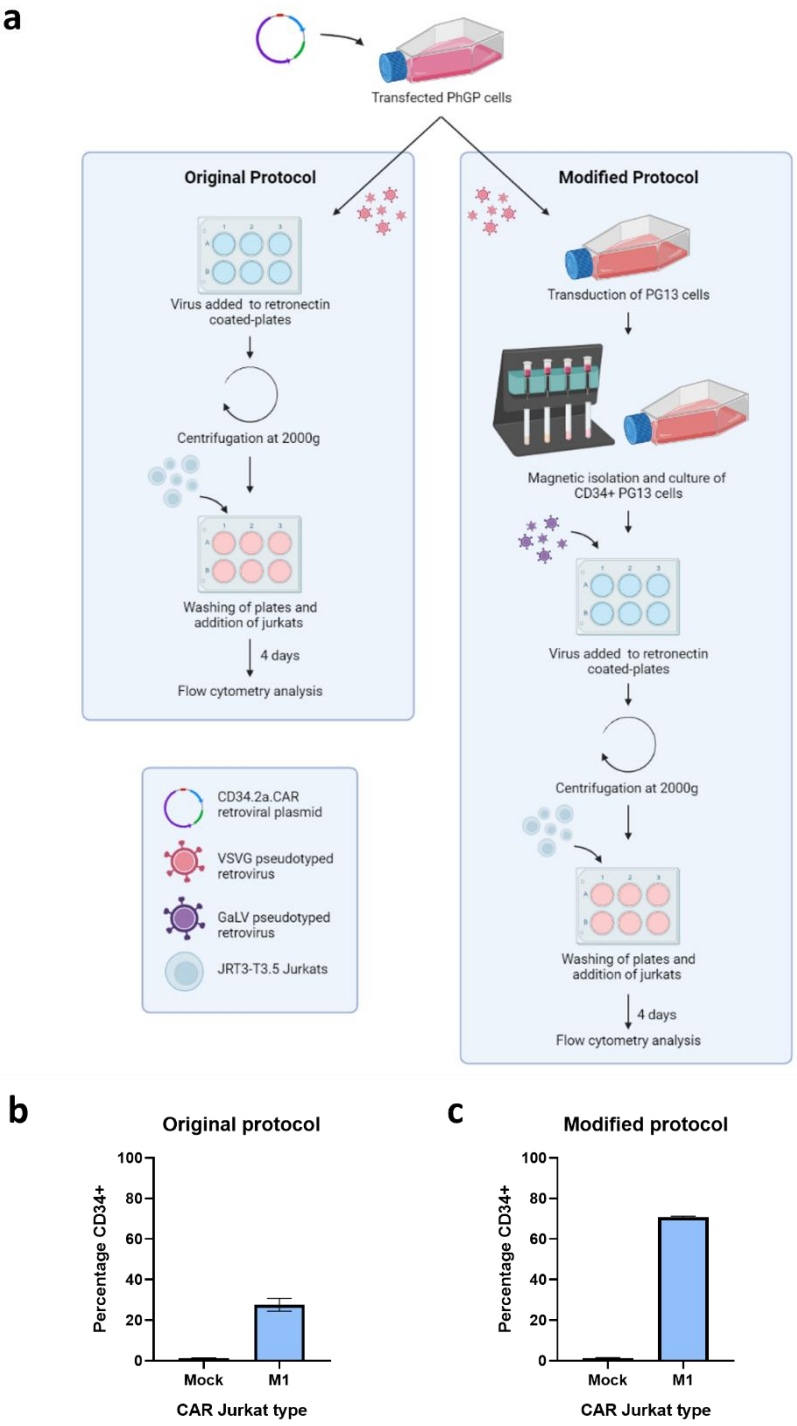

Figure 3.2 Optimisation of the retroviral transduction protocol for the JRT3-T3.5 Jurkat cells.

(a) Schematic of the original and modified transduction protocols. Retroviral supernatant was collected from transiently transfected PhGP cells (original protocol) or PG13 cells which had been transduced with the CAR constructs (modified protocol) and sorted for to isolate a successfully transduced population of stable retrovirus-producing cells. For both protocols, a RetroNectin coating process was then used to co-localise retroviral supernatant and the JRT3-T3.5 cell line. Transduction efficiencies were determined by measuring expression of the tCD34 marker protein via flow cytometry for mock and M1 JRT3-T3.5 Jurkats generated using the (b) original protocol or (c) modified protocol. Results are displayed as mean and standard deviation, and assays were performed in triplicate. Schematic made with BioRender.com.

For these reasons, further optimisation of the virus production and transduction processes was performed using Jurkats. Specifically, stable-retrovirus production was achieved using the PG13 line, a derivative of NIH 3T3 mouse embryonic fibroblasts [435]. As with PhGP, PG13 cells stably express the MoMLV *gag* and *pol* genes, however they also have the *env* gene from the gibbon ape leukaemia virus (GaLV). The broad tropism and stability of VSVG have led to its widespread use in retro and lentiviral systems, however unlike GaLV it is ultimately toxic when expressed in cells and therefore not optimal for use in stable retroviral producer systems [430]. The GaLV receptor has been identified as the sodium dependent phosphate transporter SCL20A1 [436][437], expression of which is detected on T cells [438].

The use of this PG13-based system confers 2 major advantages: Firstly, generating stocks of stable retrovirus-producing cells eliminates potential variability between different transductions introduced by the transfection of PhGP cells. Secondly, successfully transduced PG13 cells, which contain all the required elements to produce CAR-encoding retrovirus, will express cell surface tCD34. Magnetic sorting for CD34 was used to enrich for these cells, and Jurkat transductions were performed using the supernatant (Figure 3.2a, right panel). This increased the percentage of $CD34^+$ Jurkats by more than 2-fold (70.6 %; Figure 3.2c), representing a clear improvement in transduction efficiency.

3.3.3. Generating CAR expressing Jurkat cell lines

Following the above protocol, retrovirus-producing PG13 lines were generated for the anti-MCAM and anti-CD19 second generation CAR constructs. Jurkat transductions were performed as described, and the resulting CAR-Jurkat populations were characterised by flow cytometry for tCD34 and western blot. CD34 expression ranging from 61.1-81.3 % was observed for all CARs (Figure 3.3a) with the highest transduction efficiencies observed for the CD19 CAR, as measured by percentage $CD34^+$ and CD34 staining intensity (Figure 3.3b). Cells were then sorted for tCD34 expression and frozen stocks were generated for use in future assays.

To detect CAR expression in the sorted CAR-Jurkat populations, flow cytometry was first performed to confirmed that all populations were comparably enriched for CD34 (average percentage CD34 expression across all groups was 93.2 %, range 91.5 - 95.0 %). Western blots were then performed under reducing conditions using an antibody specific to the intracellular region of CD3ζ. Bands of the expected molecular weight (approximately 50kDa) were detected for all constructs apart from mock, however the intensity of expression differed, with especially low levels for the B6-11 CAR (Figure 3.3c). Of interest, the molecular weight of the B6-11 CAR was somewhat higher than expected, suggesting aberrant transgene processing may have occurred despite the plasmid sequence being correct.

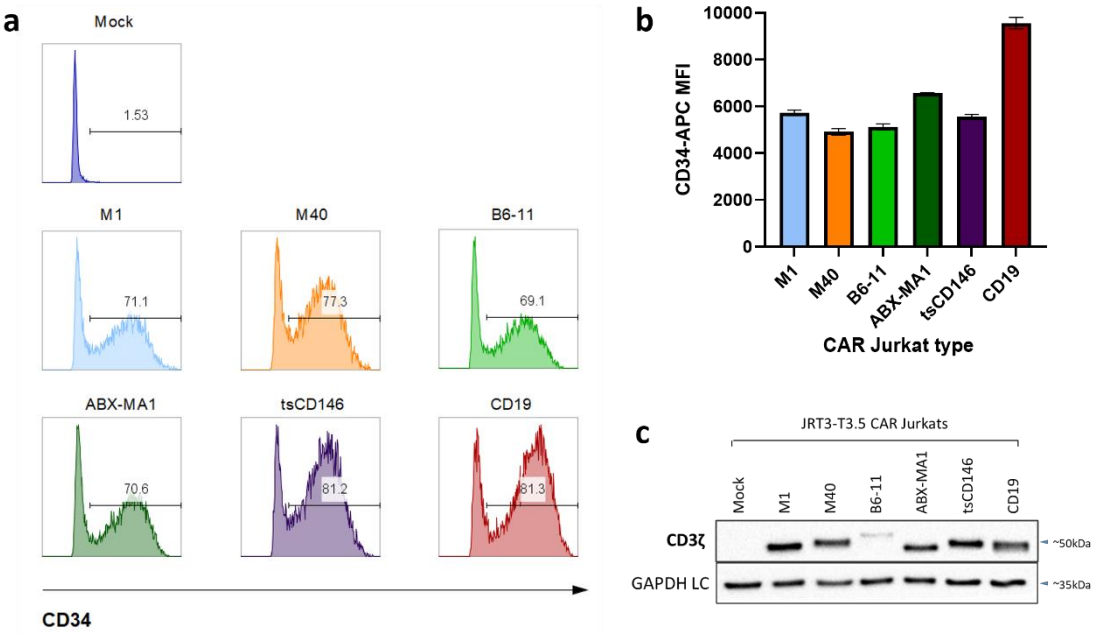

Figure 3.3 CAR expression on the Jurkat cell line
Expression of CD34, as assessed by flow cytometry, on JRT3-T3.5 Jurkats retrovirally transduced with MCAM-specific CAR constructs. Mock CAR Jurkats were transduced with OptiMEM alone. (a) percentage of live, single cells expressing CD34 and (b) CD34-APC mean fluorescence intensity (MFI) of live, single cells. (c) Confirmation of CAR expression on CD34-enriched CAR-Jurkats via western blot for CD3ζ located within the endodomain of the CAR construct. Results are displayed as mean and standard deviation and all assays were carried out in triplicate.

3.3.4. Generating 888-Mel target cell lines

The 888-Mel cell line was used to generate cellular targets for *in vitro* assays. This line was originally established from a metastatic lesion in the soft palate of a 26 year-old female melanoma patient, who later had a (non-sustained) complete response to TILs derived from the same tumour biopsy [439–442]. The lack of MCAM expression by 888-Mel has been reported in the literature [443, 444], and was confirmed by western blot for the MCAM endodomain and ectodomain (Figure 3.4b).

Transduction with a third-generation lentiviral construct was used to achieve expression of full length human MCAM with an additional cytoplasmic GFP tag under the CMV promoter (Figure 3.4a) [445]. As there is evidence that the cytoplasmic domain of MCAM has signalling and binding activity [326, 446–448], a control construct was cloned which preserves this region, but has a deletion affecting the majority of the sequence encoding the extracellular region. Termed trunc.MCAM-GFP, the resultant protein lacks the 5 immunoglobulin domains but retains a short extracellular stalk, along with the transmembrane, cytoplasmic and GFP regions (Figure 3.4a).

Targets for the control anti-CD19 CAR were generated using an alternative retroviral construct which contains full length CD19 and GFP. In this system the GFP does not take the form of an endodomain tag, but rather is independently expressed as separate protein due to an interposed IRES sequence (Figure 3.4a) [418]. While GFP in this system is found within the cytoplasm rather than associated with the membrane, it serves the same purpose as a marker of successfully transduced cells and was used for cell sorting and as a means of discriminating target cells from effectors in downstream flow cytometry-based functional assays.

888-Mel transductions were performed with the above constructs and successfully transduced GFP^+ cells were isolated by FACS. Expression of the relevant proteins was assessed by western blotting under reducing conditions along with flow cytometry, using the WM2664 melanoma cell line as a positive control on account of its widely reported expression of endogenous MCAM [256, 425, 443, 449, 450].

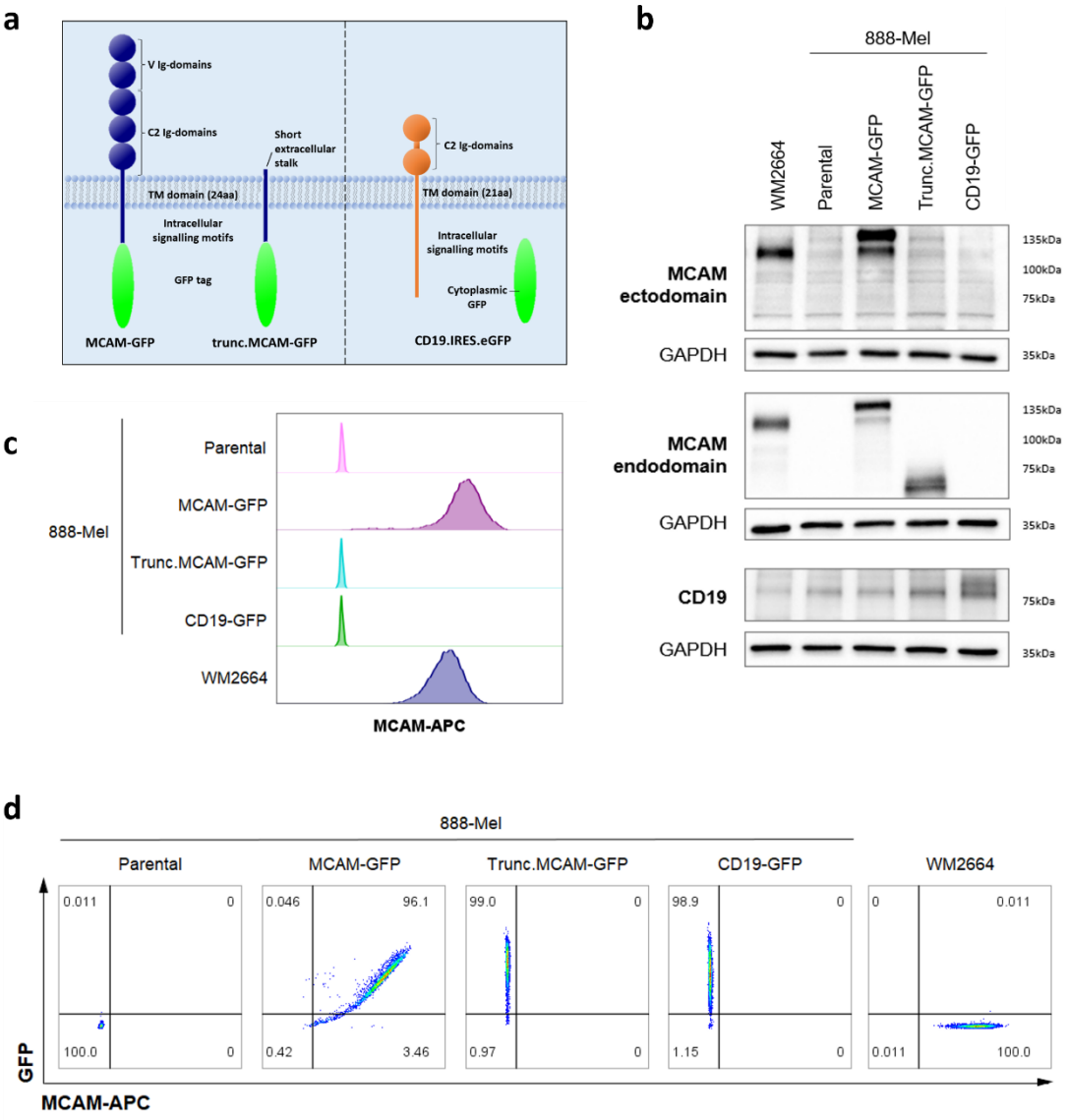

Figure 3.4 Development of 888-Mel target cell lines
(a) Schematic of proteins produced by MCAM-GFP, trunc.MCAM-GFP and CD19.IRES.eGFP constructs. (b) Western blot of parental 888-Mels, 888-Mel MCAM-GFP, 888-Mel trunc.MCAM-GFP and 888-Mel CD19-GFP cell lines with antibodies against the MCAM ecto- and endodomain and CD19. (c, d) confirmation of MCAM and GFP expression by flow cytometry.

As expected, MCAM is not detected on parental 888-Mel by western blot (Figure 3.4b) or flow cytometry (Figure 3.4c and d). Contrastingly, probing the WM2664 lysates with antibodies against the MCAM ecto- and endodomains confirms the presence of a 115kDa species corresponding to endogenous MCAM. This expression is confirmed by flow cytometry using an APC-conjugated antibody from an independent clone which binds to the extracellular domain of MCAM.

The MCAM-GFP protein has an increased expected molecular weight of 150kDa on account of the GFP tag. A species of this weight was detected by western blot with both anti-MCAM antibodies, suggesting that the 888-Mel line had been successfully transduced. These findings were confirmed by flow cytometry, which indicates that MCAM expression by the 888-Mel MCAM-GFP and WM2664 lines is broadly comparable. As expected, there is also evidence of a positive correlation between MCAM and GFP expression by 888-Mel MCAM-GFP. Interestingly a secondary band of approximately 115kDa was detected by western blot, which may represent a species of MCAM lacking the GFP tag, potentially resulting from a proteolytic cleavage event.

Western blotting of 888-Mel trunc.MCAM-GFP with the endodomain-specific antibody identifies a significantly smaller species of approximately 75kDa, in agreement with the expected molecular weight of the truncated protein. This species was not detected when lysates were probed with the ectodomain specific antibody. Furthermore, analysis of the line by flow cytometry confirmed that such cells lack expression of the target antigen of APC anti-MCAM but do retain GFP. Taken together, these findings confirm that the 888-Mel trunc.MCAM-GFP line does express a truncated protein which lacks the MCAM extracellular domain but retains the endodomain and GFP tag. The distribution of GFP within the cell was comparable with the 888-Mel MCAM-GFP line by microscopy (data not shown) suggesting that the full length and truncated proteins are localised at the cell membrane.

As expected, probing the 888-Mel CD19-GFP lysate with the anti-MCAM antibodies reveals no bands other than those representing non-specific binding by the ectodomain antibody. A CD19-specific antibody confirms the presence of a band of the predicted molecular weight (95kDa) however this band is faint and is partly obscured by a non-specific band immediately below it. Nonetheless, when combined with the expression of GFP as confirmed by microscopy and flow cytometry, such cells were deemed to have been successfully transduced. Indeed, their ability to activate CD19-CAR expressing effector cells in downstream function assays appears to validate this conclusion (see below).

3.3.5. Assessment of CAR-mediated Jurkat activation

The ability of anti-MCAM CAR constructs to induce activation in the Jurkat cell line was assessed by measuring their expression of the cell surface markers CD69 and CD62L. CD69 is an early activation marker which is upregulated on primary T cells following stimulation. Elevated expression has been detected as early as 4 hours post stimulation [451] and is generally reported to peak at around 24 hours [451–453]. Its early-stage upregulation and conserved expression by Jurkats has led to its use as a means of detecting the CAR-mediated activation of such cells [405, 406]. Furthermore, CAR constructs which mediated CD69 upregulation by Jurkats were also capable of activating primary T cells, demonstrating the utility of this marker as an initial screening tool [405, 406].

Initially, pilot experiments were carried out to optimise the assay, using Jurkats transduced with the CD19-BBz positive control CAR. Optimal cell seeding numbers were determined by incubating CAR Jurkats with either parental or CD19-GFP 888-Mels at defined effector-to-target ratios. After 24 hours the fraction of the Jurkat population expressing CD69 was determined by flow cytometry. When Jurkats were cocultured with an equal number or an excess of target cells (1:1 and 1:2 effector-to-target ratios, respectively), CD69 was upregulated in an apparently antigen-independent manner. Expression was elevated on Jurkats incubated with both the parental and CD19-expressing targets compared to baseline (Jurkats cultured in media; Figure 3.5a), potentially due to nutrient depletion due to the high cell input number. When target cells were plated at lower density (5:1 and 10:1 effector-to-target ratios), CD69 expression on Jurkats cocultured with parental 888-Mels was equivalent to baseline levels. Reducing the non-specific activation allowed the CAR-mediated increase in CD69 to be resolved. An effector-to-target ratio of 10:1 was selected for subsequent assays.

CD69 is detectable early in the activation of T cells, however the exact kinetics of this appear to be influenced by the stimulus [451–453]. To determine the optimal coculture length, CD69 upregulation by CD19-BBz Jurkats was assessed as described above, using a 10:1 effector-to-target ratio (Figure 3.5b). The incubation times

assessed appeared to have minimal impact, however there was a trend towards increasing background expression at later time points. Background activation was lowest at the 12-hour time point, however for practical reasons a 16-hour culture period was selected for subsequent assays.

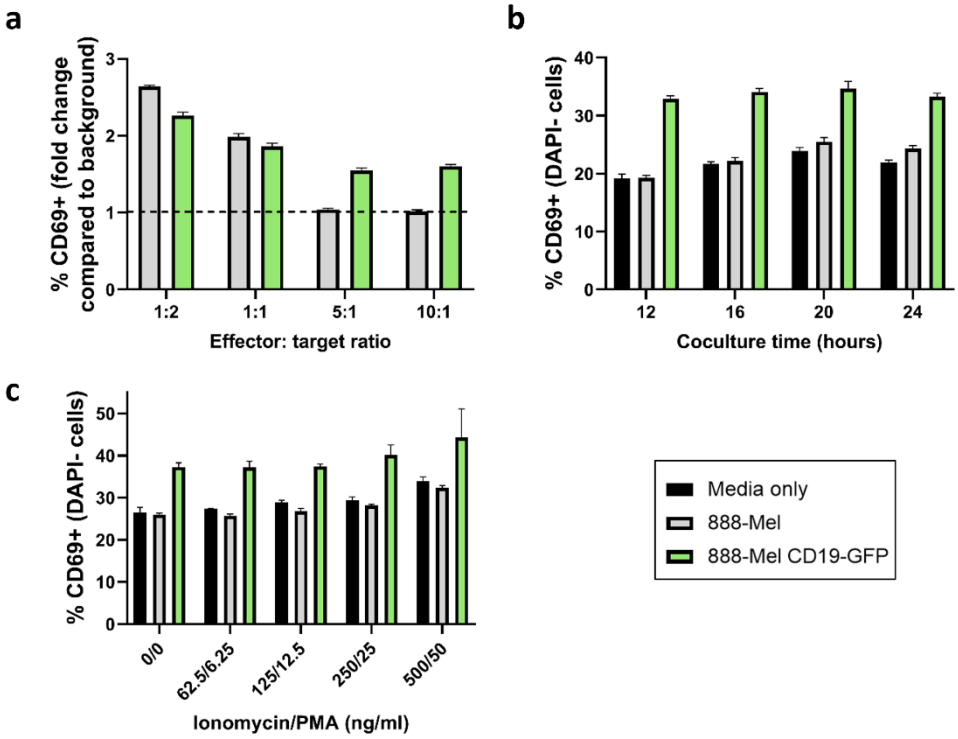

Figure 3.5 Optimisation of the CD69-based CAR-Jurkat activation assay.
Jurkats transduced with anti-CD19 CAR constructs were cultured in the presence of media, 888-Mel or 888-Mel CD19-GFP targets to identify the optimal (a) coculture time, (b) effector-to-target ratio and (c) to determine whether pre-stimulation for 2h with PMA and ionomycin was required for optimal activation. Activation was determined as the percentage of live (DAPI-) cells expressing CD69, and are presented as either fold change compared to Jurkats cocultured in media alone, or as the overall percentages. Results are displayed as mean and standard deviation and all assays were carried out in triplicate.

The extent of the CD69 upregulation observed in these preliminary assays was relatively low, and therefore we investigated whether providing an additional stimulus would improve their activity, as described in the early Jurkat literature [399, 400]. To this end, CD19-BBz Jurkats were pre-incubated with varying concentrations of PMA and ionomycin. After 2 hours cells were washed, and CD69-upregulation assays were performed as described above. While pre-treatment appeared to mediate a slight increase in both the background and CAR-mediated CD69 expression, any effect was

minimal and therefore subsequent assays were performed without pre-stimulation (Figure 3.5c).

Based on these pilot assays, activation by the full panel of CAR Jurkat lines was determined following a 16-hour coculture with the target-expressing 888-Mel cell lines, plated at a 10:1 effector-to-target ratio. In addition to CD69, CD62L served as a secondary indication of activation. CD62L (L-selectin) is a transmembrane glycoprotein expressed by naïve T cells, which plays a key role in their trafficking and migration into peripheral lymphoid organs (reviewed in [454]). Its loss from the cell membrane via enzymatic shedding occurs within 4 hours post-activation and correlates with the cytotoxic potential [455].

Cells were stained with antibodies to CD69 and CD62L as well as CD34, which allowed the analysis to be limited to CAR-expressing cells (Figure 3.6a). Of the 5 anti-MCAM CAR Jurkat lines, only M1.BBz and M40.BBz mediated CD69 upregulation (Figure 3.6b, and c) and CD62L loss (Figure 3.6d) on coculture with the 888-Mel MCAM-GFP target cell line. As expected, this effect was dependent on the presence of the MCAM-ectodomain and was not observed on coculture with the trunc.MCAM-GFP lines. While the M1.BBz and M40.BBz only activated a minority of the overall population as assessed by CD69 expression, the magnitude of the effect is equivalent to that observed with the control CD19-BBz Jurkats in the presence of the 888-Mel CD19-GFP line.

The tsCD146 antibody is reported to only bind to MCAM expressed by tumour cells, potentially due to recognition of an epitope generated by a tumour-specific post-translational modification, which may conceivably be absent from the MCAM-GFP protein. To whether the tsCD146 could bind to endogenous MCAM, preliminary CD69 upregulation assays were performed using the 888-Mel and WM2664 cell lines, which have absent and strong MCAM expression, respectively (Figure 3.4b). In this context, the tsCD146.BBz Jurkats did not display any evidence of activity above that observed with the CD19.BBz control, suggesting that this is not the case (Figure 3.6e).

To assess whether the scFvs could cross react with mouse MCAM, CD69 upregulation in response to YUMM cells was assessed. YUMM1.1, YUMM1.7 and YUMM2.1 are

mouse melanoma cell lines with common driver mutations including *Braf* activation and *Pten* inhibition [456]. Western blot analysis revealed that MCAM is expressed at low levels by YUMM1.1 but is abundant on YUMM2.1, while YUMM1.7 serves as an MCAM-negative control (Figure 3.7a). CD69 expression by CAR Jurkats following coculture with the above lines was not suggestive of CAR-driven activation, with equivalent CD69 percentages and MFI values observed for the control CD19 CAR Jurkats (Figure 3.7b and c).

Taken together, the above data suggest that second generation 4-1BB-CD3ζ CARs with M1 and M40 antigen recognition domains are able to bind selectively to the ectodomain of human MCAM and initiate Jurkat activation. No evidence was found to suggest that the B6-11, ABX-MA1 or tsCD146 scFvs were able to mediate activation in the same context. M1- and M40.BBz CAR constructs were therefore selected for further study.

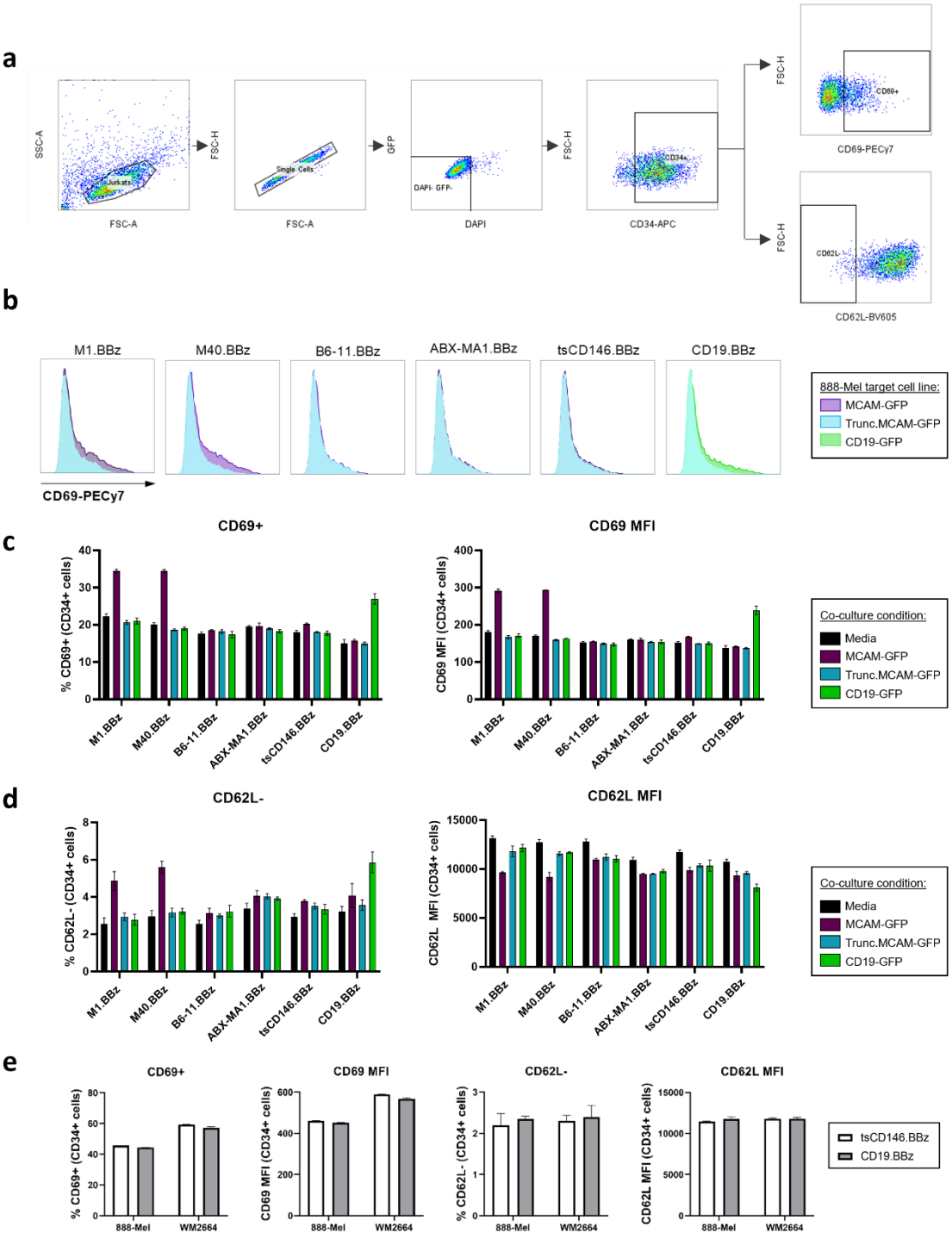

Figure 3.6 Activation of CAR-Jurkats in response to 888-Mel target cell lines.
JRT3-T3.5 Jurkats transduced with anti-MCAM and anti-CD19 CARs were cocultured for 16 h with target cell lines or media alone. Activation was determined as CD69 upregulation and CD62L loss on CD34 positive CAR Jurkats. (a) gating strategy (b) histogram overlays of CD69 expression on CD34 positive Jurkats when cocultured with 888-Mel MCAM-GFP (purple) or CD19-GFP (green) cell lines. 888-Mel trunc.MCAM-GFP (blue) is plotted as a negative control. The percentage of cells and MFI are presented for (c) CD69 and (d) CD62L. (e) Activation of tsCD146.BBz and CD19.BBz Jurkats in response to endogenous MCAM expressed by the WM2664 line.
All results displayed are for CD34 positive cells, experiments were performed in triplicate.

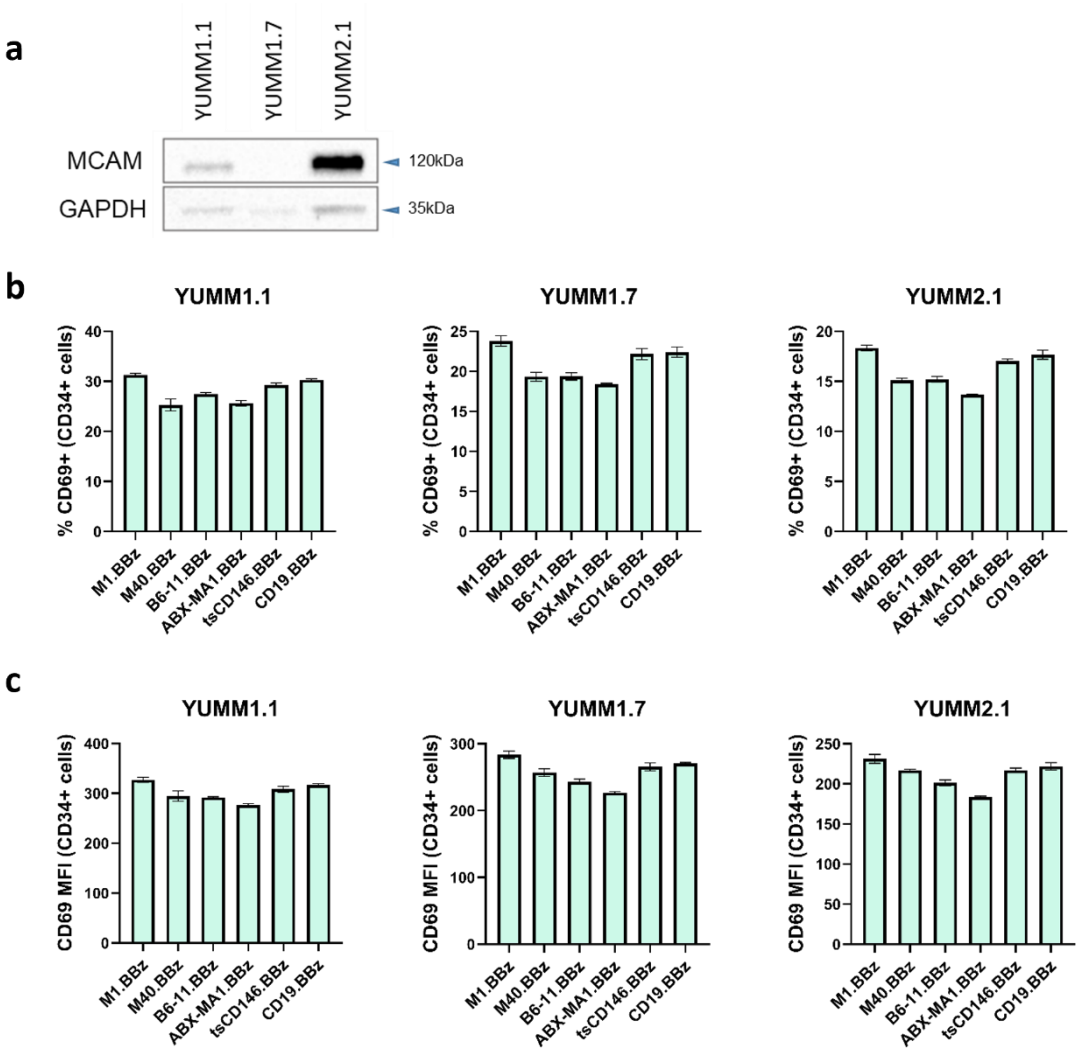

Figure 3.7 Jurkat activation in response to murine MCAM.
JRT3-T3.5 Jurkats transduced with anti-MCAM and anti-CD19 CARs were cocultured for 16 h with target cell lines or media alone. Activation was determined as CD69 upregulation on CD34 positive CAR Jurkats. (a) Western blot analysis of murine MCAM expression on a panel of mouse melanoma cell lines. (b) Percentage of CD34+ Jurkats expressing CD69, and (c) CD69 MFI on CD34+ Jurkats. Data is presented as mean and standard deviation; experiments were performed in triplicate.

3.3.6. Rearranging the vector backbone

The extent of Jurkat activation in the above assays was modest, with even the CD19.BBz construct only activating a small proportion of the overall Jurkat population, despite the scFv being previously validated. We reasoned that this could be in part due to low levels of CAR expression. In the pMP71 construct, tCD34 and the CAR are separated by a 2A linker derived from the foot-and-mouth virus. The 22 amino acid

sequence contains a 3´ glycine-proline motif, which is the site of a co-translational 'cleavage' event, thought to be due to skipping of the peptide bond [420, 421]. The upstream polypeptide (in this case tCD34 with a C-terminal 2A tag) is released from the ribosome, while the remaining mRNA is translated to produce the CAR construct, complete with an N-terminal proline residue. This system has been used in the context of T cells to mediate co-equal expression of both CAR/reporters [417] and other immune markers [457].

Although in theory the 2A linker should ensure that there is equimolar expression of the upstream and downstream transgenes, aberrant ribosome skipping could cause unequal protein expression. Incomplete cleavage has been observed with the 2A linker sequence utilised in this vector [458], and would result in the expression of a 90kDa tCD34-CAR fusion protein. Alternatively, successful cleavage followed by a failure to re-start translation would result in the sole expression of tCD34. Both scenarios would result in a reduction in functional CAR protein. Probing CAR-Jurkat lysates with a CD3ζ-specific antibody only resolved bands corresponding to the CAR, with no evidence of a tCD34-CAR fusion protein (Figure 3.3c). However, the variable intensities of CAR expression across the Jurkat lines (which had equivalent tCD34 levels) could indicate a potential failure of translation downstream of the 2A sequence.

We reasoned that expression of the protein downstream of the 2A linker is contingent on successful translation of the upstream protein, and therefore by placing the reporter gene downstream of the CAR construct we could more confidently assume that CD34+ cells also expressed the CAR. Therefore, the existing M1.BBz-encoding vector (pMP71.tCD34.2A.M1.BBz; Figure 3.8a) was re-cloned to place the CAR transgene in the 5´ position, with tCD34 located downstream of the 2A linker (pMP71.M1.BBz.2A.tCD34; Figure 3.8b). Transduction of Jurkats with the 2 constructs resulted in good CD34 expression, which was marginally lower for the rearranged construct (Figure 3.8c). By contrast, CAR expression on such cells was elevated as assessed by western blot, which demonstrated an increase in the size of the CAR construct commensurate with the 22 amino acid 2A tag which remains attached to the upstream protein (Figure 3.8d).

Given that the 2A tag is affixed to the C terminal domain of the CD3ζ CAR signalling domain, there was a risk that it could have impeded signalling. To test this, activation of M1.BBz.2A.tCD34 and tCD34.2A.M1.BBz Jurkats was assessed following coculture with MCAM-GFP and trunc-MCAM-GFP expressing 888-Mel targets. Quantification of CD69 and CD62L expression by $CD34^+$ Jurkats revealed that the M1.BBz.2A.tCD34 construct significantly increased MCAM-dependent activation when compared to the original plasmid design (Figure 3.8e-h). However, we did also observe a modest increase in the background activation of such cells, albeit only as assessed by CD69 upregulation (media only). This increased tonic signalling could potentially be caused by the presence of the 2A tag. Perhaps a more likely explanation is that this does not represent an inherent increase in the tonic signalling potential of the CAR, but rather reflects the fact that CAR expression on the M1.BBz.2A.tCD34 Jurkats is likely to be higher than when tCD34 is placed upstream of the 2A linker.

Given that the rearranged construct mediated both increased in CAR expression and efficacy of Jurkat activation, this plasmid design was selected for use in subsequent studies.

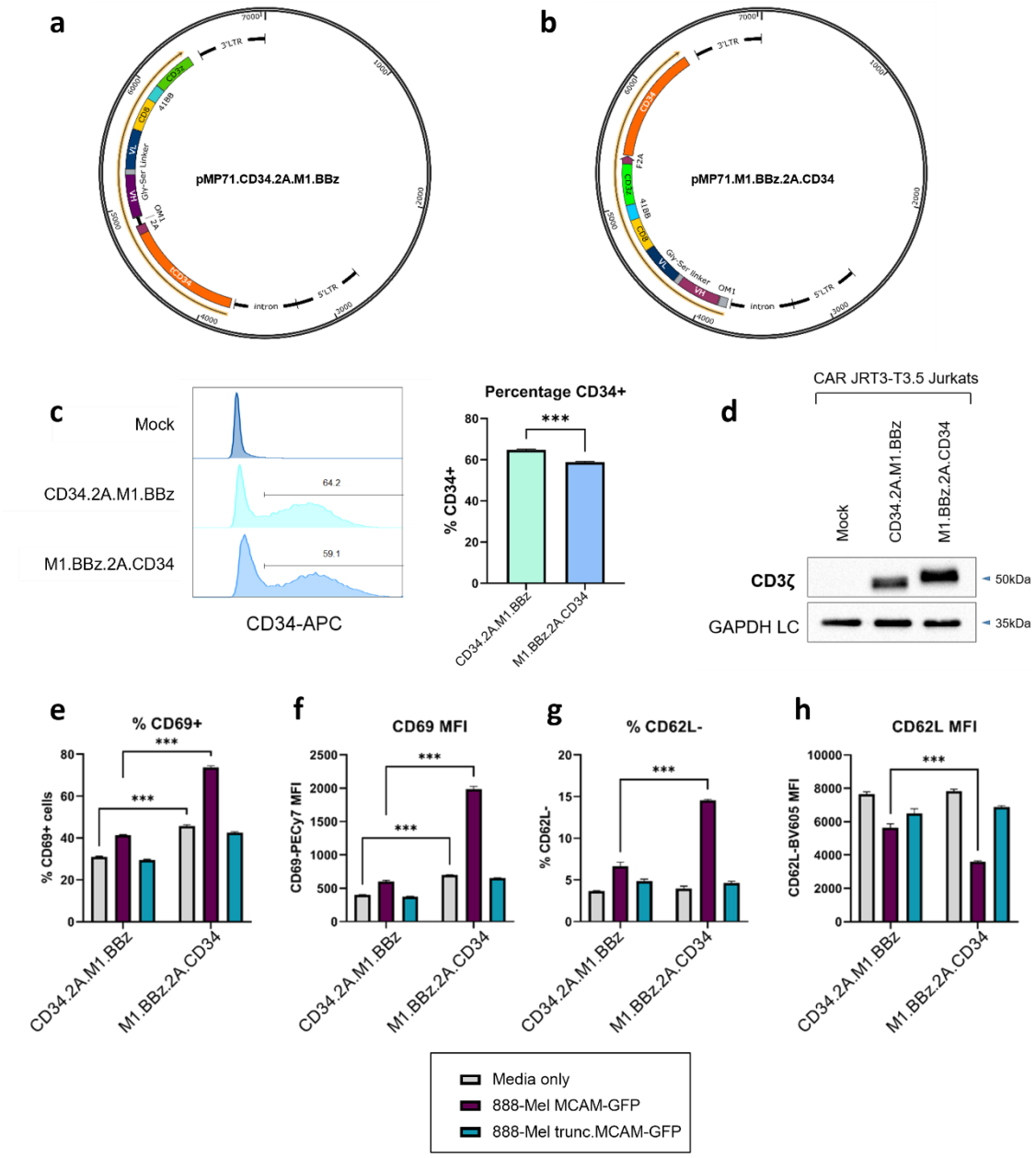

Figure 3.8 Rearrangement of the pMP71 vector.
(a) Plasmid map of the original construct, in which tCD34 is upstream of the CAR, and (b) the rearranged CAR construct with tCD34 downstream of the CAR. (c) CD34 expression as a proxy for CAR expression on JRT3-T3.5 cells transduced with the original and rearranged M1.BBz plasmids. (d) Confirmation of CAR expression via western blot for CD3ζ located within the endodomain of the CAR construct. To investigate the effect of the rearranging the pMP71 construct on JRT3-T3.5 Jurkat activation, M1.BBz CAR Jurkats were cocultured for 16 hours with target cell lines or media alone. Activation was determined as CD69 upregulation and CD62L loss on CD34 positive cells. (e) percentage of cells expressing CD69, (f) CD69 MFI, (g) percentage CD62L negative cells, and (h) CD62L MFI. All results displayed are for CD34 positive cells, experiments were performed in triplicate. Statistical analysis was by unpaired t-tests (c) or two-way ANOVA with Tukey's multiple comparisons (e-h). ** p<0.01, *** p<0.001.

3.4. Discussion

Described above is the initial preliminary characterisation of a panel of anti-MCAM CAR constructs, performed using CAR-expressing Jurkats. The Jurkat cell line is a transformed T cell line which has been widely used in the field of T cell biology to advance our understanding of T cell signalling (see [459] for review). However, as with all transformed lines, concerns remain over how closely the biology of Jurkat cells approximates that of primary human T cells. Most notably, this study made use of the JRT3-T3.5 Jurkat sub-line, which lacks expression of the TCR and CD3 due to a TCRβ gene mutation [399, 400]. For our purposes, this is advantageous as it eliminates the possibility of confounding TCR-driven Jurkat activation, however it does mean that any conclusions regarding CAR functionality must be interpreted in this context.

Subsequent research on the Jurkat parental line has identified further abnormalities which raise questions about how closely their signalling models that of normal T cells. Physiological T cell responses involve multiple signalling cascades, including those which affect lipid metabolism. TCR-driven signalling results in the activation of phospholipase C (PLC), which catalyses the hydrolysis of PIP_2 into IP_3 and DAG. Meanwhile PIP_2 is also involved in the PI3K signalling cascade, which can be activated by a multitude of drivers including cytokines and chemokines, antigenic stimulation, and costimulatory ligands. PI3K converts PIP_2 to PIP_3, to which PH-domain containing proteins bind, localising them to the cell surface. Most notably, this results in the activation of Akt. PIP_3 degradation is mediated by PTEN and SHIP, both of which are mutated in the Jurkat cell line. Their defective expression results in high basal PIP_3 levels and constitutive Akt signalling [402–404].

Furthermore, primary T cells do not just receive signalling through their TCR (or CAR) but also receive additional signals in the form of costimulatory ligands, cytokines, and chemokines, which serve to modulate their activity and control their differentiation. Primary T cell effector functions are diverse, and are not conserved in the Jurkat line, activation of which is predominantly assessed by CD69 expression [405, 406]. Put in this context, the Jurkat cell line represents a very simplified model of T cell responses which limits the conclusions that can be drawn on the efficacy of our CARs.

Nonetheless, they do allow us to address fundamental initial questions about the scFvs, specifically whether they are capable of selectively binding to antigen when expressed as part of a CAR and whether the affinity of the interaction is sufficient to initiate downstream activation signals.

Preliminary characterisation of the 5 anti-MCAM scFvs suggests that this is the case for the M1 and M40 scFvs, however it should be noted that the data that supports this conclusion has its limitations. The CD69/62L assays reported above were performed with CAR Jurkats from a single transduction, so while the assays were performed in triplicate, the work lacks biological repetition. Furthermore, CAR Jurkat activity was tested against a narrow panel of target cell lines. Further characterisation of these cell lines is required to confirm that their expression of MCAM is within a clinically relevant range. This would ideally require comparative assessment of target expression on tumour tissues from patients and on the cell lines tested.

That the responses observed in the M1.BBz and M40.BBz expressing Jurkats were of a similar magnitude to those observed with the control CD19 CAR appears promising, although caution should be taken when comparing responses between CARs directed against different antigens. Western blot analysis of the 888-Mel MCAM-GFP and CD19-GFP lines serves to confirm the presence of the respective markers. However, it cannot reliably confirm whether antigen density is equivalent as band intensity is not only determined by the amount of protein, but also the affinity of the detection antibody. Furthermore, even if it were possible to demonstrate parity of CAR response to equivalent antigen densities, this does not necessarily have clinical relevance. It may be that CD19 expression on B cell malignancies is significantly different to the magnitude of MCAM expression on melanoma or other solid tumours.

Nonetheless, the response mediated by M1.BBz and M40.BBz is in accordance with the results of Professor Bin Liu et al, who independently characterised an anti-MCAM CAR utilising the M1 scFv, which was published after the completion of the Jurkat-based assays described above [460]. By chance, the design of the CAR mirrors our second-generation CAR, with CD8α hinge and transmembrane regions and intracellular domains from 4-1BBa and CD3ζ. However, CAR expression was made conditional on the recognition of the tumour associated antigen ALPPL2 through the use of a so called

SynNotch receptor. Primary T cells redirected using this circuit were able to selectively recognise mesothelioma cells *in vitro* and mediated anti-tumour responses in mouse models.

While the performance of the M1.BBz and M40.BBz CARs in the Jurkat assays supports their further characterisation in primary T cells, the same could not be said of the other anti-MCAM CAR constructs. No evidence was observed that the B6-11, ABX-MA1 or tsCD146 constructs were capable of binding MCAM and driving Jurkat activation, as measured by CD69 upregulation and CD62L shedding. M1, M40 and B6-11 scFvs were all similarly identified through phage display [422, 424, 461], while tsCD146 [428] and ABX-MA1 [425, 427] were derived from the sequences of characterised antibodies that had not been previously validated in the form of an scFv. It is possible therefore that the lack of response from the tsCD146 and ABX-MA1 CARs stems from a failure to reconstitute the antigen recognition domain when the V_H and V_L domains are expressed in tandem. Additionally, the ABX-MA1 sequence was acquired from a lapsed patent and it was not possible for us to verify the sequence further, so we cannot rule out sequence errors as the underlying cause of the lack of response.

The tsCD146 antibody differs from the other anti-MCAM reagents in that it is reported to bind selectively to tumour-expressed MCAM, potentially due to recognition of a specific post-translational modification [428]. MCAM expressed by the 888-Mel line might lack this specific epitope, especially given the presence of the GFP tag. However, the tsCD146.BBz CAR fails to drive CD69 upregulation in response to WM2664 which expresses high levels of endogenous MCAM, suggesting that this is unlikely.

Unlike the ABX-MA1 and tsCD146 constructs, the B6-11 sequence was identified through phage display and therefore by definition should bind to MCAM when configured as an scFv. However, the B6-11.BBz construct was notable for its very low expression of CAR by western blot relative to cell surface tCD34. While the reason for this low-level CAR expression is unclear, it seems likely that it underlies the lack of response observed in B6-11 CAR Jurkats. For the B6-11 CAR to be expressed, tCD34 and the 2A linker must first be translated, and the ribosome skipping event at the C terminus of the 2A linker must occur. As evidenced by section 3.3.6, it is apparent that translation of the downstream protein does not then always proceed as it should. This

would explain the unequal expression of the B6-11 CAR and tCD34; however, the B6-11 scFv sequence is not immediately 3´ to that of the 2A linker, as all the CARs are preceded by the same oncostatin M signal peptide. More likely perhaps is that the B6-11.BBz CAR is translated but the scFv sequence results in misfolding of the CAR protein, leading to improper trafficking and/or proteosome- or lysosome-mediated degradation (reviewed in [462]). Indeed, this work has highlighted the importance of confirming cell surface CAR expression, leading to the development of an scFv-detection method for characterisation of primary CAR T cells.

The lack of response of ABX-MA1, tsCD146 and B6-11 could also be caused by the inaccessibility of their respective targets. CARs with scFvs which bind to membrane distal epitopes benefit from shorter hinge regions, while the inclusion of longer hinge regions may improve recognition of epitopes found closer to the cell surface [463]. The location of the epitopes recognised by ABX-MA1, tsCD146 and B6-11 is not known, and therefore it may be that the CD8α hinge region is not of an optimal length to facilitate scFv-MCAM interactions. Ongoing work in the Hurlstone laboratory aims to optimise the hinge for the tsCD146 scFv in light of its reported tumour-specificity; however, this fell outside the scope of this PhD project.

3.5. Conclusion

This initial programme of work, including protocol development and assay design, culminated in the generation of five JRT3-T3.5 Jurkat cell lines expressing a panel of anti-MCAM second generation CAR constructs. Challenge with target cell lines allowed identification of scFv domains which could initiate downstream Jurkat activation dependent on MCAM expression by target cells. The response of the M1.BBz and M40.BBz CARs, which was relatively low in intensity but specific to the MCAM ectodomain, justified selection of these constructs for further functional characterisation in primary T cells. Given the improved CAR expression and Jurkat activation observed when the tCD34 marker gene was placed downstream of the 2A linker, subsequent work was carried out using the rearranged vector design (pMP71.scFv.BBz.2A.tCD34).

Chapter 4. Characterisation of M1.BBz and M40.BBz primary CAR T cells

4.1. Introduction

The JRT3-T3.5 CAR Jurkat lines served as an efficient screening tool through which the M1.BBz and M40.BBz CARs were identified as capable of initiating MCAM-dependent Jurkat activation. Despite being a useful initial model, the Jurkat cell line has very limited effector functions and therefore full characterisation of CAR-driven activity necessitates their expression in primary human T cells.

Sources of human T cells for research use include leukapheresis, whole blood donations, leukocyte reduction filters (LRFs) and leukocyte reduction system (LRS) cones from NHS Blood and Transplant (NHS-BT). Blood products in the UK routinely undergo leukodepletion (defined as the removal of >99 % white blood cells [464]), which serves to reduce the risk of CMV transmission, alloimmunisation and febrile non-haemolytic transfusion reactions [465, 466].

Leukoreduction of whole blood donations is achieved by passing the blood through LRFs (physical filters which trap white blood cells) [467] meanwhile LRS cones sequester leukocytes from apheresis products by the process of elutriation [468, 469] (Figure 4.1). LRS cones are typically discarded once the apheresis procedure has been completed, however if appropriately sealed and processed these by-products provide a plentiful source of leukocytes for laboratory use [470–472]. The majority of the retained cells are CD3+ T cells, with low numbers of B cells and NK cells [470, 471, 473]. CD4+ T cells outnumber those expressing CD8 by approximately 2:1, maintaining the ratio observed in peripheral blood [470, 471, 473]. LRS-derived T cells are functional, and when stimulated by various methods upregulate activation markers [470], degranulate [473] and produce cytokines including IFNγ, TNF-α and IL-2 [472–474].

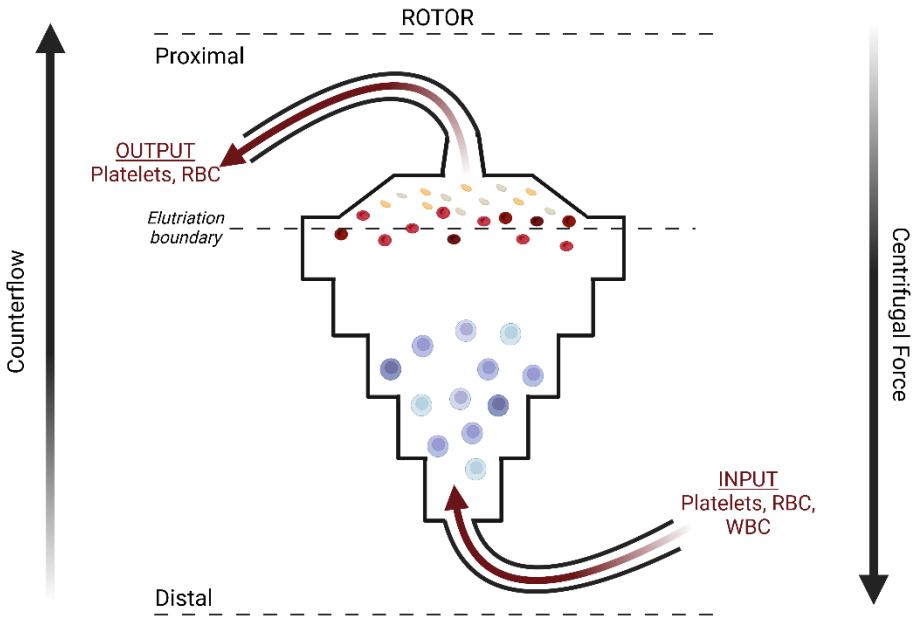

Figure 4.1 Leukocyte isolation in LRS cones
Leukocytes are retained in LRS chambers by a process of elutriation. Cells and platelets flow into the distal end of the cone, which is centrifuged. The position of the cells within the cone depends on the balance between the fluid flow rate and the counteracting centrifugal force. Due to their larger size, leukocytes are subject to stronger centrifugal forces and therefore are retained at the distal end of the chamber, while smaller platelets and red blood cells pass the elutriation boundary. The narrow shape of the proximal end of the cone causes an increase in the fluid flow, forcing red blood cells and platelets out of the cone. RBC, red blood cells; WBC, white blood cells. Adapted from Davis et al, 2001. Figure created with Biorender.com.

Potential platelet donors undergo lifestyle screening by NHS Blood and Transplant, so LRS cones have safety benefits compared to whole blood donations from research volunteers. Additionally, the consent process is simplified as donors provide generic consent for research use prior to donating. The low cost per cone, the large number of leukocytes that can be harvested and their ready availability from blood donation centres combine to make LRS cones an efficient, economical, and practical source of T cells for research. Accordingly, this chapter describes the generation and characterisation of M1.BBz and M40.BBz primary T cells derived from LRS cone leukocytes.

Functional characterisation of CARs involves the assessment of T cell effector functions, which are diverse and vary according to the CD4/CD8 T cell subtype. CAR T cell driven cytotoxicity can be achieved by 2 mechanisms: the release of cytotoxic

granules or the ligation of Fas on target cells by Fas ligand (FasL; reviewed in [475, 476]). Granules contained within cytotoxic CD8+ (and to a lesser extent CD4+ [477]) T cells have a dense core comprised of perforin and granzyme, surrounded by a lysosomal membrane coated with LAMP1 (CD107a) and LAMP2 (CD107b) glycoproteins [478, 479]. On formation of an immunological synapse between a T cell and target, granule exocytosis occurs, releasing perforin and granzyme into the synapse and resulting in the temporary presence of CD107a/b on the cell surface membrane. Granzyme enters the target cells via pores formed by perforin, and triggers apoptosis by caspase-dependent and independent mechanisms. Caspase-3 driven apoptosis is also induced to a lesser extent by Fas-FasL interactions [476]. Typically, CAR driven cytotoxicity is assessed *in vitro* either directly, by measuring target cell viability, or indirectly through the detection of cell surface CD107a as a measure of T cell degranulation [480].

While the killing of target cells by CAR T cells is arguably the most important readout of their activity, maximal anti-tumour responses *in vivo* are likely to require a broader range of effector functions. In addition to inducing target cell apoptosis, CD8+ CTLs are strong producers of pro-inflammatory cytokines, which can be quantified by ELISA or flow cytometry. IFN-γ is a type II interferon secreted by cytotoxic CD8+ effector T cells and Th1 CD4+ helper T cells (reviewed in [481, 482]). It has pleiotropic functions, promoting anti-tumour immune responses by upregulating tumour antigen presentation, enhancing the activation of tumour-associated macrophages, promoting the differentiation of CD8+ cytotoxic T cells and inhibiting tumour angiogenesis. However, it can mediate counteracting immunosuppressive effects by driving the expression of IDO and PD-L1 by tumour cells and recruiting Treg cells to the tumour stroma. Similar contradictory functions have been reported for TNF-α which is also produced by CD8+ CTLs [483]. On the one hand, it enhances the activation of innate immune cells, facilitates lymphocyte migration [483], and can synergise with IFN-γ to drive cancer cells into a senescent state [484]. However, it has also been implicated in activation induced cell death [485] and favours the accumulation and activation of Tregs [486] and MDSCs [487].

While TNF-α and IFN-γ are characteristic CD8+ CTL cytokines, IL-2 is produced predominantly by activated CD4+ T cells. A key driver of T cell proliferation, IL-2 also promotes the differentiation of CD4+ T cells into Th1 and Th2 subsets. Furthermore, it augments the functions of CD8+ CTLs, namely target cell killing and the production of IFN-γ, TNF-α, perforin and granzyme (reviewed in [488, 489]). IL-2 mediates these functions by binding to the IL-2 receptor, which is expressed as either a high affinity trimeric or low affinity dimeric form. The 2 forms are differentiated by the alpha subunit (CD25), which is expressed following TCR ligation on activated CD4+ and CD8+ T cells. The upregulation of similar cell surface proteins provides an additional method of detecting T cell activation, namely the detection of so-called activation markers by flow cytometry. Alongside the cytokine receptor CD25, other canonical activation markers include the TNF family costimulatory receptor 4-1BB/CD137 [490] and the transmembrane receptor CD69 [491], which can all be detected within the first 24 hours after T cell stimulation [451, 452]. Expression of inhibitory receptors more typically associated with an exhausted phenotype such as PD-1, LAG3 and TIM3 also provide confirmation that T cell stimulation has taken place [492].

This chapter describes the isolation of primary CAR T cells from LRS cones, their transduction with CAR-encoding retrovirus, and the expansion and characterisation of the resulting CAR T cells. The activity of the M1.BBz and M40.BBz constructs was assessed *in vitro* with the aim of determining whether the MCAM-dependent activation observed in Jurkat lines would translate into primary T cell effector functions. To this end, multiple assays were performed to quantify CAR-mediated cytokine production, degranulation, activation marker expression and target cell cytotoxicity.

4.2. Methods

4.2.1. Generating CAR T cells

PBMCs were isolated from NHS-BT LRS cones using a Ficoll gradient (section 1.2.2.9) and activated with 300IU/mL IL-2 and 50ng/mL each anti-human CD3 and anti-human CD28. After 2 days, retroviral transductions were performed according to a RetroNectin based protocol (see section 2.2.2.10), in which one full 6-well plate per CAR construct was coated with 20µg/mL RetroNectin and incubated overnight at 4 °C, then blocked with TCM for 30 minutes at room temperature. Filtered viral supernatant from pre-plated PG13 cells was added at 3mL/well. Mock CAR T cells were generated using supernatant from mock (Opti-MEM only) transduced PG13 cells. The plates were then centrifuged for 2 hours at 2000g/32 °C, with a virus exchange step at the halfway point. Plates were washed with PBS prior to the addition of 2mL/well T cell suspension, comprising 1 x 10^6 cells/mL in TCM with 200IU/mL IL-2. A brief centrifugation step (5 minutes at 200g) deposited the T cells on the base of the wells, at which point plates were placed in the incubator overnight. The following day, the cells were harvested and transduced for a second time on fresh RetroNectin-virus coated plates, according to the above protocol.

24 hours after the final transduction, T cell were expanded using G-Rex 6-well cell culture plates (Wilson Wolf) (section 2.2.2.10). T cells were seeded at a density of 15-20 x 10^6 cells/well in 40mL TCM supplemented with 200IU/mL IL-2. On day 4 post-seeding, a 75 % media exchange was performed, and fresh IL-2 was added to a final concentration of 200IU/mL. Subsequent media exchanges took place every 48 hours. The expansion phase lasted 12 days, at which point T cells were harvested, counted and frozen stocks were established (section 2.2.2.4). 2-3 days prior to their use in *in vitro* assays cells were thawed out and allowed to recover in T cell medium supplemented with 200IU/ml IL-2 (see section 2.2.2.4). The CD4:CD8 ratio and CAR transduction efficiency were determined by flow cytometry. Cells were stained with antibodies against CD3, CD4, CD8 and CD34, along with a 2-step scFv labelling process using MCAM-Fc and PE anti-IgG, prior to analysis on a BD Fortessa flow cytometer,

with appropriate single stained and FMO controls (see section 2.2.2.11 for further details).

4.2.2. Characterisation of target cell lines

CAR T cell activity was initially assessed following coculture with the 888-Mel derived cell lines described in section 3.3.4 (888-Mel MCAM-GFP, 888-Mel trunc.MCAM-GFP, 888-Mel CD19-GFP). Subsequent assays were performed using a panel of melanoma cell lines, which included 888-Mel, 501-Mel, C8161 and WM2664. Prior to their use, MCAM expression on the cell lines was quantified by flow cytometry (using Live/Dead Fixable Blue Viability Reagent and a PE anti-MCAM antibody), and western blot with an antibody to the MCAM endodomain.

To facilitate assessment of CAR-mediated target cell cytotoxicity, all the above cell lines were lentivirally transduced with a construct containing firefly luciferase under the CMV promoter, downstream of the puromycin resistance gene (see section 2.2.3.4 for more details). Target cells were then cultured in puromycin-containing culture media (at a pre-determined dose) for 5 days to select for successfully transduced cells.

To quantify growth differences between the lines, the luciferase-expressing variants were plated at varying seeding densities ($2.5 \times 10^3 – 1 \times 10^4$ cells/well) in white walled, flat-bottomed TC-treated plates in 200ul/well supplemented media. Luciferase activity as a proxy of cell growth was measured at seeding and every 24 hours thereafter, for a period of 3 days. 100ul/well Steady Glo Luciferase reagent (Promega) was added per well, the assay was incubated at room temperature with gentle agitation for 20 minutes to ensure lysis was complete, and luminescence was measured in a BioTek Synergy plate reader.

4.2.3. Characterising primary CAR T cells

To facilitate the comparison of the different CAR constructs, for each donor CAR T cells were equalised for transduction efficiency by the addition of mock T cells prior to their use in *in vitro* assays.

Cocultures were established in 96-well round bottomed plates containing 2 x 10^4 target cells and 1 x 10^5 T cells in a total volume of 200ul/well TCM. After 24 hours at 37 °C and 5 % CO_2 plates were centrifuged, and the supernatant and cells were separately isolated. Cell culture supernatant was stored at -80 °C in 96-well non-TC coated plates, prior to quantification of the levels of IFN-γ, TNF-α and IL-2 by ELISA using the respective DuoSet kit (R&D Systems) (see section 2.2.3.2 for more details). Meanwhile the expression of activation and exhaustion markers on the T cells was assessed by flow cytometry (see section 2.2.3.3 for detailed protocol). Briefly, cells were stained with Live Dead Fixable Blue (Thermo) and basic phenotyping antibodies against CD3, CD4, CD8 and CD34, with the addition of anti-CD69, CD25 and CD137 (activation markers) or anti-TIM3, PD-1 and LAG3 (exhaustion markers). PFA fixation was then performed, prior to data acquisition using the BD Fortessa flow cytometer and BD FACS DIVA.

CAR-mediated cytotoxicity was quantified by using luciferase activity as a proxy for cell viability (section 2.2.3.4). Briefly, target cells were plated at 5 x 10^3 cells/well in 96-well white-walled, clear-bottomed TC treated plates. CAR T cells were equalised for transduction efficiency and seeded at varying target-to-effector ratios in a final volume of 100ul/well TCM. Following a 24-hour incubation at 37 °C and 5 % CO_2, the assay was developed using 75ul/well Steady Glo Luciferase Reagent. Lysis was allowed to proceed for 20 minutes at room temperature with gentle agitation on an orbital shaker, and luminescence (RLU) measurements were taken on a Biotek Synergy Plate reader. Background (media-only) luminescence measurements were subtracted from test values, and the percentage target cell survival relative to coculture with mock CAR T cells was calculated as 100 x (CAR T cell coculture RLU/mock coculture RLU).

4.3. Results

4.3.1. Generating primary CAR T cells

In order to generate primary T cells expressing the M1.BBz, M40.BBz and CD19.BBz CARs, it was necessary to first optimise the protocol for their isolation, transduction and expansion, as outlined in Figure 4.2. Briefly, LRS cones from NHS-BT were used as a source of PBMCs, which were isolated using a Ficoll gradient. To activate and expand T cells, PBMCs were cultured for 2 days in the presence of medium-dose IL-2 and activating antibodies against CD3 and CD28. CAR retrovirus producing PG13 cells, which had previously been sorted for CD34 expression, were plated at a predefined density in TCM and allowed to expand. After 2 days, T cells were subjected to 2 rounds of retroviral transduction on RetroNectin coated plates, using the resulting PG13 supernatant.

The manufacturing of T cell products for clinical use generally requires a post-transduction expansion phase to generate large numbers of transduced cells for patient infusions. In pre-clinical pipelines such as described here, T cell expansion protocols similarly serve to generate sufficient cell numbers to facilitate full CAR characterisation across a range of assays. For the purposes of this project, CAR T cells were expanded in G-Rex cell culture devices (Wilson Wolf Manufacturing), which feature a specialised gas permeable silicon membrane on the base of the wells.

In typical cell culture vessels, diffusion occurs at the surface of the media while the T cells settle at the base of the vessel. In G-Rex devices, oxygen/carbon dioxide exchange occurs across the basal membrane, closer to the location of the cells. This also allows the depth of the vessels to be increased to accommodate a larger volume of media, ensuring a ready supply of nutrients and diluting out waste products, and therefore reducing the frequency with which the media must be replenished [493]. This combines to improve the viability of expanded cells compared to traditional methods [494] and has been successfully used to generate large numbers of TILs [495, 496], γδ T cells [497], Treg cells [498] and NK cells [499]. For this scheme of work the R&D grade G-Rex 24- and 6-well plates were used, which have a surface area of $2cm^2$ and $10cm^2$,

respectively. However, the system can be readily scaled up to larger GMP-compatible devices [493].

To determine the optimal seeding density for expansion, frozen PBMCs were thawed and transduced to generate mock and M1.BBz T cells, which were then incubated for 13 days at 0.5 – 2 x 10^6 cells/cm^2 in a G-Rex 24-well plate. Cells were cultured in 4 mL/cm^2 TCM with 200 IU/mL IL-2, and 75 % media changes were performed every 2-3 days, commencing on day 4 post-seeding. Samples were taken at each media change to determine the percentage cell viability, the total viable cell count and the concentration of glucose and lactate in the culture media.

Percentage viability for the various experimental conditions was generally acceptable, with an average of 91.7 % (SD 6.5 %) over all sampling points (Figure 4.2b). For both M1.BBz and mock, a seeding density of 2 x 10^6 per cm^2 gave rise to the highest total viable cell count at day 13, with M1.BBz expanding to a greater extent than mock at comparable seeding densities (Figure 4.2c). Overall, the fold change expansion for this preliminary experiment was low, ranging from 4.8-6.0 for M1.BBz and 1.8-3.8 for mock. To determine if this was due to the availability of nutrients, glucose and lactate in the culture media were measured at each sampling point. As expected, the experimental conditions with the highest seeding densities recorded the lowest glucose and highest lactate values, however the frequent media changes kept the levels within an acceptable range (Figure 4.2d and e).

During routine cell culture it was frequently observed that those PBMCs which had undergone a freeze thaw cycle displayed reduced viability and growth rates compared to freshly isolated cells. Based on the rationale that this may have explained the poor expansion rates achieved in the G-Rex plates, future experiments were conducted with PBMCs which had been freshly isolated from LRS cones immediately prior to their activation. Cells were transduced twice as described above and seeded into G-Rex 6 well plates at a density of 2 x 10^6 per cm^2 in 4 mL/cm^2 TCM with 200 IU/mL IL-2 (total capacity 40mL). Media changes were performed every 2 days from day 4, and cells were harvested after a 12-day expansion period.

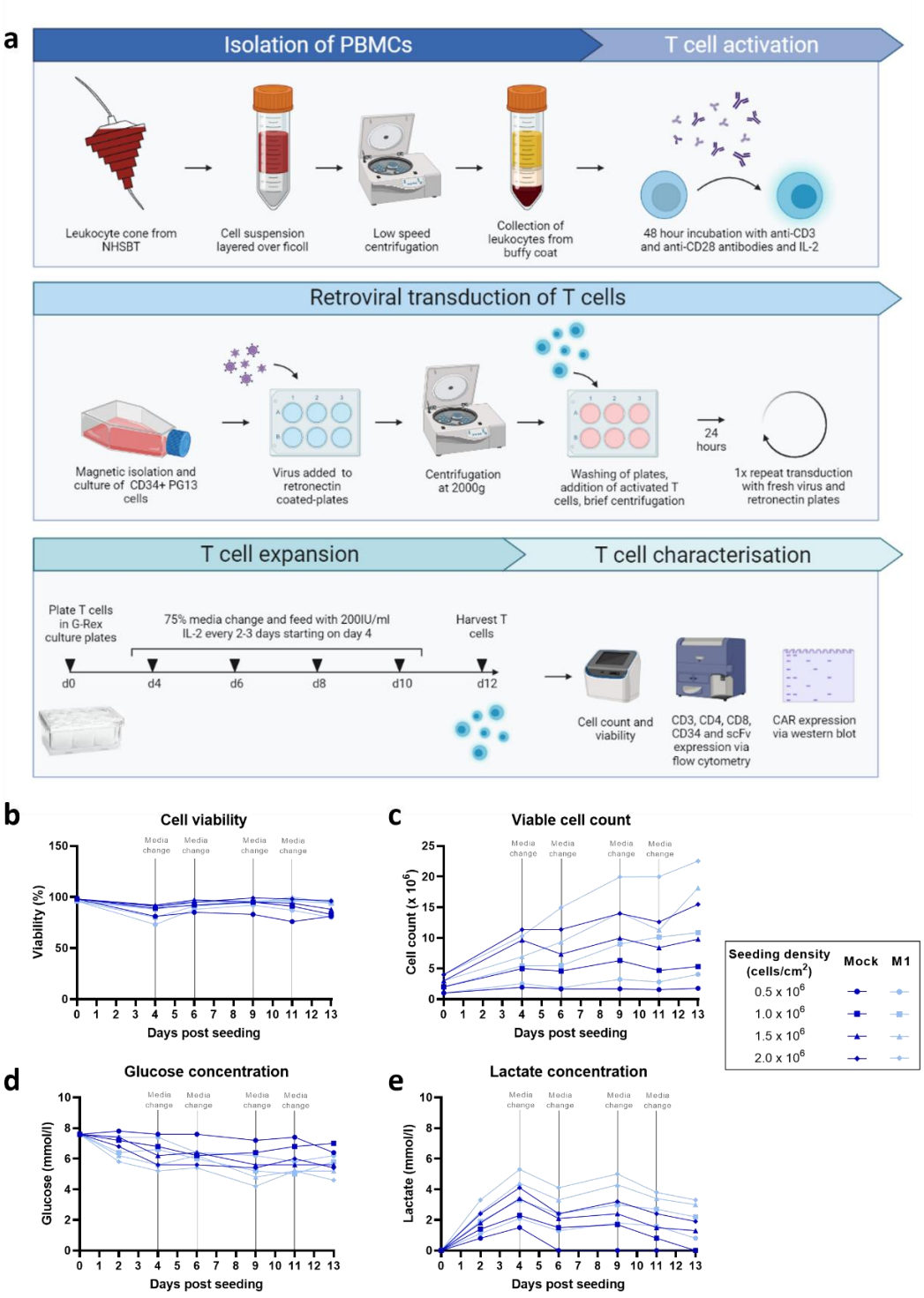

Figure 4.2 Feeder-free expansion protocol for primary CAR T cells.
(a) Schematic of the primary CAR T cell production pipeline (produced with Biorender.com). To determine optimal seeding density for CAR T cell expansion, mock and M1.BBz CAR T cells were seeded at varying cell densities in G-Rex 24-well plates and cultured in TCM with 200IU/mL IL-2. From day 4, 75 % media changes were performed every 2-3 days, with fresh IL-2 added to a final concentration of 200IU/mL. Prior to changing the media, samples were taken to monitor CAR T cell expansion in terms of (b) percentage cell viability, (c) total viable cell count, and the (d) glucose and (e) lactate levels in the media. Each condition was tested in duplicate, mean values are plotted. Results are displayed from a single donor.

4.3.2. Characterisation of CAR T cell products

The above protocol was repeated to generate M1.BBz, M40.BBz, CD19.BBz and mock CAR T cells from 3 independent donors. The G-Rex expansion process gave good yields of CAR T cells for all groups, with a mean of mean 258 x 10^6 cells (range 166 - 318 x 10^6) (Figure 4.3). Donor-to-donor variability was also observed, with donor 2 displaying significantly reduced expansion across the different CAR constructs compared to donor 1 ($p = 0.002$) and donor 3 ($p = 0.008$). Viability was acceptable for all groups, with an average of 94 % live cells (range 92 – 96 %) as measured on an automated cell counter with Trypan Blue exclusion.

Prior to their use in *in vitro* assays, cells underwent basic phenotyping by flow cytometry (Figure 4.3a). The use of stimulating antibodies against CD3 and CD28 prior to transduction, combined with continuous supplementation with IL-2 preferentially expanded T cells from an initial mixed pool of PBMCs, with most of the final population expressing CD3 (mean 94 %; range 81-99 %, Figure 4.3c). However, this process was not completely efficient, with CD3- cells present in low numbers in all preparations. Notably, the percentage of CD3+ T cells was demonstrably lower for the M1.BBz, M40.BBz and CD19.BBz populations generated from donor 2, although this was not observed in the mock group.

The CAR T cell generation protocol appeared to preferentially drive the expansion of CD8+ T cells, which significantly outnumbered CD4+ cells in the final population (mean CD8-to-CD4 ratio of 5.7, range 2.2 - 8.6; Figure 4.3d). The percentages of each subset were equivalent across the different CAR constructs for individual donors, but significant donor-to-donor variability was observed.

CAR expression was quantified by flow cytometry using either tCD34 as a proxy, or by detecting the anti-MCAM scFv itself using a 2-step staining process with MCAM-Fc and anti-IgG PE (Figure 4.4, representative data). CAR/tCD34 expression varied between donors, both in terms of the overall percentage of cells on which expression could be detected, and the intensity of staining within the positive subset. CD34 expression was low-moderate (mean 31 % excluding mock, range 18 - 46 %) and differed according to donor ($p < 0.001$), although no significant differences were detected when comparing

across CAR groups (Figure 4.4b). Interestingly, although there were significant numbers of CD3- cells in the M1.BBz, M40.BBz and CD19.BBz groups derived from donor 2, such cells appear to be CAR negative: CAR-expressing (CD34+) cells are nearly all CD3+ (Figure 4.4c). The transduction efficiency of CD8+ cells trended higher than CD4+ cells for all CAR constructs, however this did not reach statistical significance (Figure 4.4d).

As expected, there was a positive correlation between the expression of CD34 and the anti-MCAM scFvs in the M1.BBz and M40.BBz populations (Figure 4.4a, representative data). The percentage of cells with detectable scFv expression trended higher in the M40.BBz group compared to M1.BBz, however this did not reach statistical significance (M1 mean 23 %, range 15 - 28 %; M40 mean 30 %, range 23 - 36 %; Figure 4.4e). For all preparations of M1.BBz and M40.BBz CAR T cells, the percentage of tCD34+ cells exceeded the scFv+ percentage. This may in part be explained by non-specific staining observed with the IgG-PE reagent (Figure 4.4a, mock and CD19), which complicated the setting of gates and may have led to $scFv^{low}$ cells being classified as negative. However, although the absolute percentage of CD34+ scFv-, CD34- scFv+ and CD34+ scFv+ cells varied by donor and construct, there was striking consistency in the proportion of CD34+ cells which lacked the scFv (Figure 4.4f). This was significantly higher in the M1.BBz group (mean 42 %, range 40 - 44 %) compared to M40.BBz (mean 25 %, range 23 - 27 %; $p < 0.001$), suggesting that the M1.BBz CAR may have lower inherent stability.

Detection of the CAR via western blot in reducing conditions with an antibody against the intracellular CD3ζ domain appears to support this finding (Figure 4.4g and h). Fainter bands were detected for the M1.BBz lysates compared to M40.BBz across all donors, despite equivalent levels of endogenous CD3ζ and vinculin. Interestingly, there was also variation in the size of the proteins resolved, despite the close predicted molecular weights of the receptors. The primary M1.BBz band appears notably smaller than that for M40.BBz, which runs at an equivalent molecular weight to the CD19.BBz receptor. Furthermore, while the CD19.BBz lysates contained only a single CAR band, for M1.BBz and M40.BBz faint secondary bands of a marginally higher molecular weight were detected.

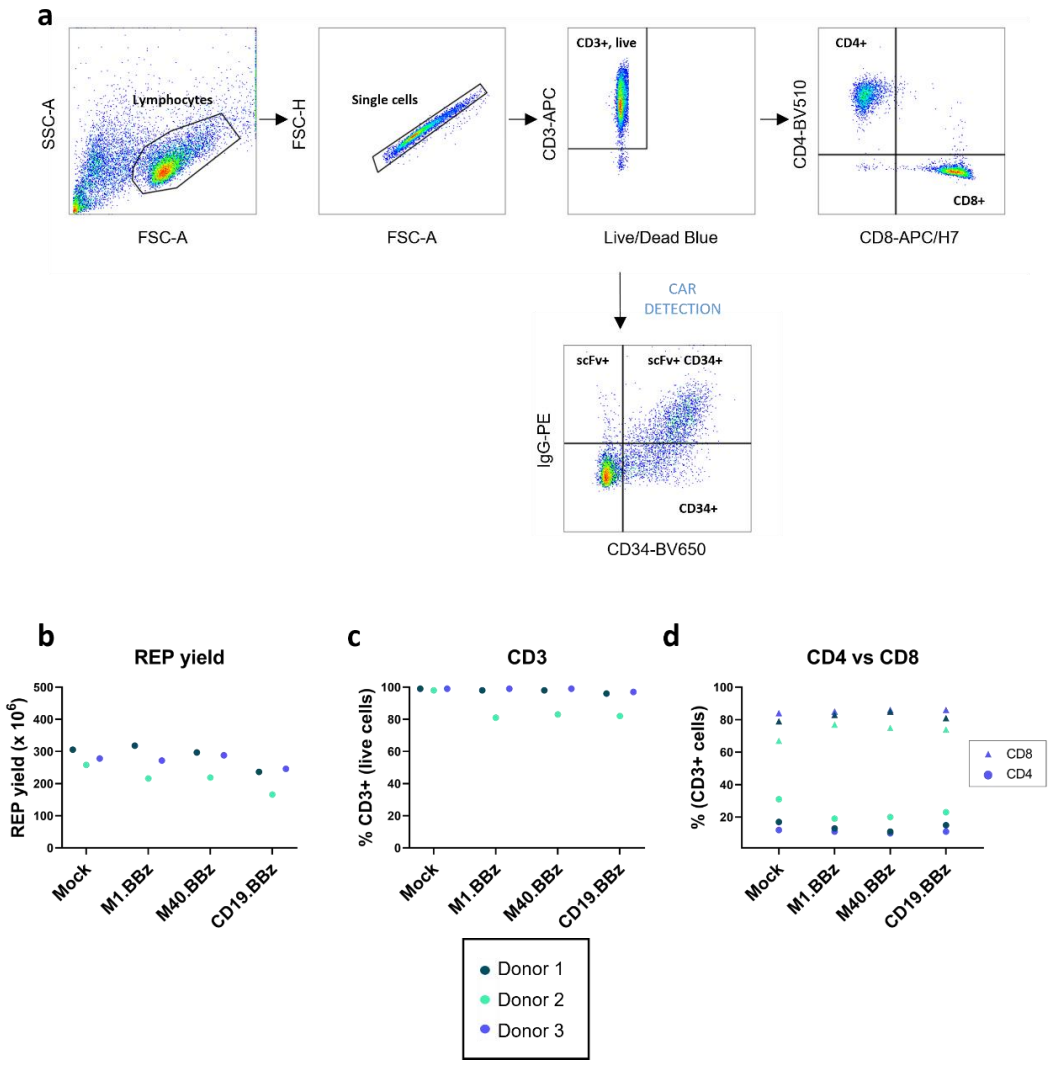

Figure 4.3 Basic phenotyping of primary CAR T cells.
On completion of the G-Rex expansion period, CAR T cells from 3 donors were harvested, counted, and stained with antibodies to detect CD3, CD4, CD8, CD34 and the anti-MCAM-scFv, prior to analysis by flow cytometry as detailed in (a). CAR T cells from 3 donors were characterised in terms of (b) the total cell number harvested from the G-Rex plate, (c) the percentage of live cells expressing CD3, and the percentage of CD3 cells expressing (d) CD4 versus CD8. For each donor, triplicate measurements were taken.

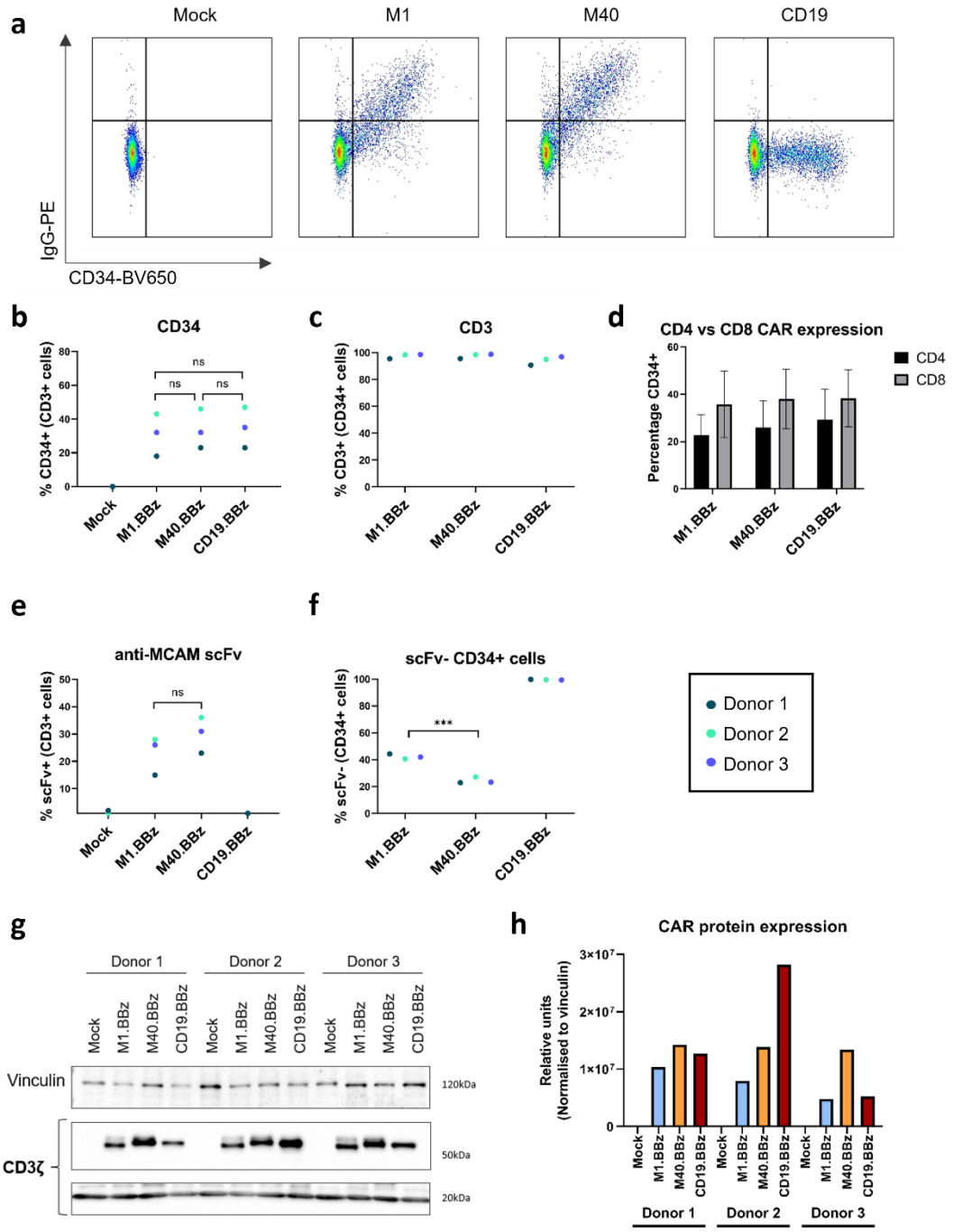

Figure 4.4 CAR expression on primary CAR T cells.
Following the REP, CAR T cell expression on primary T cells was assessed by flow cytometry to detect the CD34 marker gene or the anti-MCAM scFvs. (a) The relationship between the expression of CD34 and the anti-MCAM scFv on CAR T cells (representative dot plots from a single donor). (b) The percentage of live, CD3+ cells expressing CD34. (c) CD3 expression on CD34+ cells. (d) Relative transduction efficiencies of CD4+ and CD8+ subgroups, as determined by the percentage of CD3+ cells expressing CD34. (e) Percentage of CD3+ cells expressing anti-MCAM scFvs and (f) CD34 in the absence of scFv. (g) Confirmation of CAR expression by reducing SDS-PAGE, with antibodies against vinculin and CD3ζ, and (h) quantification of CAR protein expression, normalised to vinculin loading control. For each donor, triplicate measurements were taken. Statistical analysis of flow data was by one-way ANOVA with Tukey's multiple comparisons, * p<0.05, ** p<0.01, *** p<0.001.

Taken together, these data allow the CAR T cell products to be characterised as follows: cells harvested following activation, transduction and expansion were predominantly CD3+ T cells, of which those expressing CD8+ significantly outnumbered the CD4+ group. Across all transductions low to moderate CAR expression was achieved, which did not appear to be affected by the CAR construct itself. However, significant donor-to-donor variability was observed. This could be caused by donor specific factors such as donor age or health, or may represent differences introduced during the CAR T cell transduction process. For practical reasons it was not possible to bulk-produce CAR T cells for all donors simultaneously, and therefore each donor was prepared independently. While variables including PG13 passage number and reagent lots were controlled as far as possible, it is feasible that unforeseen variables in this process may account for the donor-to-donor variability.

While CAR expression as measured by cell surface tCD34 and scFv expression did not differ significantly between the 2 anti-MCAM CARs, there was evidence that the M1.BBz CAR was less stable, with lower expression as detected by western blot and a higher proportion of scFv- CD34+ cells. Functional characterisation of the primary CAR T cells is therefore essential to shed light on the impacts of these differences.

4.3.3. Assessment of primary CAR T cell activity against 888-Mel lines

To assess the activity of the primary anti-MCAM CAR T cells *in vitro*, cocultures were initially established with the previously validated 888-Mel lines (section 3.3.4), which express either GFP-tagged full length MCAM (MCAM-GFP), MCAM lacking the ectodomain (trunc.MCAM-GFP) or CD19 (CD19-GFP). After a 24-hour culture period at a 5:1 effector-to-target ratio, levels of pro-inflammatory cytokines in the supernatant were quantified by ELISA (Figure 4.5a). Cytokine production for all CAR constructs was modest and significant donor-to-donor variability was observed. M1.BBz and M40.BBz groups produced elevated levels of IFN-γ and TNF-α on coculture with the 888-Mel MCAM-GFP line, however this did not reach statistical significance compared to mock

as the absolute levels in pg/mL varied significantly by donor. Contrastingly, higher (albeit variable) production of IFN-γ, TNF-α and IL-2 by CD19.BBz CAR T cells on coculture with the 888-Mel CD19-GFP line was observed, which reached statistical significance compared to mock cocultures. As expected, significantly elevated cytokine production was not observed with the 888-Mel trunc.MCAM-GFP line.

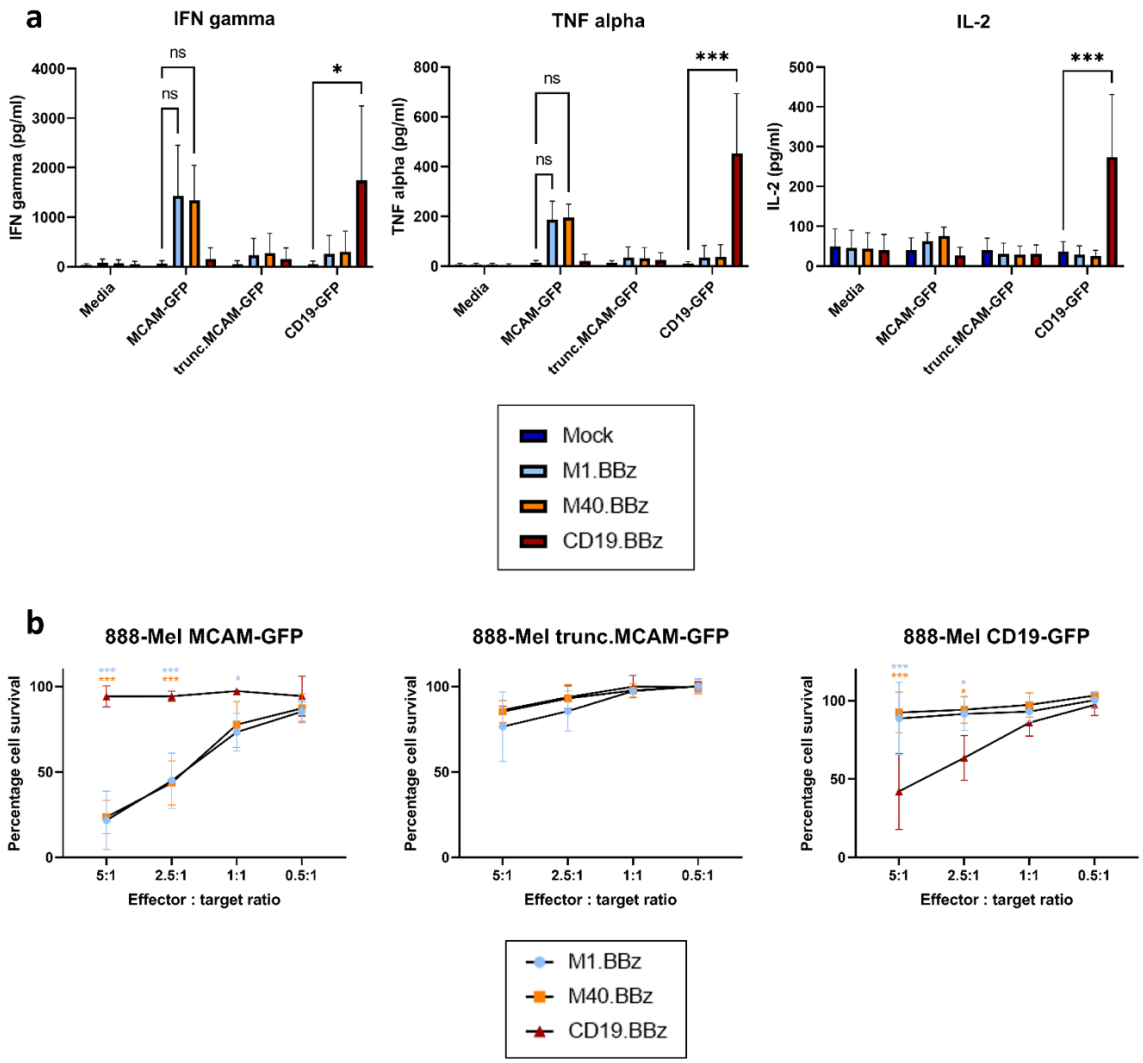

Figure 4.5 Cytotoxicity and cytokine production by CAR T cells on coculture with 888-Mel target cell lines.
(a) Production of cytokines by CAR T cells incubated with 888-Mel target cell lines at a 5:1 effector to target ratio. After 20 hours, supernatant was collected and cytokines were quantified by sandwich ELISA. (b) CAR T cells were incubated with luciferase-expressing 888-Mel target cell lines at varying effector-to-target ratios. After 20 hours, 75ul/well of Steady Glo Luciferase Assay System reagent was added, and plates were incubated for 20 minutes prior to quantification of luciferase activity (as RLU) on a plate reader. Data was normalised to RLU from mock CAR T cell coculture for the corresponding condition. Results displayed are from 3 donors, and for each donor triplicate measurements were taken. Results are displayed as mean and standard deviation. Statistical analysis is by two-way ANOVA with Tukey's multiple comparisons. * p<0.05, ** p<0.01, *** p<0.001.

Isolating out the different donors allowed the impact of the various CAR constructs on cytokine production to be more easily observed (chapter 4 appendix, Figure 4.13). The M1.BBz and M40.BBz CARs mediate MCAM-dependent IFN-γ and TNF-α production, however they fail to induce IL-2 secretion above background levels. By contrast, production of all 3 pro-inflammatory cytokines by CD19.BBz CAR T cells in response to 888-Mel CD19-GFP was robust across all donors. Of the 3 donors, donor 2-derived CAR T cells were the strongest cytokine producers, in accordance with the higher CAR expression achieved in this group (as detected by CD34 and scFv staining).

To assess M1.BBz and M40.BBz CAR mediated cytotoxicity, variants of the above 888-Mel lines were generated which constitutively express firefly luciferase under the CMV promoter. Cocultures were established using a range of target-to-effector ratios, and cytotoxicity was determined after 24 hours using luciferase activity as a proxy for target cell survival. To compensate for any non-specific impact of the coculture on target cell survival, data is presented as percentage survival relative to control (mock) cocultures and compared to the CD19.BBz control CAR (Figure 4.5b).

As expected, coculture with the CD19.BBz control CAR did not impact on the survival of the 888-Mel MCAM-GFP line across the range of seeding densities tested. However, coculture with the M1.BBz and M40.BBz CAR T cells significantly reduced viability in a dose-dependent manner, with mean survival rates at the highest effector-to-target ratio (5:1) of 21 % and 23 %, respectively. This effect was reduced at lower effector-to-target ratios, with statistical significance compared to CD19.BBz lost at the 0.5:1 (M1.BBz) and 1:1 (M40.BBz) seeding ratios. By comparison, survival of 888-Mel trunc.MCAM-GFP did not differ significantly on coculture with the anti-MCAM CARs compared to the CD19.BBz control CAR, across all effector-to-target ratios tested. Although the CD19.BBz CAR T cells proved superior in terms of cytokine production, this did not correlate with augmented cytotoxicity against the 888-Mel CD19-GFP cell line, which had a mean viability of 42 % at the 5:1 effector-to-target ratio. In agreement with the cytokine data, cytotoxicity mediated by donor 2 derived T cells trended higher than donor 1 or 3, suggesting that it may also correlate with CAR expression.

To further investigate the activity of anti-MCAM CAR T cells, the expression of T cell activation and exhaustion markers was assessed following a 24-hour culture period with media alone or with the 888-Mel MCAM-GFP lines (Figure 4.6). In non-stimulated conditions (media only) expression of CD25 and CD137 by CD3+ CD34+ cells was minimal, whereas a significant percentage of cells upregulated CD69, especially for donors 2 and 3, suggesting that some non-specific constitutive CAR signalling may occur in the absence of the target antigen. However, this does not appear to be dependent on the CAR specificity, as baseline expression of CD69, CD25 and CD137 was broadly comparable across the different CAR constructs.

Expression of the activation markers in coculture conditions broadly followed the predicted pattern, with elevated levels on M1.BBz and M40.BBz cells cocultured with 888-Mel MCAM-GFP. Meanwhile CD19.BBz CAR T cells upregulated such markers when exposed to CD19-GFP expressing target cells. Expression of CD25 and CD137 activation markers closely followed this pattern, with similar levels observed when all three CAR lines were activated by their respective target cells. The percentage of cells responding in this way was relatively low, with expression of CD25 and CD137 on only approximately one-third and one-fifth of the overall CD34+ population, respectively. This potentially reflects the longer length of time taken for these markers to be expressed at the cell surface [500].

CD69 expression does not so reliably follow the expected pattern of CAR-mediated activation. Its upregulation is observed as expected for donor 1, however very high background expression across all culture conditions and a lack of clear trends was observed for donors 2 and 3. Broadly comparable results for CD69, CD25 and CD137 were obtained when the CD34+ population was gated on CD3 alone, or when CD4+ and CD8+ subtypes were selected. Of note, due to the greater expansion of CD8+ cells during the REP, CD4+ cells represented a minority of events.

Continuous T cell stimulation eventually leads to an exhausted phenotype, identified by the expression of markers such as PD-1, TIM3 and LAG3. Baseline expression of these markers was not demonstrably different between CAR constructs, although significant donor-to-donor variability was observed in the absolute percentages of cells on which they were expressed (Figure 4.7). Expression of TIM3 and LAG3 does seem to

follow the same pattern as observed with the activation markers, although CAR-mediated upregulation is more apparent in the CD8+ population compared to CD4+ cells. By contrast, CAR-driven PD-1 upregulation is only apparent for donor 1 derived cells, and across all 3 donors CD4+ cells show high PD-1 expression independent of culture condition.

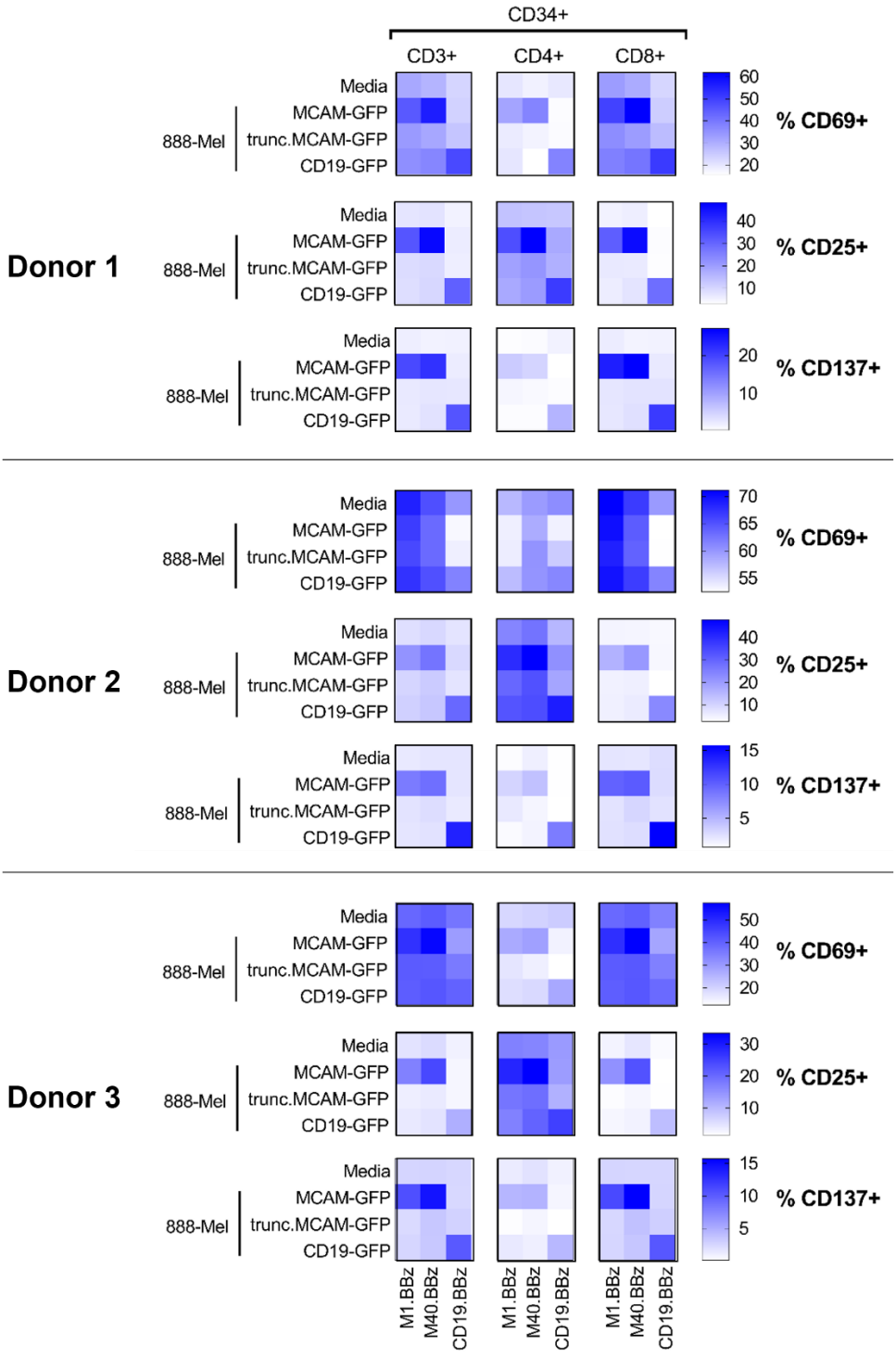

Figure 4.6 Coculture with MCAM-expressing target cells induces expression of activation markers.

CAR T cells were incubated with 888-Mel target cell lines at a 5:1 effector: target ratio. After 24 hours, T cells were harvested, washed, and stained with Live/Dead Fixable Blue viability dye and antibodies against the basic phenotyping markers (CD3, CD4, CD8 and CD34) and a limited panel of activation makers (CD69, CD25 and CD137). Data was acquired on a Fortessa flow cytometer. Data is presented for CD34+ cells, for either the entire CD3+ population or CD4+ and CD8+ subpopulations. Donor results are displayed separately.

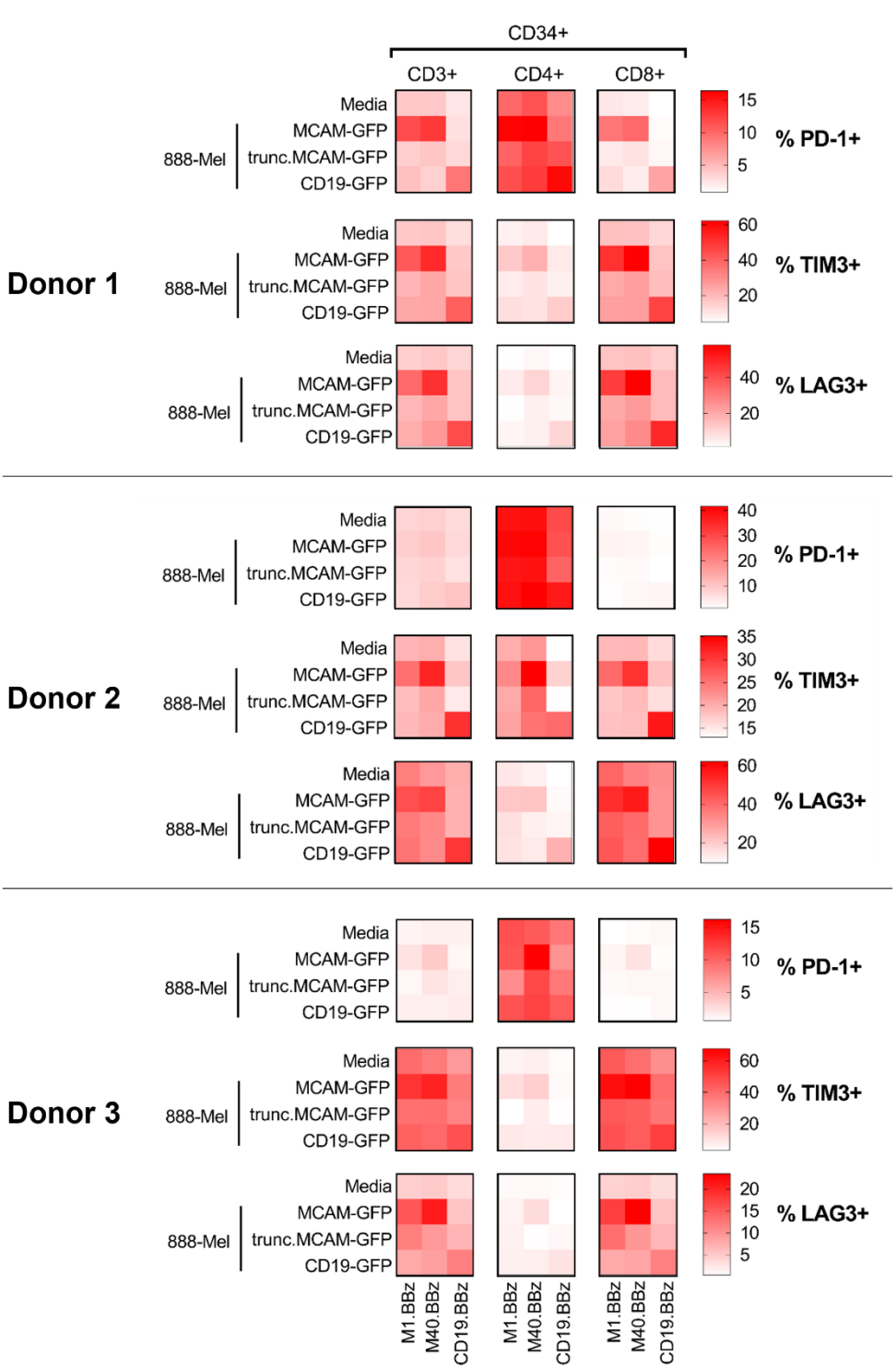

Figure 4.7 Coculture with MCAM-expressing target cells induces expression of exhaustion markers.

CAR T cells were incubated with 888-Mel target cell lines at a 5:1 effector: target ratio. After 24 hours, T cells were harvested, washed, and stained with Live/Dead Fixable Blue viability dye and antibodies against the basic phenotyping markers (CD3, CD4, CD8 and CD34) and a limited panel of exhaustion makers (PD-1, TIM3 and LAG3). Data was acquired on a Fortessa flow cytometer. Data is presented for CD34+ cells, for either the entire CD3+ population or CD4+ and CD8+ subpopulations. Donor results are displayed separately.

4.3.4. Primary CAR T cell activity against melanoma cell lines

Thus far, assessment of CAR activity against human MCAM had only been performed in the setting of the 888-Mel cell lines. These provided a useful initial model as the control (888-Mel trunc.MCAM-GFP) and test (888-Mel MCAM-GFP) lines were closely matched, differing only in the expression of the ectodomain. However, this does have its limitations. Firstly, MCAM was highly expressed on the 888-Mel MCAM-GFP line, with a mean MFI marginally higher than the WM2664 positive control (Figure 3.4). To mediate meaningful anti-tumour responses, CAR T cells would likely require the ability to lyse target cells with a range of MCAM expression levels. To model this *in vitro,* alternative cellular targets were required.

Secondly, different forms of MCAM exist: long and short isoforms are generated by an alternative splicing event which results in the truncation of the short form cytoplasmic tail, although both isoforms retain identical extracellular and transmembrane domains [501]. While the long isoform localises to the basolateral membrane of epithelial cells, the short form is found on the apical surface [269], which is likely to impact on the accessibility of the antigen to the CAR. Additionally, there is evidence that tumour expressed MCAM differs from that on normal cells, whether through dimerisation [502] or post-translational modification [428]. The 888-Mel MCAM-GFP line exclusively expresses the long isoform, which may not undergo the same post-translational modifications as tumour-expressed MCAM due to the presence of the GFP tag, and therefore may not fully model the complexity of MCAM expression.

To test the M1.BBz and M40.BBz CAR T cells against more physiologically representative cell models, a panel of melanoma cell lines was selected which displayed varying intensities of MCAM expression. As previously described the 888-Mel MCAM-negative control line was derived from a patient with recurrent metastatic melanoma [439, 442]. Similarly, WM2664 [503, 504], C8161 [505, 506] and 501-Mel [439, 507] were also derived from clinical resections of metastatic deposits.

Prior to their use in assays, the expression of MCAM on the lines was quantified by flow cytometry and western blot (Figure 4.8). As expected from previous experiments, the 888-Mel line did not express MCAM, while the other 3 melanoma lines

demonstrated varied expression levels. MCAM-PE MFI was highest for the WM2664 line, followed by the C8161 and 501-Mel lines (Figure 4.8b). While the average MCAM expression on 501-Mel was low, the population appears heterogenous: a proportion of the cells express MCAM at levels equivalent to C8161, while expression on other cells is low-absent. Western blot analysis with an antibody against the MCAM endodomain confirmed the expression profiles of the 888-Mel and WM2664 lines (Figure 4.8c). Probing for MCAM in the 501-Mel and C8161 lysates did not replicate the flow cytometry data however, with a stronger band detected for 501-Mel (potentially indicative of some intracellular MCAM deposits), although both had demonstrably lower expression than WM2664.

Luciferase-expressing variants of the melanoma cell lines were generated for use in cytotoxicity assays. Growth rates of the lines were also estimated using luciferase activity as a proxy for cell number (Figure 4.8d). In agreement with my observations when culturing the parental cell lines, the luciferase-expressing C8161 cell line showed the greatest expansion, while the WM2664 line had the slowest growth rate. However, coculture assays with CAR T cells and melanoma cells were incubated for 24-hours only, at which point differences in growth had not reached statistical significance.

To inform their use in subsequent assays, and taking into account the flow cytometry and western blot data, the melanoma lines were assigned to categories according to their MCAM expression: negative (888-Mel), low-moderate (501-Mel), moderate (C8161) and high (WM2664).

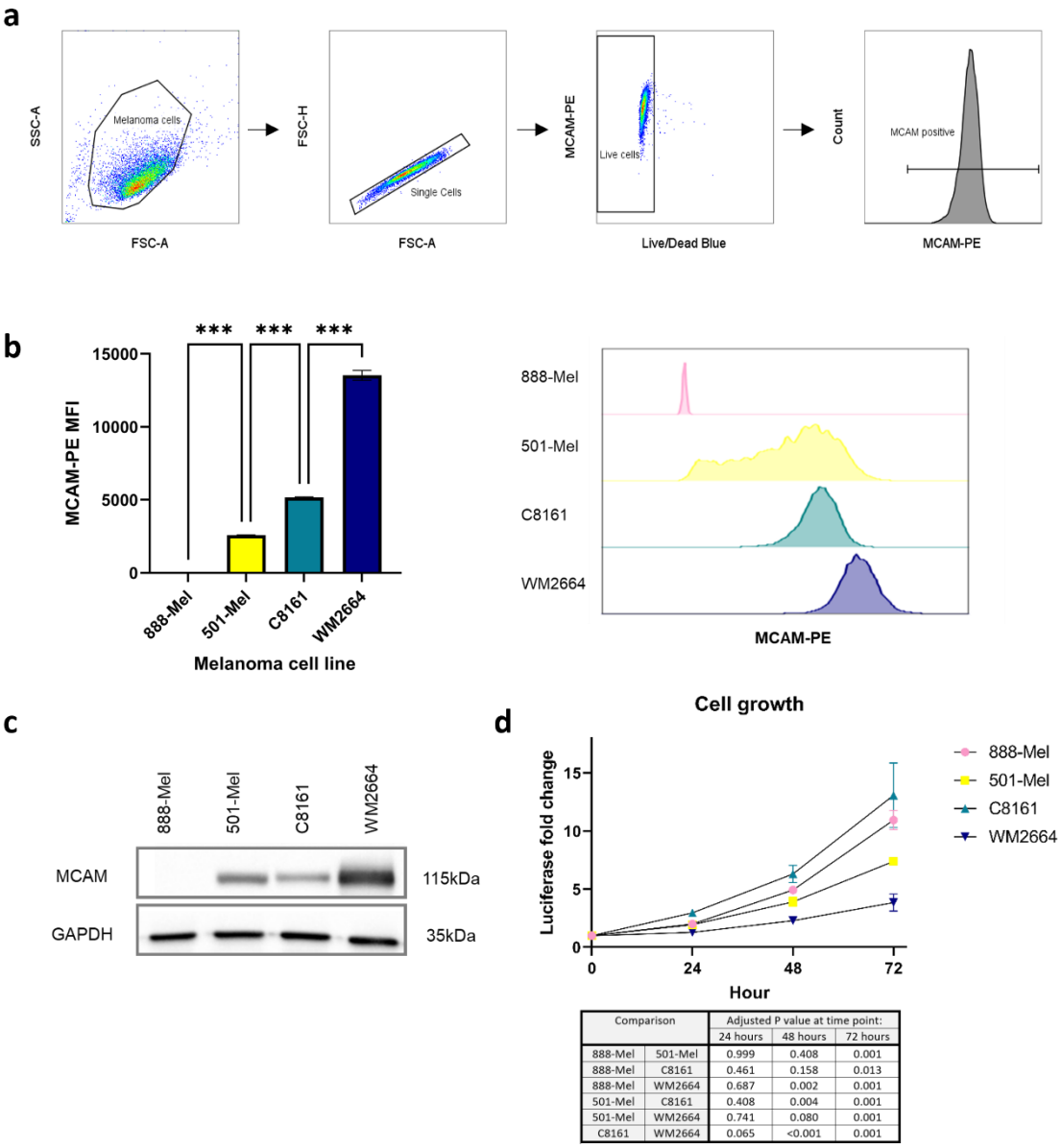

Comparison		Adjusted P value at time point:		
		24 hours	48 hours	72 hours
888-Mel	501-Mel	0.999	0.408	0.001
888-Mel	C8161	0.461	0.158	0.013
888-Mel	WM2664	0.687	0.002	0.001
501-Mel	C8161	0.408	0.004	0.001
501-Mel	WM2664	0.741	0.080	0.001
C8161	WM2664	0.065	<0.001	0.001

Figure 4.8 Characterisation of a panel of melanoma cell lines.
A panel of melanoma cell lines was stained with Live/Dead blue and anti-MCAM-PE. (a) gating strategy, (b) MCAM-PE MFI and expression histogram. (c) Western blot for the MCAM endodomain and GAPDH loading control. (d) Cell growth curve. Luciferase expressing melanoma cell lines were cultured over 3 days at different seeding densities, and cell growth was determined via measurement of luciferase activity, presented relative to RLU at day 0. All assays were conducted in triplicate. Results are displayed as mean and standard deviation. Statistical analysis is by one way (b) or two-way ANOVA (d) with Tukey's multiple comparisons. P values for the growth curve are presented below graph (d). * p<0.05, ** p<0.01, *** p<0.001.

To determine the activity of the CARs across a range of MCAM intensities, the M1.BBz, M40.BBz and CD19.BBz CAR T cells were equalised for transduction efficiency and cocultured with the melanoma lines for 24 hours at a 5:1 effector-to-target ratio. Secretion of IFN-γ and TNF-α was increased when M1.BBz and M40.BBz CAR T cells

were cultured with MCAM-expressing target cell lines with low level basal production observed with the 888-Mel MCAM-negative controls (Figure 4.9). IFN-γ was detected at higher absolute levels than TNF-α, and as expected the $MCAM^{high}$ WM2664 line stimulated robust secretion. This contrasted with the lower magnitude IFN-γ response observed on coculture with the 501-Mel cell line, in keeping with the lower MCAM expression by this line. Surprisingly, while C8161 had a lower average MCAM expression per cell than WM2664, they proved a strong stimulus for IFN-γ and TNF-α secretion. This cell line had a rapid growth rate (Figure 4.8d), which could conceivably alter the effector-to-target ratio and account for the elevated cytokine secretion.

Production of IFN-γ and TNF-α by M40.BBz in response to all MCAM+ targets trended higher than M1.BBz, but this did not achieve statistical significance across all conditions. At an individual donor level, the augmented production by M40.BBz CAR T cells is apparent (chapter 4 appendix, Figure 4.14). In agreement with the results obtained with the 888-Mel MCAM-GFP line, donor 2 derived cells proved to be the strongest cytokine producers, in keeping with the higher CAR expression detected on this batch of cells.

While CAR-mediated secretion of IFN-γ and TNF-α was clearly observed, MCAM+ target cells did not prove to be a strong stimulus for IL-2 production, mirroring the findings with the 888-Mel MCAM-GFP cocultures (Figure 4.5a and Figure 4.9). IFN-γ and TNF-α are canonical cytokines produced by cytotoxic CD8+ T cells, while CD4+ cells are the main producers of IL-2, so these results likely reflect the skewed composition of the final post-expansion CAR T cell products, in which CD8+ cells predominate.

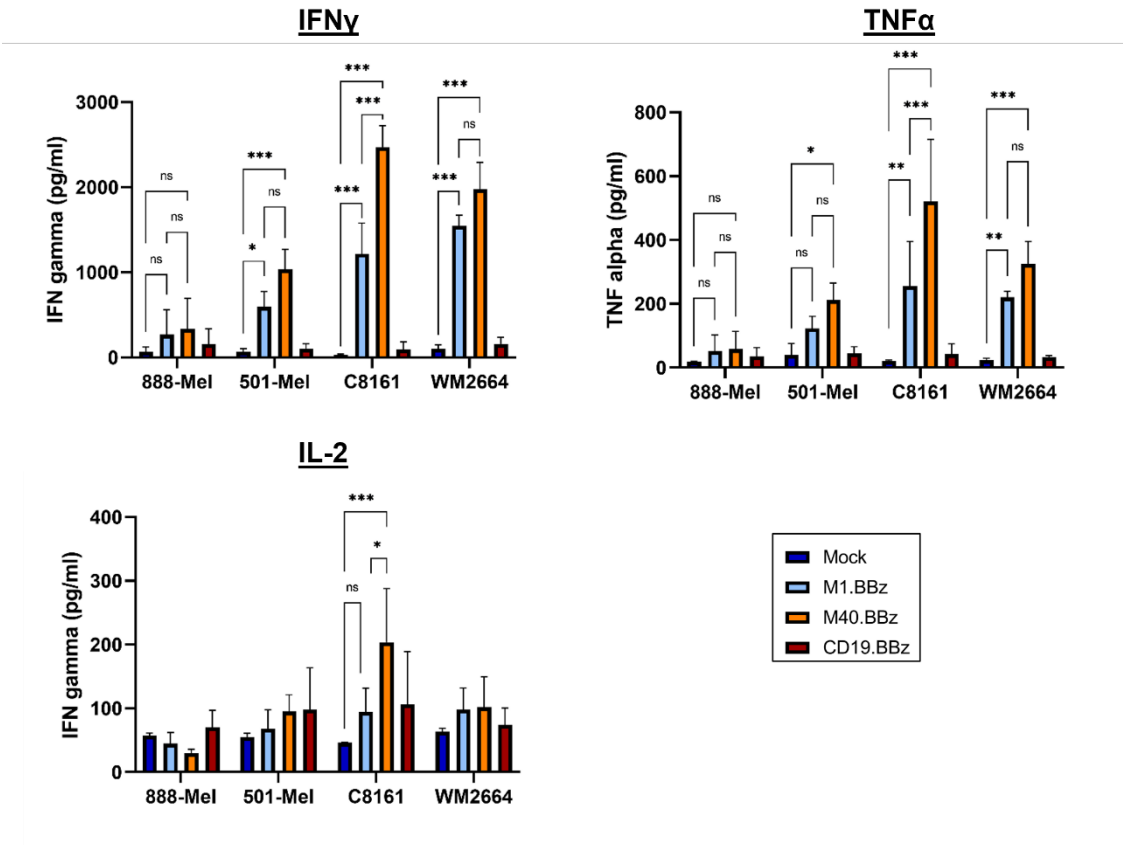

Figure 4.9 Production of cytokines by CAR T cells incubated with melanoma target cell lines at a 5:1 effector-to-target ratio.

CAR T cells and melanoma target cells were cocultured for 20 hours. Supernatant was collected, and cytokines were quantified by sandwich ELISA. (b) Cell surface CD107a expression on CD34+ T cells as a proxy of degranulation. CAR T cells were cocultured for 4 hours at a 5:1 effector-to-target ratio in the presence of monensin and anti-CD107a-PE, then stained for CD3, CD4, CD8 and CD34.

Results displayed are from 3 donors, and for each donor triplicate measurements were taken. Results are displayed as mean and standard deviation. Statistical analysis is by two-way ANOVA with Tukey's Multiple Comparisons. * p<0.05, ** p<0.01, *** p<0.001.

In addition to cytokine production, CD8+ CTLs induce target cell apoptosis though the expression of Fas-L and the release of perforin and granzyme from pre-formed granules [476]. To investigate whether this occurred *in vitro*, M1.BBz and M40.BBz T cells were cultured at a 1:1 ratio with C8161 target cells, on account of the strong cytokine response to this line. Short term (4-hour) cocultures were established in the presence of the transport inhibitor monensin and an anti-CD107a antibody, to detect CD107a which had been transferred to the cell surface following granule exocytosis.

As expected, coculture with C8161 resulted in CD107a expression above baseline on CD3+ CD34+ M1.BBz (mean 28.8 %, range 16.7-39.8 %) and M40.BBz (mean 44.9 %, range 30.7-56.5 %) CAR T cells (Figure 4.10a). Meanwhile MCAM-negative 888-Mels did not induce degranulation above baseline (media-only). Degranulation is primarily a function of CD8+ CTLs, and as expected on exposure to MCAM the percentage of CD107a+ cells was increased within the CD8+ population compared to CD4+, which did not reach statistical significance above baseline (M1.BBz – 30 % vs 23 %, M40.BBz – 48 % vs 29 %). In accordance with previous *in vitro* assays, greater degranulation was observed in the M40.BBz population compared to M1.BBz, although this did not reach statistical significance.

To confirm that CAR mediated degranulation ultimately resulted in target cell death, CAR T cells were incubated for 20 hours at varying effector-to-target ratios with the luciferase-expressing melanoma lines, and luciferase activity was measured as a proxy of target cell viability (Figure 4.10b). As previously described, cell viability is presented relative to corresponding mock cocultures to account for non-specific effects of T cells on target cell growth.

As expected, 888-Mel survival was unaffected by the CAR T cell type, although a trend towards reduced viability at higher effector-to-target ratios was observed, possibly indicative of nutrient depletion. Survival of the MCAM+ melanoma lines was significantly reduced in the presence of the M1.BBz and M40.BBz CAR T cells compared to the CD19-specific control CAR. This cytotoxic effect was strongest in the C8161 and WM2664 cell lines and is maintained even at low effector-to-target ratios. 501-Mel cells have heterogenous MCAM expression, including a subset of MCAM low-negative cells. Such cells would likely be resistant to direct CAR mediated killing, which may explain the reduced efficacy of the MCAM CAR T cells against this line. Interestingly, augmented cytotoxicity by the M40.BBz CAR T cells was observed only on coculture with 501-Mel – survival of C8161 and WM2664 was equally impacted by both anti-MCAM CAR T cell groups. This may potentially indicate that M40.BBz retains cytotoxic capabilities at lower MCAM expression densities, although it should be noted that this effect was only statistically significant at the highest effector-to-target ratio.

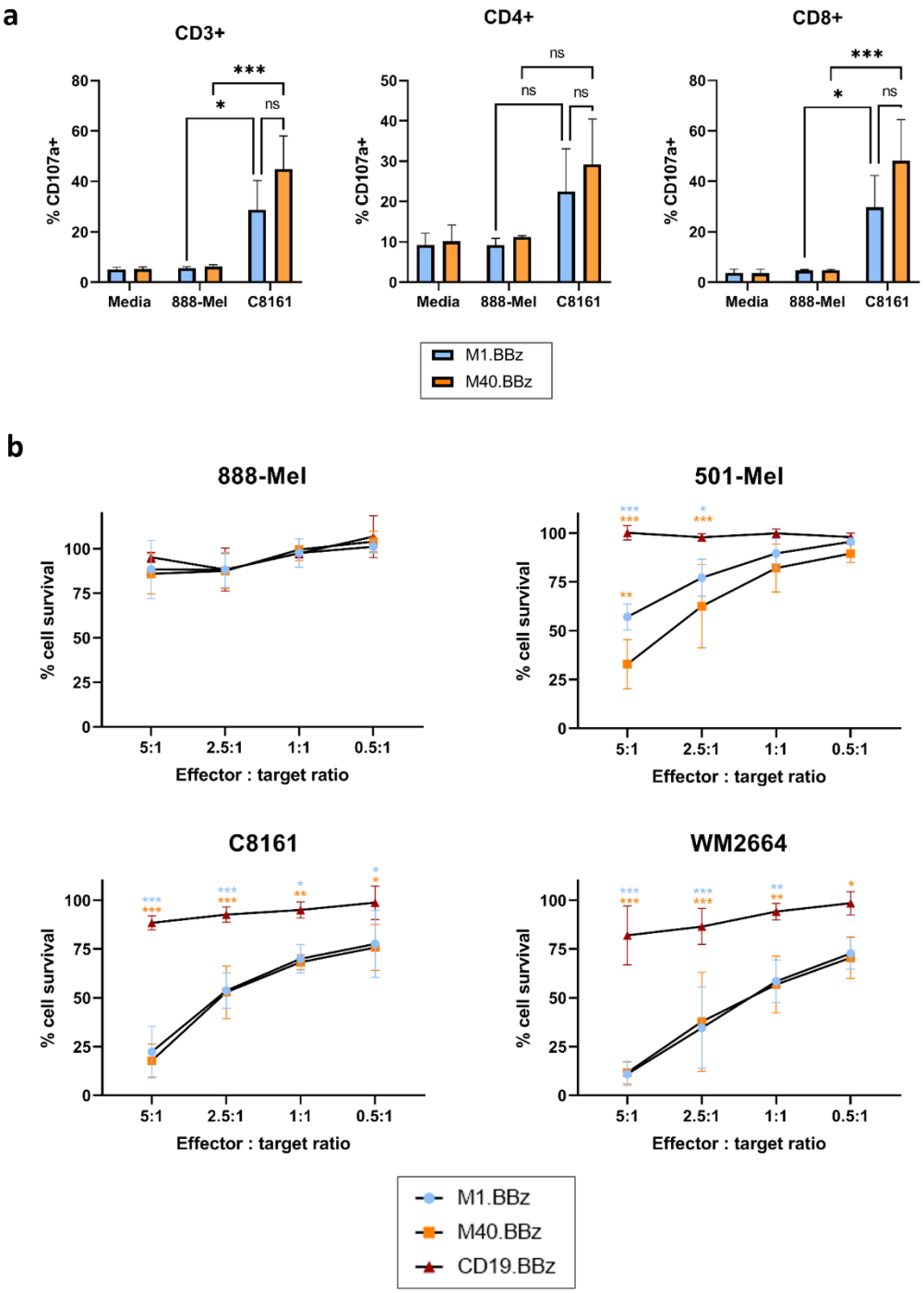

Figure 4.10 Cytotoxic effector functions of M1.BBz and M40.BBz CAR T cells.
(a) Cell surface CD107a expression on CD34+ T cells as a proxy of degranulation. CAR T cells were cocultured for 4 hours at a 5:1 effector-to-target ratio in the presence of monensin and anti-CD107a-PE, then stained for CD3, CD4, CD8 and CD34. (b) CAR-mediated cytotoxicity. CAR T cells were incubated with luciferase-expressing melanoma target cell lines. After 20 hours, 75ul/well of Steady Glo Luciferase Assay System reagent was added, and plates were incubated on an orbital shaker for 20 minutes to ensure total cell lysis. Luciferase activity was quantified as RLU, on the BioTek Synergy Plate reader. Data was normalised to RLU from mock CAR T cell coculture for the corresponding condition. Results displayed are from 3 donors, and for each donor triplicate measurements were taken. Results are displayed as mean and standard deviation. Statistical analysis is by two-way ANOVA with Tukey's multiple comparisons. * $p<0.05$, ** $p<0.01$, *** $p<0.001$.

Taken together, these assays broadly support the findings observed with the 888-Mel derived model lines previously described. Effector functions associated with CD8+ CTLs followed a CAR-mediated pattern of activity, which was reliant on the presence of the MCAM ectodomain and appears to increase in intensity according to the degree of MCAM expression on the target cell lines. Donor-to-donor variability was observed across all assays; however, the relative activities of the different donor-derived T cells were relatively consistent, with the strongest responses mediated by donor 2 derived CAR T cells, consistent with the higher transduction efficiencies achieved in these groups. Of the 2 anti-MCAM CAR designs, M40.BBz regularly outperformed M1.BBz, however the significance of this is unclear as it did not robustly reach statistical significance across all assays.

4.3.5. The effect of soluble MCAM on CAR T cell behaviour

In addition to the long and short isoforms, a soluble species of MCAM exists (sMCAM) [508], generated by the MMP-mediated proteolytic cleavage of the membrane bound protein [509]. sMCAM is produced by cultured endothelial cells [508, 509] and cancer cells, including melanoma cell lines [272]. Accordingly, it is detectable in the plasma of healthy participants [273], but is at elevated levels in cancer patients [273].

In vitro, recombinant soluble (rsMCAM) drives cancer cell proliferation, induces the expression of markers of EMT, and protects cells from DNA fragmentation in the presence of apoptotic inducing factors by inducing Bcl-X_L expression [272]. In mouse xenograft experiments, rsMCAM treatment resulted in increased tumour growth and metastatic dissemination in a variety of cell models [272, 276], which it appears to achieve by its effects on tumour neovascularisation [272, 510]. These effects were counteracted by a blocking antibody specific to the soluble form of MCAM [272, 276, 511].

Given that sMCAM contains the full extracellular domain, it would be expected to bind to the M1 and M40 scFv domains. Indeed, binding of soluble, Fc-tagged MCAM forms the basis of the flow cytometry scFv staining protocol (section 2.2.2.11). This presents

2 possible issues: Firstly, if sMCAM in the plasma is capable of binding to the receptor and driving CAR signalling, it could induce premature exhaustion before the T cells reach the tumour. Secondly, CAR T cells may be prevented from binding to tumour-cell surface expressed MCAM if the scFv antigen binding sites are already occupied by the soluble form of the protein.

To investigate this, a recombinant soluble form of MCAM which lacks the transmembrane domain (produced by Biocytex) was kindly sourced from Marcel Blot-Chabaud. To assess whether rsMCAM could increase baseline T cell activation, M1.BBz and M40.BBz cells were incubated with high level (500ng/mL) rsMCAM for 24 hours, prior to staining with antibodies for basic phenotyping and for the detection of activation and exhaustion markers. While significant donor-to-donor variability was observed in terms of the baseline marker expression on CD3+ CD34+ cells, there was no evidence of rsMCAM-induced activation or exhaustion (Figure 4.11a). Similarly, production of the cytokines IFN-γ and TNF-α by M1.BBz and M40.BBz in response to 888-Mel MCAM-GFP was not impeded by the presence of rsMCAM in the culture media (Figure 4.11b).

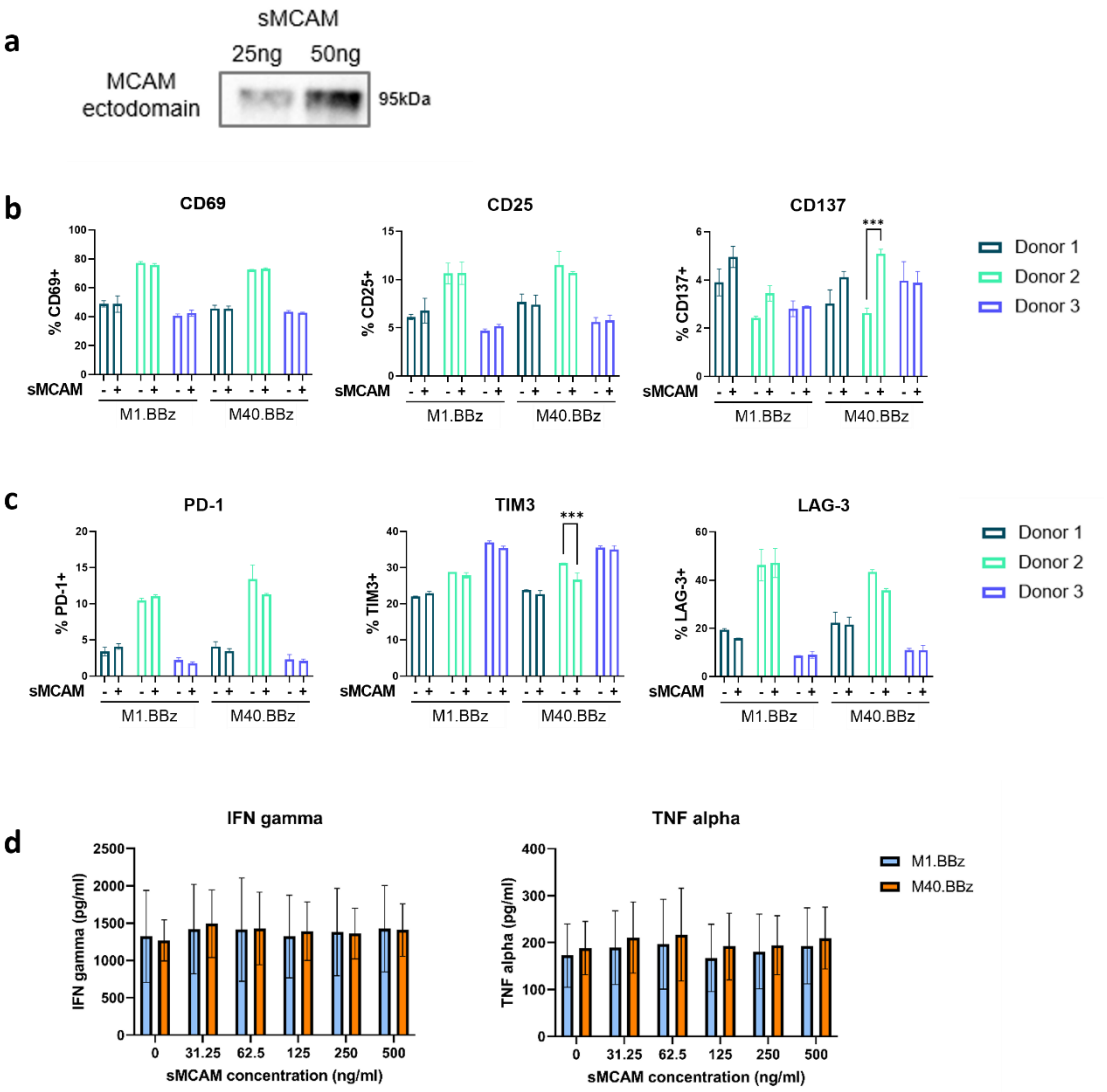

Figure 4.11 Effect of rsMCAM on M1.BBz and M40.BBz CAR T cells.
(a) Western blot analysis of soluble MCAM. M1.BBz and M40.BBz CAR T cells were incubated for 24 hours in the presence of 500ng/mL sMCAM, then stained with a basic panel to detect CD3, CD4, CD8 and CD3, plus antibodies to detect (b) activation markers CD69, CD25 and CD137 or (c) exhaustion markers PD-1, TIM-2 and LAG-3. (d) To detect changes in CAR T cell efficacy mediated by sMCAM, M1.BBz and M40.BBz CAR T cells were incubated for 20 hours with 888-Mel MCAM-GFP targets at a 5:1 effector-to-target ratio. After 20 hours, supernatant was collected, and cytokines were quantified by sandwich ELISA.
Results displayed are from 3 donors, and for each donor triplicate measurements were taken. Results are displayed as mean and standard deviation. Statistical analysis is by unpaired T tests. * p<0.05, ** p<0.01, *** p<0.001.

4.3.6. Expression of MCAM on CAR T cells

In the peripheral blood of healthy donors, MCAM is expressed by <1 % of mononuclear cells. Little expression of MCAM has been reported on B cells and NK cells, however it is detectable on approximately 2 % of peripheral T cells. In the lymphocyte compartment, MCAM identifies a population of memory CD4+ T cells which are enriched for markers of the Th17 subset (reviewed in [512]).

To assess whether MCAM could be detected on the mock, M1.BBz, M40.BBz and CD19.BBz CAR T cells, cells were maintained in standard culture conditions (TCM supplemented with 200IU/mL IL-2) prior to staining with anti-CD3 and anti-MCAM antibodies. Live Dead Fixable Blue viability dye allowed dead cells to be excluded from the analysis. In this preliminary experiment, MCAM positive cells accounted for <1.5 % of all CD3+ cells for all constructs (Figure 4.12a, representative data). Donor-to-donor variation was apparent in the overall percentages of MCAM+ cells, and it should be noted that only 2 donors were used for this experiment. However, MCAM+ cells were detected to a lesser degree in the M1.BBz and M40.BBz groups compared to mock and CD19.BBz, suggesting that clearance of such cells is potentially occurring in such cultures (Figure 4.12b).

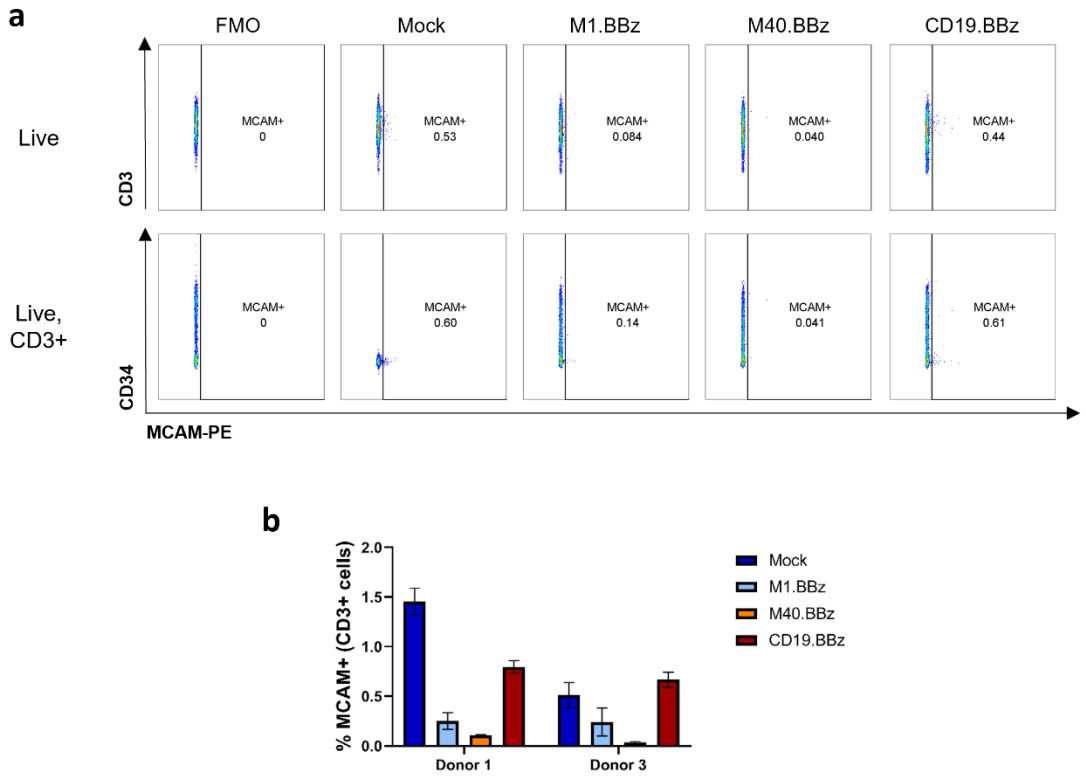

Figure 4.12 Expression of MCAM on resting CAR T cells.
CAR T cells cultured in standard conditions (TCM supplemented with 200IU/mL IL-2) were stained with Live/Dead Fixable Blue viability dye and antibodies against CD3, CD34 and MCAM.
Data was acquired on a Fortessa flow cytometer. (a) Dot plots for live (top panel) and live, CD3+ cells (bottom panel). Representative data from a single donor. (b) The percentage of CD3+ live cells expressing MCAM in the different CAR groups, separated by donor.

4.4. Discussion

Numerous manufacturing protocols for CAR T cells exist, ranging from small scale culture in traditional tissue culture plates to fully automated closed systems requiring minimal manual intervention. The selection of an appropriate method for any specific application is likely to be influenced by numerous factors, such as the number and purity of T cells required, the intended use of the final product (clinical use requiring GMP-compliant processes or laboratory research), and practical considerations such as the cost of reagents and access to highly specialised and expensive equipment [513]. To minimise manual processing, thereby reducing the risk of contamination and increasing batch-to-batch consistency, centres producing CAR T cells for clinical use have favoured semi- or fully automated, closed systems, such as the CliniMACS Prodigy or the WAVE Bioreactor [514–516]. However, due to its cost, such equipment is out of reach for many research laboratories.

The G-Rex plates were an appealing choice for this project as they strike a balance between cost and clinical relevance. From a practical perspective, the G-Rex plates are relatively low cost, can be kept in a standard laboratory incubator, and give flexibility in terms of the protocol used. However, the 6-well G-Rex plates are also part of a bigger product series, which includes high-capacity closed system devices for clinical applications [517]. Protocols are standardised according to the area of the basal membrane over which gas exchange occurs, which simplifies scaling up across the different devices [493]. Culturing mock and CAR T cells in 6 well G-Rex plates yielded plentiful cells for downstream *in vitro* assays, although the total fold expansion was modest (range 8-16 fold) compared to reported values for the G-Rex series. It is likely therefore that further protocol optimisation would be necessary as a part of any future scaling up effort.

Traditional rapid expansion protocols, especially those for the expansion of TILs, have used irradiated allogeneic feeder PBMC cells to achieve fold expansion far in excess of what was achieved in this project [518]. Similar feeder-cell dependent protocols have also been modified for use in G-Rex culture devices [494]. However, this was not adopted as part of the protocol both for practical reasons (such as difficulty accessing a

radiation source), and because feeder cells are often now not routinely used in clinical protocols.

Regardless of the expansion protocol or device used, the successful generation of CAR T cells is likely to depend on the quality of the starting material, both in terms of viability and purity. Most clinical protocols harvest lymphocytes with specialised leukapheresis equipment. However, we found that LRS cones, an easily obtained by-product of apheresis generated during the lymphodepletion process, provided a plentiful source of cells. This fraction is enriched for leukocytes, with CD3+ T cells accounting for 60-70 % of cells [470, 471, 473], but some RBCs, platelets, monocytes and neutrophils are also retained [470, 471, 474]. Density gradient purification has been shown to remove the majority of RBCs and platelets [519]; however, B cells, NK cells and monocytes still remain in the purified PBMC product. Importantly, the presence of monocytes in the starting material has been shown to impair subsequent T cell expansion [519, 520] and transduction [519, 521].

Also of concern are those cell types which are known to expand in the presence of IL-2, for example NK cells. NK cells are present in the blood, whereby they account for approximately one-tenth of PBMCs [470, 522]. They are broadly categorised into 2 types, both of which lack CD3: the majority of circulating cells are cytotoxic $CD56^{dim}$ CD16+ cells [523–525], while lymphoid organs contain a $CD56^{bright}$ CD16- population which are highly responsive to IL-2 and are strong cytokine producers [522, 525, 526]. Both populations express a range of stimulatory and inhibitory cell surface receptors, with the outcome of their interactions with target cells dependent on the balance of signalling. Importantly, CAR constructs with 4-1BB and CD3ζ signalling domains have been successfully expressed in NK cells and the resulting CAR-NK populations shown capable of mediating cytokine production, cytotoxicity and *in vivo* tumour control [527–531]. CAR NK production protocols generally also involve an IL-2 driven expansion step [528, 532], therefore there is a risk that using bulk PBMCs may result in a final product which contains both CAR+ T and NK cells.

CAR T cells derived from donors 1 and 3 were relatively comparable in terms of their expansion and percentage CD3+ cells post-expansion, however donor 2 CAR T cells proliferated to a lesser extent. Strikingly, the percentage of CD3- cells following

expansion was significantly reduced in this donor, in a manner which appeared dependent on CAR expression, as the mock group was >98 % CD3+. Why this might be is unclear. If this donor had elevated levels of NK cells, one would reasonably expect an increased CD3- fraction across the board. Although it is conceivable that tonic signalling could potentially drive preferential expansion of CAR NK cells, this does not appear to be the case here: for all donors, CAR expressing (CD34+) cells were almost exclusively CD3+. Therefore, the CD3- cells in CAR T cell products generated from donor 2 represent a CAR- population, potentially attributable to untransduced B cells, NK cells or monocytes.

Given these differences, it would be informative in future rounds of CAR T cell generation to first characterise the relative proportions of different cell types in the LRS cone harvest prior to activation and transduction. An additional approach that could be used is to enrich for CD3+ cells with immunomagnetic beads. Even this would not necessarily remove all undesirable cell types, however, as CD3+ Treg cells can also be isolated from the PBMC fraction. Inadvertent transduction of such cells would generate immunosuppressive Treg cells which have been demonstrated to impair CAR cytotoxicity [533].

Fine-tuning the specific CD3+ T cell types to be used may therefore be required for optimal product generation; however, each additional step adds complexity and does not necessarily reflect current clinical manufacturing protocols. One QC step which has been successfully incorporated into the clinical manufacturing pipeline is controlling the CD4:CD8 ratio of the starting material [534]. CD4+ T cells predominate in the blood of healthy donors, accounting for approximately 60 % of CD3+ PBMCs from LRS cones [470, 471, 473]. However, by the end of the expansion process, CD8+ cells outnumbered CD4+ T cells by an average of nearly 6:1 for all donors and CAR constructs. Such an effect has been reported by other groups using a bulk unsorted lymphocyte fraction as the starting material for CAR T generation [535, 536]. CD8+ T cells show stronger proliferation following stimulation with anti-CD3 and -CD28 antibodies [537], which would have the effect of increasing the CD4:CD8 ratio in the final product. As retrovirally mediated gene transfer can only occur in actively dividing

cells, this could also result in increased transduction efficiencies in the CD8+ population, as observed in my CAR T cell groups and reported by Moeller et al [536].

While CD8+ CAR T cells are prototypically cytotoxic and produce the cytokines IFN-γ and TNF-α, these effector functions are not limited to this subset. CD4+ CAR T cells are also capable of lysing target cells *in vitro,* albeit to a lesser extent than CD8+ cells [535, 536, 538]. Furthermore, the production of Th1 cytokines including IFN-γ and TNF-α is augmented in CD4+ CAR T cells, which are also much stronger producers of IL-2 [535, 536, 538–541]. Additionally, CD8+ cells are more prone to activation induced cell death and exhaustion [541, 542]. Indeed, at baseline conditions, expression of TIM3 and LAG3 was elevated on the CD8+ anti-MCAM and anti-CD19 CAR T cells in comparison with their CD4+ counterparts.

Not only are CD4+ CAR T cells effective in their own right, they also increase the proliferation [535, 538, 543] and lytic functions of CD8+ T cells [535]. *In vivo*, preparations containing balanced numbers of CD4 and CD8 T cells mediated stronger anti-tumour effects than CAR T cells derived from bulk unfractionated PBMCs, which typically contained an excess of CD8+ cells [535, 536, 538, 539, 543]. These differences may in part be due to increased persistence of the adoptively transferred cells in the balanced CD4:CD8 groups [536]. Furthermore, long term follow-up of some early anti-CD19 CAR T cell recipients demonstrated that although CD8+ cytotoxic cells were important in the early response, it was actually cytotoxic CD4+ T cells that formed the bulk of the long surviving CAR+ population at 10 years post treatment [544]. The optimal ratio of CD4:CD8 at the time of adoptive transfer appears to be 1:1 [536], which can be achieved by separately generating CD4+ and CD8+ CAR T cells [534] or by establishing mixed cultures with a starting CD4:CD8 ratio of 70:30 [543].

In light of this, CAR T cell preparations produced in this project, with their CD8-skewed populations, may not mediate optimal anti-tumour effects *in vivo*. Their *in vitro* lytic activity against MCAM+ target cells was reasonable and appeared to correspond to the MCAM expression by the target cells, in agreement with the findings of Hyrenius-Wittsten et al, who recently published their findings with a similar M1.BBz construct [460]. However, production of cytokines in response to target was low-moderate at best. IFN-γ was produced to the highest levels, as would be expected with a

predominantly CD8+ population, whereas only modest increases in TNF-α were detected. No convincing IL-2 response was observed at all for the M1.BBz and M40.BBz CAR constructs, which is also in accordance with Hyrenius-Wittsten et al [460].

Contrastingly, CD19.BBz CAR T cells were robust producers of IL-2 on coculture with the 888-Mel CD19-GFP cell line, despite having a comparable CD4:CD8 ratio, implying that other factors may determine the cytokine response. For individual donors, CD34 expression was broadly equivalent across all CAR groups, however it was not possible to detect cell surface CAR expression in the CD19.BBz CAR T cells due to the lack of a suitable CD19-Fc reagent. Therefore it is possible that the stronger cytokine response could be a result of elevated CAR expression. The expression of activation and exhaustion markers at rest and in response to target was relatively equivalent across the different CAR groups, however the expression of specific memory markers was not assessed. Conceivably the exposure of CD19.BBz CAR T cells to CD19+ B cells carried through from the initial PBMC preparation may have impacted on the memory status and therefore effector functions of the resulting cells [535], highlighting the importance of quantifying the proportion of naïve (T_N), central memory T cells (T_{CM}), effector memory T cells (T_{EM}) and effector T cells (T_{EFF}) in future work.

As part of the expansion process T cells were cultured in moderate dose IL-2 for a total of 16 days. While necessary for optimal cell expansion [545, 546], long term exposure to IL-2 can selectively promote CD8+ T cell expansion, as well as reducing IFN-γ and IL-2 production, degranulation and *in vitro* and *in vivo* tumour cytotoxicity [546]. It also reduces the percentage of long-lived memory CAR T cells in the final product, with a greater proportion of T_{EFF} cells, which has a negative impact on tumour control [545, 546]. A 2019 meta-analysis of CAR T cell clinical trials also found that the use of IL-2 during the *in vitro* expansion period was correlated with a lower overall response rate [176].

Therefore, it is possible that the quality of the cell product may be optimised not only by controlling the initial CD4+ and CD8+ percentages, but also by optimising the culture protocols, for example by using CD3/CD28 Dynabeads and a reduced IL-2 dosing schedule [546, 547]. Substituting IL-2 altogether for IL-7 and/or IL-15 has been suggested to increase the memory cell fraction [548, 549] and generate CAR T cells

capable of maintaining anti-tumour effector functions following repeated exposure to antigen [550]. IL-7 and IL-15 have also been shown to augment *in vivo* anti-tumour activity [550, 551].

Following the expansion phase, CAR T cells were characterised and cryopreserved, prior to thawing 2-3 days before use in *in vitro* assays. Cryopreservation is commonly used in clinical manufacturing pipelines for logistical reasons, and in a GMP setting this process is tightly controlled, reproducible and often automated [513]. Panch et al analysed the differential responses of patients receiving fresh or cryopreserved anti-CD19 or anti-CD22 CAR T cells and found that they did not differ in terms of T cell persistence, expansion or clinical responses. Nor did the composition of the product change pre- and post-thaw in terms of the percentage CD3+ cells or the CD4:CD8 ratio. However, they did find that healthy donor PBMCs subjected to CAR T cell manufacturing protocols which included a cryopreservation step were enriched for genes involved in apoptosis and damage response pathways [552].

Although best efforts were made to be consistent in the manual freezing and thawing of the CAR T cells in this project, it is likely that the cryopreservation step may have impaired their fitness and efficacy in subsequent assays. To optimise this process and to confirm whether it impacts their functionality, it would be informative to challenge matched CAR T cells before and after cryopreservation in a range of co-culture assays, especially focusing on cytokine production, cytotoxicity, and the expression of cell surface activation and exhaustion markers.

It is clear therefore that the CAR T cell generation process would benefit from further optimization, and that this may improve the effector responses observed *in vitro*. Increasing the transduction efficiency or enriching cells for CD34 would likely serve a similar purpose. On average, approximately 1/3 of T cells were CAR positive as measured by CD34 expression (although this varied significantly by donor), which could potentially be increased by switching to a lentiviral vector or modifying the activation and/or transduction procedures.

The above protocol refinements would be applicable for all future research, regardless of the specific CAR construct, however this research also aimed to address how the

M1.BBz and M40.BBz CAR constructs compared. While CD34 expression was equivalent for the 2 groups, CAR expression as measured by scFv detection trended higher in the M40.BBz group. The percentage of CD34+ cells lacking scFv expression was also consistently higher in the M1.BBz cells, which displayed reduced CAR expression as detected by western blot. Taken together, it appears that the M1.BBz CAR may be less stable than the M40.BBz construct, although why this might be is unclear, especially given that the 2 scFv sequences were highly similar, differing only at the CDR regions.

Improved effector functions were detected with the M40.BBz CAR group in certain assays; however, this effect was not detected in all conditions and did not always achieve statistical significance in the pooled groups. M1.BBz and M40.BBz CAR T cells were equalised for transduction efficiency through the addition of mock T cells from the same donor. For this purpose, CD34 expression was used as a marker of transduction: given the increased percentage of scFv- cells in the M1.BBz CD34+ fraction, it is likely that the equalised M40.BBz population still contained a higher percentage of CAR-expressing cells. As a result, it is difficult to conclude if the trend towards augmented effector functions with M40.BBz was due to increased CAR stability or mediated by inherent differences in scFv affinity.

Targeting MCAM as a tumour-associated antigen also poses some specific challenges to CAR T cell efficacy. Soluble MCAM in the plasma or tumour microenvironment could potentially drive tonic CAR signalling, leading to AICD [273, 508, 509]. However, short term culture with high level sMCAM did not cause T cell activation or exhaustion as measured by upregulation of cell surface markers. Although promising, this was only measured after 24 hours, and therefore future research should investigate the effect of prolonged exposure to sMCAM. Additionally, sMCAM does not appear to abrogate cytokine production in response to targets; however, it would be beneficial to rule out any impact on a broader range of effector functions, such as degranulation and cytotoxicity.

An additional challenge specific to anti-MCAM CAR T cells is the reported expression of MCAM on a subset of CD3+ T cells in the peripheral blood. Accounting for only around 2 % of circulating T cells [328, 329, 331–333], MCAM+ CD3+ T lymphocytes are

predominantly CD4+ [328, 338, 343], polyclonal [329, 330], and have a memory phenotype (CD45RO+ CD45RA- CCR7-) [328, 329, 331, 333, 334]. This fraction of cells is enriched for the expression of IL-17, CCR6, CXCL13 and IL-23R, identifying them as Th17 cells (reviewed in [512]. Present at low numbers in homeostasis, MCAM+ Th17 cells account for an increased percentage of the CD4+ subset in inflammatory conditions including rheumatoid arthritis [328, 336], contact dermatitis, psoriatic arthritis [336–338, 343], and multiple sclerosis [331]. MCAM+ T cells have also been isolated from the sites of active inflammation (CSF, skin lesions and synovial effusions), suggesting that they may play a causal role in such pathologies [328, 341, 343, 553].

The presence of MCAM+ cells within the M1.BBz and M40.BBz groups could conceivably result in trans-activation of the CAR expressing cells, increasing the likelihood of exhaustion and resulting in destruction of the MCAM+ Th17 subset. At baseline, the percentage of CD3+ positive cells expressing MCAM was minimal for all groups, representing <1.5 % of the total population. This is unsurprising given the paucity of CD4+ cells in the final CAR preparations, and the fact that the expansion protocol did not include any of the cytokines typically required for the expansion of Th17 cells [554, 555].

A reduction in this fraction was apparent in the M1.BBz and M40.BBz groups, suggesting that clearance of MCAM-expressing T cells may well have occurred. However, this does not appear to be a significant driver of exhaustion, as TIM3, LAG3 and PD-1 expression is relatively comparable between the anti-MCAM and CD19 control CAR groups. It should be noted that the data on MCAM expression on CAR T cells is preliminary and was only collected for 2 donors, so further repetition is required to confirm the findings. Reports suggest that Th17 cells upregulate MCAM in response to exogenous activating stimuli [329, 330, 333, 553], and therefore it would also be beneficial to assess MCAM expression on stimulated M1.BBz and M40.BBz CAR T cells over an extended timescale.

4.5. Conclusion

To conclude, the anti-MCAM activity mediated by M1.BBz and M40.BBz CARs in the JRT3-T3.5 Jurkat line was replicated in the context of primary T cells. Such cells were able to produce proinflammatory cytokines, degranulate and lyse target cells in an MCAM-dependent manner, with evidence that M40.BBz may outperform M1.BBz in certain assays. Donor-to-donor variability was high, illustrating the importance of repeating this work with additional donors. While the CAR T cell production protocol generated significant numbers of CAR+ cells, selective expansion of the CD8+ subset was observed which is likely to have had an impact on the overall anti-tumour efficacy of such cells. Therefore, protocol optimisation will be required for future studies.

4.6. Chapter 4 Appendix

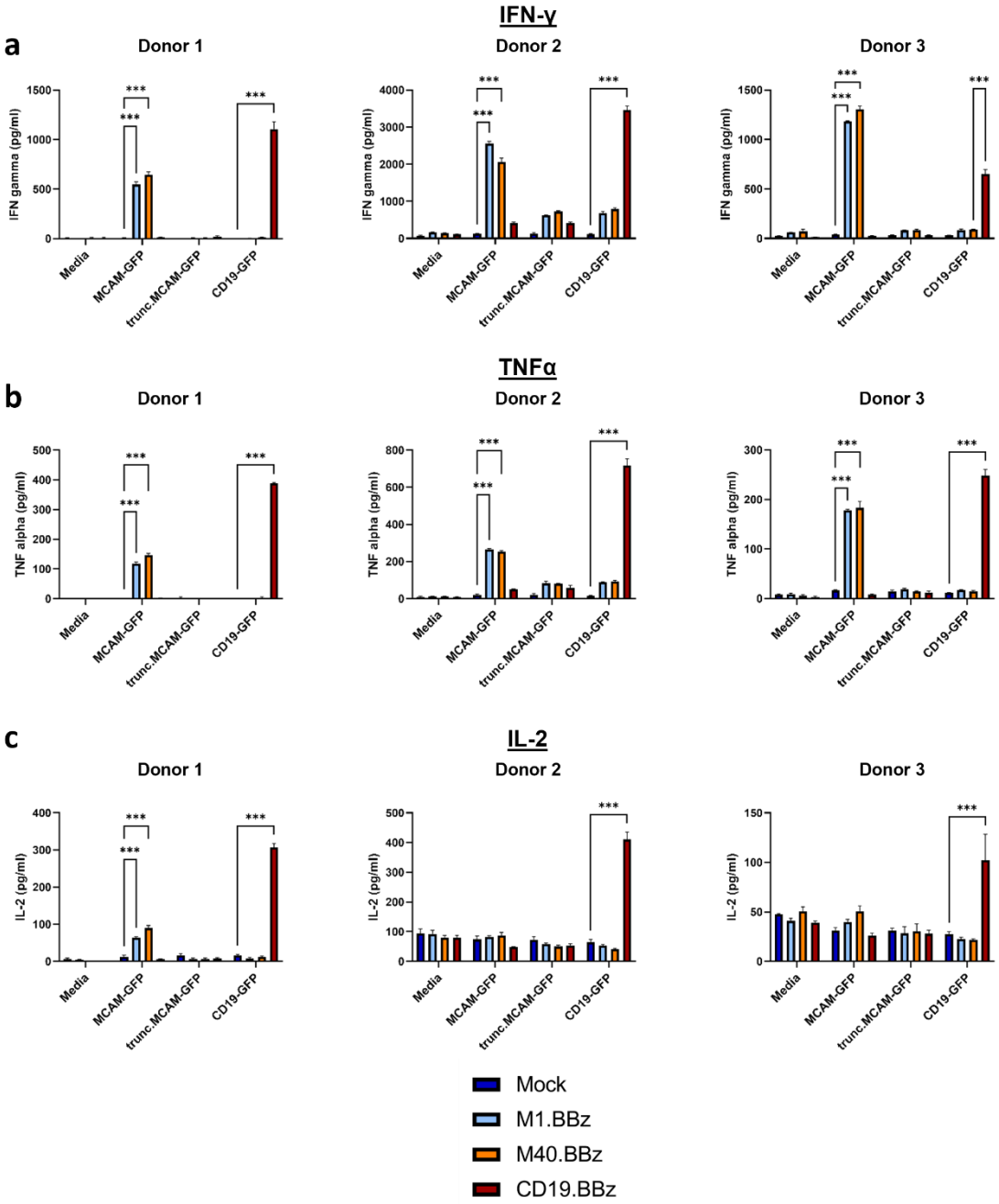

Figure 4.13 Cytokine production by CAR T cells on coculture with 888-Mel target cell lines. CAR T cells were incubated with 888-Mel target cell lines at a 5:1 effector-to-target ratio. After 20 hours, supernatant was collected, and cytokines were quantified by sandwich ELISA. For each donor triplicate measurements were taken. Results are displayed as mean and standard deviation, one donor per graph.
Statistical analysis is by two-way ANOVA with Tukey's multiple comparisons. * $p<0.05$, ** $p<0.01$, *** $p<0.001$.

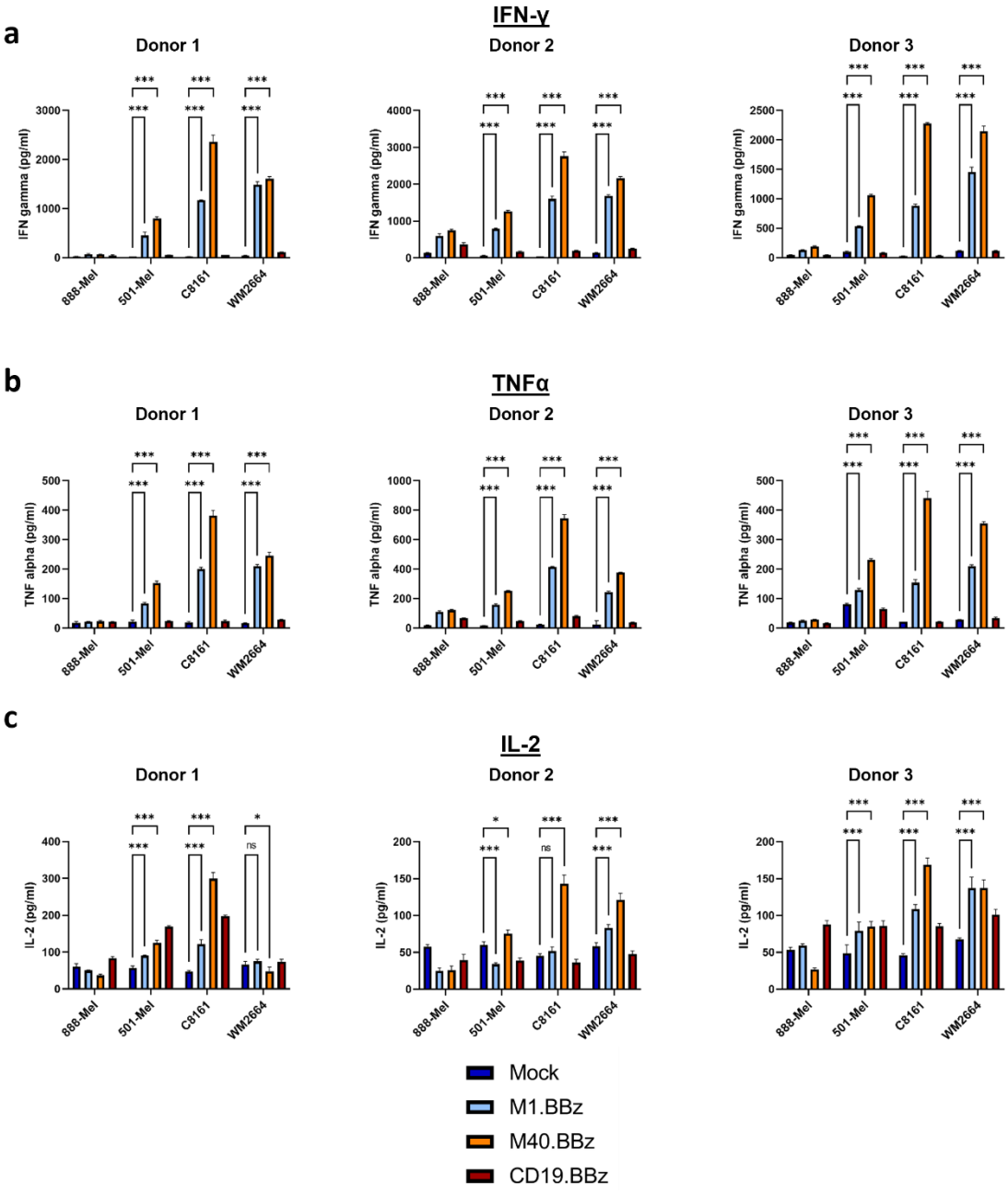

Figure 4.14 Cytokine production by CAR T cells on coculture with melanoma target cell lines.

CAR T cells were incubated with melanoma cell lines at a 5:1 effector-to-target ratio. After 20 hours, supernatant was collected and cytokines were quantified by sandwich ELISA For each donor triplicate measurements were taken. Results are displayed as mean and standard deviation, one donor per graph.

Statistical analysis is by two-way ANOVA with Tukey's multiple comparisons. * p<0.05, ** p<0.01, *** p<0.001.

Chapter 5. Developing additional models of CAR T cell functionality

5.1. Introduction

M1.BBz and M40.BBz CAR constructs proved capable of redirecting primary CAR T cells against MCAM, inducing various effector functions on exposure to target-expressing cancer cell lines *in vitro*. However, significant questions relating to their efficacy and safety remain unanswered, especially regarding their behaviour in the more complex immune-modulating environments encountered *in vivo*. The final chapter of this project aimed to address these questions through *in vitro* and *in vivo* models.

While *in vitro* assays can provide a useful readout of CAR T cell efficacy, certain essential functions, such as the ability to traffic to the site of the tumour, survive, and mediate anti-tumour responses in the face of the immunosuppressive tumour microenvironment can only be assessed *in vivo*. Typically, this has involved mouse xenograft models, commonly performed in NOD.Cg-Prkdc^{scid} Il2rg^{tm1Wjl}/SzJ (NSG) mice to avoid the problems posed by CAR T cell immunogenicity and allow the response against human cancer cell lines to be assessed [556]. Alternatively, pre-conditioning total body irradiation or artificially inducing tolerance to extracellular CAR domains can be used to reduce the likelihood of anti-CAR immune responses and improve the persistence of CAR T cells in immunocompetent mice [557].

While mouse studies may differ in terms of the mouse strain and preconditioning regimen, they generally all proceed according to a similar protocol: tumour cells are implanted and allowed to engraft, prior to the introduction of CAR T cells (of human or mouse origin, depending on the model). *In vivo* CAR efficacy is assessed according to tumour growth, signs of overt toxicity and overall mouse survival, often with no means of evaluating the intermediate steps such as CAR T cell trafficking and accumulation in the tumour microenvironment.

To address this, various strategies are under development to facilitate *in vivo* imaging of adoptively transferred CAR T cells, which can be broadly categorised into 3 groups: those which involve pre-labelling cells with radioactive isotopes such as Indium-111 [558]; those which utilise radiolabelled antibodies and immunoPET technology to

detect CAR T cells [559]; or those which leverage already available PET tracers to detect co-expressed proteins such as herpes simplex virus type 1 thymidine kinase, somatostatin receptor type 2 or the human sodium iodide symporter [560–563]. Using these technologies several groups have demonstrated that CAR T cells appear to initially traffic to the lungs, followed by the liver and spleen, with eventual accumulation in tumour sites [563, 564]. In the context of B cell malignancies, trapping of CD19 and CD20-specific CAR T cells in the lungs was attributable to their formation of aggregates with B cells [564, 565]. The feasibility of several of these techniques has also been evaluated in preliminary clinical studies, which demonstrated that Lewis Y antigen-redirected CAR T cells initially trafficked to the lung and subsequently accumulated in the spleen and bone marrow of in patients with haematological malignancies [558, 566].

Although promising, these techniques are specialised and require lengthy mouse studies. We proposed that the zebrafish (*Danio rerio*) could provide an intermediate model in between basic *in vitro* assays and *in vivo* studies, identifying CAR constructs which retain anti-tumour efficacy in a more complex 3D environment. Zebrafish are small freshwater fish named for their pattern of longitudinal pigmented stripes. They have been increasingly used as a model organism in immunological research for several key reasons, including their small size and large number of off spring. Fertilised eggs develop ex utero, and are transparent for approximately the first week, allowing easy visualisation of embryonic and larval development [567]. Several pigment deficient lines have also been created, which facilitate similar imaging in adult fish [568, 569]. Many cell types of the innate and adaptive immune systems are conserved in zebrafish, including macrophages [570], neutrophils [571], eosinophils [571, 572], dendritic-like cells [573] and B and T lymphocytes with VDJ recombined receptors [574]. These are largely absent from the early embryo; antibody responses are only mounted from 4-6 weeks post fertilisation [575].

Tumour cells, when fluorescently labelled and injected into zebrafish embryos, form distinct tumours which can be easily monitored with non-invasive imaging [576]. Such assays can be carried out in their entirety before 5 days post fertilisation, prior to the point at which zebrafish embryos acquire protected status under ASPA 1986

legislation, thereby providing a quick, high throughput assay with comparatively low barriers to access compared to mouse studies. Furthermore, the lack of adaptive immune responses at this early stage of development means that host immune responses against xenografted CAR T cells would not be expected.

With the aim of assessing the feasibility of such a model system, this chapter describes my efforts to perform pilot assays in which tumour and T cells were co-injected into zebrafish embryos. This was with a view to eventually modifying such a model to allow live *in vivo* tracking of CAR T cell trafficking and anti-tumour responses (although due to time constraints it was not possible to develop the model to this stage as part of this project).

An additional pressing concern that would require extensive investigation before M1.BBz and M40.BBz could ever be considered for human trials is their safety profile, specifically the high risk of on-target off-tumour toxicity directed against the vasculature. MCAM expression has been reported on blood vessels, generally localised to the endothelium [449, 577–581] with some evidence that it is also expressed pericytes [582] and smooth muscle cells [449, 577, 581]. It is generally found on capillaries rather than larger calibre vessels [577], although some expression on arteries and veins has been reported [579]. It has also been used as a marker of circulating endothelial cells in various pathologies, including vasculitis [583], trauma [584], atherosclerotic vascular disease [585] and breast cancer [586].

HUVECs, a widely used laboratory model of endothelial cells, are commonly reported to express MCAM [446, 448, 580, 587–589], although this is significantly upregulated by *in vitro* culture compared to in situ [577, 588]. The cellular location of MCAM on HUVECs and endothelial progenitor cells is dependent on the isoform of MCAM and the confluency of the culture. In subconfluent populations, the long isoform is primarily found intracellularly, while the short isoform is comparatively upregulated, and localised to the apical membrane, the migrating edge of the cell, and the nucleus [590]. At confluency, some diffuse expression of short-MCAM is detectable, but the strongest staining is observed at points of cell-cell contact [580, 587]. This is mediated by the long isoform of MCAM, which is located at the basolateral membranes and cell-

cell junctions (although it is not involved in adherens junctions or focal adhesions) [590, 591].

MCAM also appears to play an active role in angiogenesis. VEGF-induced micro-vessel formation in Matrigel plugs is significantly reduced in MCAM knock-out mice [447]. Similar effects were mediated by the MCAM-targeting inhibitory microRNA, miR329, which also significantly reduced vessel formation in a murine model of oxygen induced retinopathy [592]. In chick chorioallantoic membrane (CAM) assays, vasculogenesis was significantly impaired in the presence of MCAM-blocking antibodies [588]. Finally, anti-MCAM and anti-VEGF antibody treatment worked synergistically to reduce vessel number and tumour size in mice bearing pancreatic tumours [447].

As expected, targeting MCAM also alters HUVEC behaviour *in vitro.* Blocking MCAM with antibodies, siRNA or miR329 reduces HUVEC proliferation [588, 589] and migration [325, 447, 588, 589, 592], increases monolayer permeability [325, 590] and inhibits the formation of capillary-like structures on Matrigel [425, 447, 448, 592, 593]. While the short MCAM isoform appears to modulate the early stages of angiogenesis (namely HUVEC proliferation and migration), the formation and stabilisation of capillary networks is mediated by the longer isoform [590].

How exactly MCAM mediates these pro-angiogenic effects is not fully understood, but several signalling pathways have been implicated [446, 447, 594, 595]. Perhaps most importantly, it acts as a co-receptor for tumour-expressed VEGF [447], and is necessary for various VEGF induced responses, including migration, motility, and tube formation [447, 588, 596]. VEGF-VEGFR2 binding triggers homodimerisation of both MCAM and VEGFR2, leading to a downstream p38-IKK-NF-κB signalling cascade which ultimately results in the transcription of several genes involved in angiogenesis [447, 596]. Such signalling is dependent on the ability of MCAM to dimerise and interact with the cytoskeleton by binding to ERM proteins [447, 596]. A similar role has been identified for MCAM in PDGFB-PDGFRβ signal transduction, which is also dependent on its interaction with ERM proteins [582].

Given its putative role in angiogenesis, it is perhaps not surprising that MCAM has been reported to be expressed at higher levels in tumour vasculature compared to

healthy tissue sections [577, 588, 597]. Furthermore, it is unclear whether MCAM on quiescent vasculature would be accessible to CAR T cells, given its predominant expression at the basolateral membrane and areas of cell-cell contact. While this raises the possibility that there may be a therapeutic window for targeting MCAM, it is still an area of significant concern. To begin to address these safety questions I aimed to characterise CAR T cell activity against HUVECs, both in standard *in vitro* culture conditions and in response to established HUVEC capillary-like networks.

5.2. Methods

5.2.1. Pilot zebrafish embryo xenograft studies

For full details of zebrafish husbandry, breeding and xenotransplantation see section 2.2.5.

Briefly, 3 days prior to the planned assay date, pairs of *nacre* zebrafish were placed in a crossing tank with mesh insert, separated by a transparent divider. To synchronise embryo development, dividers were removed the following morning, with fertilised embryos collected 30 minutes later. Embryos were raised in petri dishes in chorion water (see section 2.1.1) until they reached approximately 52 hpf, at which point most embryos had hatched. Anaesthetised embryos were placed on pre-made injection plates and a cell suspension containing a 1:4 ratio of Vybrant DiI labelled 888-Mels and CTV-labelled CAR T cells was injected into the pericardiac space using a micromanipulator, Pico-injector micro-injection station (Warner Instruments) and inverted microscope.

Embryos were screened immediately, subsequent to embedding in 1.5 % (w/v) low-gelling temperature agarose in chorion water, to immobilise them and facilitate imaging on the Leica SP8 Upright Confocal Microscope (for full details of microscope set up see section 2.2.5.6).

For full details of the image analysis protocol using Fiji, see section 2.2.5.7. Briefly, Z-stacks were split into their respective channels, from which maximum intensity projections were generated. These images were thresholded to create new binary images, representative of the tumour and T cells. The Fiji Analyse tool was then utilised to measure the respective thresholded areas as an approximation of tumour burden and T cell persistence.

5.2.2. Assessment of anti-HUVEC CAR activity in standard culture conditions

Pooled HUVEC cells were acquired from Lonza (C2519A) and cultured in HUVEC media (EGM-2 BulletKit medium, Lonza) (section 2.2.2.1). All assays were conducted prior to passage 6. Cytokine production by CAR T cells in response to HUVECs was assessed as previously described (section 2.2.3.2), with a 4:1 effector-to-target ratio and a 24-hour culture period in standard, round-bottomed tissue culture plates. The annexin V/PI cell viability assay is described in full in section 2.2.3.6, and involved culturing HUVEC cells and CTV-stained CAR T cells at a 4:1 effector-to-target ratio for 20 hours. At the end of the culture period, non-adherent cells were harvested, and the plates were washed with PBS prior to the addition of accutase to dissociate adherent cells. RPMI + 10 % FBS was added to stop the reaction, and cells were subsequently washed twice in FACS buffer. Staining then proceeded according to the manufacturer's instructions, using the FITC Annexin V Apoptosis kit with PI (BioLegend). Samples were immediately analysed on the Fortessa flow cytometer, using BD FACS Diva software.

5.2.3. HUVEC network formation assay

To model the formation of capillary networks by HUVECs, 96-well µ angiogenesis plates (Ibidi) were coated with 10µL/well ice-cold Cultrex Basement Membrane Extract (BME, R&D Systems) (for full protocol see section 2.2.4). A 1-hour incubation at 37 °C ensured the coating was set, at which point 70µL/well HUVEC media was added to prevent the wells drying out. Plates were stored at 37 °C for 24-48 hours to ensure that the gel layer was fully hydrated. The following day, media was aspirated off prior to the addition of 1 x 10^4 HUVECs per well, which had been stained with Vybrant DiI Cell Labelling Solution (Invitrogen) according to manufacturer's instructions.

Depending on the assay in question, plates were either immediately transferred to the LiveCyte Quantitative Phase Imaging Microscope (Phasefocus, see below), or were retained in the standard incubator to allow networks to be established prior to the addition of melanoma cells and/or T cells. To investigate the effect of melanoma cells

on the network, Vybrant DiO- or DiD-labelled WM2664 cells were added at 2.5 x 10^3 cells/well to the HUVEC-containing µ angiogenesis plates, which had been incubated for 6 hours to allow the formation of visible networks. Imaging either commenced immediately, or plates were incubated for a further 4 hours prior to the addition of 1-4 x 10^4 CTV-labelled T cells.

Sequential phase contrast images were acquired for a period of 20-24 hours on the LiveCyte Quantitative Phase Imaging Microscope, during which time the attached environmental control chamber maintained cells at a temperature of 37 °C with 5 % (v/v) CO_2. Fluorescence images were acquired concurrently, using the Texas Red (Vybrant DiI), FITC (Vybrant DiO), Cy5 (Vybrant DiD) and DAPI (CTV) filter cubes.

Images were exported as Tiff stacks and were subsequently analysed in Image J (Fiji) [395]. The full image analysis protocol is described in section 2.2.4.3. Briefly, the files were split by channel into separate Tiff stacks, from which individual time point images were extracted. The total branching network length was estimated running the Angiogenesis Analyzer plug-in by Gilles Carpentier [396] on the phase contrast images.

To estimate the network area and co-localisation, each individual fluorescence time point image was thresholded to create a new binary image. The thresholded regions, corresponding to the HUVEC networks, WM2664 cells or CAR T cells (red, green and blue channels, respectively) were measured using the inbuilt Fiji measurement tools. To visualise T cell colocalization with the HUVEC (or WM2664) networks, the Fiji Image Calculator was used to output new images which displayed common thresholded areas for the matched HUVEC and T cell images. The degree of colocalization was quantified by measuring the thresholded area in these overlay images, compared to the T cell-only thresholded images. This protocol was repeated to investigate T cell co-localisation with WM2664 images.

5.3. Results

5.3.1. CAR T cell and melanoma zebrafish embryo xenografts – a pilot study

All assessments thus far had been carried out *in vitro* and therefore any conclusions on the efficacy of the M1.BBz and M40.BBz CAR T cells were tentative, pending confirmation in industry standard mouse models. Given the length and statutory requirements of such studies, a quick intermediate model to bridge the gap between *in vitro* and mouse experiments may add value to the standard CAR T cell testing pipeline. The zebrafish embryo is transparent, lacks an adaptive immune response and is not subject to ASPA 1986 regulations until 5 days post fertilisation [567, 598]. Xenografting human cancer cell lines into zebrafish has been widely used as a strategy for identifying therapeutic drugs [576], and therefore we hypothesised that a similar model may prove suitable for testing CAR T cells.

To this end, a protocol was developed which is illustrated in Figure 5.1. For the purposes of this assay, the *nacre* zebrafish line was used, which lacks melanophores due to a mutation in the *mitf* gene, thus aiding non-invasive imaging [569]. To enable their tracking, CAR T cells were labelled with CTV, while the 888-Mel MCAM-GFP line was labelled with DiI which was found to provide a stronger, more homogenous signal than GFP alone. The 888-Mel MCAM-GFP line was selected over other MCAM+ melanoma targets as 888-Mels have previously been successfully xenotransplanted into zebrafish embryos, where they form distinct tumour masses [599]. Cell suspensions containing a 4:1 mix of CAR T cells and tumour cells were injected into the pericardiac space of 52 hpf *nacre* embryos using a micromanipulator. As they had shown signs of improved functionality compared to the M1.BBz group in earlier *in vitro* assays, M40.BBz CAR T cells were selected for use in the pilot zebrafish embryo xenograft assays, along with mock control cells. Successfully injected embryos were screened and immobilised in low melt agarose, a substrate in which they can survive for >48 h. Baseline images were acquired at 2 hours post injection (hpi) with end point images taken 22-24 hours later.

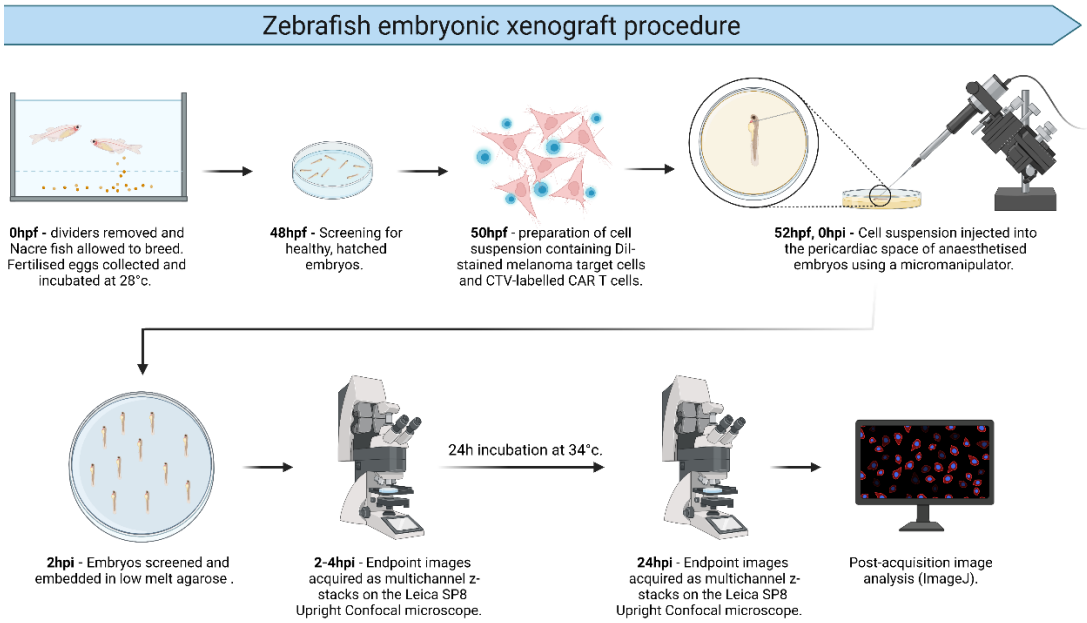

Figure 5.1 Schematic of the zebrafish xenograft model assay.
CAR T cells labelled with CTV were injected into the pericardiac space of 52 hpf *Nacre* embryos along with Vybrant DiI labelled 888-Mel MCAM-GFP cells. Embryos were screened, immobilised in low gelling temperature agarose, and imaged on the Leica SP8 Upright Confocal microscope at 2 and 24 hpi. Figure created with Biorender.com.

During the 24-hour incubation period plates must be kept at a temperature tolerated by both the embryos and the T cells, which normally require respective temperatures of 28 °C and 37 °C. Previous studies have shown that 34 °C is an acceptable compromise which allows the survival of the engrafted human cells without increased embryo mortality [599]. To test whether CAR T cells were active at this temperature, cocultures were established with the 888-Mel MCAM-GFP and 888-Mel trunc.MCAM-GFP cell lines. Production of IFN-γ and TNF-α and CAR-mediated cytotoxicity were not significantly reduced by culture at 34 °C (Figure 5.2a). Similarly, labelling CAR T cells with CTV did not impact on their activity (Figure 5.2b).

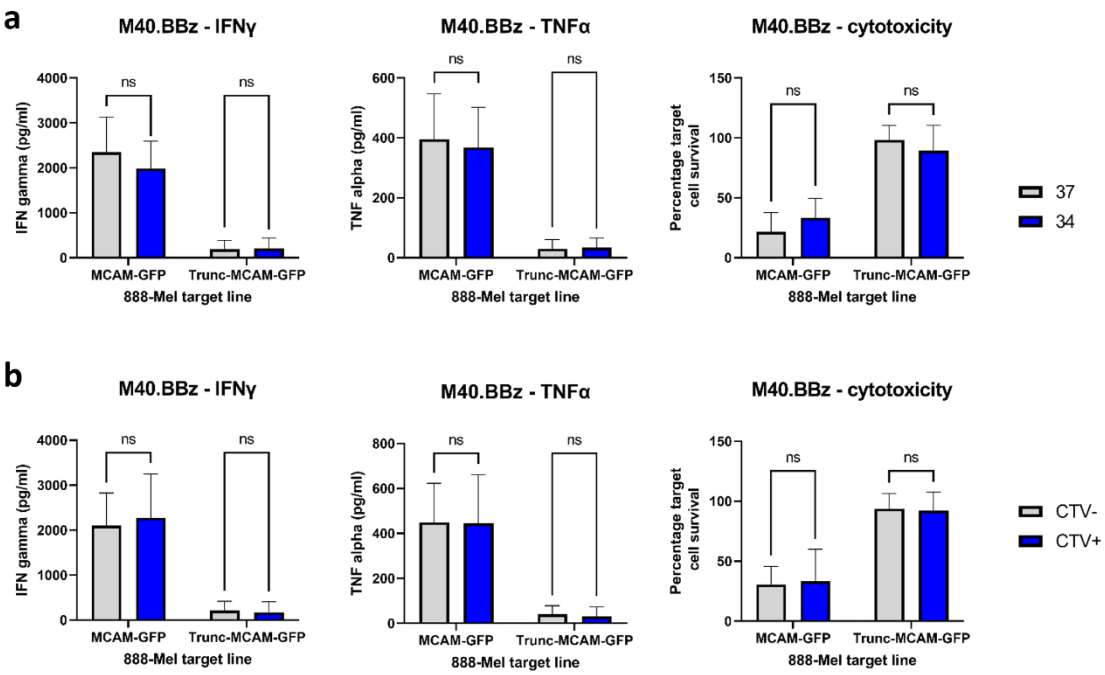

Figure 5.2 Investigating CAR T cell activity in allograft culture conditions.
(a) M40.BBz CAR T cells were incubated with 888-Mel target cell lines at a 5:1 effector-to-target ratio for 20 hours at 34 °C or 37 °C. Activity was determined by sandwich ELISA to detect IFN-γ and TNF-α. Separate cocultures were set up under the same conditions with luciferase-expressing 888-Mel cell lines. Cell survival relative to mock was determined via assay development with Steady Glo Luciferase Reagent at 20 hours. Supernatant was collected and cytokines were quantified by sandwich ELISA. (b) As in (a) except cultures were set up with T cells with and without Cell Trace Violet (CTV) labelling and were incubated at 37 °C. Results displayed are from 3 donors, and for each donor duplicate measurements were taken. Results are displayed as mean and standard deviation. Statistical analysis is by unpaired T test. * $p<0.05$, ** $p<0.01$, *** $p<0.001$.

To confirm whether T cells and tumour cells could survive in zebrafish embryos for the duration of the experiment, CTV-labelled M40.BBz CAR T cells or DiI-labelled 888-Mel MCAM-GFP cells were implanted into separate groups of 52 hpf *nacre* embryos and imaged at 2 hpi and 24 hpi (Figure 5.3a and b). While the T cells spread out over the pericardiac cavity, the tumour cells formed a more distinct mass. Tumour and T cell burden were estimated by generating a maximum intensity projection from the z-stack images and measuring the total thresholded area. This demonstrated that T cells decreased over the incubation period, which may represent cell death or their trafficking out of the pericardiac space. Meanwhile tumour area trended higher at 24 hpi but was not statistically significant at this time point.

On the basis that the CAR T cells may be preferentially retained in the pericardiac space by the presence of MCAM+ tumour cells, co-injection assays were performed with mock or M40.BBz CAR T cells (Figure 5.4a and b) and 888-Mel MCAM-GFP cells, at a 4:1 ratio. In this setting, no evidence of CAR-mediated anti-tumour activity was observed, with non-significant differences between the tumour burden in M40.BBz and mock-injected animals at 24 hours. Interestingly, for both groups tumour area decreased from baseline, at variance with the results when tumour cells were implanted alone (Figure 5.3). T cell area also decreased over the course of the experiment, to a similar degree as observed in Figure 5.3, with no significant differences in the persistence of mock and M40.BBz T cells.

It should be noted that these were early-stage pilot experiments, with a small number of fish per group. The microinjection technique required is difficult to standardise between animals, highlighting the need for alternative assays of CAR T cell function, such as HUVEC based network models.

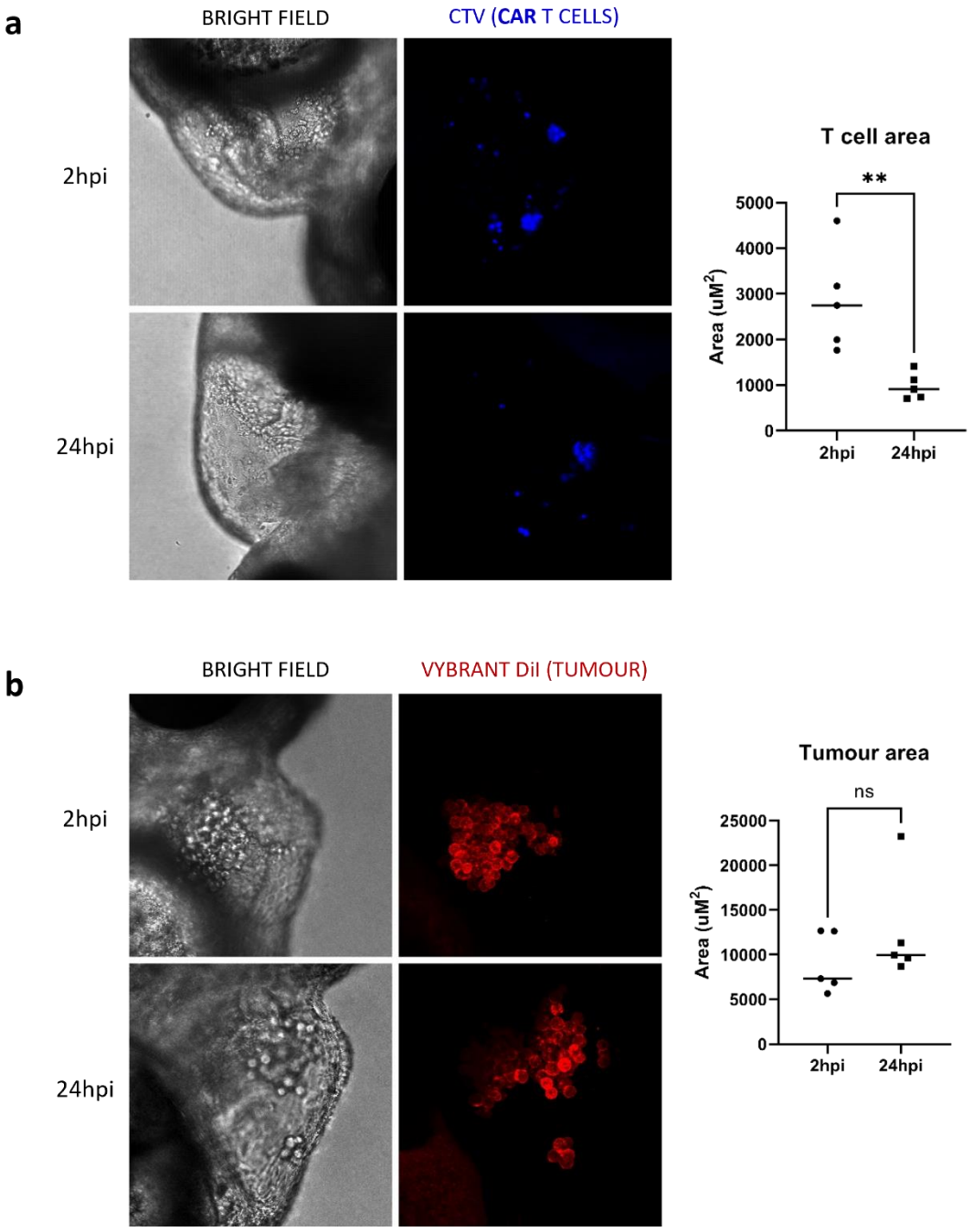

Figure 5.3 Survival of engrafted CAR T cells and tumour cells in zebrafish embryos.
(a) CTV-labelled M40.BBz CAR T cells or (b) Vybrant DiI labelled 888-Mel MCAM-GFP cells were engrafted into the pericardiac space of 52 hpf *nacre* zebrafish embryos and imaged at 2 and 24 hpi. Tumour and T cell area was estimated by generating binary maximum intensity projections from the z-stacks. Representative images are displayed. Individual results from a single experiment with a single CAR T cell donor are plotted, n = 5. Statistical analysis was by paired t-test. * $p<0.05$, ** $p<0.01$.

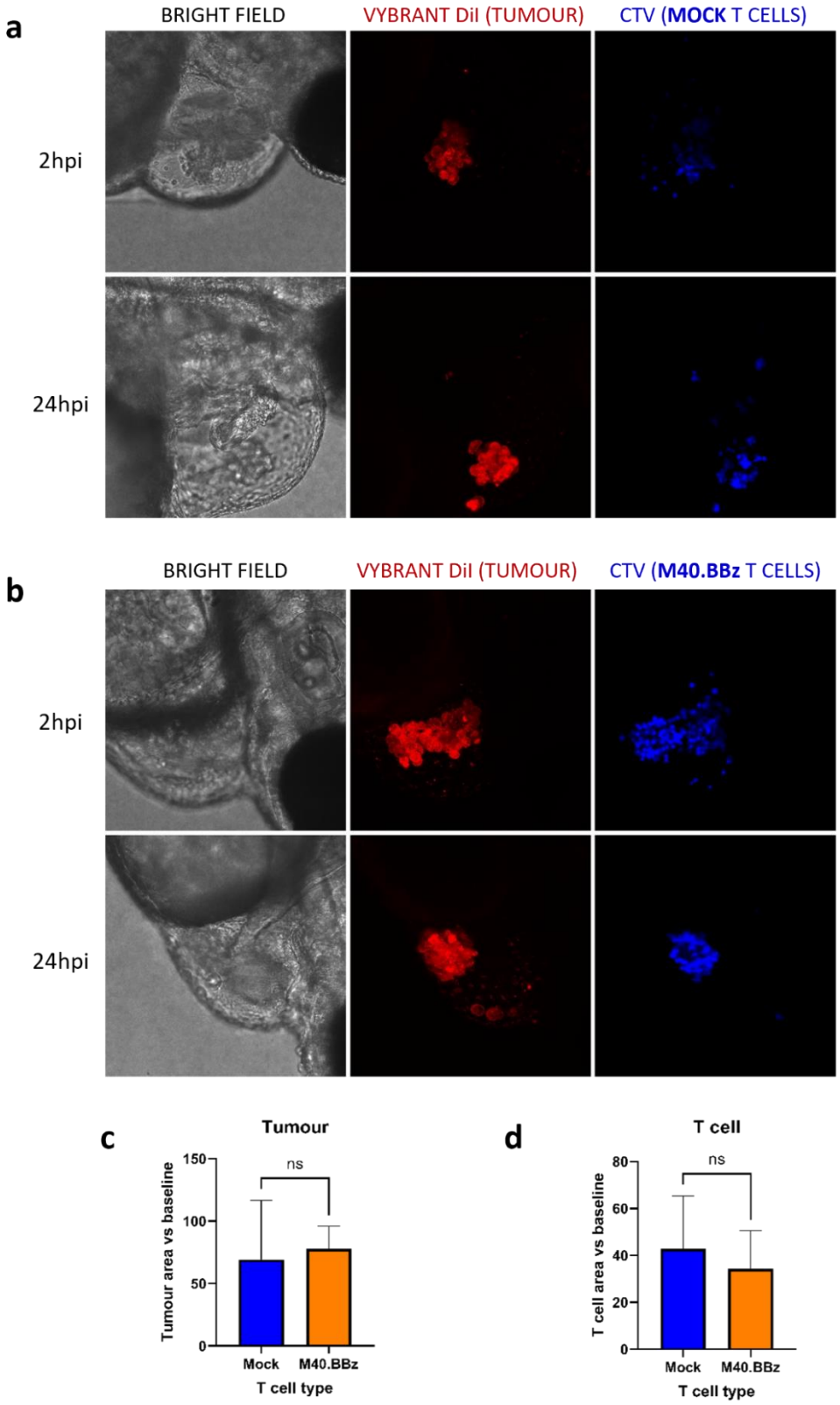

Figure 5.4 Co-injection of CAR T cells and tumour cells in zebrafish embryos.
DiI-labelled 888-Mel MCAM-GFP cells were implanted into the PCS of 52 hpf *nacre* embryos along with mock or M40.BBz CAR T cells at a 1:4 ratio. Images were acquired at baseline (2 hpi) and 24 hpi. Tumour and T cell area was estimated by generating binary maximum intensity projections from the z-stacks. Representative images are displayed. Individual results from a single experiment with a single CAR T cell donor are plotted, n = 5 (mock), n=8 (M40.BBz). Statistical analysis was by unpaired t-test. * $p<0.05$, ** $p<0.01$.

5.3.2. Anti-MCAM CAR T cell responses to standard HUVEC cultures

HUVEC cells have been reported to express MCAM, with some reports suggesting that its expression is increased on *in vitro* culture. To confirm these observations, HUVEC cells from pooled human donors (Lonza) were cultured according to established protocols, using EGM-2 (Lonza) and standard tissue culture plasticware. MCAM expression after 2 passages was assessed by western blot (Figure 5.5a) and flow cytometry (Figure 5.5b). As expected, HUVECs strongly expressed MCAM, with levels exceeding that of the WM2664 melanoma line which served as a positive control. Interestingly, this effect was especially strong in the cell lysates. Cell surface expression detected by flow cytometry was elevated to a lesser extent compared to WM2664, suggesting that a proportion of the total MCAM may be located intracellularly, as has been previously reported [590].

To assess whether M1.BBz and M40.BBz CAR T cells displayed reactivity against the HUVEC cell line, coculture assays were set up as described in section 5.2.2. Production of IFN-γ and TNF-α by the anti-MCAM CAR T cells was elevated on coculture with HUVECs, while no response occurred with CD19.BBz CAR T cells, as expected (Figure 5.5c). The magnitude of the M1.BBz and M40.BBz responses was broadly within the range that had been observed on coculture with the 888-Mel MCAM-GFP, C8161 and WM2664 cell lines (Figure 4.5 and Figure 4.9). As previously described, cytokine production was particularly impacted by donor-to-donor variability.

CAR-mediated cytotoxicity had previously been quantified through the use of luciferase-expressing target cell lines. However, this strategy was not easily applicable to HUVECs given their low transduction efficiency and the need to select for puromycin resistant cells while at the same time retaining a low passage number. Consequently, an alternative methodology was employed which used Annexin V and propidium iodide (PI) staining to identify apoptotic and necrotic HUVEC cells. Annexin V is a phospholipid binding protein which can be used to detect the translocation of phosphatidyl serine to the cell membrane, an early step in the process of apoptosis. Disrupted membrane integrity, which occurs in late apoptotic and necrotic cells, allows

PI to enter the cell and bind to nuclear DNA. Consequently, cells can be categorised as live (Annexin-/PI-), early apoptotic (Annexin+/PI-) and late apoptotic/necrotic (Annexin+/PI+) [600].

To detect CAR-driven apoptosis and necrosis, HUVEC cells were cocultured for 24 hours with CAR T cells, which were first stained with CTV to allow subsequent discrimination of targets and effectors. After 24 hours, HUVECs were stained with FITC-conjugated Annexin V and PI and analysed by flow cytometry. The percentage of live, CTV- cells is significantly reduced compared to mock for both anti-MCAM CAR T cells, with corresponding increases in the fraction of early and late apoptotic cells (Figure 5.5c). This effect is strong, with late apoptotic/necrotic cells accounting for 70 % (range 51 -81 %) and 72 % (range 52 - 84 %) of HUVEC cells in the M1.BBz and M40.BBz groups, respectively. While direct comparisons with the cytotoxicity directed against melanoma lines is difficult due to methodological differences in the Annexin V/PI and luciferase-based protocols, it is clear that M1.BBz and M40.BBz recognise MCAM on HUVEC cells in normal culture conditions, and this results in strong cytotoxic activity.

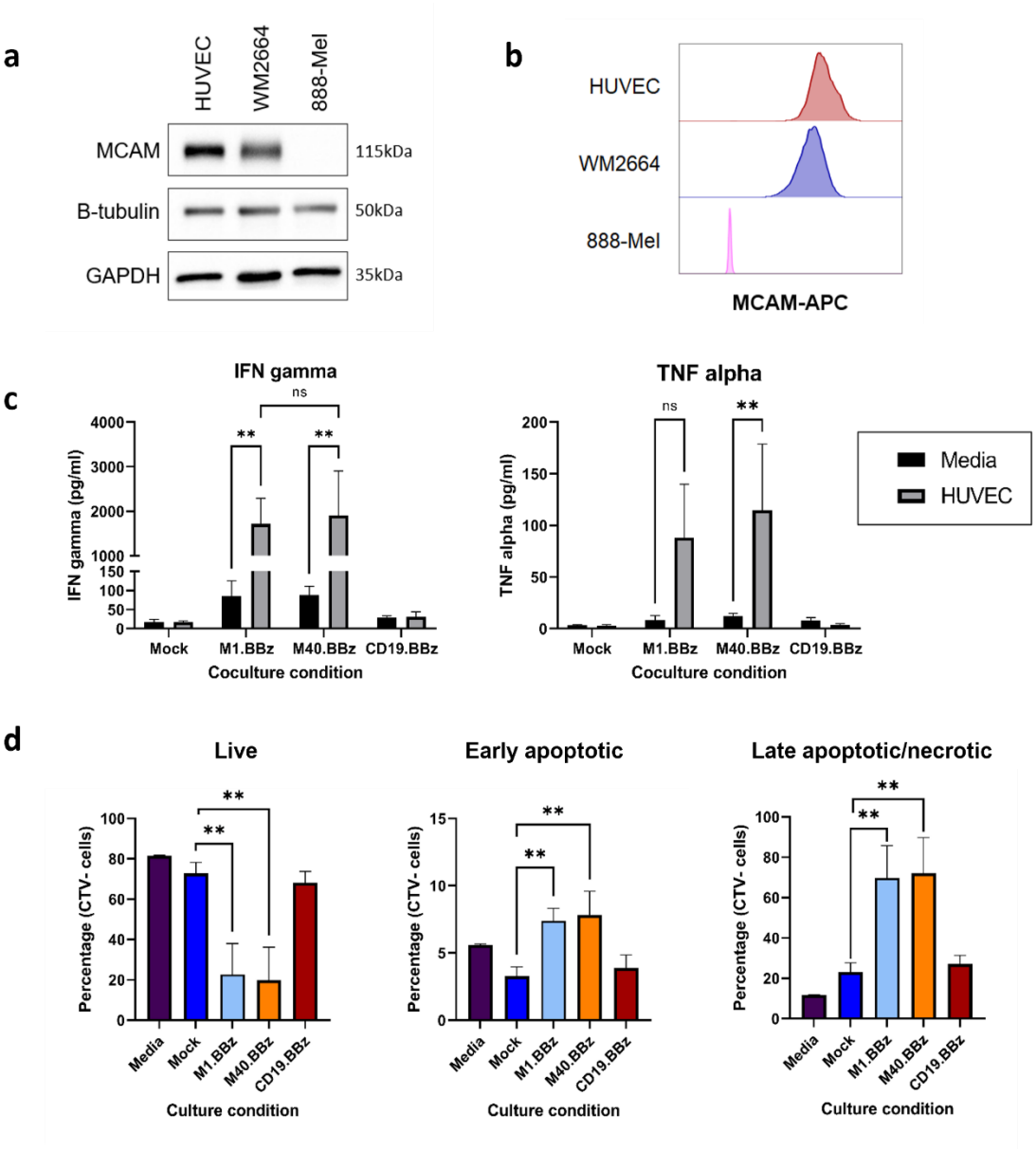

Figure 5.5 Anti-MCAM CARs T cells react against HUVEC cells in normal culture conditions. Confirmation of MCAM expression on HUVECs and WM2664s via (a) western blot and (b) flow cytometry. (c) Production of cytokines by CAR T cells incubated with HUVEC cells at a 4:1 effector-to-target ratio. After 20 hours, supernatant was collected, and cytokines were quantified by sandwich ELISA. (d) HUVEC cells were incubated with media or Cell Trace Violet (CTV) stained T cells for 20 hours at a 4:1 effector-to-target ratio. Cells were lifted with accutase, washed, and stained with Annexin-FITC and propidium iodide (PI), prior to immediate flow cytometry analysis. Single, CTV negative cells were defined as live (Annexin-negative, PI-negative), early apoptotic (Annexin single positive), and late apoptotic/necrotic (double positive). Results displayed are from 3 donors, and for each donor duplicate measurements were taken. Results are displayed as mean and standard deviation. Statistical analysis is by (c) two-way and (d) one-way ANOVA with Tukey's Multiple Comparisons. * $p<0.05$, ** $p<0.01$.

5.3.3. CAR T cell interactions with HUVECs in capillary-like networks

HUVECs grown in standard tissue culture conditions have a doubling time of approximately 24 hours (data not shown), and are therefore in a proliferating, non-quiescent state. The expression of MCAM in such actively dividing, subconfluent cultures differs from that on confluent HUVECs, with diffuse cell membrane staining at the apical surface and the migrating edge of the cell. Contrastingly, in more mature cultures, the long isoform of MCAM is found at cell-cell junctions [323, 587, 590]. Given this differential localisation pattern, it was of interest to see if the strong anti-HUVEC cytotoxic responses mediated by M1.BBz and M40.BBz were replicated when HUVECs were first allowed to form established capillary-like networks on a basement-membrane extract substrate [601–603].

To investigate the formation of such networks, DiI-labelled HUVECs were harvested and plated on either normal tissue culture plates (Figure 5.6a) or on plates pre-coated with Cultrex (R&D Systems), a commercial preparation of basement membrane extract, produced by the Engelbreth-Holm-Swarm (EHS) cell line [601]. Recurrent phase and fluorescent images were acquired over the subsequent 24 hours, during which time plates were incubated at 37 °C and 5 % (v/v) CO_2. In keeping with observations from routine culture, in the absence of BME, HUVEC cells acquired a cobblestone appearance (Figure 5.6a). During this time, cells proliferated and occupied an increasing percentage of the optical field of view. In contrast, when plated on Cultrex, HUVECs became elongated, bunching together in cords of cells which formed anastomosing networks, as described by Kubota et al [603] (Figure 5.6b). The networks had mostly formed by around 6 hours, and further matured over the remaining 18 hours, with the tubes progressively thinning. In the first few hours following plating, the optical area occupied by the HUVECs increased, likely due to them adhering to the gel layer and spreading out (Figure 5.6b). From around 4 hours post-seeding the area occupied then progressively decreased as the cells assembled into an increasingly mature network [603].

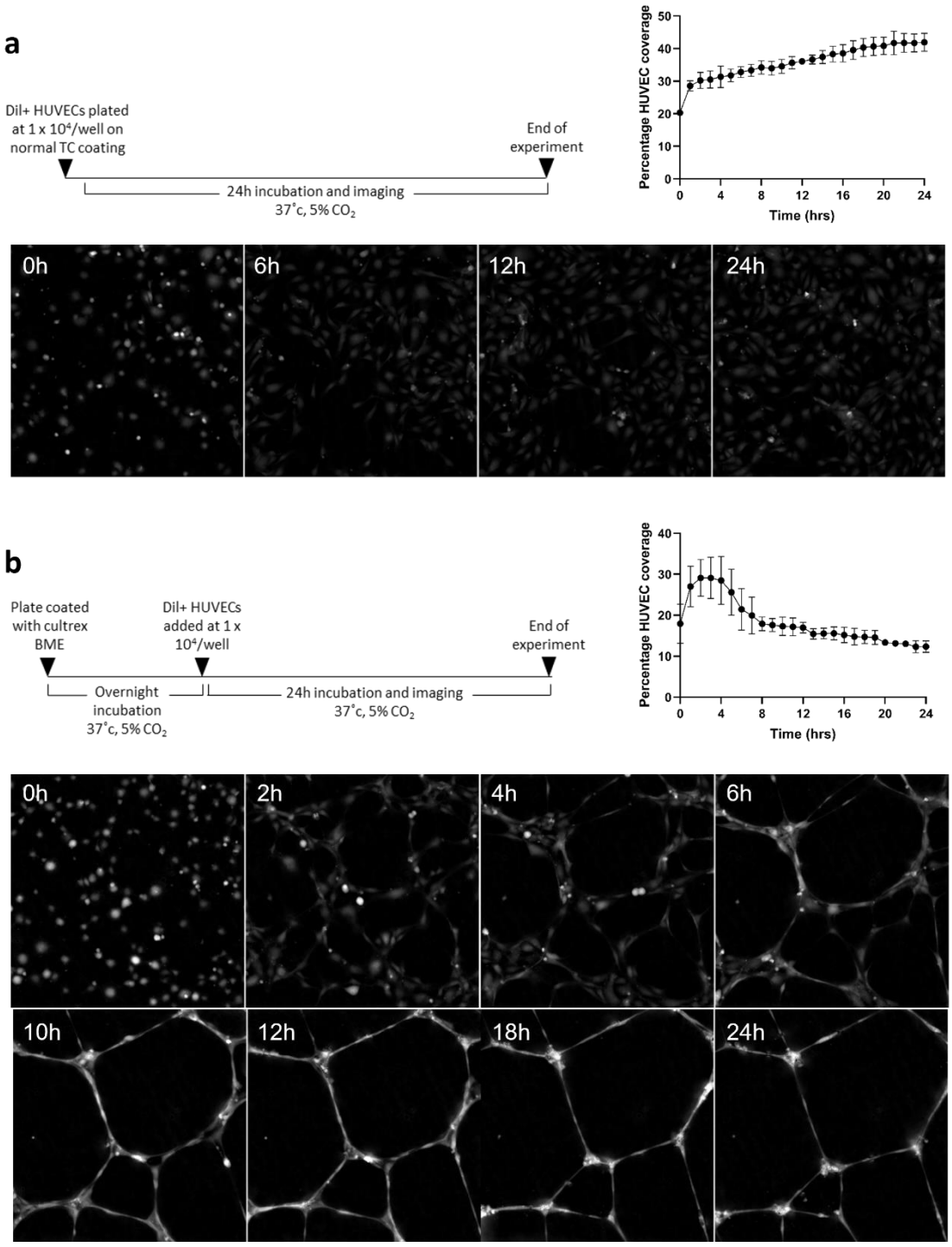

Figure 5.6 Network formation by HUVEC cells when plated on Cultrex basement membrane extract.

Vybrant DiI stained HUVEC cells were plated in Ibidi Angiogenesis plates either on (a) standard, TC coated plastic, or (b) in wells pre-coated with Cultrex basement membrane extract (BME). Plates were then incubated in the Phasefocus LiveCyte system at 37 °C, 5 % (v/v) $C0_2$ for 24 hours, with hourly imaging. Representative images are displayed, and HUVEC coverage was quantified as the percentage of the optical field occupied by DiI+ cells. All experiments were conducted in triplicate.

The differential localisation of MCAM at sub- and full confluency has only been reported for cells of endothelial origin, with no reported evidence for a similar pattern in cancer cells [590]. To investigate whether this had an impact on CAR T cell activity against the different cell types, it was first necessary to assess the interaction of melanoma cells with HUVEC networks. To this end, HUVECs were plated on Cultrex BME as previously described, and incubated for 6 hours to allow networks to form. DiO-labelled WM2664 cells were then added, with subsequent 24-hour tracking (Figure 5.7a).

In agreement with the first assay, over the course of the imaging period, the HUVEC networks matured and the area they occupied decreased (Figure 5.7b and c). This effect was observed both in monoculture and in the presence of WM2664 cells, which appear to cause a modest decrease in the HUVEC network area at later time points (Figure 5.7d). By contrast, the area occupied by the WM2664 cells increased over the course of the experiment (Figure 5.7e), suggesting that such cells are actively dividing, something which is not reportedly observed in HUVEC cells forming such networks [603]. Interestingly, the melanoma cells appear to interact with the HUVECs, rapidly assuming a similar elongated appearance and assembling into branching cords which anastomose with the existing HUVEC network.

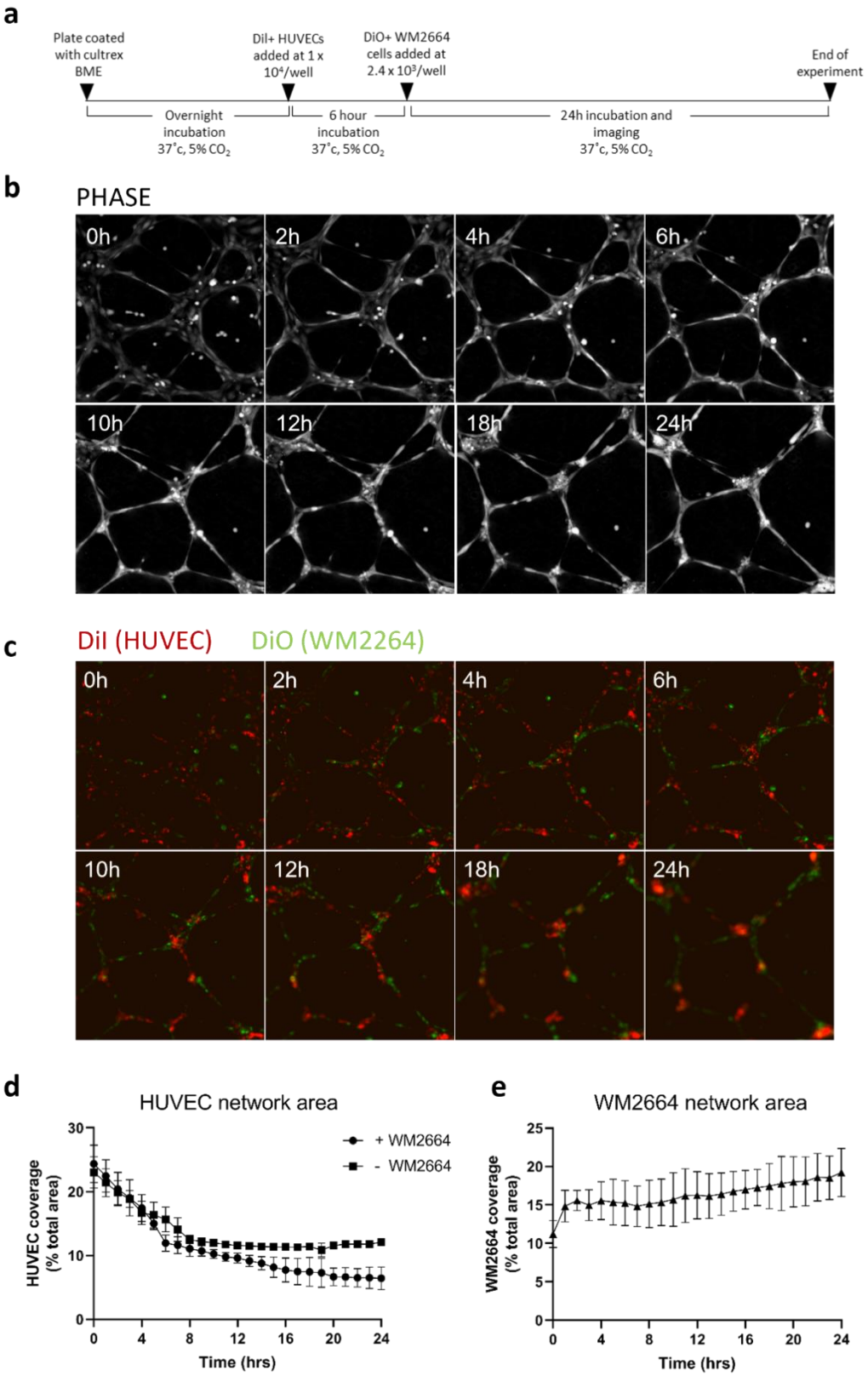

Figure 5.7 Interaction of WM2664 melanoma cells with pre-formed HUVEC networks. Vybrant DiI stained HUVEC cells were plated in Ibidi Angiogenesis plates pre-coated with Cultrex basement membrane extract (BME). After a 6-hour incubation DiO stained WM2664 melanoma cells were added at a 0.25:1 ratio. Plates were then incubated in the Phasefocus LiveCyte system at 37 °C, 5 % (v/v) CO_2 for 24 hours, with hourly imaging. Representative images are displayed, with HUVEC and WM2664 coverage quantified as the percentage of the optical field occupied by DiI+ and DiO+ cells, respectively. All experiments were conducted in triplicate.

To assess the impact of CAR T cells in the above culture system, HUVEC cultures with or without WM2664 cells were first plated as described above (Figure 5.8a and Figure 5.9a). Plates were incubated for 4 hours to allow the WM2664 cells to adhere to the gel and interpose with the HUVEC networks, at which point CTV-labelled CAR T cells were added at a 1:1 HUVEC-to-T cell ratio. Plates were then imaged for the following 20 hours.

Maturation of the HUVEC networks was observed over the time course in the absence of WM2664 cells (Figure 5.8b). Network organisation was conserved in the mock and CD19.BBz cocultures. Some evidence of disruption was observed with the M1.BBz and M40.BBz CAR T cells, with a complete loss of certain regions of the network at later time points. However, this effect was only observed with 1 of the 2 donors. Interestingly, CAR T cells of all types interacted with the network, rapidly co-localising with DiI+ cells. This was observed with mock and CD19.BBz cells in the absence of obvious toxicity, suggesting the involvement of a CAR-independent mechanism such as constitutively expressed lymphocyte adhesion receptors.

When the above assays were repeated with the addition of DiO-labelled WM2664 cells the melanoma cells interacted with the network, forming branching processes (Figure 5.9b). As observed previously, CAR T cells of all types co-localised with the networks, with some network disruption apparent only in the cocultures with M40.BBz cells, and to a lesser extent M1.BBz cells. Quantification of the total branching length of the networks reflected this disruption, with stronger effects mediated by M40.BBz cells (Figure 5.10a, c and e). Networks treated with CD19.BBz cells were comparable to those with mock cells. Similar results were obtained when the area occupied specifically by HUVECs was assessed (Figure 5.10b, d and f). This effect was observed to equivalent degrees in matched cultures with or without WM2664 cells, suggesting that T cells do not preferentially target MCAM-expressing tumour cells over mature HUVEC networks. Indeed, the total area occupied by WM2664 cells remained relatively static independent of coculture conditions, although a trend towards lower levels was observed with M1.BBz and M40.BBz (Figure 5.11a).

The interaction of the CAR T cells with the HUVEC and WM2664 populations was quantified by measuring the area of overlap across the different channels (section 2.2.4.3). While this did show that a lower proportion of the CD19.BBz CAR T cells

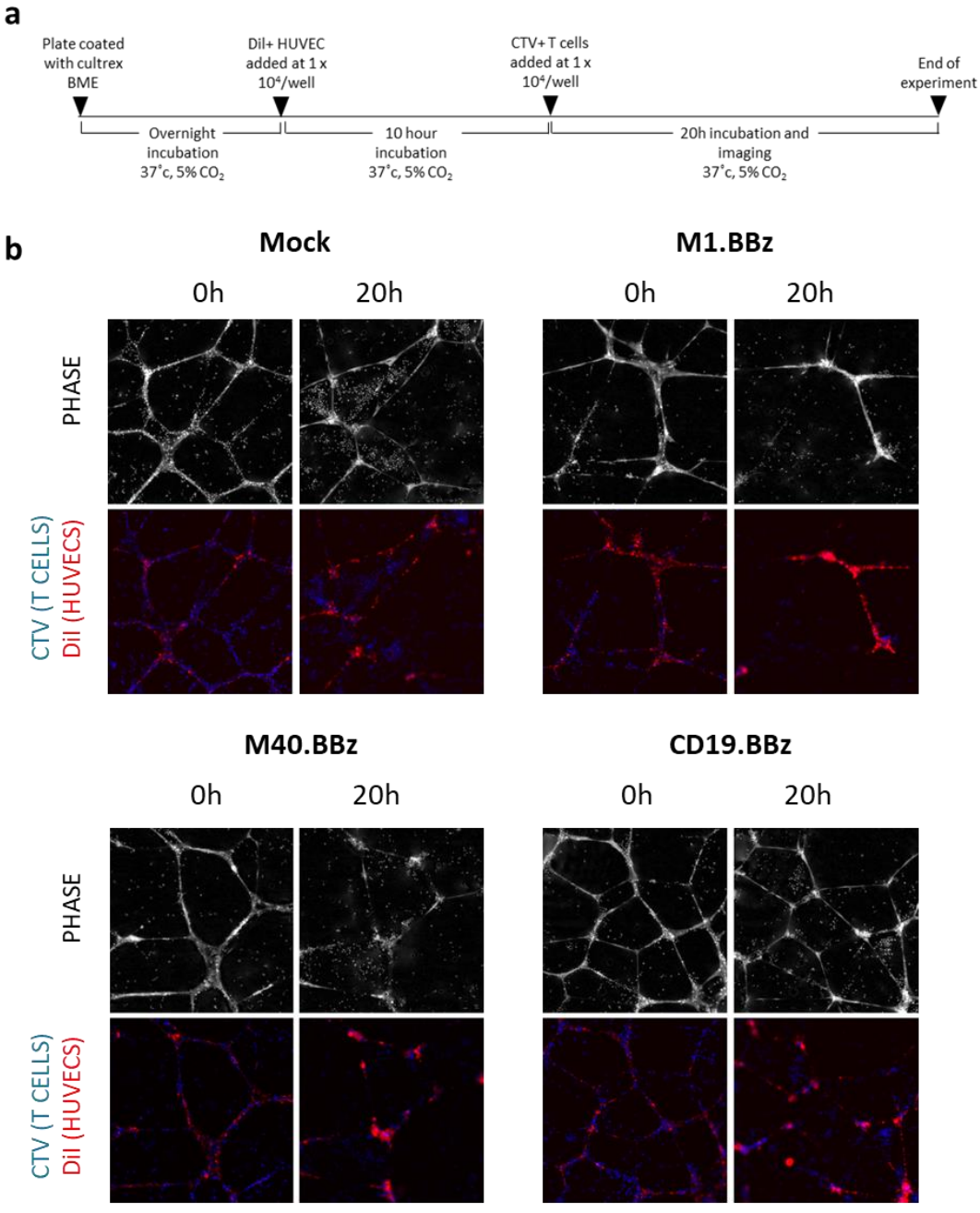

Figure 5.8 Interactions of CAR T cells with HUVEC networks.
(a) Schematic of the protocol, whereby DiI+ HUVECs were plated on Cultrex BME and incubated for 10 hours, prior to the addition of CTV-labelled CAR T cells at a 1:1 ratio. Plates were then incubated in the Phasefocus LiveCyte system at 37˚c, 5 % $C0_2$ for 20 hours, with hourly imaging. (b) Representative phase and fluorescence images are display for each CAR construct. All experiments were conducted in duplicate with 2 different T cell donors.

colocalised with the HUVEC networks and WM2664 cells, it did not demonstrate any differences between M1.BBz, M40.BBz and mock groups, although significant variability between replicates did affect the results (Figure 5.11b and c).

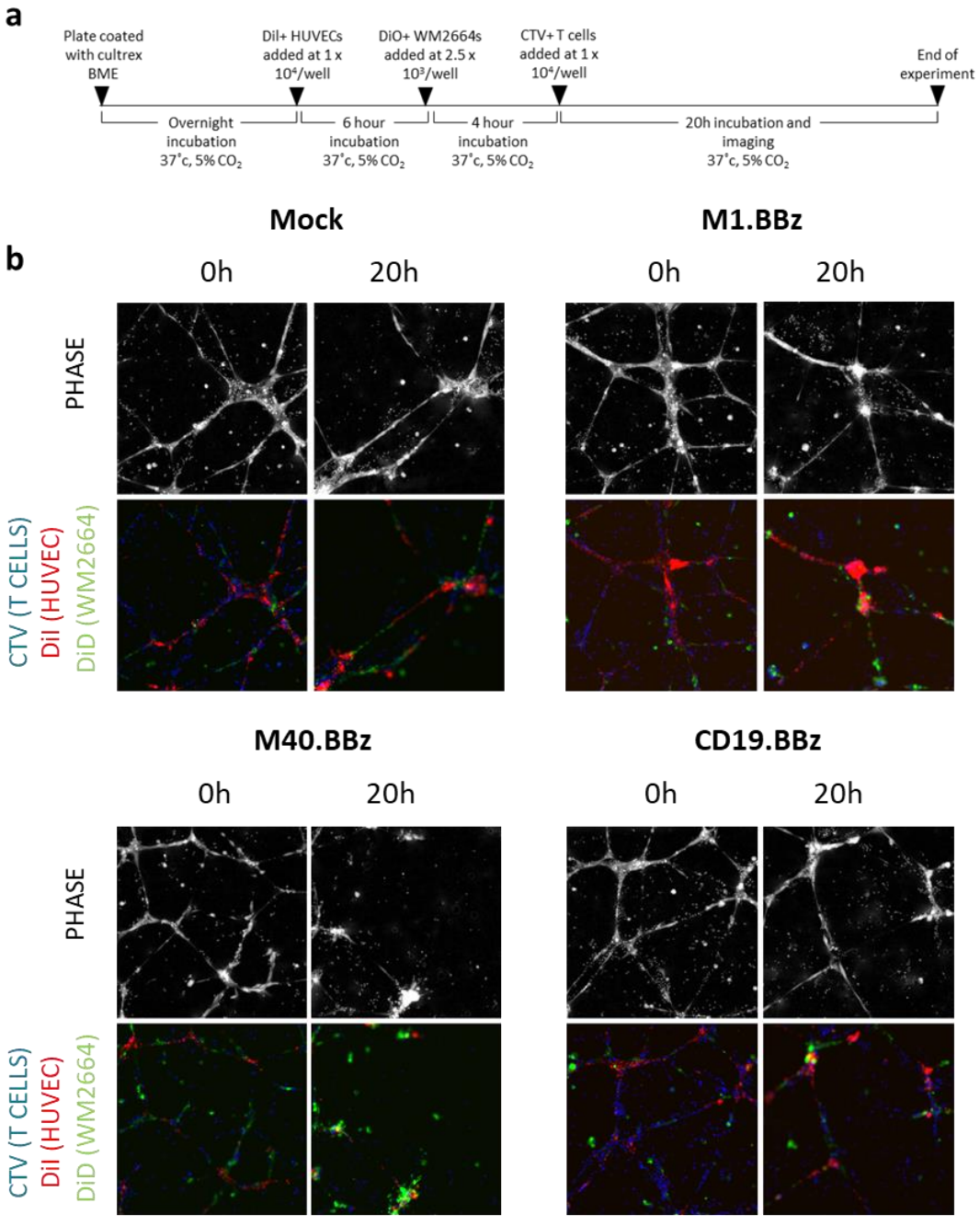

Figure 5.9 Interactions of CAR T cells with HUVEC and WM2664 networks.
(a) Schematic of the protocol, whereby DiI+ HUVECs were plated on Cultrex BME and incubated for 10 hours, prior to the addition of DiO-stained WM2664 cells at a 1:4 ratio (HUVEC:WM2664). CTV-labelled CAR T cells were added 4 hours later at a 1:1 ratio. Plates were then incubated in the Phasefocus LiveCyte system at 37 °C, 5 % (v/v) CO_2 for 20 hours, with hourly imaging. (b) Representative phase and fluorescence images are display for each CAR construct. All experiments were conducted in duplicate with 2 different T cell donors.

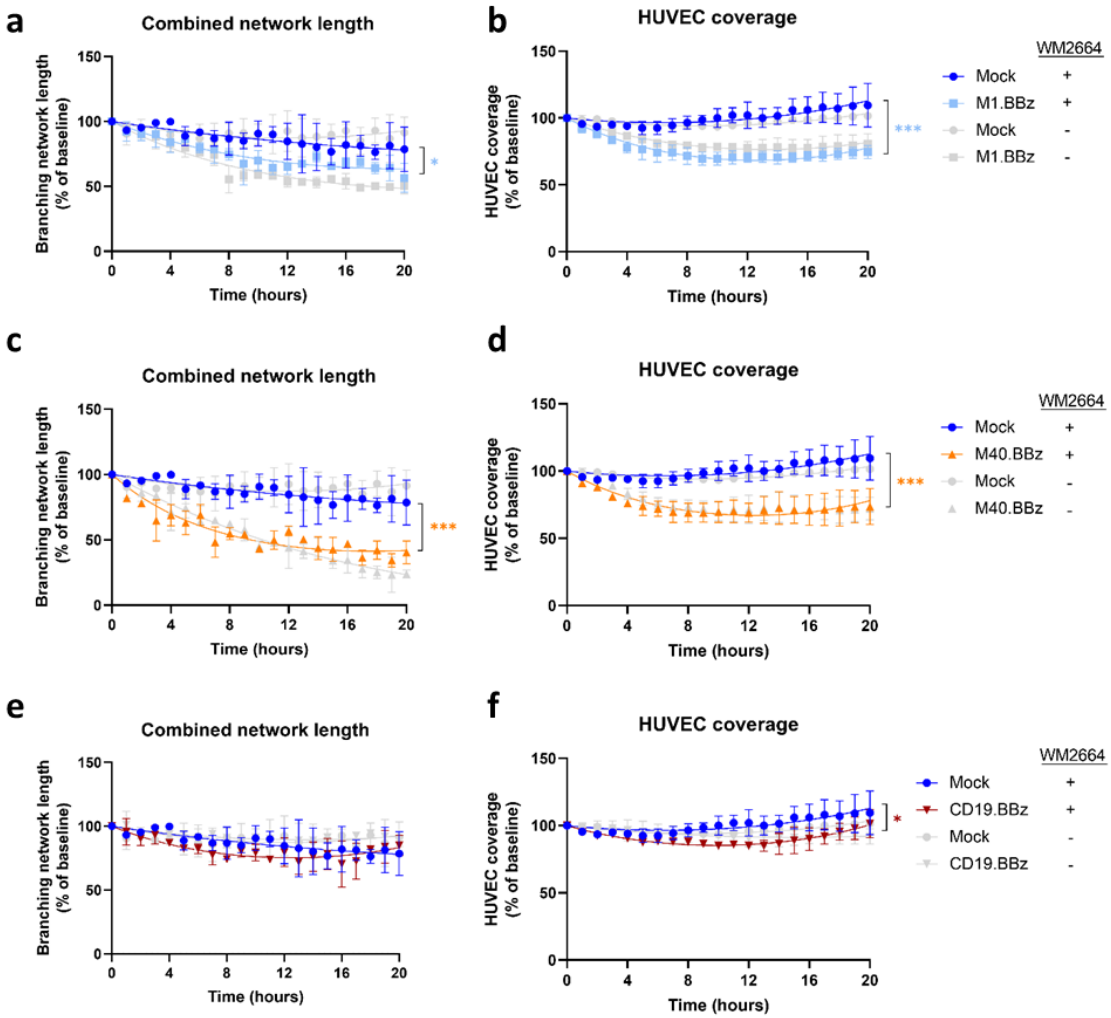

Figure 5.10 Quantification of HUVEC-WM2664 network area and length.
To quantify changes in the HUVEC-WM2664 networks on coculture with CAR T cells, timelapse images were analysed. (a)(c)(e) The total network length (HUVEC and WM2664) was estimated using the Angiogenesis Analyzer application on the phase contrast images. (b)(d)(f) Area of the HUVEC networks specifically was assessed by thresholding the appropriate fluorescence images to create binary masks, from which the area could be calculated.
Results displayed are from 2 donors, and for each donor duplicate measurements were taken. Results are displayed as mean and standard deviation, relative to baseline values.
Statistical analysis was via non-linear regression (curve fit) with subsequent comparison of curves using the extra sum of squares F test. * $p<0.05$, ** $p<0.01$, *** $p<0.001$.

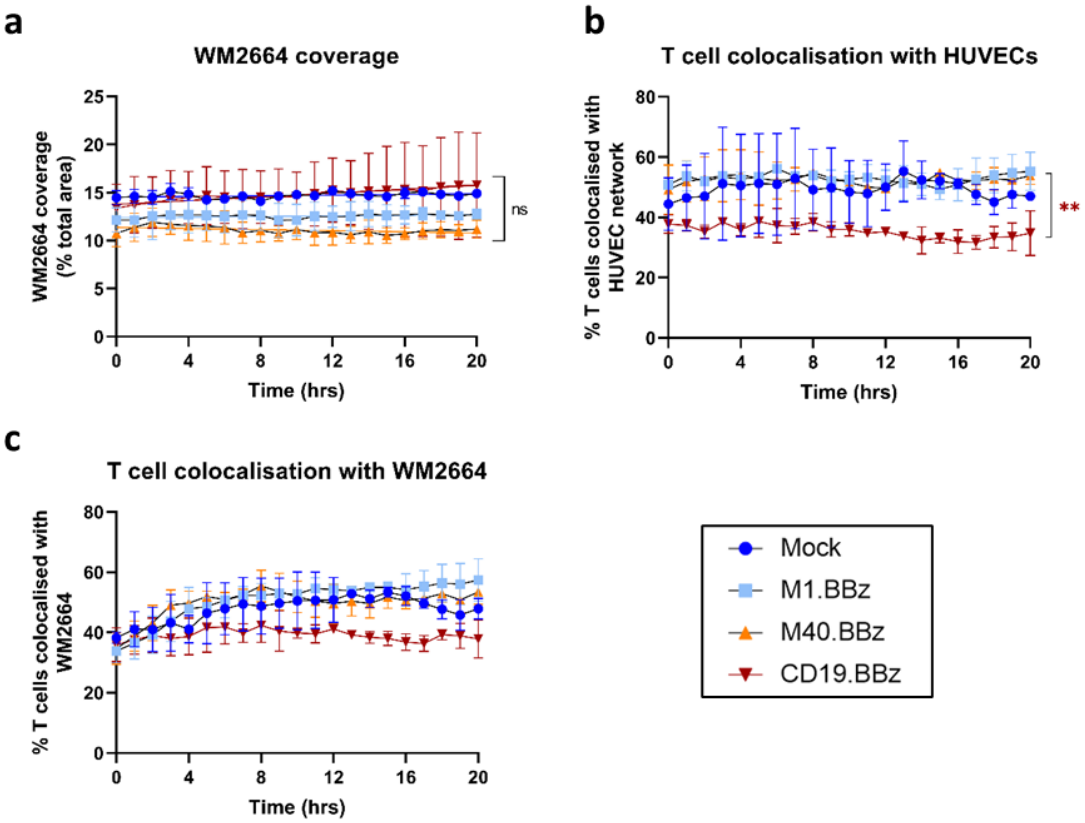

Figure 5.11 Quantification of cell-cell co-localisation in coculture assays.
To quantify the changes in the area of the HUVEC and WM2664 networks over time, images were thresholded to create a binary image, from which the area was calculated. (a) The changes in the area occupied by WM2664 cells over time, in coculture with the different CAR T cells. Binary images were also created for the T cell channel, which were combined with the respective binary HUVEC or WM2664 images to generate overlays, allowing quantification of the percentage of T cells colocalised with (b) the HUVEC network or (c) WM2664 cells. Results displayed are from 2 donors, and for each donor duplicate measurements were taken. Results are displayed as mean and standard deviation.
Statistical analysis was via simple linear regression with subsequent comparison of the gradients of the lines of best fit. * $p<0.05$, ** $p<0.01$, *** $p<0.001$.

To further investigate the potential toxicity mediated by M40.BBz CAR T cells, cultures were established as above with DiI- and DiD-stained HUVEC and WM2664 cells. CTV-stained M40.BBz CAR T cells were then added at a 4:1 effector-to-HUVEC ratio. M40.BBz cytotoxicity was clearly apparent from an early time point, with an almost complete loss of the network organisation and a corresponding decrease in the total branching length. This occurred in cultures with (Figure 5.12) and without (Figure 5.13) WM2664 cells and was accompanied by WM2664-independent IFN-γ production.

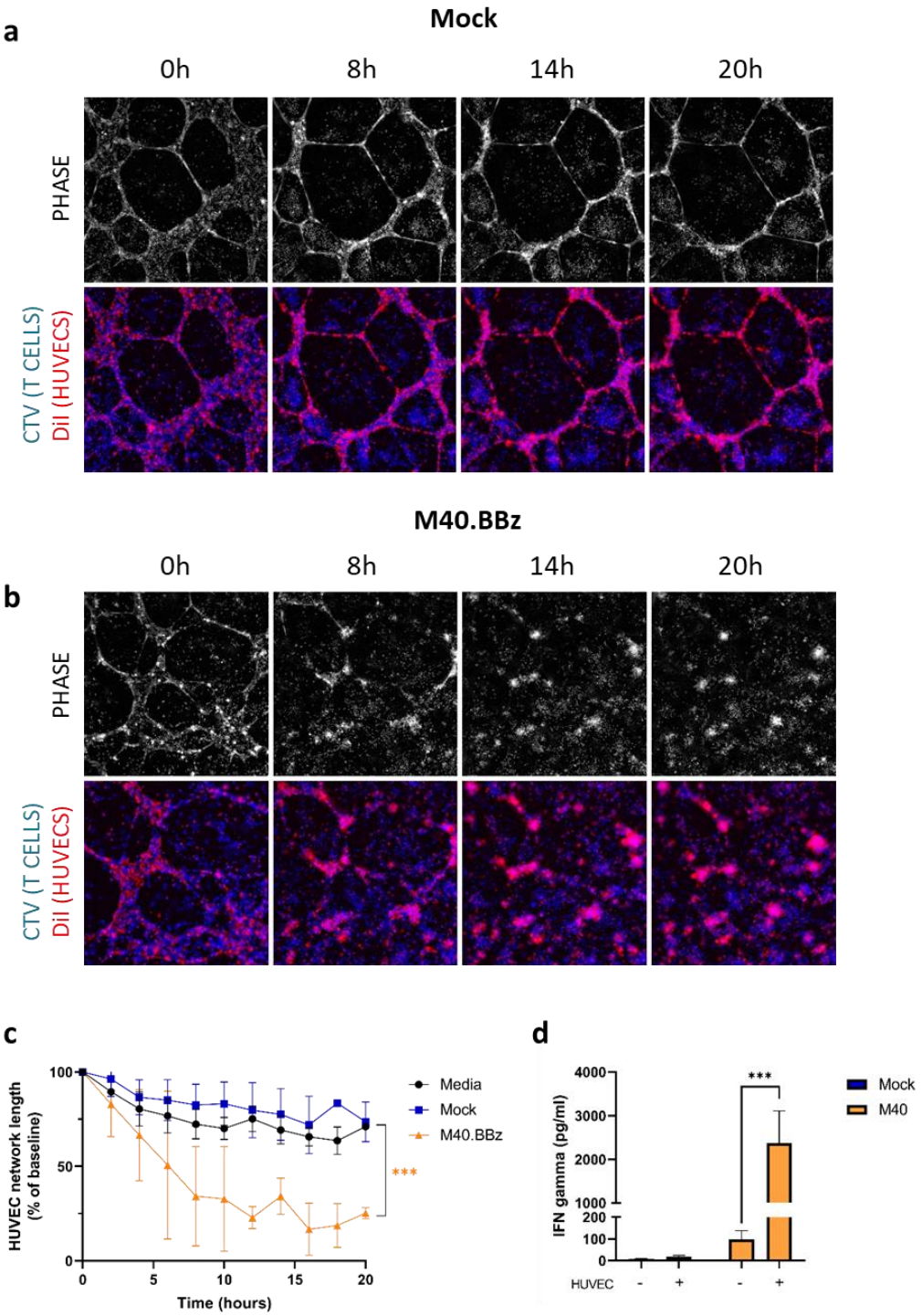

Figure 5.12 M40.BBz CAR T cells destroy HUVEC networks at a high E:T ratio.
HUVEC were plated on Cultrex BME and incubated for 10 hours, prior to the addition of mock and M40.BBz CAR T cells at a 4:1 ratio. Plates were imaged on a 2-hourly basis for the next 20 hours in the Phasefocus LiveCyte system. Representative images are presented for cocultures with (a) mock and (b) M40.BBz CAR T cells. (c) The total network length was estimated by using the Angiogenesis Analyzer on the phase contrast images. (d) IFN-gamma in the culture supernatant, collected at the 20-hour time point. Results displayed are from 3 donors, and for each donor duplicate measurements were taken. Results are displayed as mean and standard deviation. Statistical analysis was via non-linear regression (curve fit) with subsequent comparison of curves using the extra sum of squares F test for (c) by two-way ANOVA with Tukey's Multiple Comparisons in (d). * $p<0.05$, ** $p<0.01$, *** $p<0.001$.

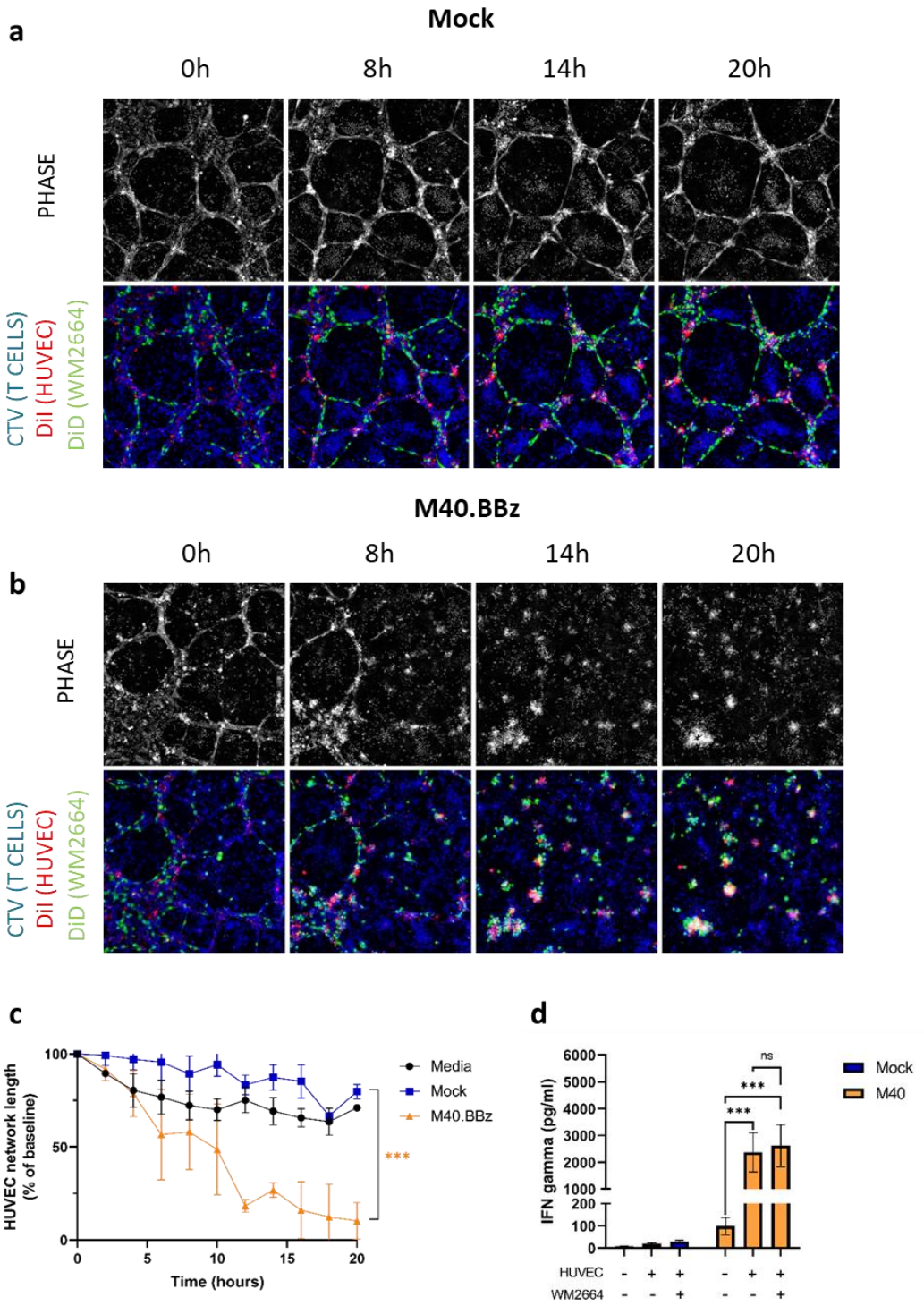

Figure 5.13 M40.BBz CAR T cells at high E:T ratios destroy HUVEC-WM2664 networks. HUVEC were plated on Cultrex BME. DiD-labelled WM2664 cells were added at hour 6, followed by mock and M40.BBz CAR T cells at a 4:1 ratio at hour 10. Plates were imaged on a 2-hourly basis for the next 20 hours in the Phasefocus LiveCyte system. Representative images are presented for cocultures with (a) mock and (b) M40.BBz CAR T cells. (c) The total network length was estimated by using the Angiogenesis Analyzer on the phase contrast images. (d) IFN-gamma in the culture supernatant, collected at the 20-hour time point. Results displayed are from 3 donors, and for each donor duplicate measurements were taken. Results are displayed as mean and standard deviation. Statistical analysis was via non-linear regression (curve fit) with subsequent comparison of curves using the extra sum of squares F test for (c) and by two-way ANOVA with Tukey's Multiple Comparisons in (d). * p<0.05, ** p<0.01, *** p<0.001.

5.4. Discussion

Whilst the standard procedure is to assess CAR T cell efficacy in mouse models, these experiments can be expensive and time consuming, and do not necessarily allow the infused CAR T cells to be tracked *in vivo.* We hypothesised that the zebrafish embryo could provide a unique model system in which to screen CAR T cells, thereby ensuring that only the best CAR constructs are selected for further analysis in industry-standard mouse studies.

However, the experiments conducted to date were very early-stage pilot studies, utilising a small number of fish and T cells derived from a single donor. These models were technically challenging for several reasons. Injecting the cells into the pericardiac space requires considerable skill, and standardising the number of cells delivered is difficult, especially as cells sediment over time in the injection suspension. When imaging the embryos, obtaining higher definition images of the injection site was prioritised over imaging the entire animal (which would have necessitated a lower resolution). However, as the number of T cells in the pericardiac space decreased over the course of the experiment, imaging the entire embryo could have confirmed whether this was due to the migration or the death of these cells. To address this question, it would also have been informative to fix and stain the embryos to allow apoptotic and proliferating cells to be detected.

To quantify the tumour volume, maximum intensity projections were generated from the z-stack images, but more accurate measurements could have been achieved using 3D volumetric analysis. Unfortunately, labelling the tumour cells with DiI did not give provide sufficiently homogenous signal to facilitate this. Additionally, the use of the pericardiac space as the injection site caused further complications. While this potential space is easily accessible, if the engrafted cells adhere to the heart the movement caused by the heartbeat makes acquiring high resolution images difficult. Other injection sites, such as the perivitelline space [604] or common cardinal vein [604, 605], are more technically challenging to access but may facilitate imaging.

Unfortunately, it was not possible to surmount the above technical challenges in the time available, so it is not possible to draw meaningful conclusions either on the

suitability of zebrafish as a model or on the *in vivo* behaviour of the anti-MCAM CAR T cells. More work is required to optimise the procedures and repeat the assays with a larger group of animals and with CAR T cells from multiple donors. Obviously significantly more time needs to be invested to establish the zebrafish embryo as a reliable and reproducible model in which to test CAR T cells, but the utility of such an assay has recently been confirmed by 2 other groups, who published similar models during the course of this project. Both Pascoal et al [605] and He et al [604] utilised CD19+ lymphoma cell lines and established anti-CD19 CAR T cells, which were sequentially injected into the circulation of 48 hpf zebrafish embryos to model metastasis. Cells preferentially accumulated in the tail region, facilitating imaging, with the anti-CD19 CAR T cells eradicating the tumour cells over the subsequent 24 hours. He at al also engrafted human primary melanoma cells which were selectively cleared by TILs isolated from the same patient, demonstrating that such assays could potentially be used in future to model patient-specific responses to therapy.

While these models are low-cost and can provide a rapid indication of CAR T cell functionality, they do have their limitations. The short duration of the assay means that it is not possible to detect immune escape or progressive T cell exhaustion. Additionally, it is unlikely that implanted tumour cells are fully engrafted by 24 hours, and embryos cannot be kept at 37 °C, the normal physiological temperature at which CAR T cells would be required to function in a clinical setting.

To address these limitations, Yan et al [606] generated a mutant zebrafish line lacking functional recombination activating gene 2 and IL-2 receptor gamma proteins (*rag2*$^{\Delta/\Delta}$, *il2rga*$^{-/-}$). Adult fish lacked pigment and had no mature B, T and NK cells, enabling human tumour and T cells to be engrafted. T cells persisted for at least 14 days post-injection and were found in the peripheral blood and kidney marrow. Using this model, Yan et al demonstrated that EGFRvIII-positive glioma cells could form established tumours when implanted into the peritoneal space. Intra-peritoneal injection of suitably targeted CAR T cells at 7- and 14-days post-engraftment efficiently cleared such tumours. Additionally, CAR T cells were able to migrate from a distal injection site to an established tumour. 3D modelling of individual cell-cell interactions confirmed that CAR T cells infiltrated the tumour mass to engage with, and kill, target-expressing

tumour cells. The model was also used to demonstrate the relative effectiveness of other immunotherapies, namely bi-specific T cell engagers (BiTEs) and antibody-peptide epitope conjugates (APECs). Interestingly, while T cell accumulation at the tumour site was strongest with BiTE therapies, CAR T cells were the best at tumour cell killing.

The above studies clearly illustrate the utility of the zebrafish-based assays as an intermediate model to bridge the gap between *in vitro* work and mouse studies. They have their advantages, such as the low cost, the high number of animals which can be used per experiment, and the ease of live imaging which facilitates the tracking of engrafted cells. It is therefore unfortunate that it was not possible to make sufficient progress in developing a model of our own. However, conclusions drawn from such models are limited in terms of their clinical applicability due to the lack of similarity between zebrafish and human protein sequences. For any given target antigen it is unlikely that scFv domains specific to the human protein will bind to the zebrafish ortholog with equivalent specificity, if indeed they bind at all. For example, the zebrafish ortholog of CD146 only has approximately 30% sequence similarity to human forms [279]. This lack of cross reactivity, combined with species-specific expression patterns, prevents any meaningful assessment of CAR-mediated toxicities. Any conclusions on the efficacy of CAR T cells must also be cautiously interpreted on account of the sequence differences in many other key proteins with which CAR T cells might normally interact, such as cytokines or adhesion molecules. Where they exist, zebrafish orthologs of such proteins are unlikely to bind to human receptors. Given the limited uptake of similar models, their inability to model toxicities, and the time and resources required for optimisation, this line of research was not prioritised further.

Instead, as arguably the biggest obstacle to the progression of M1.BBz and M40.BBz CAR T cells is the risk of on-target, off-tumour toxicities, I chose to investigate the interactions between them and HUVEC cells as a model of the vasculature. MCAM is expressed on blood vessels, with particular enrichment on endothelial cells [449, 577–581]. Nonetheless, its expression on tumour vasculature has been reported to exceed that on healthy, quiescent blood vessels [577, 588, 597]. Targeting the endothelial cells of tumour blood vessels could theoretically provide an effective tumour control

strategy for several reasons: endothelial antigens are easily accessible to circulating T cells, and antigen escape is less likely as endothelial cells do not display the same genetic instability as tumour cells. T cells would not need to infiltrate the tumour (with its immunosuppressive microenvironment) to lyse target-expressing endothelial cells, and the resulting destruction could starve the tumour of nutrients and oxygen, with widespread anti-tumour effects [607, 608]. Indeed, several groups have generated CAR T cells against a range of vascular antigens with elevated expression on angiogenic blood vessels [609–611].

However, for such a strategy to be clinically acceptable, expression of the target antigen on healthy vasculature needs to be very minimal; it is unlikely that MCAM, with its widespread expression, could be targeted in such a way without significant toxicity. To confirm whether this was the case *in vitro*, CAR T cells were incubated with HUVECs. In standard culture conditions anti-MCAM CAR T cells produced proinflammatory cytokines and killed HUVEC cells. While the expression of MCAM by HUVEC cells is well established [446, 448, 580, 587–589], it is unclear whether this is representative of the *in vivo* situation, or whether its expression and localisation is altered on *in vitro* culture [577, 588].

To assess CAR T cell behaviour against HUVECs in a more physiological configuration, capillary-like networks were established on basement membrane extract. Ideally, this would have been accompanied by visualisation of MCAM and comparison with HUVEC grown under standard conditions. At a 1:1 effector-to-target ratio some network disruption was detected with MCAM-specific CAR T cells from one donor. Increasing the T cell dose fourfold led to almost complete destruction of the networks across 3 independent donors, demonstrating a clear potential for catastrophic on-target/off-tumour toxicities. No selective responses against tumour-expressed MCAM were detected - this could be on account of the low number of melanoma cells seeded (1:4 WM2664-to-HUVEC ratio), a number designed to challenge them. Additionally, MCAM was expressed at comparably high levels by both HUVEC and WM2664 cells in culture. As ex vivo culture is thought to increase MCAM expression on HUVECs, it is possible that this is artificially elevated compared to the *in vivo* situation [577, 588]. It is not clear whether HUVEC culture in networks would induce its return to physiological

levels, nor how long this would take. The use of growth factor-containing commercial media preparations further limits the extent to which the networks could be considered representative of quiescent vasculature. Interestingly, all T cell types co-localised to the vasculature to some extent, suggesting that this is not an exclusively CAR-induced behaviour and instead may be mediated by leukocyte adhesion molecules, such as selectins or integrins [612, 613].

The experiments conducted to date relied on the capture of sequential microscopy images to assess CAR behaviour; although this demonstrates gross network disruption it is not possible to identify the outcome of these interactions at the level of the individual cell. Repeating these assays with CAR T cells from additional donors and including a means of detecting cell death would therefore be informative, especially at low effector-to-target ratios. Networks could also be fixed at the endpoint and IHC techniques employed to detect markers of apoptosis along with T cell effector proteins such as granzyme and perforin.

Furthermore, the capillary-like networks formed by HUVECs are a basic model of the vasculature. The cells are arranged largely in 2D, and lack the pericytes, smooth muscle cells and fibroblasts which contribute to the normal micro- and macro-vessel architecture. Although there is some evidence that small 'lumens' might form in the cords of HUVEC cells [603], this is difficult to visualise using standard techniques and could not be confirmed in our assays. If lumens were present, the fact remains that it is not possible to administer T cells directly into the network; rather they are added into the surrounding area, more akin to a situation in which T cells have already extravasated. Therefore, it is not possible to exclusively model the interaction between CAR T cells and the luminal surface of HUVECs, which is likely to have a different MCAM expression pattern to the basolateral surface [580, 587][590, 591], which is more easily assessed by CAR T cells in this assay. Therefore, CAR activity should be assessed in a more physiologically relevant context, through tissue engineering to generate *in vitro* models of blood vessels or using tissue explants [614]. This would also potentially allow CAR T cells to be delivered to the lumens of the vessels, something that is not possible with the HUVEC network models.

5.5. Conclusions

Reflecting the early-stage nature of these final sub-projects, the results are somewhat inconclusive with significant further work required. Data collected to date demonstrate that M1.BBz and M40.BBz do recognise HUVEC-expressed MCAM, both in standard culture conditions and in capillary-like networks. It remains to be seen what their response would be to MCAM on more physiological models of the vasculature, however it seems clear that this would impede their safe clinical use in the current CAR context.

Chapter 6. Final discussion

Melanoma is the 5th most common cancer in the UK, and its incidence is increasing [252]. Nearly half of patients with stage 4 metastatic melanoma do not survive the first year following diagnosis [251]. While immunotherapies including checkpoint inhibitors and TIL therapies have been transformative, there remains an ongoing unmet clinical need as such therapies are not suitable or effective in all patients [253, 615, 616].

With this in mind, this project aimed to generate CAR T cells suitable for use in the context of melanoma. A panel of anti-MCAM scFv domains was incorporated into a retroviral, second-generation CAR construct, complete with CD8α hinge and transmembrane regions and a 4-1BB-derived costimulatory domain. These constructs were first screened for their ability to activate the JRT3-T3.5 Jurkat cell line in response to target antigen. Based on their activity in this context, M1.BBz and M40.BBz CARs were subsequently expressed in primary human T cells. This efficiently redirected the T cells, leading to MCAM-induced cytokine production, degranulation, and target cell lysis, albeit in a manner which displayed significant donor-to-donor variation in terms of the magnitude of the response.

Although upregulated on numerous cancers, MCAM is also expressed on healthy tissues throughout the body, creating a significant risk of on-target/off-tumour toxicities. MCAM is detected on 2-3 % of circulating lymphocytes, where it is enriched on a population of memory CD4+ cells with a Th17 phenotype [512]. This creates a potential risk that targeting MCAM with CAR T cells could result in trans-activation, leading to exhaustion and loss of transferred cells. MCAM expression on all CAR T cells groups was rare (<1.5 % of cells at baseline), and the percentage of positive cells was reduced in the M1.BBz and M40.BBz groups, suggesting that some level of targeting may be occurring. Despite this, these CAR T cells had minimal expression of exhaustion markers at rest. Whether this would be the case clinically, where CAR T cells would potentially encounter a greater number of MCAM+ T cells, is unclear. Furthermore, there is evidence that T cell stimulation results in increased MCAM expression [329, 330, 333, 553]. T cell viability and expression of exhaustion and activation markers was

broadly comparable between the MCAM-stimulated M1.BBz and M40.BBz and CD19-stimulated CD19.BBz groups. However, these cocultures were analysed after 24 hours at which point MCAM upregulation may not have fully occurred. This area requires further investigation and would benefit from longer assays involving repeated CAR stimulation.

The expression of MCAM on endothelial cells across the vasculature poses a particular risk of toxicities. To investigate this, CAR T cells were administered to capillary-like networks of HUVEC cells, in anticipation that this might more closely mimic the expression of MCAM *in vivo* where it is expressed at sites of cell–cell contact. Coculture with M40.BBz at high effector-to-target ratios led to almost complete destruction of the networks. Concurrent cytokine production suggests that this was a result of T cell activation in response to HUVEC-expressed MCAM. Network disruption was also detected to a lesser extent at a 1:1 ratio. Predicting likely *in vivo* effector-to-target ratios is difficult, but nonetheless these results suggest that significant on-target/off-tumour toxicity could be expected.

We did not detect any evidence to suggest that WM2664 melanoma cells were preferentially targeted, despite previously seeing nearly 50 % lysis at a 1:1 ratio in standard cytotoxicity assays. Although further assay optimisation is required, these experiments do not support the existence of a therapeutic window in which the required threshold for MCAM expression intensity to drive CAR activation is only surpassed by malignant cells.

The HUVEC network model has some significant limitations: it was not possible to characterise the polarity or the localisation of MCAM on HUVECs due to time constraints; HUVECs cultured *in vitro* with growth factor-containing commercial media preparations may have artificially elevated MCAM expression [617] and may be more representative of angiogenic rather than quiescent vasculature; the assay was limited in terms of duration and the effector-to-target ratios tested. Furthermore, unlike mature blood vessels the system does not contain supporting pericytes, smooth muscle cells or fibroblasts, and lacks a ‘luminal’ surface within the cords. Modelling normal tissue architecture is essential as it is likely that the degree of on-target/off-tumour toxicity for a given protein will depend not simply on how frequently

expressed it is at a tissue level, but on how accessible it is to circulating CAR T cells, as evidenced by the successful targeting of GUCY2C and CLDN18.2. These proteins are abundantly expressed on the gastrointestinal epithelium but can be safety targeted by CAR T cells due to their sequestration at the luminal epithelial surface or within tight junctions [196, 199]. Therefore, this basic model of the vasculature is a long way from faithfully recreating the conditions CAR T cells would encounter in the body and more complex models are required to detect tumour lysis and on-target/off-tumour toxicity.

In addition to on-target/off-tumour toxicity, off-target toxicity also poses a substantial risk. Typically, antibody-based therapeutics are tested for cross-reactivity using immunohistochemistry tissue cross reactivity (IHC-TCR) assays, in which a panel of frozen human tissues was probed with the test antibody or scFv to detect unexpected staining [618, 619]. Although they are still frequently used, IHC-TCR assays have their limitations, including the effect of processing and fixing tissues on tissue architecture and antigen availability, the high rate of false positives, and the inability to determine if unexpected staining is due to on-target or off-target reactivity.

Various microarray-based techniques have subsequently been developed to facilitate cross-reactivity testing. The HuProt Human Proteome Microarray (Cambridge Protein Assays) allows users to test antibody-based therapeutics against a panel of purified proteins from more than 16,000 human genes [227]. Although this method provides coverage of a large number of proteins, the proteins are produced in yeast which could potentially lead to differential post-translational modifications. The glutathione-S-transferase tag, necessary for protein purification, may further impact protein conformation. The Membrane Proteome Array (Integral Molecular) and Cell Microarray (Retrogenix) systems avoid these issues by using transfected HEK-293 cells. In the Membrane Proteome Array, HEK293 cells are transfected with a library of expression plasmids encompassing more than 6000 proteins [230]. They are subsequently incubated with the antibody in question and a suitable secondary antibody, and binding is identified by flow cytometry. By contrast, Retrogenix's Cell Microarray system deposits expression vectors in distinct locations on specialised slides [228, 229]. HEK293 cells are then seeded onto the slides and become reverse

transfected with the library of membrane proteins. Incubation with the test antibody allows detection of cross-reactivity.

Comprehensive screening for scFv cross-reactivity requires a broad and exhaustive library of proteins which is technically challenging to achieve. It was not possible to perform this type of screening during the time course of this project, and therefore it is not currently possible to comment on the potential cross reactivity of M1 and M40 scFvs. This represents a significant risk which would need further investigation using the above techniques if these CAR T cells were to progress further in the development pipeline.

More generally, the strength of any conclusions as to the function, specificity, and toxicity of M1.BBz and M40.BBz constructs is limited by the nature of the experiments conducted to date. These assays are a drastic simplification of the conditions in which such T cells would be expected to function if given clinically, where they would have to survive in the circulation, traffic to the tumour, extravasate and survive in the immunosuppressive tumour microenvironment [189]. Additionally, T cell activity was only tested against a limited panel of cell lines. Therefore, further assays are required to thoroughly characterise the M1.BBz and M40.BBz CAR constructs in more challenging conditions and address the potential risk of toxicities.

Efficacious CAR T cell therapies must recognise and kill malignant cells with heterogenous antigen expression within the tumour microenvironment. M1.BBz and M40.BBz were cytotoxic against the cell lines tested, but it is not possible to make predictions as to their clinical efficacy based on these assays. Although the cell lines selected were originally isolated from metastatic melanoma lesions, further work is required to confirm whether their expression of MCAM is comparable to that of clinical specimens. To fully address this issue, a range of tumour samples from patients with stage IV melanoma should be characterised by IHC, flow cytometry or RT-qPCR to determine what the clinically relevant range of MCAM expression is. Characterisation of a variety of cell lines in parallel would facilitate rational selection of cell models approximating target antigen density in MCAM-low, -medium and -high tumours. *In vitro* assessment of CAR T cell activity against such a panel would increase confidence that CAR affinity, avidity and activity may be sufficient to mediate anti-tumour

responses if tested clinically. This would also help inform the design of subsequent *in vivo* efficacy studies in mice.

Clonal cell lines are inherently a simplification of the diverse cellular composition of solid tumours, which contain genetically heterogenous tumour cells alongside multiple other cell types. Moreover, the simplistic *in vitro* assays conducted to date do not attempt to recreate the 3D structure of malignant lesions. A potential alternative model is the use of patient-derived organoids (PDOs), which may better replicate the heterogenous nature of tumours whilst providing a more physically and spatially complex environment in which to test CAR T cells [620].

In one such study [621], PDOs generated from glioblastoma biopsies were shown to closely resemble parental tumours in terms of cellular morphology and gene expression. When EGFR-vIII-specific CAR T cells were administered to the organoids, Jacobs et al observed CAR T cell infiltration, proliferation, cytokine production and cytotoxicity, which was dependent on EGFR-vIII expression by the organoids. Similar systems have been deployed to test anti-HER2 CAR T cells and EPCAM and EGFR-vIII-specific CAR-NK cells [622]. Whilst protocols for culturing melanoma organoids have been developed [623], to date their use to test CAR T cells has not been reported. Such systems have clear potential; generating matched PDOs and CAR T cells could better identify suitable candidates for CAR T cell therapy. Additionally, the flexibility offered by these assays could allow rapid testing of different CAR constructs, modelling their effectiveness at low effector-to-target ratios and over extended time periods. Whilst establishing melanoma organoids did not fall within the scope of this project, it would be a valuable tool to develop to facilitate the assessment of CAR T cell efficacy.

Although a significant improvement on basic cell line models, CAR T cells are still tested in isolation in these PDO systems. To understand the behaviour of M1.BBz and M40.BBz in an *in vivo* setting, where they would need to interact with endogenous immune cells, circulate systemically and traffic into the tumour, mouse models will be an essential next step.

Multiple factors must inform the choice of the model required for a given project; the cross reactivity of the scFv, the desired primary endpoint (efficacy versus safety) and

the expression profile of the target antigen, as well as pragmatic considerations such as cost and available expertise. In the CAR T cell research field, mouse studies often take the form of a 'stress test,' where T cells are administered at a suboptimal dose [624]. They broadly fall into 3 categories: immune competent syngeneic models, immune compromised xenograft models, and HSC-humanised mouse models.

In immunocompetent mice models, histocompatible tumour lines are implanted into mice and allowed to engraft, prior to treatment with syngeneic mouse T cells transduced with CAR constructs containing murine costimulatory and activation domains. By contrast, immunocompromised models allow human CAR T cells to be xenografted. These models frequently use NOD.Cg-Prkdc^{scid} Il2rg^{tm1Wjl}/SzJ (NSG) mice, which lack mature B, T and NK cells, and have defective macrophages and dendritic cells [625]. As a result, human CAR T cells can be tested against human tumour cells so such models are typically well suited for efficacy studies. Lastly, advances in genetic engineering have allowed the development of HSC-humanised mouse models. When engrafted into NSG mice, human haematopoietic stem cells can reconstitute the immune system, allowing CAR T cells administered at a later date to interact with fully human innate and adaptive immune compartments [626]. Given that cytokine release syndrome is a common toxicity in CD19-CAR trials, these models are valuable tools and allow the detection of CRS-like syndromes [627, 628].

Immunocompromised mouse models typically involve the engraftment of human tumour cells, which can take 2 forms: cell line derived xenografts (CDX) or patient derived xenografts (PDX). CDX models are commonly used in preclinical testing, allowing CAR T cells to be tested in solid tumours. However, the limitations of cell lines discussed above still apply. Cells are clonal and do not necessarily model tumour heterogeneity, and the intensity and pattern of target antigen expression may not be clinically representative. By contrast, in PDX models small tumour fragments are surgically isolated from patients and transplanted subcutaneously or orthotopically into immunocompromised mice [629]. PDX tumours have been established for many cancers, including melanoma [630–632], and have been demonstrated to maintain the characteristics of the parental tumours [629]. Therefore they represent an optimal system in which to evaluate CAR T cell efficacy [633, 634].

Further development of the M1 and M40 CAR T cells would also require compelling evidence of a therapeutic window for targeting MCAM; the ability to detect on-target/off-tumour toxicities in mouse models is therefore a priority. Where CARs cross-react against the mouse form of the protein, such toxicities can be detected in immunocompetent, immunocompromised, and HSC-humanised mice, albeit with the caveat that this assumes that target protein expression intensity and location in mice is representative of the situation in humans [635, 636]. However, early work indicated that the M1 and M40 scFvs do not recognise murine MCAM and therefore the only way to test the anti-MCAM CAR strategy in an immunocompetent setting would be to generate fully murine CAR constructs with scFvs specific to the mouse form of the protein [637]. This assumes that scFvs against the same target can be used interchangeably, however their affinities for their respective targets and the accessibility of the epitopes may be significantly different. Additionally, it would be difficult to reliably generate murine versions of scFvs which recognise certain tumour specific epitopes, such as tsCD146.

Whilst NSG models would still provide a means of assessing the anti-tumour efficacy of human-MCAM specific CAR constructs, the lack of cross reactivity would again prevent any conclusions being drawn on their safety. This could however be addressed using transgenic mice. CRISPR-Cas9 technology allows the human tumour associated antigen to be knocked in alongside its required regulatory elements, thereby driving its expression at normal locations [638]. Chimlewski et al [639] utilised a transgenic mouse expressing human CEA, demonstrating that anti-CEA CAR T cells accumulated in tissues with known CEA expression. Whilst such models are clearly advantageous, they are expensive and time consuming to develop, requiring a level of technical expertise which may not be accessible for many labs. Additionally, generating humanised lines for multiple alternative targets is not practical.

For the reasons set out above, properly addressing the issue of the safety of M1.BBz and M40.BBz CARs would require a longer-term approach involving the generation of a humanised MCAM mouse. Whether this would be a worthwhile investment in terms of time and funding remains to be seen, especially given the lack of evidence so far for a therapeutic window. In the short term, M1 and M40-targeted CAR T cells will be tested

in preliminary cell line derived xenograft experiments in immunocompromised NSG mice, to give an indication of their *in vivo* activity.

If M1.BBz and M40.BBz failed to mediate anti-tumour effects *in vivo*, a multitude of potential techniques have been developed which aim to augment CAR activity, although to date their effectiveness has generally only been proven in a pre-clinical setting. Firstly, this could involve intrinsic changes to the CAR construct itself, such as including additional costimulatory domains, substituting the CD8 transmembrane domain for that of CD28, and optimising the hinge length. Optimising the CAR T cell generation process by more stringent selection of starting material to remove contaminating non-T cells [519, 520], controlling the CD4:CD8 ratio [536] and utilising alternative cytokines during expansion may also help increase activity [550, 551].

Compared to CAR T cells for haematological malignancies, those targeting solid tumours face unique challenges and several strategies have been developed to address these. Migration into the tumour microenvironment can be supported by the co-expression of chemokine receptors [640] or heparinase, which degrades heparin sulphate proteoglycans, facilitating T cell migration through the ECM [641]. Where the pathology permits it may be possible to bypass this step by administering CAR T cells via injection into the tumour or surrounding area [538, 642, 643].

Once in the tumour microenvironment, CAR T cells are exposed to numerous exhaustion-inducing factors, from immunosuppressive cytokines to immune checkpoint ligands [189]. TGF-β is a pleiotropic cytokine which often accumulates in the tumour microenvironment and can function to both suppress and promote tumour growth and progression [644]. It's immunosuppressive effects on T cells are numerous, and include the inhibition of T cell proliferation, interference with TCR receptor signalling, and suppression of T cell effector functions [645]. Several groups have sought to circumvent these effects through the development of dominant negative TGF-β receptors which can rescue CAR T cell proliferation, persistence and tumour control *in vivo* [646–648]. Similar results were obtained by blocking PD-1 signalling with anti-PD-1 antibodies [649] or using dominant negative receptors for PD-L1 [117, 650]. Other groups have developed a variety of strategies to prevent the exhaustion of CAR T cells, including reducing the impact of tonic signalling through fine

spatiotemporal control of CAR expression [161, 651–653], knocking-down Fas [654], or overexpressing c-Jun [655, 656] or the anti-apoptotic protein Bcl-X_L [657].

Whilst such strategies could be employed to augment the anti-tumour activity of M1 and M40 directed CAR T cells, it is likely that this would also lead to increased toxicity against normal tissues. Even if a therapeutic window for targeting MCAM exists, it is likely that further engineering would be required to increase CAR T cell selectivity and controllability. Several strategies have been developed which act as permanent or temporary 'brakes' on CAR T cell activity. Early attempts centred around the introduction of so-called 'suicide systems,' which in the event of toxicities would allow the rapid clearance of CAR T cells on administration of an exogenous agent. In the inducible caspase 9 (iCasp9) suicide system, cells are transduced with a construct formed of truncated caspase 9 joined to an FKBP domain. Treatment with a chemical inducer of dimerization (CID) results in FKBP-mediated caspase 9 dimerisation and activation, triggering the intrinsic pathway of apoptosis [658–660]. Use in the context of graft-versus host disease following stem cell transplants resulted in a loss of greater than 85 % of transduced donor T cells [661, 662]. iCASP9 expressing CD19-CAR T cells have been tested in recent clinical trials [663]. Similar systems have been suggested which involve the transduction of cells with the gene for herpes simplex virus thymidine kinase or CD20, conferring sensitivity to ganciclovir or rituximab, respectively [664]. Temporary inhibition of CAR activity has been achieved through the use of ligand induced degradation domains, which lead to reversible intracellular CAR destruction on administration of a small molecule [665, 666]. Alternatively, administration of dasatinib (a tyrosine kinase inhibitor used for the treatment of CML) can suppress CAR T cell effector functions by inhibiting essential signalling proteins [667, 668].

In the event of severe on-target/off-tumour toxicity temporary systems would be inappropriate, and whilst suicide systems could remove reactive M1.BBz or M40.BBz CAR T cells, they are inherently reactive; potentially permanent tissue damage may have already occurred by the time they are deployed. Therefore, there is a need for more proactive safety mechanisms to provide better temporal and spatial control of CAR T cell activation to reduce on-target/off-tumour and off-target effects. It is

possible to remotely control CAR T cell activity at the level of transcription through the use of synthetic promoters, which have been used to titrate activity in response to doxycycline [669–671]. Alternatively, using Synthetic Notch (SynNotch) circuits T cells can be 'armed' by one antigen and activated by another, improving their specificity [672]. SynNotch receptors bind to their target antigen via an scFv which leads to cleavage of a portion of the intracellular region, allowing it to enter the nucleus where it acts as a transcription factor, inducing expression of the CAR construct. Given that the half-life of CAR expression was 8 hours in one study, there is a risk that T cells could be 'armed' in one location and then traffic to other tissues where the CAR may mediate off-tumour toxicities, although there was no evidence of this in mouse models [460, 673].

Hyrenius-Wittsten et al [460] incorporated a similar second generation M1 CAR construct into such a circuit, where its expression was driven by a SynNotch receptor specific to alkaline phosphatase placental-like 2 (ALPPL2), a tumour-associated antigen common in mesothelioma. These SynNotch CAR T cells retained full functionality across a range of antigen densities, and the conditional CAR expression appeared to protect cells from the deleterious effects of tonic signalling, preventing exhaustion and premature differentiation. *In vivo*, the SynNotch CAR T cells mediated superior anti-tumour immunity against $ALPPL2^+$ $MCAM^+$ tumours. Importantly, MCAM-single positive tumours in the same mice did not regress, suggesting that the SynNotch CAR T cells were not capable of being primed in the $ALPPL2^+$ environment before trafficking elsewhere. Of note, these experiments were conducted in non-humanised NSG mice, and therefore could not detect on-target/off-tumour toxicities specific to the MCAM CAR.

In order to remotely control the activity of cells post infusion, recent research has focused on making CAR T cell activity dependent on an external user-generated signal. Novel small-molecule gated CARs have been developed to this end in which the activation and costimulatory domains are separated on different proteins which are brought together into a functional signalling molecule on administration of a chemical inducer of dimerisation [653, 674–676]. Alternatively, so called SUPRA- or zip-CAR T

cells rely on the titratable administration of soluble scFv to bind to target antigens [674, 677–679].

Bispecific antibodies provide an alternative means of targeting T cells to tumour antigens without the expense and difficulties inherent to adoptive cell transfer. They include 2 antigen binding domains, one of which typically binds CD3 on T cells whilst the other is specific for a pre-defined tumour-associated antigen. Antigen binding creates an immune synapse between endogenous T cells and tumour cells, driving T cell mediated tumour lysis. Numerous bispecific antibody formats have been designed, with the most common being bispecific T cell engagers (BiTE), comprised of 2 linked scFv domains [680, 681]. Numerous clinical trials of BiTEs and other bispecific engager molecules are currently underway, with several therapies recently receiving FDA approval [682–684]. Due to their small size and lack of Fc domain, BiTE molecules have a short half-life, so are typically administered by continuous infusion [685]. Although this does not allow for long term memory formation, it would provide a method of targeting MCAM in a titratable manner, allowing treatment to be rapidly withdrawn if toxicities developed.

Despite recent advances in this area, the fact remains that many of the strategies discussed above are inherently reactive. By the time control mechanisms such as suicide systems are initiated, self-reactive T cells may have already mediated significant damage. Furthermore, the efficacy of many of these systems is yet to be proven in the clinic. This returns to the central question, specifically whether it would ever be safe to target MCAM given the potential reactivity of such CAR T cells against normal tissues and even activated self-T cells [512]. Although there is some suggestion in the literature that they may be a therapeutic window for targeting MCAM with certain immunotherapeutics [355, 386, 387, 595, 686, 687], this is based on limited pre-clinical modelling. MCAM expression by human tissues is also likely to be dynamic; a hypothesis that assumes expression is uniformly high on tumours and low on healthy cells is probably an oversimplification.

Although the potential for on-target/off-tumour reactivity of the anti-MCAM scFvs may ultimately preclude their safe use as part of a standard CAR, they could be used to target chimeric costimulatory receptors (CCRs). In combinatorial antigen recognition

systems, T cells express a first generation scFv-CD3ζ CAR alongside a chimeric costimulatory receptor (CCR) comprised of a different scFv and a costimulatory domain. Provided that the scFvs recognise different tumour associated antigens, the CAR T cell will receive both activation and costimulatory signals on interaction with the tumour. However, encounter with normal cells expressing only one of the antigens will not provide both signals for full T cell activation [688, 689]. M1 or M40-targeted chimeric costimulatory receptors could be co-expressed with alternative CARs or on TILs, providing an additional boost in the tumour microenvironment whilst reducing the danger of antigen encounter on normal tissues. The expression of MCAM in a variety of cancer types would mean this strategy could have broad applicability.

The tsCD146 scFv presented a possible solution to this challenge in that it has been reported to be highly selective for tumour-expressed MCAM, potentially due to recognition of a specific motif accessible following MCAM homodimerisation [428]. Whilst second generation tsCD146.BBz CARs were unable to activate the JRT3-T3.5 cell line, ongoing work by other colleagues in the Hurlstone lab has subsequently optimised the CAR design. By reducing the length of the hinge region and incorporating the CD28 transmembrane/costimulatory domain it was possible to partially rescue tsCD146 activity, highlighting the need for a systematic approach to CAR development. M1.BBz and M40.BBz may therefore be useful as 'pan-MCAM' control CARs, supporting the characterisation of the more promising tsCD146 reagent.

To conclude, the present study identified 2 MCAM-specific scFv domains capable of redirecting T cell effector functions against melanoma cells *in vitro* when expressed as part of a second-generation, 4-1BB costimulated CAR. Targeting tumour associated antigens in this way carries a risk of on-target/off-tumour toxicity. The expression of MCAM on the vasculature and the endothelial-cytotoxicity of MCAM-specific CAR T cells will likely ultimately preclude their clinical use. Although M1.BBz and M40.BBz CARs in their current form may not necessarily represent clinically applicable therapies, their development has generated a base of protocols in the lab, providing a foundation on which future research can take place.

References

[1] Ruella M, Kalos M. Adoptive immunotherapy for cancer. *Immunol Rev* 2014; 257: 14–38.

[2] Bonini C, Mondino A. Adoptive T-cell therapy for cancer: The era of engineered T cells. *Eur J Immunol* 2015; 45: 2457–2469.

[3] June CH, Maus M V, Plesa G, et al. Engineered T cells for cancer therapy. *Cancer Immunol Immunother* 2014; 63: 969–975.

[4] Gao GF, Rao Z, Bell JI. Molecular coordination of αβ T-cell receptors and coreceptors CD8 and CD4 in their recognition of peptide-MHC ligands. *Trends Immunol* 2002; 23: 408–413.

[5] Murphy C. KW. *Janeways Immunobiology*. New York: Garland Science, 2017.

[6] Garcia KC, Degano M, Stanfield RL, et al. An αβ T Cell Receptor Structure at 2.5 Å and Its Orientation in the TCR-MHC Complex. *Science (1979)* 1996; 274: 209–219.

[7] Veillette A, Bookman MA, Horak EM, et al. The CD4 and CD8 T cell surface antigens are associated with the internal membrane tyrosine-protein kinase p56lck. *Cell* 1988; 55: 301–308.

[8] Iwashima M, Irving BA, van Oers NSC, et al. Sequential Interactions of the TCR with Two Distinct Cytoplasmic Tyrosine Kinases. *Science (1979)* 1994; 263: 1136–1139.

[9] van Oers NS, Killeen N, Weiss A. Lck regulates the tyrosine phosphorylation of the T cell receptor subunits and ZAP-70 in murine thymocytes. *Journal of Experimental Medicine* 1996; 183: 1053–1062.

[10] Martin PJ, Ledbetter JA, Morishita Y, et al. A 44 kilodalton cell surface homodimer regulates interleukin 2 production by activated human T lymphocytes. *J Immunol* 1986; 136: 3282–7.

[11] Read KA, Powell MD, Sreekumar BK, et al. In Vitro Differentiation of Effector CD4+ T Helper Cell Subsets. In: *Methods Mol Biol*. 2019, pp. 75–84.

[12] Zhu X, Zhu J. CD4 T Helper Cell Subsets and Related Human Immunological Disorders. *Int J Mol Sci* 2020; 21: 8011.

[13] Xie Y, Akpinarli A, Maris C, et al. Naive tumor-specific CD4+ T cells differentiated in vivo eradicate established melanoma. *Journal of Experimental Medicine* 2010; 207: 651–667.

[14] Brown DM, Lee S, Garcia-Hernandez M de la L, et al. Multifunctional CD4 Cells Expressing Gamma Interferon and Perforin Mediate Protection against Lethal Influenza Virus Infection. *J Virol* 2012; 86: 6792–6803.

[15] Aslan N, Yurdaydin C, Wiegand J, et al. Cytotoxic CD4+ T cells in viral hepatitis. *J Viral Hepat* 2006; 13: 505–514.

[16] Appay V, Zaunders JJ, Papagno L, et al. Characterization of CD4+ CTLs Ex Vivo. *The Journal of Immunology* 2002; 168: 5954–5958.

[17] st. Paul M, Ohashi PS. The Roles of CD8+ T Cell Subsets in Antitumor Immunity. *Trends Cell Biol* 2020; 30: 695–704.

[18] Hodi FS, O'Day SJ, McDermott DF, et al. Improved Survival with Ipilimumab in Patients with Metastatic Melanoma. *N Engl J Med* 2010; 363: 711–723.

[19] Robert C, Long G V, Brady B, et al. Nivolumab in Previously Untreated Melanoma without BRAF Mutation. *N Engl J Med* 2015; 372: 320–330.

[20] Robert C, Schachter J, Long G V, et al. Pembrolizumab versus Ipilimumab in Advanced Melanoma. *N Engl J Med* 2015; 372: 2521–2532.

[21] Pasquali S, Hadjinicolaou A V, Chiarion Sileni V, et al. Systemic treatments for metastatic cutaneous melanoma. *Cochrane Database Syst Rev* 2018; 2: CD011123.

[22] Rosenberg SA, Packard BS, Aebersold PM, et al. Use of tumor-infiltrating lymphocytes and interleukin-2 in the immunotherapy of patients with

metastatic melanoma. A preliminary report. *N Engl J Med* 1988; 319: 1676–1680.

[23] Rohaan MW, van den Berg JH, Kvistborg P, et al. Adoptive transfer of tumor-infiltrating lymphocytes in melanoma: a viable treatment option. *J Immunother Cancer* 2018; 6: 102.

[24] Dafni U, Michielin O, Lluesma SM, et al. Efficacy of adoptive therapy with tumor-infiltrating lymphocytes and recombinant interleukin-2 in advanced cutaneous melanoma: a systematic review and meta-analysis. *Annals of Oncology* 2019; 30: 1902–1913.

[25] Stevanović S, Helman SR, Wunderlich JR, et al. A Phase II Study of Tumor-infiltrating Lymphocyte Therapy for Human Papillomavirus–associated Epithelial Cancers. *Clinical Cancer Research* 2019; 25: 1486–1493.

[26] Tran E, Robbins PF, Lu Y-C, et al. T-Cell Transfer Therapy Targeting Mutant KRAS in Cancer. *N Engl J Med* 2016; 375: 2255–2262.

[27] Tran E, Turcotte S, Gros A, et al. Cancer Immunotherapy Based on Mutation-Specific CD4+ T Cells in a Patient with Epithelial Cancer. *Science (1979)* 2014; 344: 641–645.

[28] Zacharakis N, Chinnasamy H, Black M, et al. Immune recognition of somatic mutations leading to complete durable regression in metastatic breast cancer. *Nat Med* 2018; 24: 724–730.

[29] Creelan BC, Wang C, Teer JK, et al. Tumor-infiltrating lymphocyte treatment for anti-PD-1-resistant metastatic lung cancer: a phase 1 trial. *Nat Med* 2021; 27: 1410–1418.

[30] Yeh S, Karne NK, Kerkar SP, et al. Ocular and Systemic Autoimmunity after Successful Tumor-Infiltrating Lymphocyte Immunotherapy for Recurrent, Metastatic Melanoma. *Ophthalmology* 2009; 116: 981-989.e1.

[31] Shafer P, Kelly LM, Hoyos V. Cancer Therapy With TCR-Engineered T Cells: Current Strategies, Challenges, and Prospects. *Front Immunol*; 13. Epub ahead of print 3 March 2022. DOI: 10.3389/fimmu.2022.835762.

[32] Stadtmauer EA, Faitg TH, Lowther DE, et al. Long-term safety and activity of NY-ESO-1 SPEAR T cells after autologous stem cell transplant for myeloma. *Blood Adv* 2019; 3: 2022–2034.

[33] Butler MO, Sotov V, Saibil S, et al. Adoptive T cell therapy with TBI-1301 results in gene-engineered T cell persistence and anti-tumour responses in patients with NY-ESO-1 expressing solid tumours. *Annals of Oncology* 2019; 30: v481.

[34] Ramachandran I, Lowther DE, Dryer-Minnerly R, et al. Systemic and local immunity following adoptive transfer of NY-ESO-1 SPEAR T cells in synovial sarcoma. *J Immunother Cancer* 2019; 7: 276.

[35] Ishihara M, Kitano S, Hattori H, et al. Tumor responses and early onset cytokine release syndrome in synovial sarcoma patients treated with a novel affinity-enhanced NY-ESO-1-targeting TCR-redirected T cell transfer. *Journal of Clinical Oncology* 2019; 37: 2530–2530.

[36] Nowicki TS, Berent-Maoz B, Cheung-Lau G, et al. A Pilot Trial of the Combination of Transgenic NY-ESO-1–reactive Adoptive Cellular Therapy with Dendritic Cell Vaccination with or without Ipilimumab. *Clinical Cancer Research* 2019; 25: 2096–2108.

[37] Robbins PF, Kassim SH, Tran TLN, et al. A Pilot Trial Using Lymphocytes Genetically Engineered with an NY-ESO-1–Reactive T-cell Receptor: Long-term Follow-up and Correlates with Response. *Clinical Cancer Research* 2015; 21: 1019–1027.

[38] Moore T, Wagner CR, Scurti GM, et al. Clinical and immunologic evaluation of three metastatic melanoma patients treated with autologous melanoma-reactive TCR-transduced T cells. *Cancer Immunology, Immunotherapy* 2018; 67: 311–325.

[39] Parkhurst MR, Yang JC, Langan RC, et al. T Cells Targeting Carcinoembryonic Antigen Can Mediate Regression of Metastatic Colorectal Cancer but Induce Severe Transient Colitis. *Molecular Therapy* 2011; 19: 620–626.

[40] Johnson LA, Morgan RA, Dudley ME, et al. Gene therapy with human and mouse T-cell receptors mediates cancer regression and targets normal tissues expressing cognate antigen. *Blood* 2009; 114: 535–546.

[41] Morgan RA, Chinnasamy N, Abate-Daga D, et al. Cancer Regression and Neurological Toxicity Following Anti-MAGE-A3 TCR Gene Therapy. *Journal of Immunotherapy* 2013; 36: 133–151.

[42] Cameron BJ, Gerry AB, Dukes J, et al. Identification of a Titin-Derived HLA-A1–Presented Peptide as a Cross-Reactive Target for Engineered MAGE A3–Directed T Cells. *Sci Transl Med*; 5. Epub ahead of print 7 August 2013. DOI: 10.1126/scitranslmed.3006034.

[43] Salter AI, Rajan A, Kennedy JJ, et al. Comparative analysis of TCR and CAR signaling informs CAR designs with superior antigen sensitivity and in vivo function. *Sci Signal*; 14. Epub ahead of print 24 August 2021. DOI: 10.1126/scisignal.abe2606.

[44] Harris DT, Hager M V., Smith SN, et al. Comparison of T Cell Activities Mediated by Human TCRs and CARs That Use the Same Recognition Domains. *The Journal of Immunology* 2018; 200: 1088–1100.

[45] Cornel AM, Mimpen IL, Nierkens S. MHC Class I Downregulation in Cancer: Underlying Mechanisms and Potential Targets for Cancer Immunotherapy. *Cancers (Basel)* 2020; 12: 1760.

[46] Lu Y-C, Parker LL, Lu T, et al. Treatment of Patients With Metastatic Cancer Using a Major Histocompatibility Complex Class II-Restricted T-Cell Receptor Targeting the Cancer Germline Antigen MAGE-A3. *J Clin Oncol* 2017; 35: 3322–3329.

[47] Huston JS, Levinson D, Mudgett-Hunter M, et al. Protein engineering of antibody binding sites: recovery of specific activity in an anti-digoxin single-chain Fv

analogue produced in Escherichia coli. *Proc Natl Acad Sci U S A* 1988; 85: 5879–5883.

[48] Cheadle EJ, Gornall H, Baldan V, et al. CAR T cells: driving the road from the laboratory to the clinic. *Immunol Rev* 2014; 257: 91–106.

[49] Sadelain M, Brentjens R, Rivière I. The Basic Principles of Chimeric Antigen Receptor Design. *Cancer Discov* 2013; 3: 388–398.

[50] Benmebarek M-R, Karches C, Cadilha B, et al. Killing Mechanisms of Chimeric Antigen Receptor (CAR) T Cells. *Int J Mol Sci* 2019; 20: 1283.

[51] Kuwana Y, Asakura Y, Utsunomiya N, et al. Expression of chimeric receptor composed of immunoglobulin-derived V regions and T-cell receptor-derived C regions. *Biochem Biophys Res Commun* 1987; 149: 960–968.

[52] Irving BA, Weiss A. The cytoplasmic domain of the T cell receptor zeta chain is sufficient to couple to receptor-associated signal transduction pathways. *Cell* 1991; 64: 891–901.

[53] Letourneur F, Klausner RD. T-cell and basophil activation through the cytoplasmic tail of T-cell-receptor zeta family proteins. *Proc Natl Acad Sci U S A* 1991; 88: 8905–8909.

[54] Romeo C, Seed B. Cellular immunity to HIV activated by CD4 fused to T cell or Fc receptor polypeptides. *Cell* 1991; 64: 1037–1046.

[55] Eshhar Z, Waks T, Gross G, et al. Specific activation and targeting of cytotoxic lymphocytes through chimeric single chains consisting of antibody-binding domains and the gamma or zeta subunits of the immunoglobulin and T-cell receptors. *Proc Natl Acad Sci U S A* 1993; 90: 720–724.

[56] Brocker T, Karjalainen K. Signals through T cell receptor-zeta chain alone are insufficient to prime resting T lymphocytes. *J Exp Med* 1995; 181: 1653–1659.

[57] Gong MC, Latouche JB, Krause A, et al. Cancer patient T cells genetically targeted to prostate-specific membrane antigen specifically lyse prostate cancer

cells and release cytokines in response to prostate-specific membrane antigen. *Neoplasia* 1999; 1: 123–127.

[58] Finney HM, Akbar AN, Lawson AD. Activation of resting human primary T cells with chimeric receptors: costimulation from CD28, inducible costimulator, CD134, and CD137 in series with signals from the TCR zeta chain. *J Immunol* 2004; 172: 104–113.

[59] Maher J, Brentjens RJ, Gunset G, et al. Human T-lymphocyte cytotoxicity and proliferation directed by a single chimeric TCRzeta /CD28 receptor. *Nat Biotechnol* 2002; 20: 70–75.

[60] Zhong XS, Matsushita M, Plotkin J, et al. Chimeric antigen receptors combining 4-1BB and CD28 signaling domains augment PI3kinase/AKT/Bcl-XL activation and CD8+ T cell-mediated tumor eradication. *Mol Ther* 2010; 18: 413–420.

[61] Milone MC, Fish JD, Carpenito C, et al. Chimeric receptors containing CD137 signal transduction domains mediate enhanced survival of T cells and increased antileukemic efficacy in vivo. 17. Epub ahead of print 2009. DOI: 10.1038/mt.2009.83.

[62] Brentjens RJ, Santos E, Nikhamin Y, et al. Genetically targeted T cells eradicate systemic acute lymphoblastic leukemia xenografts. *Clin Cancer Res* 2007; 13: 5426–5435.

[63] Carpenito C, Milone MC, Hassan R, et al. Control of large, established tumor xenografts with genetically retargeted human T cells containing CD28 and CD137 domains. *Proc Natl Acad Sci U S A* 2009; 106: 3360–3365.

[64] Pule MA, Straathof KC, Dotti G, et al. A chimeric T cell antigen receptor that augments cytokine release and supports clonal expansion of primary human T cells. *Mol Ther* 2005; 12: 933–941.

[65] You F, Jiang L, Zhang B, et al. Phase 1 clinical trial demonstrated that MUC1 positive metastatic seminal vesicle cancer can be effectively eradicated by modified Anti-MUC1 chimeric antigen receptor transduced T cells. *Sci China Life Sci* 2016; 59: 386–397.

[66] Enblad G, Karlsson H, Gammelgård G, et al. A Phase I/IIa Trial Using CD19-Targeted Third-Generation CAR T Cells for Lymphoma and Leukemia. *Clinical Cancer Research* 2018; 24: 6185–6194.

[67] Schubert M-L, Schmitt A, Neuber B, et al. Third-Generation CAR T Cells Targeting CD19 Are Associated with an Excellent Safety Profile and Might Improve Persistence of CAR T Cells in Treated Patients. *Blood* 2019; 134: 51–51.

[68] Tokarew N, Ogonek J, Endres S, et al. Teaching an old dog new tricks: next-generation CAR T cells. *Br J Cancer* 2019; 120: 26–37.

[69] Adachi K, Kano Y, Nagai T, et al. IL-7 and CCL19 expression in CAR-T cells improves immune cell infiltration and CAR-T cell survival in the tumor. *Nat Biotechnol* 2018; 36: 346–351.

[70] Goto S, Sakoda Y, Adachi K, et al. Enhanced anti-tumor efficacy of IL-7/CCL19-producing human CAR-T cells in orthotopic and patient-derived xenograft tumor models. *Cancer Immunology, Immunotherapy* 2021; 70: 2503–2515.

[71] Luo H, Su J, Sun R, et al. Coexpression of IL7 and CCL21 Increases Efficacy of CAR-T Cells in Solid Tumors without Requiring Preconditioned Lymphodepletion. *Clinical Cancer Research* 2020; 26: 5494–5505.

[72] Pang N, Shi J, Qin L, et al. IL-7 and CCL19-secreting CAR-T cell therapy for tumors with positive glypican-3 or mesothelin. *J Hematol Oncol* 2021; 14: 118.

[73] Hoyos V, Savoldo B, Quintarelli C, et al. Engineering CD19-specific T lymphocytes with interleukin-15 and a suicide gene to enhance their anti-lymphoma/leukemia effects and safety. *Leukemia* 2010; 24: 1160–1170.

[74] Koneru M, Purdon TJ, Spriggs D, et al. IL-12 secreting tumor-targeted chimeric antigen receptor T cells eradicate ovarian tumors *in vivo*. *Oncoimmunology* 2015; 4: e994446.

[75] Yeku OO, Purdon TJ, Koneru M, et al. Armored CAR T cells enhance antitumor efficacy and overcome the tumor microenvironment. *Sci Rep* 2017; 7: 10541.

[76] Chmielewski M, Kopecky C, Hombach AA, et al. IL-12 Release by Engineered T Cells Expressing Chimeric Antigen Receptors Can Effectively Muster an Antigen-Independent Macrophage Response on Tumor Cells That Have Shut Down Tumor Antigen Expression. *Cancer Res* 2011; 71: 5697–5706.

[77] Avanzi MP, Yeku O, Li X, et al. Engineered Tumor-Targeted T Cells Mediate Enhanced Anti-Tumor Efficacy Both Directly and through Activation of the Endogenous Immune System. *Cell Rep* 2018; 23: 2130–2141.

[78] Kagoya Y, Tanaka S, Guo T, et al. A novel chimeric antigen receptor containing a JAK–STAT signaling domain mediates superior antitumor effects. *Nat Med* 2018; 24: 352–359.

[79] Barros LRC, Couto SCF, da Silva Santurio D, et al. Systematic Review of Available CAR-T Cell Trials around the World. *Cancers (Basel)* 2022; 14: 2667.

[80] Drent E, Poels R, Ruiter R, et al. Combined CD28 and 4-1BB Costimulation Potentiates Affinity-tuned Chimeric Antigen Receptor–engineered T Cells. *Clinical Cancer Research* 2019; 25: 4014–4025.

[81] Long AH, Haso WM, Shern JF, et al. 4-1BB costimulation ameliorates T cell exhaustion induced by tonic signaling of chimeric antigen receptors. *Nature Medicine 2015 21:6* 2015; 21: 581–590.

[82] Wagner DL, Fritsche E, Pulsipher MA, et al. Immunogenicity of CAR T cells in cancer therapy. *Nat Rev Clin Oncol* 2021; 18: 379–393.

[83] Kershaw MH, Westwood JA, Parker LL, et al. A phase I study on adoptive immunotherapy using gene-modified T cells for ovarian cancer. *Clin Cancer Res* 2006; 12: 6106–6115.

[84] Lamers CHJ, Willemsen R, van Elzakker P, et al. Immune responses to transgene and retroviral vector in patients treated with ex vivo–engineered T cells. *Blood* 2011; 117: 72–82.

[85] Maus M v, Haas AR, Beatty GL, et al. T cells expressing chimeric antigen receptors can cause anaphylaxis in humans. *Cancer Immunol Res* 2013; 1: 26–31.

[86] Jensen MC, Popplewell L, Cooper LJ, et al. Antitransgene Rejection Responses Contribute to Attenuated Persistence of Adoptively Transferred CD20/CD19-Specific Chimeric Antigen Receptor Redirected T Cells in Humans. *Biology of Blood and Marrow Transplantation* 2010; 16: 1245–1256.

[87] Turtle CJ, Hanafi L-A, Berger C, et al. CD19 CAR–T cells of defined CD4+:CD8+ composition in adult B cell ALL patients. *Journal of Clinical Investigation* 2016; 126: 2123–2138.

[88] Turtle CJ, Hanafi L-A, Berger C, et al. Immunotherapy of non-Hodgkin's lymphoma with a defined ratio of CD8+ and CD4+ CD19-specific chimeric antigen receptor–modified T cells. *Sci Transl Med*; 8. Epub ahead of print 7 September 2016. DOI: 10.1126/scitranslmed.aaf8621.

[89] Brudno JN, Lam N, Vanasse D, et al. Safety and feasibility of anti-CD19 CAR T cells with fully human binding domains in patients with B-cell lymphoma. *Nat Med* 2020; 26: 270–280.

[90] Heng G, Jia J, Li S, et al. Sustained Therapeutic Efficacy of Humanized Anti-CD19 Chimeric Antigen Receptor T Cells in Relapsed/Refractory Acute Lymphoblastic Leukemia. *Clinical Cancer Research* 2020; 26: 1606–1615.

[91] Singh N, Frey N v., Engels B, et al. Antigen-independent activation enhances the efficacy of 4-1BB-costimulated CD22 CAR T cells. *Nat Med* 2021; 27: 842–850.

[92] Shah NN, Highfill SL, Shalabi H, et al. CD4/CD8 T-Cell Selection Affects Chimeric Antigen Receptor (CAR) T-Cell Potency and Toxicity: Updated Results From a Phase I Anti-CD22 CAR T-Cell Trial. *Journal of Clinical Oncology* 2020; 38: 1938–1950.

[93] Fry TJ, Shah NN, Orentas RJ, et al. CD22-targeted CAR T cells induce remission in B-ALL that is naive or resistant to CD19-targeted CAR immunotherapy. *Nat Med* 2018; 24: 20–28.

[94] Tong C, Zhang Y, Liu Y, et al. Optimized tandem CD19/CD20 CAR-engineered T cells in refractory/relapsed B cell lymphoma. *Blood*. Epub ahead of print 18 June 2020. DOI: 10.1182/blood.2020005278.

[95] Hegde M, Mukherjee M, Grada Z, et al. Tandem CAR T cells targeting HER2 and IL13Rα2 mitigate tumor antigen escape. *Journal of Clinical Investigation* 2016; 126: 3036–3052.

[96] Yang M, Tang X, Zhang Z, et al. Tandem CAR-T cells targeting CD70 and B7-H3 exhibit potent preclinical activity against multiple solid tumors. *Theranostics* 2020; 10: 7622–7634.

[97] Crunkhorn S. First-in-human trial of bispecific CAR-T cells. *Nat Rev Drug Discov* 2020; 19: 838–838.

[98] Orlando EJ, Han X, Tribouley C, et al. Genetic mechanisms of target antigen loss in CAR19 therapy of acute lymphoblastic leukemia. *Nat Med* 2018; 24: 1504–1506.

[99] Guest RD, Hawkins RE, Kirillova N, et al. The role of extracellular spacer regions in the optimal design of chimeric immune receptors: Evaluation of four different scFvs and antigens. *Journal of Immunotherapy* 2005; 28: 203–211.

[100] James SE, Greenberg PD, Jensen MC, et al. Antigen sensitivity of CD22-specific chimeric TCR is modulated by target epitope distance from the cell membrane. *J Immunol* 2008; 180: 7028–7038.

[101] Wilkie S, Picco G, Foster J, et al. Retargeting of Human T Cells to Tumor-Associated MUC1: The Evolution of a Chimeric Antigen Receptor. *The Journal of Immunology* 2008; 180: 4901–4909.

[102] Hombach A, Hombach AA, Abken H. Adoptive immunotherapy with genetically engineered T cells: modification of the IgG1 Fc 'spacer' domain in the extracellular moiety of chimeric antigen receptors avoids 'off-target' activation and unintended initiation of an innate immune response. *Gene Ther* 2010; 17: 1206–1213.

[103] Hudecek M, Sommermeyer D, Kosasih PL, et al. The non-signaling extracellular spacer domain of chimeric antigen receptors is decisive for in vivo antitumor activity HHS Public Access. *Cancer Immunol Res* 2015; 3: 125–135.

[104] Watanabe N, Bajgain P, Sukumaran S, et al. Fine-tuning the CAR spacer improves T-cell potency. *Oncoimmunology* 2016; 5: e1253656.

[105] Jonnalagadda M, Mardiros A, Urak R, et al. Chimeric antigen receptors with mutated IgG4 Fc spacer avoid fc receptor binding and improve T cell persistence and antitumor efficacy. *Molecular Therapy* 2015; 23: 757–768.

[106] Majzner RG, Rietberg SP, Sotillo E, et al. Tuning the Antigen Density Requirement for CAR T-cell Activity. *Cancer Discov* 2020; 10: 702–723.

[107] Alabanza L, Pegues M, Geldres C, et al. Function of Novel Anti-CD19 Chimeric Antigen Receptors with Human Variable Regions Is Affected by Hinge and Transmembrane Domains. Epub ahead of print 2017. DOI: 10.1016/j.ymthe.2017.07.013.

[108] Cappell KM, Kochenderfer JN. A comparison of chimeric antigen receptors containing CD28 versus 4-1BB costimulatory domains. *Nat Rev Clin Oncol* 2021; 18: 715–727.

[109] Riha P, Rudd CE. CD28 co-signaling in the adaptive immune response. *Self Nonself* 2010; 1: 231–240.

[110] Riha P, Rudd CE. CD28 co-signaling in the adaptive immune response. *Self Nonself* 2010; 1: 231–240.

[111] Sanchez-Paulete AR, Labiano S, Rodriguez-Ruiz ME, et al. Deciphering CD137 (4-1BB) signaling in T-cell costimulation for translation into successful cancer immunotherapy. *Eur J Immunol* 2016; 46: 513–522.

[112] Salter AI, Ivey RG, Kennedy JJ, et al. Phosphoproteomic analysis of chimeric antigen receptor signaling reveals kinetic and quantitative differences that affect cell function. *Sci Signal*; 11. Epub ahead of print 21 August 2018. DOI: 10.1126/scisignal.aat6753.

[113] Sun C, Shou P, Du H, et al. THEMIS-SHP1 Recruitment by 4-1BB Tunes LCK-Mediated Priming of Chimeric Antigen Receptor-Redirected T Cells. *Cancer Cell* 2020; 37: 216-225.e6.

[114] Philipson BI, O'Connor RS, May MJ, et al. 4-1BB costimulation promotes CAR T cell survival through noncanonical NF-κB signaling. *Sci Signal*; 13. Epub ahead of print 31 March 2020. DOI: 10.1126/scisignal.aay8248.

[115] Li G, Boucher JC, Kotani H, et al. 4-1BB enhancement of CAR T function requires NF-κB and TRAFs. *JCI Insight*; 3. Epub ahead of print 20 September 2018. DOI: 10.1172/jci.insight.121322.

[116] Guedan S, Posey AD, Shaw C, et al. Enhancing CAR T cell persistence through ICOS and 4-1BB costimulation. *JCI Insight*; 3. Epub ahead of print 11 January 2018. DOI: 10.1172/JCI.INSIGHT.96976.

[117] Cherkassky L, Morello A, Villena-Vargas J, et al. Human CAR T cells with cell-intrinsic PD-1 checkpoint blockade resist tumor-mediated inhibition. *Journal of Clinical Investigation* 2016; 126: 3130–3144.

[118] Zhao Z, Condomines M, van der Stegen SJC, et al. Structural Design of Engineered Costimulation Determines Tumor Rejection Kinetics and Persistence of CAR T Cells. *Cancer Cell* 2015; 28: 415–428.

[119] Kawalekar OU, O'Connor RS, Fraietta JA, et al. Distinct Signaling of Coreceptors Regulates Specific Metabolism Pathways and Impacts Memory Development in CAR T Cells. *Immunity* 2016; 44: 380–90.

[120] Boroughs AC, Larson RC, Marjanovic ND, et al. A Distinct Transcriptional Program in Human CAR T Cells Bearing the 4-1BB Signaling Domain Revealed by scRNA-Seq. *Molecular Therapy* 2020; 28: 2577–2592.

[121] Fraietta JA, Lacey SF, Orlando EJ, et al. Determinants of response and resistance to CD19 chimeric antigen receptor (CAR) T cell therapy of chronic lymphocytic leukemia. *Nat Med* 2018; 24: 563–571.

[122] Finney OC, Brakke H, Rawlings-Rhea S, et al. CD19 CAR T cell product and disease attributes predict leukemia remission durability. *Journal of Clinical Investigation* 2019; 129: 2123–2132.

[123] Maude SL, Laetsch TW, Buechner J, et al. Tisagenlecleucel in Children and Young Adults with B-Cell Lymphoblastic Leukemia. *N Engl J Med* 2018; 378: 439–448.

[124] Lee DW, Kochenderfer JN, Stetler-Stevenson M, et al. T cells expressing CD19 chimeric antigen receptors for acute lymphoblastic leukaemia in children and young adults: a phase 1 dose-escalation trial. 385. Epub ahead of print 2015. DOI: 10.1016/s0140-6736(14)61403-3.

[125] Park JH, Riviere I, Gonen M, et al. Long-Term Follow-up of CD19 CAR Therapy in Acute Lymphoblastic Leukemia. *N Engl J Med* 2018; 378: 449–459.

[126] Gardner RA, Finney O, Annesley C, et al. Intent-to-treat leukemia remission by CD19 CAR T cells of defined formulation and dose in children and young adults. *Blood* 2017; 129: 3322–3331.

[127] Zhao Z, Zhang J, Bian J, et al. The efficacy and safety of chimeric antigen receptor T cells in digestive system cancers: a systematic review and meta-analysis. *Ann Transl Med* 2022; 10: 508–508.

[128] Anagnostou T, Riaz IB, Hashmi SK, et al. Anti-CD19 chimeric antigen receptor T-cell therapy in acute lymphocytic leukaemia: a systematic review and meta-analysis. *Lancet Haematol* 2020; 7: e816–e826.

[129] Bridgeman JS, Hawkins RE, Bagley S, et al. The optimal antigen response of chimeric antigen receptors harboring the CD3zeta transmembrane domain is dependent upon incorporation of the receptor into the endogenous TCR/CD3 complex. *J Immunol* 2010; 184: 6938–49.

[130] Feucht J, Sun J, Eyquem J, et al. Calibration of CAR activation potential directs alternative T cell fates and therapeutic potency. *Nat Med* 2019; 25: 82–88.

[131] Wu W, Zhou Q, Masubuchi T, et al. Multiple Signaling Roles of CD3ε and Its Application in CAR-T Cell Therapy. *Cell* 2020; 182: 855-871.e23.

[132] Hartl FA, Beck-Garcìa E, Woessner NM, et al. Noncanonical binding of Lck to CD3ε promotes TCR signaling and CAR function. *Nat Immunol* 2020; 21: 902–913.

[133] Parente-Pereira AC, Wilkie S, Van der Stegen SJC, et al. Use of retroviral-mediated gene transfer to deliver and test function of chimeric antigen receptors in human T-cells. *J Biol Methods* 2014; 1: 7.

[134] Circosta P, Granziero L, Follenzi A, et al. T cell receptor (TCR) gene transfer with lentiviral vectors allows efficient redirection of tumor specificity in naive and memory T cells without prior stimulation of endogenous TCR. *Hum Gene Ther* 2009; 20: 1576–1588.

[135] Amirache F, Lévy C, Costa C, et al. Mystery solved: VSV-G-LVs do not allow efficient gene transfer into unstimulated T cells, B cells, and HSCs because they lack the LDL receptor. *Blood*. Epub ahead of print 2014. DOI: 10.1182/blood-2013-11-540641.

[136] Yacoub N al, Romanowska M, Haritonova N, et al. Optimized production and concentration of lentiviral vectors containing large inserts. *J Gene Med* 2007; 9: 579–584.

[137] Hacein-Bey-Abina S, Garrigue A, Wang GP, et al. Insertional oncogenesis in 4 patients after retrovirus-mediated gene therapy of SCID-X1. *Journal of Clinical Investigation* 2008; 118: 3132–3142.

[138] Hacein-Bey-Abina S, Von Kalle C, Schmidt M, et al. LMO2-Associated Clonal T Cell Proliferation in Two Patients after Gene Therapy for SCID-X1. *Science (1979)* 2003; 302: 415–419.

[139] Cattoglio C, Facchini G, Sartori D, et al. Hot spots of retroviral integration in human CD34+ hematopoietic cells. *Blood* 2007; 110: 1770–1778.

[140] De Ravin SS, Su L, Theobald N, et al. Enhancers Are Major Targets for Murine Leukemia Virus Vector Integration. *J Virol* 2014; 88: 4504–4513.

[141] LaFave MC, Varshney GK, Gildea DE, et al. MLV integration site selection is driven by strong enhancers and active promoters. *Nucleic Acids Res* 2014; 42: 4257–4269.

[142] Fraietta JA, Nobles CL, Sammons MA, et al. Disruption of TET2 promotes the therapeutic efficacy of CD19-targeted T cells. *Nature* 2018; 558: 307–312.

[143] Rodrigues A, M. P, Coroadinh A. Production of Retroviral and Lentiviral Gene Therapy Vectors: Challenges in the Manufacturing of Lipid Enveloped Virus. In: *Viral Gene Therapy*. InTech, 2011. Epub ahead of print 20 July 2011. DOI: 10.5772/18615.

[144] Cornetta K, Duffy L, Turtle CJ, et al. Absence of Replication-Competent Lentivirus in the Clinic: Analysis of Infused T Cell Products. *Molecular Therapy* 2018; 26: 280–288.

[145] Marcucci KT, Jadlowsky JK, Hwang WT, et al. Retroviral and Lentiviral Safety Analysis of Gene-Modified T Cell Products and Infused HIV and Oncology Patients. *Molecular Therapy* 2018; 26: 269.

[146] Bear AS, Morgan RA, Cornetta K, et al. Replication-Competent Retroviruses in Gene-Modified T Cells Used in Clinical Trials: Is It Time to Revise the Testing Requirements? *Molecular Therapy* 2012; 20: 246–249.

[147] Cornetta K, Duffy L, Feldman SA, et al. Screening Clinical Cell Products for Replication Competent Retrovirus: The National Gene Vector Biorepository Experience. *Mol Ther Methods Clin Dev* 2018; 10: 371–378.

[148] Munoz-Lopez M, Garcia-Perez J. DNA Transposons: Nature and Applications in Genomics. *Curr Genomics* 2010; 11: 115–128.

[149] Magnani CF, Tettamanti S, Alberti G, et al. Transposon-Based CAR T Cells in Acute Leukemias: Where Are We Going? *Cells* 2020; 9: 1337.

[150] Manuri P V, Wilson MH, Maiti SN, et al. piggyBac transposon/transposase system to generate CD19-specific T cells for the treatment of B-lineage malignancies. *Hum Gene Ther* 2010; 21: 427–437.

[151] Chicaybam L, Abdo L, Viegas M, et al. Transposon-mediated generation of CAR-T cells shows efficient anti B-cell leukemia response after ex vivo expansion. *Gene Ther* 2020; 27: 85–95.

[152] Lock D, Monjezi R, Brandes C, et al. Automated, scaled, transposon-based production of CAR T cells. *J Immunother Cancer* 2022; 10: e005189.

[153] Ptáčková P, Musil J, Štach M, et al. A new approach to CAR T-cell gene engineering and cultivation using piggyBac transposon in the presence of IL-4, IL-7 and IL-21. *Cytotherapy* 2018; 20: 507–520.

[154] Kebriaei P, Singh H, Huls MH, et al. Phase I trials using Sleeping Beauty to generate CD19-specific CAR T cells. *Journal of Clinical Investigation* 2016; 126: 3363–3376.

[155] Zhang Y, Zhang Z, Ding Y, et al. Phase I clinical trial of EGFR-specific CAR-T cells generated by the piggyBac transposon system in advanced relapsed/refractory non-small cell lung cancer patients. *J Cancer Res Clin Oncol* 2021; 147: 3725–3734.

[156] Magnani CF, Gaipa G, Lussana F, et al. Sleeping Beauty–engineered CAR T cells achieve antileukemic activity without severe toxicities. *Journal of Clinical Investigation* 2020; 130: 6021–6033.

[157] Zhao Y, Zheng Z, Cohen CJ, et al. High-efficiency transfection of primary human and mouse T lymphocytes using RNA electroporation. *Mol Ther* 2006; 13: 151–159.

[158] Barrett DM, Zhao Y, Liu X, et al. Treatment of Advanced Leukemia in Mice with mRNA Engineered T Cells. *Hum Gene Ther* 2011; 22: 1575.

[159] Jayasooriya V, Ringwelski B, Dorsam G, et al. mRNA-based CAR T-cells Manufactured by Miniaturized Two-step Electroporation Produce Selective Cytotoxicity Toward Target Cancer Cells. *Lab Chip* 2021; 21: 3748.

[160] Jin C, Fotaki G, Ramachandran M, et al. Safe engineering of CAR T cells for adoptive cell therapy of cancer using long-term episomal gene transfer. *EMBO Mol Med* 2016; 8: 702–711.

[161] Eyquem J, Mansilla-Soto J, Giavridis T, et al. Targeting a CAR to the TRAC locus with CRISPR/Cas9 enhances tumour rejection. *Nature* 2017; 543: 113–117.

[162] Stadtmauer EA, Fraietta JA, Davis MM, et al. CRISPR-engineered T cells in patients with refractory cancer. *Science (1979)*; 367. Epub ahead of print 28 February 2020. DOI: 10.1126/science.aba7365.

[163] Gao Q, Dong X, Xu Q, et al. Therapeutic potential of CRISPR/Cas9 gene editing in engineered T-cell therapy. *Cancer Med* 2019; 8: 4254–4264.

[164] Gattinoni L, Klebanoff CA, Restifo NP. Paths to stemness: building the ultimate antitumour T cell. *Nat Rev Cancer* 2012; 12: 671–684.

[165] Zhou J, Shen X, Huang J, et al. Telomere length of transferred lymphocytes correlates with in vivo persistence and tumor regression in melanoma patients receiving cell transfer therapy. *J Immunol* 2005; 175: 7046–7052.

[166] Rosenberg SA, Yang JC, Sherry RM, et al. Durable complete responses in heavily pretreated patients with metastatic melanoma using T-cell transfer immunotherapy. *Clin Cancer Res* 2011; 17: 4550–4557.

[167] Klebanoff CA, Gattinoni L, Torabi-Parizi P, et al. Central memory self/tumor-reactive CD8+ T cells confer superior antitumor immunity compared with effector memory T cells. *Proc Natl Acad Sci U S A* 2005; 102: 9571–9576.

[168] Hinrichs CS, Borman ZA, Cassard L, et al. Adoptively transferred effector cells derived from naive rather than central memory CD8+ T cells mediate superior antitumor immunity. *Proc Natl Acad Sci U S A* 2009; 106: 17469–17474.

[169] Pule MA, Savoldo B, Myers GD, et al. Virus-specific T cells engineered to coexpress tumor-specific receptors: persistence and antitumor activity in individuals with neuroblastoma. *Nat Med* 2008; 14: 1264–1270.

[170] Kershaw MH, Westwood JA, Parker LL, et al. A phase I study on adoptive immunotherapy using gene-modified T cells for ovarian cancer. *Clin Cancer Res* 2006; 12: 6106–6115.

[171] Park JR, Digiusto DL, Slovak M, et al. Adoptive transfer of chimeric antigen receptor re-directed cytolytic T lymphocyte clones in patients with neuroblastoma. *Mol Ther* 2007; 15: 825–833.

[172] Lamers CH, Langeveld SC, Groot-van Ruijven CM, et al. Gene-modified T cells for adoptive immunotherapy of renal cell cancer maintain transgene-specific immune functions in vivo. *Cancer Immunol Immunother* 2007; 56: 1875–1883.

[173] Kalos M, Levine BL, Porter DL, et al. T cells with chimeric antigen receptors have potent antitumor effects and can establish memory in patients with advanced leukemia. *Sci Transl Med* 2011; 3: 95ra73.

[174] Melenhorst JJ, Chen GM, Wang M, et al. Decade-long leukaemia remissions with persistence of CD4+ CAR T cells. *Nature 2022 602:7897* 2022; 602: 503–509.

[175] Maude SL, Barrett D, Teachey DT, et al. Managing cytokine release syndrome associated with novel T cell-engaging therapies. *Cancer J* 2014; 20: 119–122.

[176] Yu W-L, Hua Z-C. Chimeric Antigen Receptor T-cell (CAR T) Therapy for Hematologic and Solid Malignancies: Efficacy and Safety—A Systematic Review with Meta-Analysis. *Cancers (Basel)* 2019; 11: 47.

[177] Lei W, Xie M, Jiang Q, et al. Treatment-Related Adverse Events of Chimeric Antigen Receptor T-Cell (CAR T) in Clinical Trials: A Systematic Review and Meta-Analysis. *Cancers (Basel)* 2021; 13: 3912.

[178] Grigor EJM, Fergusson D, Kekre N, et al. Risks and Benefits of Chimeric Antigen Receptor T-Cell (CAR-T) Therapy in Cancer: A Systematic Review and Meta-Analysis. *Transfus Med Rev* 2019; 33: 98–110.

[179] Summers C, Wu QV, Annesley C, et al. Hematopoietic Cell Transplantation after CD19 Chimeric Antigen Receptor T Cell-Induced Acute Lymphoblastic Leukemia

Remission Confers a Leukemia-Free Survival Advantage. *Transplant Cell Ther* 2022; 28: 21–29.

[180] Chiesa R, Georgiadis C, Ottaviano G, et al. Tvt CAR7: Phase 1 Clinical Trial of Base-Edited "Universal" CAR7 T Cells for Paediatric Relapsed/Refractory T-ALL. *Blood* 2022; 140: 4579–4580.

[181] FDA. Approval Letter - KYMRIAH. *U.S. Food and Drug Administration, Center for Drug Evaluation and Research*, https://www.fda.gov/vaccines-blood-biologics/cellular-gene-therapy-products/kymriah-tisagenlecleucel (2017, accessed 8 January 2023).

[182] Technology appraisal guidance [TA554] Tisagenlecleucel for treating relapsed or refractory B-cell acute lymphoblastic leukaemia in people aged up to 25 years. 2018, https://www.nice.org.uk/guidance/ta554/chapter/1-Recommendations (2018).

[183] FDA. Approval Letter - YESCARTA. *U.S. Food and Drug Administration, Center for Drug Evaluation and Research*, https://www.fda.gov/vaccines-blood-biologics/cellular-gene-therapy-products/yescarta-axicabtagene-ciloleucel (2017, accessed 8 January 2023).

[184] FDA. Approval Letter - TECARTUS. *U.S. Food and Drug Administration, Center for Drug Evaluation and Research.*, https://www.fda.gov/vaccines-blood-biologics/cellular-gene-therapy-products/tecartus-brexucabtagene-autoleucel (2020, accessed 8 January 2023).

[185] FDA. Approval Letter - BREYANZI. *U.S. Food and Drug Administration, Center for Drug Evaluation and Research.*, https://www.fda.gov/vaccines-blood-biologics/cellular-gene-therapy-products/breyanzi-lisocabtagene-maraleucel (2021, accessed 8 January 2023).

[186] FDA. Approval Letter - ABECMA. *U.S. Food and Drug Administration, Center for Drug Evaluation and Research*, https://www.fda.gov/vaccines-blood-biologics/abecma-idecabtagene-vicleucel (2021, accessed 8 January 2023).

[187] FDA. Approval Letter - CARVYKTI. *U.S. Food and Drug Administration, Center for Drug Evaluation and Research.*, https://www.fda.gov/vaccines-blood-biologics/carvykti (2022, accessed 8 January 2023).

[188] Hou B, Tang Y, Li W, et al. Efficiency of CAR-T Therapy for Treatment of Solid Tumor in Clinical Trials: A Meta-Analysis. *Dis Markers* 2019; 2019: 1–11.

[189] Gajewski TF, Meng Y, Blank C, et al. Immune resistance orchestrated by the tumor microenvironment. *Immunol Rev* 2006; 213: 131–145.

[190] Louis CU, Savoldo B, Dotti G, et al. Antitumor activity and long-term fate of chimeric antigen receptor-positive T cells in patients with neuroblastoma. 118. Epub ahead of print 2011. DOI: 10.1182/blood-2011-05-354449.

[191] Pule MA, Savoldo B, Myers GD, et al. Virus-specific T cells engineered to coexpress tumor-specific receptors: persistence and antitumor activity in individuals with neuroblastoma. *Nat Med* 2008; 14: 1264–1270.

[192] Hegde M, DeRenzo CC, Zhang H, et al. Expansion of HER2-CAR T cells after lymphodepletion and clinical responses in patients with advanced sarcoma. *Journal of Clinical Oncology* 2017; 35: 10508–10508.

[193] Cao W, Xing H, Li Y, et al. Claudin18.2 is a novel molecular biomarker for tumor-targeted immunotherapy. *Biomark Res* 2022; 10: 1–21.

[194] Jiang H, Shi Z, Wang P, et al. Claudin18.2-Specific Chimeric Antigen Receptor Engineered T Cells for the Treatment of Gastric Cancer. *JNCI: Journal of the National Cancer Institute* 2019; 111: 409–418.

[195] Mathur D, Root AR, Bugaj-Gaweda B, et al. A Novel GUCY2C-CD3 T-Cell Engaging Bispecific Construct (PF-07062119) for the Treatment of Gastrointestinal Cancers. *Clinical Cancer Research* 2020; 26: 2188–2202.

[196] Qi C, Gong J, Li J, et al. Claudin18.2-specific CAR T cells in gastrointestinal cancers: phase 1 trial interim results. *Nat Med* 2022; 28: 1189–1198.

[197] Botta GP, Becerra CR, Jin Z, et al. Multicenter phase Ib trial in the U.S. of salvage CT041 CLDN18.2-specific chimeric antigen receptor T-cell therapy for patients

with advanced gastric and pancreatic adenocarcinoma. *Journal of Clinical Oncology* 2022; 40: 2538–2538.

[198] QI C, Liu C, Gong J, et al. Safety, tolerability, and preliminary efficacy results in patients with advanced gastric/gastroesophageal junction adenocarcinoma from a phase Ib/II study of CLDN18.2 CAR T-cell therapy (CT041). *Journal of Clinical Oncology* 2022; 40: 4017–4017.

[199] Magee MS, Kraft CL, Abraham TS, et al. GUCY2C-directed CAR-T cells oppose colorectal cancer metastases without autoimmunity. *Oncoimmunology* 2016; 5: e1227897.

[200] Magee MS, Abraham TS, Baybutt TR, et al. Human GUCY2C-Targeted Chimeric Antigen Receptor (CAR)-Expressing T Cells Eliminate Colorectal Cancer Metastases. *Cancer Immunol Res* 2018; 6: 509–516.

[201] Root AR, Guntas G, Katragadda M, et al. Discovery and optimization of a novel anti-GUCY2c x CD3 bispecific antibody for the treatment of solid tumors. *MAbs*; 13. Epub ahead of print 1 January 2021. DOI: 10.1080/19420862.2020.1850395.

[202] Reinhard K, Rengstl B, Oehm P, et al. An RNA vaccine drives expansion and efficacy of claudin-CAR-T cells against solid tumors. *Science (1979)* 2020; 367: 446–453.

[203] Mackensen A, Haanen J, Koenecke C, et al. LBA38 - BNT211-01: A phase I trial to evaluate safety and efficacy of CLDN6 CAR T cells and CLDN6-encoding mRNA vaccine-mediated in vivo expansion in patients with CLDN6-positive advanced solid tumours. In: *Annals of Oncology (2022) 33 (suppl_7): S808-S869. 10.1016/annonc/annonc1089*. Annals of Oncology (2022), 2022.

[204] Wang X, Rivière I. Clinical manufacturing of CAR T cells: foundation of a promising therapy. *Mol Ther Oncolytics* 2016; 3: 16015.

[205] Beatty GL, Haas AR, Maus M v, et al. Mesothelin-specific chimeric antigen receptor mRNA-engineered T cells induce anti-tumor activity in solid malignancies. *Cancer Immunol Res* 2014; 2: 112–120.

[206] Singh H, Huls H, Kebriaei P, et al. A new approach to gene therapy using *Sleeping Beauty* to genetically modify clinical-grade T cells to target CD19. *Immunol Rev* 2014; 257: 181–190.

[207] Vormittag P, Gunn R, Ghorashian S, et al. A guide to manufacturing CAR T cell therapies. *Curr Opin Biotechnol* 2018; 53: 164–181.

[208] Ghassemi S, Nunez-Cruz S, O'Connor RS, et al. Reducing Ex Vivo Culture Improves the Antileukemic Activity of Chimeric Antigen Receptor (CAR) T Cells. *Cancer Immunol Res* 2018; 6: 1100–1109.

[209] Ghassemi S, Durgin JS, Nunez-Cruz S, et al. Rapid manufacturing of non-activated potent CAR T cells. *Nat Biomed Eng* 2022; 6: 118–128.

[210] Turtle CJ, Hanafi LA, Berger C, et al. CD19 CAR-T cells of defined CD4+:CD8+ composition in adult B cell ALL patients. *J Clin Invest* 2016; 126: 2123–2138.

[211] Gattinoni L, Finkelstein SE, Klebanoff CA, et al. Removal of homeostatic cytokine sinks by lymphodepletion enhances the efficacy of adoptively transferred tumor-specific CD8+ T cells. 202. Epub ahead of print 2005. DOI: 10.1084/jem.20050732.

[212] Klebanoff CA, Khong HT, Antony PA, et al. Sinks, suppressors and antigen presenters: how lymphodepletion enhances T cell-mediated tumor immunotherapy. 26. Epub ahead of print 2005. DOI: 10.1016/j.it.2004.12.003.

[213] Chernysheva AD, Kirou KA, Crow MK. T Cell Proliferation Induced by Autologous Non-T Cells Is a Response to Apoptotic Cells Processed by Dendritic Cells. *The Journal of Immunology* 2002; 169: 1241–1250.

[214] Zhang Y, Louboutin J-P, Zhu J, et al. Preterminal host dendritic cells in irradiated mice prime CD8+ T cell–mediated acute graft-versus-host disease. *Journal of Clinical Investigation* 2002; 109: 1335–1344.

[215] Schuster SJ, Svoboda J, Chong EA, et al. Chimeric Antigen Receptor T Cells in Refractory B-Cell Lymphomas. *N Engl J Med* 2017; 377: 2545–2554.

[216] Shimabukuro-Vornhagen A, Godel P, Subklewe M, et al. Cytokine release syndrome. *J Immunother Cancer* 2018; 6: 56.

[217] Grupp SA, Kalos M, Barrett D, et al. Chimeric antigen receptor-modified T cells for acute lymphoid leukemia. *N Engl J Med* 2013; 368: 1509–1518.

[218] Kochenderfer JN, Dudley ME, Carpenter RO, et al. Donor-derived CD19-targeted T cells cause regression of malignancy persisting after allogeneic hematopoietic stem cell transplantation. *Blood* 2013; 122: 4129–4139.

[219] Wong SW, Richard S, Lin Y, et al. Anakinra Targeting Cytokine Release Syndrome Associated with Chimeric Antigen Receptor T-Cell Therapies. *Blood* 2021; 138: 2812–2812.

[220] Porter DL, Hwang WT, Frey N v, et al. Chimeric antigen receptor T cells persist and induce sustained remissions in relapsed refractory chronic lymphocytic leukemia. 7. Epub ahead of print 2015. DOI: 10.1126/scitranslmed.aac5415.

[221] Kochenderfer JN, Dudley ME, Kassim SH, et al. Chemotherapy-refractory diffuse large B-cell lymphoma and indolent B-cell malignancies can be effectively treated with autologous T cells expressing an anti-CD19 chimeric antigen receptor. 33. Epub ahead of print 2015. DOI: 10.1200/jco.2014.56.2025.

[222] Maude SL, Frey N, Shaw PA, et al. Chimeric antigen receptor T cells for sustained remissions in leukemia. *N Engl J Med* 2014; 371: 1507–1517.

[223] Morris EC, Neelapu SS, Giavridis T, et al. Cytokine release syndrome and associated neurotoxicity in cancer immunotherapy. *Nat Rev Immunol* 2022; 22: 85–96.

[224] Kochenderfer JN, Dudley ME, Feldman SA, et al. B-cell depletion and remissions of malignancy along with cytokine-associated toxicity in a clinical trial of anti-CD19 chimeric-antigen-receptor-transduced T cells. 119. Epub ahead of print 2012. DOI: 10.1182/blood-2011-10-384388.

[225] Kochenderfer JN, Wilson WH, Janik JE, et al. Eradication of B-lineage cells and regression of lymphoma in a patient treated with autologous T cells genetically engineered to recognize CD19. *Blood* 2010; 116: 4099–4102.

[226] Morgan RA, Yang JC, Kitano M, et al. Case report of a serious adverse event following the administration of T cells transduced with a chimeric antigen receptor recognizing ERBB2. *Mol Ther* 2010; 18: 843–851.

[227] Cambridge Protein Arrays. About HuProt, https://cambridgeproteinarrays.com/about-huprot.php (2023, accessed 12 April 2023).

[228] Freeth J, Soden J. New Advances in Cell Microarray Technology to Expand Applications in Target Deconvolution and Off-Target Screening. *SLAS Discovery* 2020; 25: 223–230.

[229] Charles River. Retrogenix Cell Microarray Technology , https://www.criver.com/products-services/discovery-services/screening-and-profiling-assays/retrogenix-cell-microarray-technology?region=3696 (2023, accessed 12 April 2023).

[230] Integral Molecular. Membrane Proteome Array (MPA), https://www.integralmolecular.com/membrane-proteome-array/ (2023, accessed 12 April 2023).

[231] Linette GP, Stadtmauer EA, Maus M v, et al. Cardiovascular toxicity and titin cross-reactivity of affinity-enhanced T cells in myeloma and melanoma. *Blood* 2013; 122: 863–871.

[232] Martin AD, Wang X, Sandberg ML, et al. Re-examination of MAGE-A3 as a T-cell Therapeutic Target. *Journal of Immunotherapy* 2021; 44: 95–105.

[233] Lu Y-C, Parker LL, Lu T, et al. Treatment of Patients With Metastatic Cancer Using a Major Histocompatibility Complex Class II-Restricted T-Cell Receptor Targeting the Cancer Germline Antigen MAGE-A3. *J Clin Oncol* 2017; 35: 3322–3329.

[234] Milone MC, O'Doherty U. Clinical use of lentiviral vectors. *Leukemia* 2018; 32: 1529–1541.

[235] Dull T, Zufferey R, Kelly M, et al. A Third-Generation Lentivirus Vector with a Conditional Packaging System. *J Virol* 1998; 72: 8463–8471.

[236] Zufferey R, Dull T, Mandel RJ, et al. Self-Inactivating Lentivirus Vector for Safe and Efficient In Vivo Gene Delivery. *J Virol* 1998; 72: 9873–9880.

[237] Donahue RE, Kessler SW, Bodine D, et al. Helper virus induced T cell lymphoma in nonhuman primates after retroviral mediated gene transfer. *Journal of Experimental Medicine* 1992; 176: 1125–1135.

[238] Hacein-Bey-Abina S, Hauer J, Lim A, et al. Efficacy of Gene Therapy for X-Linked Severe Combined Immunodeficiency. *N Engl J Med* 2010; 363: 355–364.

[239] Wu X, Li Y, Crise B, et al. Transcription Start Regions in the Human Genome Are Favored Targets for MLV Integration. *Science (1979)* 2003; 300: 1749–1751.

[240] Schröder ARW, Shinn P, Chen H, et al. HIV-1 Integration in the Human Genome Favors Active Genes and Local Hotspots. *Cell* 2002; 110: 521–529.

[241] Shah NN, Qin H, Yates B, et al. Clonal expansion of CAR T cells harboring lentivector integration in the CBL gene following anti-CD22 CAR T-cell therapy. *Blood Adv* 2019; 3: 2317–2322.

[242] Brown KF, Rumgay H, Dunlop C, et al. The fraction of cancer attributable to modifiable risk factors in England, Wales, Scotland, Northern Ireland, and the United Kingdom in 2015. *Br J Cancer* 2018; 118: 1130–1141.

[243] Boniol M, Autier P, Boyle P, et al. Cutaneous melanoma attributable to sunbed use: systematic review and meta-analysis. *BMJ* 2012; 345: e4757–e4757.

[244] Cogliano VJ, Baan R, Straif K, et al. Preventable Exposures Associated With Human Cancers. *JNCI Journal of the National Cancer Institute* 2011; 103: 1827–1839.

[245] Guo W, Wang H, Li C. Signal pathways of melanoma and targeted therapy. *Signal Transduct Target Ther* 2021; 6: 424.

[246] Davies H, Bignell GR, Cox C, et al. Mutations of the BRAF gene in human cancer. *Nature* 2002; 417: 949–954.

[247] Prior IA, Lewis PD, Mattos C. A Comprehensive Survey of Ras Mutations in Cancer. *Cancer Res* 2012; 72: 2457–2467.

[248] Maertens O, Johnson B, Hollstein P, et al. Elucidating Distinct Roles for NF1 in Melanomagenesis. *Cancer Discov* 2013; 3: 338–349.

[249] Miller AJ, Mihm MC. Melanoma. *New England Journal of Medicine* 2006; 355: 51–65.

[250] Clark WH, Elder DE, Guerry D, et al. A study of tumor progression: The precursor lesions of superficial spreading and nodular melanoma. *Hum Pathol* 1984; 15: 1147–1165.

[251] Cancer Research UK. Melanoma Skin Cancer Survival Statistics .

[252] Cancer Research UK. Melanoma Skin Cancer Incidence Statistics, https://www.cancerresearchuk.org/health-professional/cancer-statistics/statistics-by-cancer-type/melanoma-skin-cancer#heading-Zero (2019, accessed 10 January 2023).

[253] Merhavi-Shoham E, Itzhaki O, Markel G, et al. Adoptive Cell Therapy for Metastatic Melanoma. *Cancer J* 2017; 23: 48–53.

[254] Wu MR, Zhang T, Alcon A, et al. DNAM-1-based chimeric antigen receptors enhance T cell effector function and exhibit in vivo efficacy against melanoma. *Cancer Immunol Immunother* 2015; 64: 409–418.

[255] Zhang G, Wang L, Cui H, et al. Anti-melanoma activity of T cells redirected with a TCR-like chimeric antigen receptor. *Sci Rep* 2014; 4: 3571.

[256] Burns WR, Zhao Y, Frankel TL, et al. A high molecular weight melanoma-associated antigen-specific chimeric antigen receptor redirects lymphocytes to target human melanomas. *Cancer Res* 2010; 70: 3027–3033.

[257] Lehmann JM, Holzmann B, Breitbart EW, et al. Discrimination between benign and malignant cells of melanocytic lineage by two novel antigens, a glycoprotein

with a molecular weight of 113,000 and a protein with a molecular weight of 76,000. *Cancer Res* 1987; 47: 841–845.

[258] Kersey PJ, Allen JE, Allot A, et al. Ensembl Genomes 2018: an integrated omics infrastructure for non-vertebrate species. *Nucleic Acids Res* 2018; 46: D802–D808.

[259] Kuske MD, Johnson JP. Assignment of the human melanoma cell adhesion molecule gene (MCAM) to chromosome 11 band q23.3 by radiation hybrid mapping. *Cytogenet Cell Genet* 1999; 87: 258.

[260] Sers C, Kirsch K, Rothbacher U, et al. Genomic organization of the melanoma-associated glycoprotein MUC18: implications for the evolution of the immunoglobulin domains. *Proc Natl Acad Sci U S A* 1993; 90: 8514–8518.

[261] Kohama K, Tsukamoto Y, Furuya M, et al. Molecular cloning and analysis of the mouse gicerin gene. *Neurochem Int* 2005; 46: 465–470.

[262] Lehmann JM, Riethmuller G, Johnson JP. MUC18, a marker of tumor progression in human melanoma, shows sequence similarity to the neural cell adhesion molecules of the immunoglobulin superfamily. *Proc Natl Acad Sci U S A* 1989; 86: 9891–9895.

[263] Shih IM, Elder DE, Speicher D, et al. Isolation and functional characterization of the A32 melanoma-associated antigen. *Cancer Res* 1994; 54: 2514–2520.

[264] Zheng C, Qiu Y, Zeng Q, et al. Endothelial CD146 is required for in vitro tumor-induced angiogenesis: the role of a disulfide bond in signaling and dimerization. *Int J Biochem Cell Biol* 2009; 41: 2163–2172.

[265] Sers C, Riethmuller G, Johnson JP. MUC18, a melanoma-progression associated molecule, and its potential role in tumor vascularization and hematogenous spread. *Cancer Res* 1994; 54: 5689–5694.

[266] Jiang T, Zhuang J, Duan H, et al. CD146 is a coreceptor for VEGFR-2 in tumor angiogenesis. *Blood* 2012; 120: 2330–2339.

[267] Luo Y, Zheng C, Zhang J, et al. Recognition of CD146 as an ERM-binding protein offers novel mechanisms for melanoma cell migration. *Oncogene* 2012; 31: 306–321.

[268] Xu W, Hua H, Chiu Y-H, et al. CD146 Regulates Growth Factor-Induced mTORC2 Activity Independent of the PI3K and mTORC1 Pathways. *Cell Rep* 2019; 29: 1311-1322.e5.

[269] Guezguez B, Vigneron P, Alais S, et al. A dileucine motif targets MCAM-l cell adhesion molecule to the basolateral membrane in MDCK cells. *FEBS Lett* 2006; 580: 3649–3656.

[270] Bardin N, Frances V, Combes V, et al. CD146: biosynthesis and production of a soluble form in human cultured endothelial cells. *FEBS Lett* 1998; 421: 12–14.

[271] Boneberg EM, Illges H, Legler DF, et al. Soluble CD146 is generated by ectodomain shedding of membrane CD146 in a calcium-induced, matrix metalloprotease-dependent process. *Microvasc Res* 2009; 78: 325–331.

[272] Stalin J, Nollet M, Garigue P, et al. Targeting soluble CD146 with a neutralizing antibody inhibits vascularization, growth and survival of CD146-positive tumors. *Nature Publishing Group* 2016; 35: 5489–5500.

[273] Bardin N, Moal V, Anfosso F, et al. Soluble CD146, a novel endothelial marker, is increased in physiopathological settings linked to endothelial junctional alteration. *Thromb Haemost* 2003; 90: 915–920.

[274] Meijers WC, Bayes-Genis A, Mebazaa A, et al. Circulating heart failure biomarkers beyond natriuretic peptides: review from the Biomarker Study Group of the Heart Failure Association. *Eur J Heart Fail* 2021; 23: 1610–1632.

[275] Abu El-Asrar AM, Nawaz MI, Ahmad A, et al. CD146/Soluble CD146 Pathway Is a Novel Biomarker of Angiogenesis and Inflammation in Proliferative Diabetic Retinopathy. *Investigative Opthalmology & Visual Science* 2021; 62: 32.

[276] Stalin J, Traboulsi W, Vivancos-Stalin L, et al. Therapeutic targeting of soluble CD146/MCAM with the M2J-1 monoclonal antibody prevents metastasis

development and procoagulant activity in CD146-positive invasive tumors. *Int J Cancer*. Epub ahead of print 22 February 2020. DOI: 10.1002/ijc.32909.

[277] Wu G-J, Wu M-WH, Wang S-W, et al. Isolation and characterization of the major form of human MUC18 cDNA gene and correlation of MUC18 over-expression in prostate cancer cell lines and tissues with malignant progression. *Gene* 2001; 279: 17–31.

[278] Johnson JP, Rothbacher U, Sers C. The progression associated antigen MUC18: a unique member of the immunoglobulin supergene family. *Melanoma Res* 1993; 3: 337–340.

[279] Chan B, Sinha S, Cho D, et al. Critical roles of CD146 in zebrafish vascular development. *Dev Dyn* 2005; 232: 232–244.

[280] Leroyer AS, Blin MG, Bachelier R, et al. CD146 (Cluster of Differentiation 146). *Arterioscler Thromb Vasc Biol* 2019; 39: 1026–1033.

[281] Shih IM, Elder DE, Hsu MY, et al. Regulation of Mel-CAM/MUC18 expression on melanocytes of different stages of tumor progression by normal keratinocytes. *Am J Pathol* 1994; 145: 837–845.

[282] Dudzik P, Trojan SE, Ostrowska B, et al. Aberrant promoter methylation may be responsible for the control of CD146 (MCAM) gene expression during breast cancer progression. *Acta Biochim Pol*. Epub ahead of print 11 December 2019. DOI: 10.18388/abp.2019_2907.

[283] Li X, Wang Y, Zhang Y, et al. Overexpression of MCAM induced by SMYD2-H3K36me2 in breast cancer stem cell properties. *Breast Cancer* 2022; 29: 854–868.

[284] Mintz-Weber CS, Johnson JP. Identification of the elements regulating the expression of the cell adhesion molecule MCAM/MUC18. Loss of AP-2 is not required for MCAM expression in melanoma cell lines. *J Biol Chem* 2000; 275: 34672–34680.

[285] Sapio L, Salzillo A, Ragone A, et al. Targeting CREB in Cancer Therapy: A Key Candidate or One of Many? An Update. *Cancers (Basel)* 2020; 12: 3166.

[286] Mayr B, Montminy M. Transcriptional regulation by the phosphorylation-dependent factor CREB. *Nat Rev Mol Cell Biol* 2001; 2: 599–609.

[287] Rummel MM, Sers C, Johnson JP. Phorbol ester and cyclic AMP-mediated regulation of the melanoma-associated cell adhesion molecule MUC18/MCAM. *Cancer Res* 1996; 56: 2218–2223.

[288] Vizcaíno C, Mansilla S, Portugal J. Sp1 transcription factor: A long-standing target in cancer chemotherapy. *Pharmacol Ther* 2015; 152: 111–124.

[289] Chen J, Dang Y, Feng W, et al. SOX18 promotes gastric cancer metastasis through transactivating MCAM and CCL7. *Oncogene* 2020; 39: 5536–5552.

[290] Jean D, Gershenwald JE, Huang S, et al. Loss of AP-2 results in up-regulation of MCAM/MUC18 and an increase in tumor growth and metastasis of human melanoma cells. *J Biol Chem* 1998; 273: 16501–16508.

[291] Karjalainen JM, Kellokoski JK, Eskelinen MJ, et al. Downregulation of transcription factor AP-2 predicts poor survival in stage I cutaneous malignant melanoma. *Journal of Clinical Oncology* 1998; 16: 3584–3591.

[292] Bar-Eli M. Role of AP-2 in tumor growth and metastasis of human melanoma. *Cancer Metastasis Rev* 1999; 18: 377–385.

[293] McPherson LA, Loktev A v., Weigel RJ. Tumor Suppressor Activity of AP2α Mediated through a Direct Interaction with p53. *Journal of Biological Chemistry* 2002; 277: 45028–45033.

[294] Liu XS, Genet MD, Haines JE, et al. ZBTB7A Suppresses Melanoma Metastasis by Transcriptionally Repressing MCAM. *Mol Cancer Res* 2015; 13: 1206–1217.

[295] Wang P, Luo Y, Duan H, et al. MicroRNA 329 suppresses angiogenesis by targeting CD146. *Mol Cell Biol* 2013; 33: 3689–3699.

[296] Holzmann B, Brocker EB, Lehmann JM, et al. Tumor progression in human malignant melanoma: five stages defined by their antigenic phenotypes. *Int J Cancer* 1987; 39: 466–471.

[297] Liu WF, Ji SR, Sun JJ, et al. CD146 expression correlates with epithelial-mesenchymal transition markers and a poor prognosis in gastric cancer. *Int J Mol Sci* 2012; 13: 6399–6406.

[298] Zabouo G, Imbert AM, Jacquemier J, et al. CD146 expression is associated with a poor prognosis in human breast tumors and with enhanced motility in breast cancer cell lines. *Breast Cancer Res* 2009; 11: R1.

[299] Li C, Kang L, Fan K, et al. ImmunoPET of CD146 in Orthotopic and Metastatic Breast Cancer Models. *Bioconjug Chem* 2021; 32: 1306–1314.

[300] Ferreira CA, Kang L, Li C, et al. ImmunoPET of the differential expression of CD146 in breast cancer. *Am J Cancer Res* 2021; 11: 1586–1599.

[301] Wu Z, Wu Z, Li J, et al. MCAM is a novel metastasis marker and regulates spreading, apoptosis and invasion of ovarian cancer cells. *Tumour Biol* 2012; 33: 1619–1628.

[302] Thomann S, Longerich T, Bazhin A v, et al. Selective targeting of liver cancer with the endothelial marker CD146. *Oncotarget* 2014; 5: 8614–8624.

[303] Liu JW, Nagpal JK, Jeronimo C, et al. Hypermethylation of MCAM gene is associated with advanced tumor stage in prostate cancer. *Prostate* 2008; 68: 418–426.

[304] Bu P, Gao L, Zhuang J, et al. Anti-CD146 monoclonal antibody AA98 inhibits angiogenesis via suppression of nuclear factor-kappaB activation. *Mol Cancer Ther* 2006; 5: 2872–2878.

[305] Shih IM, Nesbit M, Herlyn M, et al. A new Mel-CAM (CD146)-specific monoclonal antibody, MN-4, on paraffin-embedded tissue. *Mod Pathol* 1998; 11: 1098–1106.

[306] Shih IM, Wang TL, Westra WH. Diagnostic and biological implications of mel-CAM expression in mesenchymal neoplasms. *Clin Cancer Res* 1996; 2: 569–575.

[307] Zhang Y, Lei X, He R, et al. Identification and preliminary validation of a four-gene signature to predict metastasis and survival in osteosarcoma. *Am J Transl Res* 2021; 13: 12264–12284.

[308] Pacifico MD, Grover R, Richman PI, et al. Development of a tissue array for primary melanoma with long-term follow-up: discovering melanoma cell adhesion molecule as an important prognostic marker. *Plast Reconstr Surg* 2005; 115: 367–375.

[309] Reid AL, Millward M, Pearce R, et al. Markers of circulating tumour cells in the peripheral blood of patients with melanoma correlate with disease recurrence and progression. *Br J Dermatol* 2013; 168: 85–92.

[310] Rapanotti MC, Bianchi L, Ricozzi I, et al. Melanoma-associated markers expression in blood: MUC-18 is associated with advanced stages in melanoma patients. *Br J Dermatol* 2009; 160: 338–344.

[311] de Kruijff I, Timmermans A, den Bakker M, et al. The Prevalence of CD146 Expression in Breast Cancer Subtypes and Its Relation to Outcome. *Cancers (Basel)* 2018; 10: 134.

[312] Onisim An, Vlad C, Simon I, et al. The role of CD146 in serous ovarian carcinoma. *JBUON* 2019; 24: 1009–1019.

[313] Dufies M, Nollet M, Ambrosetti D, et al. Soluble CD146 is a predictive marker of pejorative evolution and of sunitinib efficacy in clear cell renal cell carcinoma. *Theranostics* 2018; 8: 2447–2458.

[314] Du X, Zhang Q, Wang S, et al. MCAM is associated with metastasis and poor prognosis in osteosarcoma by modulating tumor cell migration. *J Clin Lab Anal*; 36. Epub ahead of print 27 February 2022. DOI: 10.1002/jcla.24214.

[315] Wang J, Wu Z, Zheng M, et al. CD146 is closely associated with the prognosis and molecular features of osteosarcoma: Guidance for personalized clinical

treatment. *Front Genet*; 13. Epub ahead of print 21 October 2022. DOI: 10.3389/fgene.2022.1025306.

[316] Joshkon A, Tabouret E, Traboulsi W, et al. Soluble CD146, a biomarker and a target for preventing resistance to anti-angiogenic therapy in glioblastoma. *Acta Neuropathol Commun* 2022; 10: 151.

[317] Zeng P, Li H, Lu P-H, et al. Prognostic value of CD146 in solid tumor: A Systematic Review and Meta-analysis. *Sci Rep* 2017; 7: 4223–4223.

[318] Pasquier E, Bardin N, Martin LD saint, et al. The first assessment of soluble CD146 in women with unexplained pregnancy loss. *Thromb Haemost* 2005; 94: 1280–1284.

[319] Liu Y-Y, Bin Y, Wang X, et al. Increased serum levels of soluble CD146 and vascular endothelial growth factor receptor 2 in patients with exudative age-related macular degeneration. *Int J Ophthalmol* 2019; 12: 457–463.

[320] Nollet M, Bachelier R, Joshkon A, et al. Involvement of Multiple Variants of Soluble CD146 in Systemic Sclerosis: Identification of a Novel Profibrotic Factor. *Arthritis & Rheumatology* 2022; 74: 1027–1038.

[321] George F, Poncelet P, Laurent JC, et al. Cytofluorometric detection of human endothelial cells in whole blood using S-Endo 1 monoclonal antibody. *J Immunol Methods* 1991; 139: 65–75.

[322] Kebir A, Harhouri K, Guillet B, et al. CD146 short isoform increases the proangiogenic potential of endothelial progenitor cells in vitro and in vivo. *Circ Res* 2010; 107: 66–75.

[323] Bardin N, Frances V, Lesaule G, et al. Identification of the S-Endo 1 endothelial-associated antigen. *Biochem Biophys Res Commun* 1996; 218: 210–216.

[324] Bardin N, Anfosso F, Masse JM, et al. Identification of CD146 as a component of the endothelial junction involved in the control of cell-cell cohesion. *Blood* 2001; 98: 3677–3684.

[325] Solovey AN, Gui L, Chang L, et al. Identification and functional assessment of endothelial P1H12. *Journal of Laboratory and Clinical Medicine* 2001; 138: 322–331.

[326] Anfosso F, Bardin N, Vivier E, et al. Outside-in signaling pathway linked to CD146 engagement in human endothelial cells. *J Biol Chem* 2001; 276: 1564–1569.

[327] Shih IM, Kurman RJ. Expression of melanoma cell adhesion molecule in intermediate trophoblast. *Lab Invest* 1996; 75: 377–388.

[328] Dagur PK, Tatlici G, Gourley M, et al. CD146+ T lymphocytes are increased in both the peripheral circulation and in the synovial effusions of patients with various musculoskeletal diseases and display pro-inflammatory gene profiles. *Cytometry B Clin Cytom* 2010; 78: 88–95.

[329] Elshal MF, Khan SS, Raghavachari N, et al. A unique population of effector memory lymphocytes identified by CD146 having a distinct immunophenotypic and genomic profile. Epub ahead of print 2007. DOI: 10.1186/1471-2172-8-29.

[330] Elshal MF, Khan SS, Takahashi Y, et al. CD146 (Mel-CAM), an adhesion marker of endothelial cells, is a novel marker of lymphocyte subset activation in normal peripheral blood. *Blood* 2005; 106: 2923–2924.

[331] Larochelle C, Cayrol R, Kebir H, et al. Melanoma cell adhesion molecule identifies encephalitogenic T lymphocytes and promotes their recruitment to the central nervous system. *Brain* 2012; 135: 2906–2924.

[332] Dagur PK, Biancotto A, Stansky E, et al. Secretion of Interleukin-17 by CD8+ T Cells Expressing CD146 (MCAM). DOI: 10.1016/j.clim.2014.01.009.

[333] Dagur PK, Biancotto A, Wei L, et al. MCAM-expressing CD4 + T cells in Peripheral Blood Secrete IL-17A and are Significantly Elevated in Inflammatory Autoimmune Diseases. *National Institutes of Health* 2011; 37: 319–327.

[334] Hadjinicolaou A v, Wu L, Fang B, et al. Relationship of CD146 expression to activation of circulating T cells: exploratory studies in healthy donors and

patients with connective tissue diseases. Epub ahead of print 2013. DOI: 10.1111/cei.12151.

[335] Ikeguchi R, Shimizu Y, Kondo A, et al. Melanoma Cell Adhesion Molecule Expressing Helper T Cells in CNS Inflammatory Demyelinating Diseases. Epub ahead of print 2021. DOI: 10.1212/NXI.0000000000001069.

[336] Raychaudhuri SK, Abria C, Siba ·, et al. Phenotype and pathological significance of MCAM + (CD146 +) T cell subset in psoriatic arthritis. 2021; 48: 6787–6796.

[337] Kamiyama T, Watanabe H, Iijima M, et al. Coexpression of CCR6 and CD146 (MCAM) is a marker of effector memory T-helper 17 cells. *J Dermatol* 2012; 39: 838–842.

[338] Wu C, Goodall † J C, Busch R, et al. Relationship of CD146 expression to secretion of interleukin (IL)-17, IL-22 and interferon-γ by CD4 + T cells in patients with inflammatory arthritis. Epub ahead of print 2014. DOI: 10.1111/cei.12434.

[339] Seftalioglu A, Karakoc L. Expression of CD146 adhesion molecules (MUC18 or MCAM) in the thymic microenvironment. *Acta Histochem* 2000; 102: 69–83.

[340] Duan H, Jing L, Jiang X, et al. CD146 bound to LCK promotes T cell receptor signaling and antitumor immune responses in mice. *Journal of Clinical Investigation*; 131. Epub ahead of print 1 November 2021. DOI: 10.1172/JCI148568.

[341] Brucklacher-Waldert V, Stuerner K, Kolster M, et al. Phenotypical and functional characterization of T helper 17 cells in multiple sclerosis. *Brain* 2009; 132: 3329–3341.

[342] Pickl WF, Majdic O, Fischer GF, et al. MUC18/MCAM (CD146), an activation antigen of human T lymphocytes. *J Immunol* 1997; 158: 2107–2115.

[343] Mehta NN, Dagur PK, Rose SM, et al. IL-17A Production in Human Psoriatic Blood and Lesions by CD146+ T Cells. *Journal of Investigative Dermatology* 2015; 135: 311–314.

[344] Xie S, Luca M, Huang S, et al. Expression of MCAM/MUC18 by human melanoma cells leads to increased tumor growth and metastasis. *Cancer Res* 1997; 57: 2295–2303.

[345] Wu GJ. Ectopic expression of MCAM/MUC18 increases in vitro motility and invasiveness, but decreases in vivo tumorigenesis and metastasis of a mouse melanoma K1735-9 subline in a syngeneic mouse model. *Clin Exp Metastasis* 2016; 33: 817–828.

[346] Imbert AM, Garulli C, Choquet E, et al. CD146 expression in human breast cancer cell lines induces phenotypic and functional changes observed in Epithelial to Mesenchymal Transition. *PLoS One* 2012; 7: e43752.

[347] Wu GJ, Fu P, Wang SW, et al. Enforced expression of MCAM/MUC18 increases in vitro motility and invasiveness and in vivo metastasis of two mouse melanoma K1735 sublines in a syngeneic mouse model. *Mol Cancer Res* 2008; 6: 1666–1677.

[348] Kang Y, Wang F, Feng J, et al. Knockdown of CD146 reduces the migration and proliferation of human endothelial cells. *Cell Res* 2006; 16: 313–318.

[349] Heerboth S, Housman G, Leary M, et al. EMT and tumor metastasis. *Clin Transl Med* 2015; 4: 6.

[350] Satyamoorthy K, Muyrers J, Meier F, et al. Mel-CAM-specific genetic suppressor elements inhibit melanoma growth and invasion through loss of gap junctional communication. *Oncogene* 2001; 20: 4676–4684.

[351] Schlagbauer-Wadl H, Jansen B, Muller M, et al. Influence of MUC18/MCAM/CD146 expression on human melanoma growth and metastasis in SCID mice. *Int J Cancer* 1999; 81: 951–955.

[352] Prosen L, Markelc B, Dolinsek T, et al. Mcam Silencing With RNA Interference Using Magnetofection has Antitumor Effect in Murine Melanoma. *Mol Ther Nucleic Acids* 2014; 3: e205.

[353] Shih LM, Hsu MY, Palazzo JP, et al. The cell-cell adhesion receptor Mel-CAM acts as a tumor suppressor in breast carcinoma. *Am J Pathol* 1997; 151: 745–751.

[354] So JH, Hong SK, Kim HT, et al. Gicerin/Cd146 is involved in zebrafish cardiovascular development and tumor angiogenesis. *Genes Cells* 2010; 15: 1099–1110.

[355] Yan X, Lin Y, Yang D, et al. A novel anti-CD146 monoclonal antibody, AA98, inhibits angiogenesis and tumor growth. *Blood* 2003; 102: 184–191.

[356] Wang Z, Xu Q, Zhang N, et al. CD146, from a melanoma cell adhesion molecule to a signaling receptor. *Signal Transduction and Targeted Therapy 2020 5:1* 2020; 5: 1–15.

[357] Johnson JP, Bar-Eli M, Jansen B, et al. Melanoma progression-associated glycoprotein MUC18/MCAM mediates homotypic cell adhesion through interaction with a heterophilic ligand. *Int J Cancer* 1997; 73: 769–774.

[358] Domogatskaya A, Rodin S, Tryggvason K. Functional Diversity of Laminins. *Annu Rev Cell Dev Biol* 2012; 28: 523–553.

[359] Saito N, Hamada J, Furukawa H, et al. Laminin-421 produced by lymphatic endothelial cells induces chemotaxis for human melanoma cells. *Pigment Cell Melanoma Res* 2009; 22: 601–610.

[360] Graf F, Horn P, Ho AD, et al. The extracellular matrix proteins type I collagen, type III collagen, fibronectin, and laminin 421 stimulate migration of cancer cells. *The FASEB Journal*; 35. Epub ahead of print 12 July 2021. DOI: 10.1096/fj.202002558RR.

[361] Ishikawa T, Wondimu Z, Oikawa Y, et al. Monoclonal antibodies to human laminin α4 chain globular domain inhibit tumor cell adhesion and migration on laminins 411 and 421, and binding of α6β1 integrin and MCAM to α4-laminins. *Matrix Biology* 2014; 36: 5–14.

[362] Ishikawa T, Wondimu Z, Oikawa Y, et al. Laminins 411 and 421 differentially promote tumor cell migration via α6β1 integrin and MCAM (CD146). *Matrix Biology* 2014; 38: 69–83.

[363] Flanagan K, Fitzgerald K, Baker J, et al. Laminin-411 is a vascular ligand for MCAM and facilitates TH17 cell entry into the CNS. *PLoS One* 2012; 7: e40443–e40443.

[364] Ebrahim AH, Alalawi Z, Mirandola L, et al. Galectins in cancer: carcinogenesis, diagnosis and therapy. *Ann Transl Med* 2014; 2: 88.

[365] Thijssen VL, Heusschen R, Caers J, et al. Galectin expression in cancer diagnosis and prognosis: A systematic review. *Biochimica et Biophysica Acta (BBA) - Reviews on Cancer* 2015; 1855: 235–247.

[366] Jouve N, Despoix N, Espeli M, et al. The involvement of CD146 and its novel ligand Galectin-1 in apoptotic regulation of endothelial cells. *J Biol Chem* 2013; 288: 2571–2579.

[367] Yazawa EM, Geddes-Sweeney JE, Cedeno-Laurent F, et al. Melanoma Cell Galectin-1 Ligands Functionally Correlate with Malignant Potential. *Journal of Investigative Dermatology* 2015; 135: 1849–1862.

[368] Colomb F, Wang W, Simpson D, et al. Galectin-3 interacts with the cell-surface glycoprotein CD146 (MCAM, MUC18) and induces secretion of metastasis-promoting cytokines from vascular endothelial cells. *Journal of Biological Chemistry* 2017; 292: 8381–8389.

[369] Pang Y, Maxwell E, Sindrewicz-Goral P, et al. Galectin-3 Is a Natural Binding Ligand of MCAM (CD146, MUC18) in Melanoma Cells and Their Interaction Promotes Melanoma Progression. *Biomolecules* 2022; 12: 1451.

[370] Bresnick AR, Weber DJ, Zimmer DB. S100 proteins in cancer. *Nat Rev Cancer* 2015; 15: 96–109.

[371] Ruma IMW, Putranto EW, Kondo E, et al. MCAM, as a novel receptor for S100A8/A9, mediates progression of malignant melanoma through prominent

activation of NF-κB and ROS formation upon ligand binding. *Clin Exp Metastasis* 2016; 33: 609–627.

[372] Chen Y, Sumardika IW, Tomonobu N, et al. Melanoma cell adhesion molecule is the driving force behind the dissemination of melanoma upon S100A8/A9 binding in the original skin lesion. *Cancer Lett* 2019; 452: 178–190.

[373] Fife CM, McCarroll JA, Kavallaris M. Movers and shakers: cell cytoskeleton in cancer metastasis. *Br J Pharmacol* 2014; 171: 5507–5523.

[374] Lamouille S, Xu J, Derynck R. Molecular mechanisms of epithelial–mesenchymal transition. *Nat Rev Mol Cell Biol* 2014; 15: 178–196.

[375] Anfosso F, Bardin N, Frances V, et al. Activation of human endothelial cells via S-endo-1 antigen (CD146) stimulates the tyrosine phosphorylation of focal adhesion kinase p125(FAK). *J Biol Chem* 1998; 273: 26852–26856.

[376] Ye Z, Zhang C, Tu T, et al. Wnt5a uses CD146 as a receptor to regulate cell motility and convergent extension. *Nat Commun* 2013; 4: 2803.

[377] Yan H, Zhang C, Wang Z, et al. CD146 is required for VEGF-C-induced lymphatic sprouting during lymphangiogenesis. *Sci Rep* 2017; 7: 7442.

[378] Stalin J, Harhouri K, Hubert L, et al. Soluble Melanoma Cell Adhesion Molecule (sMCAM/sCD146) Promotes Angiogenic Effects on Endothelial Progenitor Cells through Angiomotin. Epub ahead of print 2013. DOI: 10.1074/jbc.M112.446518.

[379] Stalin J, Nollet M, Dignat-George F, et al. Therapeutic and Diagnostic Antibodies to CD146: Thirty Years of Research on Its Potential for Detection and Treatment of Tumors. *Antibodies*; 6. Epub ahead of print 2017. DOI: 10.3390/antib6040017.

[380] Mills L, Tellez C, Huang S, et al. Fully human antibodies to MCAM/MUC18 inhibit tumor growth and metastasis of human melanoma. *Cancer Res* 2002; 62: 5106–5114.

[381] McGary EC, Heimberger A, Mills L, et al. A fully human antimelanoma cellular adhesion molecule/MUC18 antibody inhibits spontaneous pulmonary metastasis of osteosarcoma cells in vivo. *Clin Cancer Res* 2003; 9: 6560–6566.

[382] Chen X, Yan H, Liu D, et al. Structure basis for AA98 inhibition on the activation of endothelial cells mediated by CD146. *iScience* 2021; 24: 102417.

[383] Zhang R, Chen X, Chen S, et al. Inhibition of CD146 lessens uveal melanoma progression through reducing angiogenesis and vasculogenic mimicry. *Cellular Oncology* 2022; 45: 557–572.

[384] Nollet M, Stalin J, Moyon A, et al. A novel anti-CD146 antibody specifically targets cancer cells by internalizing the molecule. *Oncotarget* 2017; 8: 112283–112296.

[385] Zoni E, Astrologo L, Ng CKY, et al. Therapeutic Targeting of CD146/MCAM Reduces Bone Metastasis in Prostate Cancer. *Molecular Cancer Research* 2019; 17: 1049–1062.

[386] Prothena Reports Results from Phase 1b Multiple Ascending Dose Study of PRX003 in Patients with Psoriasis Nasdaq:PRTA.

[387] Prothena Reports Results of Phase 1 Single Ascending Dose Study of PRX003, Demonstrating Target Engagement of the Novel Anti-MCAM Antibody for Inflammatory Diseases | Prothena Corporation plc.

[388] Ogawa M, Takakura H. Photoimmunotherapy: A new cancer treatment using photochemical reactions. *Bioorg Med Chem* 2021; 43: 116274.

[389] Wei W, Jiang D, Ehlerding EB, et al. CD146-Targeted Multimodal Image-Guided Photoimmunotherapy of Melanoma. *Advanced Science* 2019; 6: 1801237.

[390] Leslie MC, Zhao YJ, Lachman LB, et al. Immunization against MUC18/MCAM, a novel antigen that drives melanoma invasion and metastasis. *Gene Ther* 2007; 14: 316–323.

[391] Schrage A, Loddenkemper C, Erben U, et al. Murine CD146 is widely expressed on endothelial cells and is recognized by the monoclonal antibody ME-9F1. *Histochem Cell Biol* 2008; 129: 441–451.

[392] National Cancer Institute (NCI). CAR T Cell Receptor Immunotherapy Targeting VEGFR2 for Patients With Metastatic Cancer. Trial identifier: NCT01218867.

ClinicalTrials.Gov, https://clinicaltrials.gov/ct2/show/results/NCT01218867 (accessed 18 January 2023).

[393] Feng K, Guo Y, Dai H, et al. Chimeric antigen receptor-modified T cells for the immunotherapy of patients with EGFR-expressing advanced relapsed/refractory non-small cell lung cancer. *Sci China Life Sci* 2016; 59: 468–479.

[394] Liu Y, Guo Y, Wu Z, et al. Anti-EGFR chimeric antigen receptor-modified T cells in metastatic pancreatic carcinoma: A phase I clinical trial. *Cytotherapy* 2020; 22: 573–580.

[395] Schindelin J, Arganda-Carreras I, Frise E, et al. Fiji: an open-source platform for biological-image analysis. *Nat Methods* 2012; 9: 676–682.

[396] Gilles Carpentier. Angiogenesis Analyzer for ImageJ. *Gilles Carpentier Research Web Site: Computer Image Analysis* , http://image.bio.methods.free.fr/ImageJ/?Angiogenesis-Analyzer-for-ImageJ&lang=en#outil_sommaire_0 (2012, accessed 10 January 2023).

[397] Lister JA, Robertson CP, Lepage T, et al. nacre encodes a zebrafish microphthalmia-related protein that regulates neural-crest-derived pigment cell fate. *Development* 1999; 126: 3757–3767.

[398] Schneider U, Schwenk H -U, Bornkamm G. Characterization of EBV-genome negative “null” and “T” cell lines derived from children with acute lymphoblastic leukemia and leukemic transformed non-Hodgkin lymphoma. *Int J Cancer* 1977; 19: 621–626.

[399] Weiss A, Stobo JD. Requirement for the coexpression of T3 and the T cell antigen receptor on a malignant human T cell line. *Journal of Experimental Medicine* 1984; 160: 1284–1299.

[400] Ohashi PS, Mak TW, van den Elsen P, et al. Reconstitution of an active surface T3/T-cell antigen receptor by DNA transfer. *Nature* 1985; 316: 606–609.

[401] Giacomini CP, Sun S, Varma S, et al. Breakpoint Analysis of Transcriptional and Genomic Profiles Uncovers Novel Gene Fusions Spanning Multiple Human Cancer Types. *PLoS Genet* 2013; 9: 1003464.

[402] Freeburn RW, Wright KL, Burgess SJ, et al. Evidence that SHIP-1 contributes to phosphatidylinositol 3,4,5-trisphosphate metabolism in T lymphocytes and can regulate novel phosphoinositide 3-kinase effectors. *J Immunol* 2002; 169: 5441–50.

[403] Shan X, Czar MJ, Bunnell SC, et al. Deficiency of PTEN in Jurkat T Cells Causes Constitutive Localization of Itk to the Plasma Membrane and Hyperresponsiveness to CD3 Stimulation. *Mol Cell Biol* 2000; 20: 6945–6957.

[404] Astoul E, Cantrell DA, Edmunds C, et al. PI 3-K and T-cell activation: Limitations of T-leukemic cell lines as signaling models. *Trends Immunol* 2001; 22: 490–496.

[405] Bloemberg D, Nguyen T, MacLean S, et al. A High-Throughput Method for Characterizing Novel Chimeric Antigen Receptors in Jurkat Cells. *Mol Ther Methods Clin Dev*. Epub ahead of print 2020. DOI: 10.1016/j.omtm.2020.01.012.

[406] Duong CPM, Westwood JA, Yong CSM, et al. Engineering T cell function using chimeric antigen receptors identified using a DNA library approach. *PLoS One* 2013; 8: e63037–e63037.

[407] Vairy S, Garcia JL, Teira P, et al. CTL019 (Tisagenlecleucel): CAR-T therapy for relapsed and refractory B-cell acute lymphoblastic leukemia. *Drug Design, Development and Therapy* 2018; 12: 3885–3898.

[408] Grupp SA, Frey N v., Aplenc R, et al. T Cells Engineered With a Chimeric Antigen Receptor (CAR) Targeting CD19 (CTL019) Produce Significant In Vivo Proliferation, Complete Responses and Long-Term Persistence Without Gvhd In Children and Adults With Relapsed, Refractory ALL. *Blood* 2013; 122: 67–67.

[409] Locke FL, Neelapu SS, Bartlett NL, et al. Phase 1 Results of ZUMA-1: A Multicenter Study of KTE-C19 Anti-CD19 CAR T Cell Therapy in Refractory Aggressive Lymphoma. *Molecular Therapy* 2017; 25: 285–295.

[410] Locke FL, Ghobadi A, Jacobson CA, et al. Long-term safety and activity of axicabtagene ciloleucel in refractory large B-cell lymphoma (ZUMA-1): a single-arm, multicentre, phase 1–2 trial. *Lancet Oncol* 2019; 20: 31–42.

[411] Iacoboni G, Rejeski K, Villacampa G, et al. Real-world evidence of brexucabtagene autoleucel for the treatment of relapsed or refractory mantle cell lymphoma. Epub ahead of print 2022. DOI: 10.1182/bloodadvances.2021006922.

[412] Abramson JS, Palomba ML, Gordon LI, et al. Lisocabtagene maraleucel for patients with relapsed or refractory large B-cell lymphomas (TRANSCEND NHL 001): a multicentre seamless design study. *The Lancet* 2020; 396: 839–852.

[413] Munshi NC, Anderson LD, Shah N, et al. Idecabtagene Vicleucel in Relapsed and Refractory Multiple Myeloma. *New England Journal of Medicine* 2021; 384: 705–716.

[414] Berdeja JG, Madduri D, Usmani SZ, et al. Ciltacabtagene autoleucel, a B-cell maturation antigen-directed chimeric antigen receptor T-cell therapy in patients with relapsed or refractory multiple myeloma (CARTITUDE-1): a phase 1b/2 open-label study. *The Lancet* 2021; 398: 314–324.

[415] Nolan Lab. The Phoenix System. *University of Stanford*, https://web.stanford.edu/group/nolan/_OldWebsite/tutorials/retpkg_7_phx_sys.html (accessed 15 August 2022).

[416] Rein A. Murine Leukemia Viruses: Objects and Organisms. *Adv Virol* 2011; 2011: 14.

[417] Cheadle EJ, Gilham DE, Hawkins RE. The combination of cyclophosphamide and human T cells genetically engineered to target CD19 can eradicate established B-cell lymphoma. *Br J Haematol*. Epub ahead of print 2008. DOI: 10.1111/j.1365-2141.2008.07145.x.

[418] Cheadle EJ, Hawkins RE, Batha H, et al. Eradication of Established B-cell Lymphoma by CD19-specific Murine T Cells is Dependent on Host Lymphopenic

Environment and Can be Mediated by CD4+ and CD8+ T Cells. *Journal of Immunotherapy* 2009; 32: 207–218.

[419] Engels B, Cam H, Schüler T, et al. Retroviral Vectors for High-Level Transgene Expression in T Lymphocytes. *Hum Gene Ther* 2003; 14: 1155–1168.

[420] Ryan MD, King AMQ, Thomas GP. Cleavage of foot-and-mouth disease virus polyprotein is mediated by residues located within a 19 amino acid sequence. *Journal of General Virology* 1991; 72: 2727–2732.

[421] Ryan MD, Donnelly M, Lewis A, et al. A model for nonstoichiometric, cotranslational protein scission in eukaryotic ribosomes. *Bioorg Chem* 1999; 27: 55–79.

[422] An F, Drummond DC, Wilson S, et al. Targeted drug delivery to mesothelioma cells using functionally selected internalizing human single-chain antibodies. *Mol Cancer Ther* 2008; 7: 569–578.

[423] Bidlingmaier S, He J, Wang Y, et al. Identification of MCAM/CD146 as the target antigen of a human monoclonal antibody that recognizes both epithelioid and sarcomatoid types of mesothelioma. *Cancer Res* 2009; 69: 1570–1577.

[424] Keller T, Kalt R, Raab I, et al. Selection of scFv Antibody Fragments Binding to Human Blood versus Lymphatic Endothelial Surface Antigens by Direct Cell Phage Display. *PLoS One* 2015; 10: e0127169–e0127169.

[425] Mills L, Tellez C, Huang S, et al. Fully human antibodies to MCAM/MUC18 inhibit tumor growth and metastasis of human melanoma. *Cancer Res* 2002; 62: 5106–5114.

[426] Mendez MJ, Green LL, Corvalan JR, et al. *Functional transplant of megabase human immunoglobulin loci recapitulates human antibody response in mice*, http://www.nature.com/naturegenetics (1997).

[427] McGary EC, Heimberger A, Mills L, et al. A fully human antimelanoma cellular adhesion molecule/MUC18 antibody inhibits spontaneous pulmonary metastasis of osteosarcoma cells in vivo. *Clin Cancer Res* 2003; 9: 6560–6566.

[428] Nollet M, Stalin J, Moyon A, et al. A novel anti-CD146 antibody specifically targets cancer cells by internalizing the molecule. *Oncotarget* 2017; 8: 112283–112296.

[429] Pezzutto A, Dörken B, Rabinovitch PS, et al. CD19 monoclonal antibody HD37 inhibits anti-immunoglobulin-induced B cell activation and proliferation. *J Immunol* 1987; 138: 2793–9.

[430] Burns JC, Friedmann T, Driever W, et al. Vesicular stomatitis virus G glycoprotein pseudotyped retroviral vectors: concentration to very high titer and efficient gene transfer into mammalian and nonmammalian cells. *Proc Natl Acad Sci U S A* 1993; 90: 8033.

[431] RetroNectin reagent, https://www.takarabio.com/products/gene-function/t-cell-transduction-and-culture/retronectin-reagent (accessed 11 August 2022).

[432] Finkelshtein D, Werman A, Novick D, et al. LDL receptor and its family members serve as the cellular receptors for vesicular stomatitis virus. *Proc Natl Acad Sci U S A* 2013; 110: 7306–7311.

[433] Matlin KS, Reggio H, Helenius A, et al. Pathway of vesicular stomatitis virus entry leading to infection. *J Mol Biol* 1982; 156: 609–631.

[434] Martinez I, Wertz GW. Biological Differences between Vesicular Stomatitis Virus Indiana and New Jersey Serotype Glycoproteins: Identification of Amino Acid Residues Modulating pH-Dependent Infectivity. *J Virol* 2005; 79: 3578–3585.

[435] Miller A, Garcia J, von Suhr N, et al. Construction and Properties of Retrovirus Packaging Cells Based on Gibbon Ape Leukemia Virus. *J Virol* 1991; 65: 2220–2224.

[436] O'Hara B, Johann S v, Klinger HP, et al. Characterization of a human gene conferring sensitivity to infection by gibbon ape leukemia virus. *Cell Growth Differ* 1990; 1: 119–27.

[437] Overbaugh J, Miller AD, Eiden M v. Receptors and Entry Cofactors for Retroviruses Include Single and Multiple Transmembrane-Spanning Proteins as

well as Newly Described Glycophosphatidylinositol-Anchored and Secreted Proteins. *Microbiology and Molecular Biology Reviews* 2001; 65: 371.

[438] Immune cell - SLC20A1 - The Human Protein Atlas, https://www.proteinatlas.org/ENSG00000144136-SLC20A1/immune+cell (accessed 11 August 2022).

[439] Marincola FM, Shamamian P, Alexander RB, et al. Loss of HLA haplotype and B locus down-regulation in melanoma cell lines. *J Immunol*.

[440] Wang E, Voiculescu S, le Poole IC, et al. Clonal Persistence and Evolution During a Decade of Recurrent Melanoma. *Journal of Investigative Dermatology* 2006; 126: 1372–1377.

[441] Robbins PF, El-Gamil M, Li YF, et al. Multiple HLA Class II-Restricted Melanocyte Differentiation Antigens Are Recognized by Tumor-Infiltrating Lymphocytes from a Patient with Melanoma. *The Journal of Immunology* 2002; 169: 6036–6047.

[442] Cellosaurus cell line 888-mel (CVCL_4632), https://web.expasy.org/cellosaurus/CVCL_4632 (accessed 3 August 2022).

[443] Mintz-Weber CS, Johnson JP. Identification of the elements regulating the expression of the cell adhesion molecule MCAM/MUC18. Loss of AP-2 is not required for MCAM expression in melanoma cell lines. *J Biol Chem* 2000; 275: 34672–34680.

[444] Johnson JP, Bar-Eli M, Jansen B, et al. Melanoma progression-associated glycoprotein MUC18/MCAM mediates homotypic cell adhesion through interaction with a heterophilic ligand. *Int J Cancer* 1997; 73: 769–774.

[445] Witze ES, Litman ES, Argast GM, et al. Wnt5a Control of Cell Polarity and Directional Movement by Polarized Redistribution of Adhesion Receptors. *Science* 2008; 320: 365.

[446] Anfosso F, Bardin N, Frances V, et al. Activation of human endothelial cells via S-endo-1 antigen (CD146) stimulates the tyrosine phosphorylation of focal adhesion kinase p125(FAK). *J Biol Chem* 1998; 273: 26852–26856.

[447] Jiang T, Zhuang J, Duan H, et al. CD146 is a coreceptor for VEGFR-2 in tumor angiogenesis. *Blood* 2012; 120: 2330–2339.

[448] Zheng C, Qiu Y, Zeng Q, et al. Endothelial CD146 is required for in vitro tumor-induced angiogenesis: the role of a disulfide bond in signaling and dimerization. *Int J Biochem Cell Biol* 2009; 41: 2163–2172.

[449] Shih IM, Elder DE, Speicher D, et al. Isolation and functional characterization of the A32 melanoma-associated antigen. *Cancer Res* 1994; 54: 2514–2520.

[450] Mangahas CR, dela Cruz G v, Schneider RJ, et al. Endothelin-1 upregulates MCAM in melanocytes. *J Invest Dermatol* 2004; 123: 1135–1139.

[451] Caruso A, Licenziati S, Corulli M, et al. Flow cytometric analysis of activation markers on stimulated T cells and their correlation with cell proliferation. *Cytometry* 1997; 27: 71–6.

[452] Wolfl M, Rgen Kuball J, Ho WY, et al. Activation-induced expression of CD137 permits detection, isolation, and expansion of the full repertoire of CD8 T cells responding to antigen without requiring knowledge of epitope specificities. Epub ahead of print 2007. DOI: 10.1182/blood-2006-11.

[453] Simms PE, Ellis TM. Utility of Flow Cytometric Detection of CD69 Expression as a Rapid Method for Determining Poly-and Oligoclonal Lymphocyte Activation. *Clin Diagn Lab Immunol* 1996; 3: 301–304.

[454] Ivetic A, Green HLH, Hart SJ. L-selectin: A major regulator of leukocyte adhesion, migration and signaling. *Front Immunol* 2019; 10: 1068.

[455] Yang S, Liu F, Wang QJ, et al. The Shedding of CD62L (L-Selectin) Regulates the Acquisition of Lytic Activity in Human Tumor Reactive T Lymphocytes. *PLoS One* 2011; 6: 22560.

[456] Meeth K, Wang JX, Micevic G, et al. The YUMM lines: a series of congenic mouse melanoma cell lines with defined genetic alterations. *Pigment Cell Melanoma Res* 2016; 29: 590.

[457] Szymczak AL, Workman CJ, Wang Y, et al. Correction of multi-gene deficiency in vivo using a single 'self-cleaving' 2A peptide–based retroviral vector. *Nature Biotechnology 2004 22:5* 2004; 22: 589–594.

[458] Minskaia E, Nicholson J, Ryan MD. Optimisation of the foot-and-mouth disease virus 2A co-expression system for biomedical applications. *BMC Biotechnol* 2013; 13: 1–11.

[459] Abraham RT, Weiss A %J N reviews I. Jurkat T cells and development of the T-cell receptor signalling paradigm. 4. Epub ahead of print 2004. DOI: 10.1038/nri1330.

[460] Hyrenius-Wittsten A, Su Y, Park M, et al. SynNotch CAR Circuits Enhance Solid Tumor Recognition and Promote Persistent Anti-tumor Activity in Mouse Models HHS Public Access. *Sci Transl Med*; 13. Epub ahead of print 2021. DOI: 10.1126/scitranslmed.abd8836.

[461] Bidlingmaier S, He J, Wang Y, et al. Identification of MCAM/CD146 as the target antigen of a human monoclonal antibody that recognizes both epithelioid and sarcomatoid types of mesothelioma. *Cancer Res* 2009; 69: 1570–1577.

[462] Ciechanover A. Proteolysis: from the lysosome to ubiquitin and the proteasome. *Nature Reviews Molecular Cell Biology 2005 6:1* 2005; 6: 79–87.

[463] Guest RD, Hawkins RE, Kirillova N, et al. The role of extracellular spacer regions in the optimal design of chimeric immune receptors: evaluation of four different scFvs and antigens. *J Immunother* 2005; 28: 203–211.

[464] Joint United Kingdom (UK) Blood Transfusion and Tissue Transplantation Services Professional Advisory Committee. 7.1 Leucocyte depletion. *Guidelines for the Blood Transfusion Services*, https://www.transfusionguidelines.org/red-book/chapter-7-specifications-for-blood-components/7-1-leucocyte-depletion (accessed 24 August 2022).

[465] Bianchi M, Vaglio S, Pupella S, et al. Leucoreduction of blood components: an effective way to increase blood safety? *Blood Transfusion* 2016; 14: 214.

[466] Singh S, Kumar A. Leukocyte depletion for safe blood transfusion. *Biotechnol J* 2009; 4: 1140–1151.

[467] Dzik S. Leukodepletion Blood Filters: Filter Design and Mechanisms of Leukocyte Removal. *Transfus Med Rev* 1993; 7: 65–77.

[468] Sahoo D, Prakash S, Mukherjee S, et al. Trapping of platelets in leukocyte reduction chamber leads to failure of plateletpheresis procedure: a rare troubleshooting during apheresis. *Hematol Transfus Cell Ther* 2020; 42: 173.

[469] Davis PK, Ho A, Dowdy SF. Biological methods for cell-cycle synchronization of mammalian cells. *Biotechniques* 2001; 30: 1322–1331.

[470] Dietz AB, Bulur PA, Emery RL, et al. A novel source of viable peripheral blood mononuclear cells from leukoreduction system chambers. *Transfusion (Paris)* 2006; 46: 2083–9.

[471] Néron S, Thibault L, Dussault N, et al. Characterization of mononuclear cells remaining in the leukoreduction system chambers of apheresis instruments after routine platelet collection: A new source of viable human blood cells. *Transfusion (Paris)* 2007; 47: 1042–1049.

[472] Tremblay MM, Houtman JCD. TCR-Mediated Functions Are Enhanced in Activated Peripheral Blood T Cells Isolated From Leucocyte Reduction Systems. Epub ahead of print 2014. DOI: 10.1016/j.jim.2014.11.009.

[473] Boudreau G, Carli C, Lamarche C, et al. Leukoreduction system chambers are a reliable cellular source for the manufacturing of T-cell therapeutics. *Transfusion (Paris)* 2019; 59: 1300–1311.

[474] Pfeiffer IA, Zinser E, Strasser E, et al. Leukoreduction system chambers are an efficient, valid, and economic source of functional monocyte-derived dendritic cells and lymphocytes. *Immunobiology* 2013; 218: 1392–1401.

[475] Trapani JA, Smyth MJ. Functional significance of the perforin/granzyme cell death pathway. *Nat Rev Immunol* 2002; 2: 735–747.

[476] Benmebarek M-R, Karches CH, Loureiro Cadilha B, et al. Molecular Sciences Killing Mechanisms of Chimeric Antigen Receptor (CAR) T Cells. Epub ahead of print 2019. DOI: 10.3390/ijms20061283.

[477] Marshall NB, Swain SL. Cytotoxic CD4 T Cells in Antiviral Immunity. *J Biomed Biotechnol*; 2011. Epub ahead of print 2011. DOI: 10.1155/2011/954602.

[478] Peters PJ, Borst J, Oorschot V, et al. Cytotoxic T Lymphocyte Granules Are Secretory Lysosomes, Containing Both Perforin and Granzymes, http://rupress.org/jem/article-pdf/173/5/1099/1394679/1099.pdf (accessed 9 September 2022).

[479] Fukuda M. Lysosomal membrane glycoproteins: Structure, biosynthesis, and intracellular trafficking. *Journal of Biological Chemistry* 1991; 266: 21327–21330.

[480] Betts MR, Brenchley JM, Price DA, et al. Sensitive and viable identification of antigen-specific CD8+ T cells by a flow cytometric assay for degranulation. *J Immunol Methods* 2003; 281: 65–78.

[481] Castro F, Cardoso AP, Gonçalves RM, et al. Interferon-Gamma at the Crossroads of Tumor Immune Surveillance or Evasion. *Front Immunol* 2018; 9: 847.

[482] Jorgovanovic D, Song M, Wang L, et al. Roles of IFN-γ in tumor progression and regression: a review. *Biomark Res* 2020; 8: 49.

[483] Mahdavi Sharif P, Jabbari P, Razi S, et al. Importance of TNF-alpha and its alterations in the development of cancers. *Cytokine*; 130. Epub ahead of print 1 June 2020. DOI: 10.1016/J.CYTO.2020.155066.

[484] Braumüller H, Wieder T, Brenner E, et al. T-helper-1-cell cytokines drive cancer into senescence. *Nature* 2013; 494: 361–5.

[485] Zhang M, Wang J, Jia L, et al. Transmembrane TNF-α promotes activation-induced cell death by forward and reverse signaling. *Oncotarget* 2017; 8: 63799–63812.

[486] Chen X, Bäumel M, Männel DN, et al. Interaction of TNF with TNF receptor type 2 promotes expansion and function of mouse CD4+CD25+ T regulatory cells. *J Immunol* 2007; 179: 154–61.

[487] Zhao X, Rong L, Zhao X, et al. TNF signaling drives myeloid-derived suppressor cell accumulation. *J Clin Invest* 2012; 122: 4094–4104.

[488] Boyman O, Sprent J. The role of interleukin-2 during homeostasis and activation of the immune system. *Nat Rev Immunol* 2012; 12: 180–190.

[489] Ross SH, Cantrell DA. Signaling and Function of Interleukin-2 in T Lymphocytes. *Annu Rev Immunol* 2018; 36: 411–433.

[490] Watts TH. TNF/TNFR family members in costimulation of T cell responses. *Annu Rev Immunol* 2005; 23: 23–68.

[491] Cibrián D, Sánchez-Madrid F. CD69: from activation marker to metabolic gatekeeper. *Eur J Immunol* 2017; 47: 946–953.

[492] Yi JS, Cox MA, Zajac AJ. T-cell exhaustion: characteristics, causes and conversion. *Immunology* 2010; 129: 474–81.

[493] Bajgain P, Mucharla R, Wilson J, et al. Optimizing the production of suspension cells using the G-Rex 'M' series. *Mol Ther Methods Clin Dev* 2014; 1: 14015.

[494] Vera JF, Brenner LJ, Gerdemann U, et al. Accelerated production of antigen-specific T cells for preclinical and clinical applications using gas-permeable rapid expansion cultureware (G-Rex). *J Immunother* 2010; 33: 305–15.

[495] Jin J, Sabatino M, Somerville R, et al. Simplified method of the growth of human tumor infiltrating lymphocytes in gas-permeable flasks to numbers needed for patient treatment. *J Immunother* 2012; 35: 283–92.

[496] Forget M-A, Haymaker C, Dennison JB, et al. The beneficial effects of a gas-permeable flask for expansion of Tumor-Infiltrating lymphocytes as reflected in their mitochondrial function and respiration capacity. *Oncoimmunology* 2016; 5: e1057386.

[497] Xiao L, Chen C, Li Z, et al. Large-scale expansion of Vγ9Vδ2 T cells with engineered K562 feeder cells in G-Rex vessels and their use as chimeric antigen receptor-modified effector cells. *Cytotherapy* 2018; 20: 420–435.

[498] Chakraborty R, Mahendravada A, Perna SK, et al. Robust and cost effective expansion of human regulatory T cells highly functional in a xenograft model of graft-versus-host disease. *Haematologica* 2013; 98: 533–537.

[499] Lapteva N, Durett AG, Sun J, et al. Large-scale ex vivo expansion and characterization of natural killer cells for clinical applications. *Cytotherapy* 2012; 14: 1131–43.

[500] Caruso A, Licenziati S, Corulli M, et al. Flow cytometric analysis of activation markers on stimulated T cells and their correlation with cell proliferation. *Cytometry* 1997; 27: 71–76.

[501] Alais S, Allioli N, Pujades C, et al. HEMCAM/CD146 downregulates cell surface expression of beta1 integrins. *J Cell Sci* 2001; 114: 1847–1859.

[502] Bu P, Zhuang J, Feng J, et al. Visualization of CD146 dimerization and its regulation in living cells. *Biochim Biophys Acta Mol Cell Res* 2007; 1773: 513–520.

[503] Herlyn M. Human melanoma: Development and progression. *Cancer and Metastasis Reviews* 1990; 9: 101–112.

[504] Herlyn M, Balaban G, Bennicelli J, et al. Primary Melanoma Cells of the Vertical Growth Phase: Similarities to Metastatic Cells. *J Natl Cancer Inst* 1985; 74: 283–289.

[505] Welch DR, Bisi JE, Miller BE, et al. Characterization of a highly invasive and spontaneously metastatic human malignant melanoma cell line. *Int J Cancer* 1991; 47: 227–237.

[506] Cellosaurus. C8161 (CVCL_6813). *Expasy* , https://web.expasy.org/cellosaurus/CVCL_6813 (2021, accessed 25 August 2022).

[507] Expasy. 501-mel (CVCL_4633). *Cellosaurus* , https://web.expasy.org/cellosaurus/CVCL_4633 (2021, accessed 25 August 2022).

[508] Bardin N, Francès V, Combes V, et al. CD146: biosynthesis and production of a soluble form in human cultured endothelial cells. *FEBS Lett* 1998; 421: 12–14.

[509] Boneberg EM, Illges H, Legler DF, et al. Soluble CD146 is generated by ectodomain shedding of membrane CD146 in a calcium-induced, matrix metalloprotease-dependent process. *Microvasc Res* 2009; 78: 325–331.

[510] Harhouri K, Kebir A, Guillet B, et al. Soluble CD146 displays angiogenic properties and promotes neovascularization in experimental hind-limb ischemia. Epub ahead of print 2010. DOI: 10.1182/blood-2009-06-229591.

[511] Sharma A, Joshkon A, Ladjimi A, et al. Soluble CD146 as a Potential Target for Preventing Triple Negative Breast Cancer MDA-MB-231 Cell Growth and Dissemination. *Int J Mol Sci* 2022; 23: 974.

[512] Dagur PK, McCoy JP. Endothelial-binding, proinflammatory T cells identified by MCAM (CD146) expression: Characterization and role in human autoimmune diseases. *Autoimmun Rev* 2015; 14: 415–422.

[513] Abou-el-Enein M, Elsallab M, Feldman SA, et al. Scalable Manufacturing of CAR T Cells for Cancer Immunotherapy. *Blood Cancer Discov* 2021; 2: 408–422.

[514] Somerville RPT, Devillier L, Parkhurst MR, et al. Clinical scale rapid expansion of lymphocytes for adoptive cell transfer therapy in the WAVE ®bioreactor. *J Transl Med* 2012; 10: 1–11.

[515] Fernández L, Fernández A, Mirones I, et al. GMP-Compliant Manufacturing of NKG2D CAR Memory T Cells Using CliniMACS Prodigy. *Front Immunol*; 10. Epub ahead of print 10 October 2019. DOI: 10.3389/FIMMU.2019.02361.

[516] Shah NN, Johnson BD, Schneider D, et al. Bispecific anti-CD20, anti-CD19 CAR T cells for relapsed B cell malignancies: a phase 1 dose escalation and expansion trial. *Nat Med* 2020; 26: 1569–1575.

[517] Gagliardi C, Khalil M, Foster AE. Streamlined production of genetically modified T cells with activation, transduction and expansion in closed-system G-Rex bioreactors. *Cytotherapy* 2019; 21: 1246–1257.

[518] Dudley ME, Wunderlich JR, Shelton TE, et al. Generation of tumor-infiltrating lymphocyte cultures for use in adoptive transfer therapy for melanoma patients. *J Immunother*; 26: 332–42.

[519] Elavia N, Panch SR, McManus A, et al. Effects of starting cellular material composition on chimeric antigen receptor T-cell expansion and characteristics. *Transfusion (Paris)* 2019; 59: 1755–1764.

[520] Stroncek DF, Ren J, Lee DW, et al. Myeloid cells in peripheral blood mononuclear cell concentrates inhibit the expansion of chimeric antigen receptor T cells. *Cytotherapy* 2016; 18: 893–901.

[521] Noaks E, Peticone C, Kotsopoulou E, et al. Enriching leukapheresis improves T cell activation and transduction efficiency during CAR T processing. *Mol Ther Methods Clin Dev* 2021; 20: 675–687.

[522] Fehniger TA, Cooper MA, Nuovo GJ, et al. CD56bright natural killer cells are present in human lymph nodes and are activated by T cell–derived IL-2: a potential new link between adaptive and innate immunity. *Blood* 2003; 101: 3052–3057.

[523] Screpanti V, Wallin RPA, Ljunggren H-G, et al. A Central Role for Death Receptor-Mediated Apoptosis in the Rejection of Tumors by NK Cells. *The Journal of Immunology* 2001; 167: 2068–2073.

[524] Voskoboinik I, Smyth MJ, Trapani JA. Perforin-mediated target-cell death and immune homeostasis. *Nat Rev Immunol* 2006; 6: 940–52.

[525] Bollino D, Webb TJ. Chimeric antigen receptor-engineered natural killer and natural killer T cells for cancer immunotherapy. *Transl Res* 2017; 187: 32–43.

[526] Wu Y, Tian Z, Wei H. Developmental and functional control of natural killer cells by cytokines. *Front Immunol* 2017; 8: 930.

[527] Chang YH, Connolly J, Shimasaki N, et al. A chimeric receptor with NKG2D specificity enhances natural killer cell activation and killing of tumor cells. *Cancer Res* 2013; 73: 1777–1786.

[528] Kruschinski A, Moosmann A, Poschke I, et al. Engineering antigen-specific primary human NK cells against HER-2 positive carcinomas. *Proc Natl Acad Sci U S A* 2008; 105: 17481–17486.

[529] Imai C, Iwamoto S, Campana D. Genetic modification of primary natural killer cells overcomes inhibitory signals and induces specific killing of leukemic cells. *Blood* 2005; 106: 376–83.

[530] Chu Y, Hochberg J, Yahr A, et al. Targeting CD20+ Aggressive B-cell Non-Hodgkin Lymphoma by Anti-CD20 CAR mRNA-Modified Expanded Natural Killer Cells In Vitro and in NSG Mice. *Cancer Immunol Res* 2015; 3: 333–44.

[531] Shimasaki N, Fujisaki H, Cho D, et al. A clinically adaptable method to enhance the cytotoxicity of natural killer cells against B-cell malignancies. *Cytotherapy* 2012; 14: 830–40.

[532] Chen M, Li Y, Wu Y, et al. Anti-Tumor Activity of Expanded PBMC-Derived NK Cells by Feeder-Free Protocol in Ovarian Cancer. *Cancers (Basel)*; 13. Epub ahead of print 1 November 2021. DOI: 10.3390/CANCERS13225866.

[533] Hoyos V, Savoldo B, Vera JF, et al. 61. Effects of Chimeric Antigen Receptor (CAR) Expression on Regulatory T Cells. *Molecular Therapy* 2009; 17: S25.

[534] Turtle CJ, Hanafi LA, Berger C, et al. CD19 CAR-T cells of defined CD4+:CD8+ composition in adult B cell ALL patients. *J Clin Invest* 2016; 126: 2123–2138.

[535] Sommermeyer D, Hudecek M, Kosasih PL, et al. Chimeric antigen receptor-modified T cells derived from defined CD8+ and CD4+ subsets confer superior antitumor reactivity in vivo. *Leukemia* 2016; 30: 492–500.

[536] Moeller M, Haynes NM, Kershaw MH, et al. Adoptive transfer of gene-engineered CD4 helper T cells induces potent primary and secondary tumor rejection. Epub ahead of print 2005. DOI: 10.1182/blood-2004-12-4906.

[537] Li Y, Kurlander RJ. Comparison of anti-CD3 and anti-CD28-coated beads with soluble anti-CD3 for expanding human T cells: differing impact on CD8 T cell phenotype and responsiveness to restimulation. *J Transl Med*; 8. Epub ahead of print 26 October 2010. DOI: 10.1186/1479-5876-8-104.

[538] Adusumilli PS, Cherkassky L, Villena-Vargas J, et al. Regional delivery of mesothelin-targeted CAR T cell therapy generates potent and long-lasting CD4-dependent tumor immunity. *Sci Transl Med* 2014; 6: 261ra151.

[539] Moeller M, Kershaw MH, Cameron R, et al. Sustained Antigen-Specific Antitumor Recall Response Mediated by Gene-Modified CD4 + T Helper-1 and CD8 + T Cells. *Cancer Res* 2007; 67: 11428–11465.

[540] Ngai P, McCormick S, Small C, et al. Gamma interferon responses of CD4 and CD8 T-cell subsets are quantitatively different and independent of each other during pulmonary Mycobacterium bovis BCG infection. *Infect Immun* 2007; 75: 2244–2252.

[541] Yang Y, Kohler ME, Chien CD, et al. TCR engagement negatively affects CD8 but not CD4 CAR T cell expansion and leukemic clearance. *Sci Transl Med*; 9. Epub ahead of print 22 November 2017. DOI: 10.1126/SCITRANSLMED.AAG1209.

[542] Agarwal S, Hanauer JDS, Frank AM, et al. In Vivo Generation of CAR T Cells Selectively in Human CD4+ Lymphocytes. *Molecular Therapy* 2020; 28: 1783–1794.

[543] Lee DH, Cervantes-Contreras F, Lee SY, et al. Improved Expansion and Function of CAR T Cell Products from Cultures Initiated at Defined CD4:CD8 Ratios. *Blood* 2018; 132: 3334.

[544] Melenhorst JJ, Chen GM, Wang M, et al. Decade-long leukaemia remissions with persistence of CD4+ CAR T cells. *Nature* 2022; 602: 503–509.

[545] Kaartinen T, Luostarinen A, Maliniemi P, et al. Low interleukin-2 concentration favors generation of early memory T cells over effector phenotypes during chimeric antigen receptor T-cell expansion. *Cytotherapy* 2017; 19: 689–702.

[546] Zhang X, Lv X, Song Y. Short-term culture with IL-2 is beneficial for potent memory chimeric antigen receptor T cell production. *Biochem Biophys Res Commun* 2018; 495: 1833–1838.

[547] Barrett DM, Singh N, Liu X, et al. Relation of clinical culture method to T-cell memory status and efficacy in xenograft models of adoptive immunotherapy. *Cytotherapy* 2014; 16: 619–630.

[548] Giuffrida L, Sek K, Henderson MA, et al. IL-15 Preconditioning Augments CAR T Cell Responses to Checkpoint Blockade for Improved Treatment of Solid Tumors. *Molecular Therapy* 2020; 28: 2379–2393.

[549] Alizadeh D, Wong RA, Yang X, et al. IL15 enhances CAR-T cell antitumor activity by reducing mTORC1 activity and preserving their stem cell memory phenotype. *Cancer Immunol Res* 2019; 7: 759–772.

[550] Xu Y, Zhang M, Ramos CA, et al. Closely related T-memory stem cells correlate with in vivo expansion of CAR.CD19-T cells and are preserved by IL-7 and IL-15. *Blood* 2014; 123: 3750–3759.

[551] Zhou J, Jin L, Wang F, et al. Chimeric antigen receptor T (CAR-T) cells expanded with IL-7/IL-15 mediate superior antitumor effects. DOI: 10.1007/s13238-019-0643-y.

[552] Panch SR, Srivastava SK, Elavia N, et al. Effect of Cryopreservation on Autologous Chimeric Antigen Receptor T Cell Characteristics. *Molecular Therapy* 2019; 27: 1275–1285.

[553] Pickl WF, Majdic O, Fischer GF, et al. MUC18/MCAM (CD146), an activation antigen of human T lymphocytes. *J Immunol* 1997; 158: 2107–2115.

[554] Bedoya SK, Wilson TD, Collins EL, et al. Isolation and Th17 Differentiation of Naïve CD4 T Lymphocytes. *J Vis Exp* 2013; 50765.

[555] Revu S, Wu J, Henkel M, et al. IL-23 and IL-1β Drive Human Th17 Cell Differentiation and Metabolic Reprogramming in Absence of CD28 Costimulation. *CellReports* 2018; 22: 2642–2653.

[556] Majzner RG, Theruvath JL, Nellan A, et al. CAR T Cells Targeting B7-H3, a Pan-Cancer Antigen, Demonstrate Potent Preclinical Activity Against Pediatric Solid Tumors and Brain Tumors. *Clin Cancer Res* 2019; 25: 2560–2574.

[557] Festag MM, Festag J, Fräßle SP, et al. Evaluation of a Fully Human, Hepatitis B Virus-Specific Chimeric Antigen Receptor in an Immunocompetent Mouse Model. *Molecular Therapy* 2019; 27: 947–959.

[558] Ritchie DS, Neeson PJ, Khot A, et al. Persistence and Efficacy of Second Generation CAR T Cell Against the LeY Antigen in Acute Myeloid Leukemia. *Molecular Therapy* 2013; 21: 2122–2129.

[559] Simonetta F, Alam IS, Lohmeyer JK, et al. Molecular Imaging of Chimeric Antigen Receptor T Cells by ICOS-ImmunoPET. *Clinical Cancer Research* 2021; 27: 1058–1068.

[560] Vedvyas Y, Shevlin E, Zaman M, et al. Longitudinal PET imaging demonstrates biphasic CAR T cell responses in survivors. *JCI Insight*; 1. Epub ahead of print 17 November 2016. DOI: 10.1172/jci.insight.90064.

[561] Keu KV, Witney TH, Yaghoubi S, et al. Reporter gene imaging of targeted T cell immunotherapy in recurrent glioma. *Sci Transl Med*; 9. Epub ahead of print 18 January 2017. DOI: 10.1126/scitranslmed.aag2196.

[562] Emami-Shahri N, Foster J, Kashani R, et al. Clinically compliant spatial and temporal imaging of chimeric antigen receptor T-cells. *Nat Commun* 2018; 9: 1081.

[563] Dobrenkov K, Olszewska M, Likar Y, et al. Monitoring the Efficacy of Adoptively Transferred Prostate Cancer–Targeted Human T Lymphocytes with PET and Bioluminescence Imaging. *Journal of Nuclear Medicine* 2008; 49: 1162–1170.

[564] Cazaux M, Grandjean CL, Lemaître F, et al. Single-cell imaging of CAR T cell activity in vivo reveals extensive functional and anatomical heterogeneity. *Journal of Experimental Medicine* 2019; 216: 1038–1049.

[565] James SE, Orgun NN, Tedder TF, et al. Antibody-mediated B-cell depletion before adoptive immunotherapy with T cells expressing CD20-specific chimeric T-cell receptors facilitates eradication of leukemia in immunocompetent mice. *Blood* 2009; 114: 5454–5463.

[566] Singla R, Wall D, Anderson S, et al. First in Human Study of In-vivo Imaging of Ex-Vivo Labelled CAR T Cells with Dual PET-MR. *Cytotherapy* 2020; 22: S201.

[567] Lawrence C. The husbandry of zebrafish (Danio rerio): A review. *Aquaculture* 2007; 269: 1–20.

[568] White RM, Sessa A, Burke C, et al. Transparent adult zebrafish as a tool for in vivo transplantation analysis. *Cell Stem Cell* 2008; 2: 183–189.

[569] Lister JA, Robertson CP, Lepage T, et al. nacre encodes a zebrafish microphthalmia-related protein that regulates neural-crest-derived pigment cell fate. *Development* 1999; 126: 3757–67.

[570] Herbomel P, Thisse B, Thisse C. Ontogeny and behaviour of early macrophages in the zebrafish embryo. *Development* 1999; 126: 3735–3745.

[571] Lieschke GJ, Oates AC, Crowhurst MO, et al. Morphologic and functional characterization of granulocytes and macrophages in embryonic and adult zebrafish. *Blood* 2001; 98: 3087–3096.

[572] Balla KM, Lugo-Villarino G, Spitsbergen JM, et al. Eosinophils in the zebrafish: prospective isolation, characterization, and eosinophilia induction by helminth determinants. *Blood* 2010; 116: 3944–3954.

[573] Lugo-Villarino G, Balla KM, Stachura DL, et al. Identification of dendritic antigen-presenting cells in the zebrafish. *Proc Natl Acad Sci U S A* 2010; 107: 15850–15855.

[574] Page DM, Wittamer V, Bertrand JY, et al. An evolutionarily conserved program of B-cell development and activation in zebrafish. *Blood* 2013; 122: e1-11.

[575] Lam SH, Chua HL, Gong Z, et al. Development and maturation of the immune system in zebrafish, Danio rerio: a gene expression profiling, in situ hybridization and immunological study. *Dev Comp Immunol* 2004; 28: 9–28.

[576] Wertman J, Veinotte CJ, Dellaire G, et al. The zebrafish xenograft platform: Evolution of a novel cancer model and preclinical screening tool. *Adv Exp Med Biol* 2016; 916: 289–314.

[577] Sers C, Riethmuller G, Johnson JP. MUC18, a melanoma-progression associated molecule, and its potential role in tumor vascularization and hematogenous spread. *Cancer Res* 1994; 54: 5689–5694.

[578] Shih IM, Nesbit M, Herlyn M, et al. A new Mel-CAM (CD146)-specific monoclonal antibody, MN-4, on paraffin-embedded tissue. *Mod Pathol* 1998; 11: 1098–1106.

[579] Schrage A, Loddenkemper C, Erben U, et al. Murine CD146 is widely expressed on endothelial cells and is recognized by the monoclonal antibody ME-9F1. *Histochem Cell Biol* 2008; 129: 441–451.

[580] Bardin N, Frances V, Lesaule G, et al. Identification of the S-Endo 1 endothelial-associated antigen. *Biochem Biophys Res Commun* 1996; 218: 210–216.

[581] Shih IM, Wang TL, Westra WH. Diagnostic and biological implications of mel-CAM expression in mesenchymal neoplasms. *Clin Cancer Res* 1996; 2: 569–575.

[582] Chen J, Luo Y, Huang H, et al. CD146 is essential for PDGFRβ-induced pericyte recruitment. *Protein Cell* 2018; 9: 743–747.

[583] Clarke LA, Shah V, Arrigoni F, et al. Quantitative detection of circulating endothelial cells in vasculitis: comparison of flow cytometry and immunomagnetic bead extraction. *Journal of Thrombosis and Haemostasis* 2008; 6: 1025–1032.

[584] George F, Poncelet P, Laurent JC, et al. Cytofluorometric detection of human endothelial cells in whole blood using S-Endo 1 monoclonal antibody. *J Immunol Methods* 1991; 139: 65–75.

[585] Makin AJ, Blann AD, Chung NAY, et al. Assessment of endothelial damage in atherosclerotic vascular disease by quantification of circulating endothelial cells. Relationship with von Willebrand factor and tissue factor. *Eur Heart J* 2004; 25: 371–376.

[586] Fürstenberger G, von Moos R, Senn HJ, et al. Real-time PCR of CD146 mRNA in peripheral blood enables the relative quantification of circulating endothelial cells and is an indicator of angiogenesis. *Br J Cancer* 2005; 93: 793–798.

[587] Bardin N, Anfosso F, Masse JM, et al. Identification of CD146 as a component of the endothelial junction involved in the control of cell-cell cohesion. *Blood* 2001; 98: 3677–3684.

[588] Yan X, Lin Y, Yang D, et al. A novel anti-CD146 monoclonal antibody, AA98, inhibits angiogenesis and tumor growth. *Blood* 2003; 102: 184–191.

[589] Kang Y, Wang F, Feng J, et al. Knockdown of CD146 reduces the migration and proliferation of human endothelial cells. *Cell Res* 2006; 16: 313–318.

[590] Kebir A, Harhouri K, Guillet B, et al. CD146 short isoform increases the proangiogenic potential of endothelial progenitor cells in vitro and in vivo. *Circ Res* 2010; 107: 66–75.

[591] Guezguez B, Vigneron P, Alais S, et al. A dileucine motif targets MCAM-l cell adhesion molecule to the basolateral membrane in MDCK cells. *FEBS Lett* 2006; 580: 3649–3656.

[592] Wang P, Luo Y, Duan H, et al. MicroRNA 329 suppresses angiogenesis by targeting CD146. *Mol Cell Biol* 2013; 33: 3689–3699.

[593] Prosen L, Markelc B, Dolinsek T, et al. Mcam Silencing With RNA Interference Using Magnetofection has Antitumor Effect in Murine Melanoma. *Mol Ther Nucleic Acids* 2014; 3: e205.

[594] Zhang Z, Zheng Y, Wang H, et al. CD146 interacts with galectin-3 to mediate endothelial cell migration. *FEBS Letters* 2018; 592: 1817–1828.

[595] Tu T, Zhang C, Yan H, et al. CD146 acts as a novel receptor for netrin-1 in promoting angiogenesis and vascular development. *Cell Res* 2015; 25: 275–287.

[596] Bu P, Zhuang J, Feng J, et al. Visualization of CD146 dimerization and its regulation in living cells. *Biochim Biophys Acta Mol Cell Res* 2007; 1773: 513–520.

[597] Wwragg J, Finnity JP, Anderson JA, et al. MCAM and LAMA4 are highly enriched in tumor blood vessels of renal cell carcinoma and predict patient outcome. *Cancer Res* 2016; 76: 2314–2326.

[598] Lam SH, Chua HL, Gong Z, et al. Development and maturation of the immune system in zebrafish, Danio rerio: a gene expression profiling, in situ hybridization and immunological study. *Dev Comp Immunol* 2004; 28: 9–28.

[599] Letrado P, Mole H, Montoya M, et al. Systematic Roadmap for Cancer Drug Screening Using Zebrafish Embryo Xenograft Cancer Models: Melanoma Cell Line as a Case Study. *Cancers 2021, Vol 13, Page 3705* 2021; 13: 3705.

[600] Vermes I, Haanen C, Steffens-Nakken H, et al. A novel assay for apoptosis Flow cytometric detection of phosphatidylserine expression on early apoptotic cells using fluorescein labelled Annexin V. *J Immunol Methods* 1995; 184: 39–51.

[601] Kleinman HK, Martin GR. Matrigel: Basement membrane matrix with biological activity. *Semin Cancer Biol* 2005; 15: 378–386.

[602] Arnaoutova I, Jay AE, Ae G, et al. The endothelial cell tube formation assay on basement membrane turns 20: state of the science and the art. DOI: 10.1007/s10456-009-9146-4.

[603] Kubota Y, Kleinman HK, Martin GR, et al. Role of laminin and basement membrane in the morphological differentiation of human endothelial cells into capillary-like structures. *Journal of Cell Biology* 1988; 107: 1589–1598.

[604] He X, Yin X, Wu J, et al. Visualization of human T lymphocyte-mediated eradication of cancer cells in vivo. *Proc Natl Acad Sci U S A* 2020; 117: 22910–22919.

[605] Pascoal S, Salzer B, Scheuringer E, et al. A Preclinical Embryonic Zebrafish Xenograft Model to Investigate CAR T Cells in Vivo. *Cancers (Basel)* 2020; 12: 567.

[606] Yan C, Yang Q, Zhang S, et al. Single-cell imaging of T cell immunotherapy responses in vivo. Epub ahead of print 2021. DOI: 10.1084/jem.20210314.

[607] Lanitis E, Irving M, Coukos G. Targeting the tumor vasculature to enhance T cell activity. *Curr Opin Immunol* 2015; 33: 55–63.

[608] Akbari P, Katsarou A, Daghighian R, et al. Directing CAR T cells towards the tumor vasculature for the treatment of solid tumors. *Biochim Biophys Acta Rev Cancer*; 1877. Epub ahead of print 1 May 2022. DOI: 10.1016/J.BBCAN.2022.188701.

[609] Zhuang X, Maione F, Robinson J, et al. CAR T cells targeting tumor endothelial marker CLEC14A inhibit tumor growth. *JCI Insight*; 5. Epub ahead of print 7 December 2020. DOI: 10.1172/JCI.INSIGHT.138808.

[610] Xing H, Yang X, Xu Y, et al. Anti-tumor effects of vascular endothelial growth factor/vascular endothelial growth factor receptor binding domain-modified chimeric antigen receptor T cells. *Cytotherapy* 2021; 23: 810–819.

[611] Byrd TT, Fousek K, Pignata A, et al. TEM8/ANTXR1-Specific CAR T cells as a targeted therapy for triple-negative breast cancer. *Cancer Res* 2018; 78: 489–500.

[612] Rutledge NS, Muller WA. Understanding Molecules that Mediate Leukocyte Extravasation. *Curr Pathobiol Rep* 2020; 8: 25–35.

[613] Mitroulis I, Alexaki VI, Kourtzelis I, et al. Leukocyte integrins: Role in leukocyte recruitment and as therapeutic targets in inflammatory disease. *Pharmacol Ther* 2015; 0: 123.

[614] Cochrane A, Albers HJ, Passier R, et al. Advanced in vitro models of vascular biology: Human induced pluripotent stem cells and organ-on-chip technology. *Adv Drug Deliv Rev* 2019; 140: 68–77.

[615] Pasquali S, Hadjinicolaou A v, Chiarion Sileni V, et al. Systemic treatments for metastatic cutaneous melanoma. *Cochrane Database Syst Rev* 2018; 2: CD011123.

[616] Herzberg B, Fisher DE. Metastatic melanoma and immunotherapy. *Clinical Immunology* 2016; 172: 105–110.

[617] Wragg JW, Finnity JP, Anderson JA, et al. MCAM and LAMA4 Are Highly Enriched in Tumor Blood Vessels of Renal Cell Carcinoma and Predict Patient Outcome. *Cancer Res* 2016; 76: 2314–2326.

[618] Leach MW, Halpern WG, Johnson CW, et al. Use of Tissue Cross-reactivity Studies in the Development of Antibody-based Biopharmaceuticals. *Toxicol Pathol* 2010; 38: 1138–1166.

[619] MacLachlan TK, Price S, Cavagnaro J, et al. Classic and evolving approaches to evaluating cross reactivity of mAb and mAb-like molecules – A survey of industry 2008–2019. *Regulatory Toxicology and Pharmacology* 2021; 121: 104872.

[620] Liu Y, Wu W, Cai C, et al. Patient-derived xenograft models in cancer therapy: technologies and applications. *Signal Transduct Target Ther* 2023; 8: 160.

[621] Jacob F, Salinas RD, Zhang DY, et al. A Patient-Derived Glioblastoma Organoid Model and Biobank Recapitulates Inter- and Intra-tumoral Heterogeneity. *Cell* 2020; 180: 188-204.e22.

[622] Schnalzger TE, de Groot MH, Zhang C, et al. 3D model for CAR-mediated cytotoxicity using patient-derived colorectal cancer organoids. *EMBO J*; 38. Epub ahead of print 2019. DOI: 10.15252/embj.2018100928.

[623] Rebecca VW, Somasundaram R, Herlyn M. Pre-clinical modeling of cutaneous melanoma. *Nat Commun* 2020; 11: 2858.

[624] Si X, Xiao L, Brown CE, et al. Preclinical Evaluation of CAR T Cell Function: In Vitro and In Vivo Models. *Int J Mol Sci*; 23. Epub ahead of print 15 March 2022. DOI: 10.3390/ijms23063154.

[625] Ishikawa F, Yasukawa M, Lyons B, et al. Development of functional human blood and immune systems in NOD/SCID/IL2 receptor γ chainnull mice. *Blood* 2005; 106: 1565–1573.

[626] Mhaidly R, Verhoeyen E. Humanized Mice Are Precious Tools for Preclinical Evaluation of CAR T and CAR NK Cell Therapies. *Cancers (Basel)*; 12. Epub ahead of print 15 July 2020. DOI: 10.3390/cancers12071915.

[627] Norelli M, Camisa B, Barbiera G, et al. Monocyte-derived IL-1 and IL-6 are differentially required for cytokine-release syndrome and neurotoxicity due to CAR T cells. *Nat Med* 2018; 24: 739–748.

[628] Jin C-H, Xia J, Rafiq S, et al. Modeling anti-CD19 CAR T cell therapy in humanized mice with human immunity and autologous leukemia. *EBioMedicine* 2019; 39: 173–181.

[629] Liu Y, Wu W, Cai C, et al. Patient-derived xenograft models in cancer therapy: technologies and applications. *Signal Transduct Target Ther* 2023; 8: 160.

[630] Ny L, Rizzo LY, Belgrano V, et al. Supporting clinical decision making in advanced melanoma by preclinical testing in personalized immune-humanized xenograft mouse models. *Annals of Oncology* 2020; 31: 266–273.

[631] Ice RJ, Chen M, Sidorov M, et al. Drug responses are conserved across patient-derived xenograft models of melanoma leading to identification of novel drug combination therapies. *Br J Cancer* 2020; 122: 648–657.

[632] Shattuck-Brandt RL, Chen S-C, Murray E, et al. Metastatic Melanoma Patient–Derived Xenografts Respond to MDM2 Inhibition as a Single Agent or in Combination with BRAF/MEK Inhibition. *Clinical Cancer Research* 2020; 26: 3803–3818.

[633] Teng R, Zhao J, Zhao Y, et al. Chimeric Antigen Receptor–modified T Cells Repressed Solid Tumors and Their Relapse in an Established Patient-derived Colon Carcinoma Xenograft Model. *Journal of Immunotherapy* 2019; 42: 33–42.

[634] Jiang Z, Jiang X, Chen S, et al. Anti-GPC3-CAR T Cells Suppress the Growth of Tumor Cells in Patient-Derived Xenografts of Hepatocellular Carcinoma. *Front Immunol*; 7. Epub ahead of print 11 January 2017. DOI: 10.3389/fimmu.2016.00690.

[635] Richman SA, Nunez-Cruz S, Moghimi B, et al. High-Affinity GD2-Specific CAR T Cells Induce Fatal Encephalitis in a Preclinical Neuroblastoma Model. *Cancer Immunol Res* 2018; 6: 36–46.

[636] Du H, Hirabayashi K, Ahn S, et al. Antitumor Responses in the Absence of Toxicity in Solid Tumors by Targeting B7-H3 via Chimeric Antigen Receptor T Cells. *Cancer Cell* 2019; 35: 221-237.e8.

[637] Parker KR, Migliorini D, Perkey E, et al. Single-Cell Analyses Identify Brain Mural Cells Expressing CD19 as Potential Off-Tumor Targets for CAR-T Immunotherapies. *Cell* 2020; 183: 126-142.e17.

[638] Donnadieu E, Luu M, Alb M, et al. Time to evolve: predicting engineered T cell-associated toxicity with next-generation models. *J Immunother Cancer*; 10. Epub ahead of print 2022. DOI: 10.1136/jitc-2021-003486.

[639] Chmielewski M, Hahn O, Rappl G, et al. T cells that target carcinoembryonic antigen eradicate orthotopic pancreatic carcinomas without inducing autoimmune colitis in mice. *Gastroenterology* 2012; 143: 1095–107.e2.

[640] Craddock JA, Lu A, Bear A, et al. Enhanced Tumor Trafficking of GD2 Chimeric Antigen Receptor T Cells by Expression of the Chemokine Receptor CCR2b. *Journal of Immunotherapy* 2010; 33: 780–788.

[641] Caruana I, Savoldo B, Hoyos V, et al. Heparanase promotes tumor infiltration and antitumor activity of CAR-redirected T lymphocytes. *Nat Med* 2015; 21: 524–529.

[642] Brown CE, Aguilar B, Starr R, et al. Optimization of IL13Rα2-Targeted Chimeric Antigen Receptor T Cells for Improved Anti-tumor Efficacy against Glioblastoma. *Molecular Therapy* 2018; 26: 31–44.

[643] Priceman SJ, Tilakawardane D, Jeang B, et al. Regional Delivery of Chimeric Antigen Receptor–Engineered T Cells Effectively Targets HER2+ Breast Cancer Metastasis to the Brain. *Clinical Cancer Research* 2018; 24: 95–105.

[644] Pickup M, Novitskiy S, Moses HL. The roles of TGFβ in the tumour microenvironment. *Nat Rev Cancer* 2013; 13: 788–799.

[645] Dahmani A, Delisle J-S. TGF-β in T Cell Biology: Implications for Cancer Immunotherapy. *Cancers (Basel)* 2018; 10: 194.

[646] Kloss CC, Lee J, Zhang A, et al. Dominant-Negative TGF-β Receptor Enhances PSMA-Targeted Human CAR T Cell Proliferation And Augments Prostate Cancer Eradication. *Molecular Therapy* 2018; 26: 1855–1866.

[647] Foster AE, Dotti G, Lu A, et al. Antitumor activity of EBV-specific T lymphocytes transduced with a dominant negative TGF-beta receptor. *J Immunother* 2008; 31: 500–505.

[648] Bollard CM, Rossig C, Calonge MJ, et al. Adapting a transforming growth factor beta-related tumor protection strategy to enhance antitumor immunity. *Blood* 2002; 99: 3179–3187.

[649] John LB, Devaud C, Duong CPM, et al. Anti-PD-1 Antibody Therapy Potently Enhances the Eradication of Established Tumors By Gene-Modified T Cells. *Clinical Cancer Research* 2013; 19: 5636–5646.

[650] Liu X, Ranganathan R, Jiang S, et al. A Chimeric Switch-Receptor Targeting PD1 Augments the Efficacy of Second-Generation CAR T Cells in Advanced Solid Tumors. *Cancer Res* 2016; 76: 1578–1590.

[651] Webster B, Xiong Y, Hu P, et al. Self-driving armored CAR-T cells overcome a suppressive milieu and eradicate CD19+ Raji lymphoma in preclinical models. *Molecular Therapy* 2021; 29: 2691–2706.

[652] Greenshpan Y, Sharabi O, Ottolenghi A, et al. Synthetic promoters to induce immune-effectors into the tumor microenvironment. *Commun Biol* 2021; 4: 143.

[653] Wu C-Y, Roybal KT, Puchner EM, et al. Remote control of therapeutic T cells through a small molecule-gated chimeric receptor. *Science* 2015; 350: aab4077–aab4077.

[654] Dotti G, Savoldo B, Pule M, et al. Human cytotoxic T lymphocytes with reduced sensitivity to Fas-induced apoptosis. *Blood* 2005; 105: 4677–4684.

[655] Lynn RC, Weber EW, Sotillo E, et al. c-Jun overexpression in CAR T cells induces exhaustion resistance. *Nature* 2019; 576: 293–300.

[656] Heitzeneder S, Bosse KR, Zhu Z, et al. GPC2-CAR T cells tuned for low antigen density mediate potent activity against neuroblastoma without toxicity. *Cancer Cell* 2022; 40: 53-69.e9.

[657] Eaton D, Gilham DE, O'Neill A, et al. Retroviral transduction of human peripheral blood lymphocytes with Bcl-X(L) promotes in vitro lymphocyte survival in pro-apoptotic conditions. *Gene Ther* 2002; 9: 527–535.

[658] Diaconu I, Ballard B, Zhang M, et al. Inducible Caspase-9 Selectively Modulates the Toxicities of CD19-Specific Chimeric Antigen Receptor-Modified T Cells. *Mol Ther* 2017; 25: 580–592.

[659] Straathof KC, Pule MA, Yotnda P, et al. An inducible caspase 9 safety switch for T-cell therapy. *Blood* 2005; 105: 4247–4254.

[660] Gargett T, Brown MP. The inducible caspase-9 suicide gene system as a 'safety switch' to limit on-target, off-tumor toxicities of chimeric antigen receptor T cells. *Front Pharmacol* 2014; 5: 235.

[661] Di Stasi A, Tey S-K, Dotti G, et al. Inducible apoptosis as a safety switch for adoptive cell therapy. *N Engl J Med* 2011; 365: 1673–1683.

[662] Zhou X, Dotti G, Krance RA, et al. Inducible caspase-9 suicide gene controls adverse effects from alloreplete T cells after haploidentical stem cell transplantation. *Blood* 2015; 125: 4103–13.

[663] Chen Y, Cheng Y, Suo P, et al. Donor-derived CD19-targeted T cell infusion induces minimal residual disease-negative remission in relapsed B-cell acute

lymphoblastic leukaemia with no response to donor lymphocyte infusions after haploidentical haematopoietic stem cell transplantation. *Br J Haematol* 2017; 179: 598–605.

[664] Resetca D, Neschadim A, Medin JA. Engineering Hematopoietic Cells for Cancer Immunotherapy: Strategies to Address Safety and Toxicity Concerns. *J Immunother* 2016; 39: 249–259.

[665] Richman SA, Wang LC, Moon EK, et al. Ligand-Induced Degradation of a CAR Permits Reversible Remote Control of CAR T Cell Activity In Vitro and In Vivo. *Molecular Therapy* 2020; 28: 1600–1613.

[666] Juillerat A, Tkach D, Busser BW, et al. Modulation of chimeric antigen receptor surface expression by a small molecule switch. *BMC Biotechnol*; 19. Epub ahead of print 3 July 2019. DOI: 10.1186/S12896-019-0537-3.

[667] Mestermann K, Giavridis T, Weber J, et al. The tyrosine kinase inhibitor dasatinib acts as a pharmacologic on/off switch for CAR T cells. *Sci Transl Med* 2019; 11: 5907.

[668] Weber EW, Lynn RC, Sotillo E, et al. Pharmacologic control of CAR-T cell function using dasatinib. Epub ahead of print 2019. DOI: 10.1182/bloodadvances.2018028720.

[669] Drent E, Poels R, Mulders MJ, et al. Feasibility of controlling CD38-CAR T cell activity with a Tet-on inducible CAR design. *PLoS One* 2018; 13: e0197349.

[670] Zhang RY, Wei D, Liu ZK, et al. Doxycycline Inducible Chimeric Antigen Receptor T Cells Targeting CD147 for Hepatocellular Carcinoma Therapy. *Front Cell Dev Biol* 2019; 7: 233.

[671] Gu X, He D, Li C, et al. Development of Inducible CD19-CAR T Cells with a Tet-On System for Controlled Activity and Enhanced Clinical Safety. *International Journal of Molecular Sciences 2018, Vol 19, Page 3455* 2018; 19: 3455.

[672] Morsut L, Roybal KT, Xiong X, et al. Engineering Customized Cell Sensing and Response Behaviors Using Synthetic Notch Receptors. *Cell* 2016; 164: 780–791.

[673] Roybal KT, Rupp LJ, Morsut L, et al. Precision Tumor Recognition by T Cells With Combinatorial Antigen-Sensing Circuits. *Cell* 2016; 164: 770–779.

[674] Leung W-H, Gay J, Martin U, et al. Sensitive and adaptable pharmacological control of CAR T cells through extracellular receptor dimerization. *Reference information: JCI Insight*; 4. Epub ahead of print 2019. DOI: 10.1172/jci.insight.124430.

[675] Mata M, Gerken C, Nguyen P, et al. Inducible activation of myD88 and CD40 in CAR T cells results in controllable and potent antitumor activity in preclinical solid tumor models. *Cancer Discov* 2017; 7: 1306–1319.

[676] Foster AE, Mahendravada A, Shinners NP, et al. Regulated Expansion and Survival of Chimeric Antigen Receptor-Modified T Cells Using Small Molecule-Dependent Inducible MyD88/CD40. *Molecular Therapy* 2017; 25: 2176–2188.

[677] Liu X, Wen J, Yi H, et al. Split chimeric antigen receptor-modified T cells targeting glypican-3 suppress hepatocellular carcinoma growth with reduced cytokine release. *https://doi.org/101177/1758835920910347*; 12. Epub ahead of print 9 March 2020. DOI: 10.1177/1758835920910347.

[678] Viaud S, Ma JSY, Hardy IR, et al. Switchable control over in vivo CAR T expansion, B cell depletion, and induction of memory. *Proc Natl Acad Sci U S A* 2018; 115: E10898–E10906.

[679] Lee YG, Chu H, Lu Y, et al. Regulation of CAR T cell-mediated cytokine release syndrome-like toxicity using low molecular weight adapters. *Nat Commun* 2019; 10: 2681.

[680] Goebeler ME, Bargou RC. T cell-engaging therapies — BiTEs and beyond. *Nature Reviews Clinical Oncology 2020 17:7* 2020; 17: 418–434.

[681] Labrijn AF, Janmaat ML, Reichert JM, et al. Bispecific antibodies: a mechanistic review of the pipeline. *Nat Rev Drug Discov* 2019; 18: 585–608.

[682] Nathan P, Hassel JC, Rutkowski P, et al. Overall Survival Benefit with Tebentafusp in Metastatic Uveal Melanoma. *New England Journal of Medicine* 2021; 385: 1196–1206.

[683] FDA. FDA grants accelerated approval to mosunetuzumab-axgb for relapsed or refractory follicular lymphoma. *FDA*, https://www.fda.gov/drugs/resources-information-approved-drugs/fda-grants-accelerated-approval-mosunetuzumab-axgb-relapsed-or-refractory-follicular-lymphoma (2022, accessed 27 April 2023).

[684] FDA. FDA approves teclistamab-cqyv for relapsed or refractory multiple myeloma. *FDA*, https://www.fda.gov/drugs/resources-information-approved-drugs/fda-approves-teclistamab-cqyv-relapsed-or-refractory-multiple-myeloma (2022, accessed 27 April 2023).

[685] Klinger M, Brandl C, Zugmaier G, et al. Immunopharmacologic response of patients with B-lineage acute lymphoblastic leukemia to continuous infusion of T cell-engaging CD19/CD3-bispecific BiTE antibody blinatumomab. *Blood* 2012; 119: 6226–6233.

[686] Zoni E, Astrologo L, Ng CKY, et al. Therapeutic targeting of CD146/MCAM reduces bone metastasis in prostate cancer. *Molecular Cancer Research* 2019; 17: 1049–1062.

[687] Leslie MC, Zhao YJ, Lachman LB, et al. Immunization against MUC18/MCAM, a novel antigen that drives melanoma invasion and metastasis. *Gene Ther* 2007; 14: 316–323.

[688] Lanitis E, Poussin M, Klattenhoff AW, et al. Chimeric antigen receptor T Cells with dissociated signaling domains exhibit focused antitumor activity with reduced potential for toxicity in vivo. *Cancer Immunol Res* 2013; 1: 43–53.

[689] Kloss CC, Condomines M, Cartellieri M, et al. Combinatorial antigen recognition with balanced signaling promotes selective tumor eradication by engineered T cells. *Nat Biotechnol* 2013; 31: 71–75.